2038-5625

Italian Journal of Agrometeorology

Rivista Italiana di Agrometeorologia

n. 1 – 2024

FIRENZE UNIVERSITY PRESS

Cover photo by Maurizio Borin

Italian Journal of Agrometeorology

n. 1 - 2024

Firenze University Press

The ***Italian Journal of Agrometeorology*** (***IJAm - Rivista Italiana di Agrometeorologia***) is the official periodical of the Italian Association of Agrometeorology (AIAM) and aims to publish original scientific contributions in English on agrometerology, as a science that studies the interactions of hydrological and meteorological factors with the agricultural and forest ecosystems, and with agriculture in its broadest sense (including livestock and fisheries).

SUBSCRIPTION INFORMATION
IJAm articles are freely available online, but print editions are available to paying subscribers. Subscription rates are in Eur and are applicable worldwide.
Annual Subscription: € 50,00 Single Issue: € 25,00

CONTACT INFORMATION
Please contact ordini@fupress.com, if you have any questions about your subscription or if you would like to place an order for the print edition. Information on payment methods will be provided after your initial correspondence.

Published by
Firenze University Press – University of Florence, Italy
Via Cittadella, 7 - 50144 Florence - Italy
http://www.fupress.com/ijam

Italian Journal of Agrometeorology
Rivista Italiana di Agrometeorologia

Firenze University Press
www.fupress.com/ijam

OPEN ACCESS

Citation: de Almeida, A.M., Coelho, R.D., da Silva Barros, T.H., Quiloango-Chimarro, C.A., Azevedo, A.T. & de Oliveira Costa, J. (2024). Water use efficiency and canopy temperature response of soybean subjected to deficit irrigation. *Italian Journal of Agrometeorology* (1): 3-16. doi: 10.36253/ijam-2445

Received: January 20, 2024

Accepted: June 14, 2024

Published: August 2, 2024

Data Availability Statement: All relevant data are within the paper and its Supporting Information files.

Competing Interests: The Author(s) declare(s) no conflict of interest.

Water use efficiency and canopy temperature response of soybean subjected to deficit irrigation

Ailson Maciel de Almeida[1,*], Rubens Duarte Coelho[1], Timóteo Herculino da Silva Barros[2], Carlos Alberto Quiloango-Chimarro[1], Angelo Tiago Azevedo[1], Jéfferson de Oliveira Costa[3]

[1] *University of São Paulo/USP-ESALQ, Biosystems Engineering Department, C.P. 09, 13418-900 Piracicaba, SP, Brazil*
[2] *University of São Paulo/USP-CENA, Center of Nuclear Energy in Agriculture, 13416-000 Piracicaba, SP, Brazil*
[3] *Minas Gerais Agricultural Research Agency/EPAMIG, Experimental Field of Gorutuba, 39525-000 Nova Porteirinha, MG, Brazil*
*Corresponding author. Email: ailson.m.almeida@gmail.com

Abstract. Deficit irrigation is a key strategy for improving water use efficiency (WUE) under irrigated conditions. However, there is a lack of information regarding the optimal water replacement that have minimal negative effects on soybean productivity. The objective of this study was to determine the water replacement levels associated with insignificant grain yield (GY) losses in soybean crops. A rain shelter experiment was conducted using a randomized complete block design with six replicates. Eight irrigation replacement levels, L120, L100, L90, L80, L70, L60, L50, and L40, were applied, where L100 was the reference treatment that kept soil moisture content along the soil profile under field capacity conditions and all other replacement levels were a fraction of this reference level. Grain yield ranged from 2.2 Mg ha^{-1} in L40 to 4.4 Mg ha^{-1} in L100, with a significant GY reduction in irrigation levels below 70%. The average crop water stress index (CWSI) ranged between 0.26 at L120 and 0.66 at L40 irrigation levels. WUE varied significantly only for the extreme irrigation levels studied, with the greatest value at the L40 irrigation level (1.2 kg m^{-3}) and the lowest value at the L120 irrigation level (0.65 kg m^{-3}), whereas for the intermediate irrigation levels from 50 to 100%, the WUE was equal to approximately 1.1 kg m^{-3}. The relationship between CWSI and GY (R^2 = 0.85) suggested that the maximum GY occurred at a CWSI of 0.34. In addition, the relationship between CWSI and WUE (R^2 = 0.73) showed that as evapotranspiration decreased, crop temperature increased. In conclusion, the implementation of a continuous water deficit in soybeans is feasible for farmers in water-scarce areas, but the minimum value of area productivity must be considered, even though WUE increases under more intensive values of water deficit.

Keywords: *Glycine max* L., water deficit strategies, canopy temperature, morphological responses.

HIGHLIGHTS

- Water replacement levels below 70% of required irrigation depth causes significant grain yield losses;
- Water replacement level of 40% of required irrigation depth improving water use efficiency;
- Long-term irrigation deficit reduces biomass of pods, leaves and stalks;
- CWSI showed significant quadratic relations with grain yield and water use efficiency.

1. INTRODUCTION

Currently, Brazil is the world's leading producer of soybeans (*Glycine max* L.), with a cropped area of roughly 38 million hectares and an average yield of 3517 kg ha^{-1} (Conab, 2023). This crop is one of the main commodities in the world, is of great importance in human and animal nutrition, and plays an important role in the bioenergy industry (Vale et al., 2019). However, soybean-cropped areas in Brazil are under rainfed conditions (90%) (Battisti et al., 2018), most of which are susceptible to drought stress, and hence yield gaps (Battisti and Sentelhas, 2019).

Water stress during the soybean growing cycle causes yield reductions between 46 and 74% (Sentelhas et al., 2015; Battisti et al., 2018). Furthermore, these negative effects may increase in the future because of water scarcity for agricultural activities related to climate change (Singh et al., 2014; Kang et al., 2021). Consequently, new irrigated areas for soybean production are being developed in this country (Fernandes et al., 2022). However, irrigated areas require technologies that contribute to the rational use of water in agriculture (Blum, 2009; Quiloango-Chimarro et al., 2022). Among these technologies, deficit irrigation appears to be the primary strategy to promote water saving, which can be quantified through water use efficiency (WUE) (Geerts and Raes, 2009; Kang et al., 2021). For example, a meta-analysis in China showed that deficit irrigation strategies in wheat and maize increased WUE by 9.25% and 6.38%, respectively, and water saving varied between 100 and 200 mm per growing cycle (Li et al., 2022). In soybean, a recent study showed that differences between full (80% of required irrigation depth) and deficit irrigation (60% of required irrigation depth) were only 2.9% in grain yield (GY) (Kocar et al., 2022). This finding highlights the benefits of deficit irrigation in soybean; however, further research is needed to determine the specific deficit irrigation levels that improve WUE with incipient GY reductions.

The effects of water stress can be evaluated using several methods in both plants and soil (Petrie et al., 2019). An important cost-effective indicator of crop water status in real time is canopy temperature (Bian et al., 2019; Costa et al., 2020). This method of assessing the water deficit in plants is based on the principle that the reduction in temperature is proportional to the rate of plant transpiration due to the evaporative cooling process (Zia et al., 2013; Costa et al., 2018; Khorsandi et al., 2018). Temperature data acquisition has advanced over the last 50 years (Craparo et al., 2017; Kirnak et al., 2019). Currently, thermal cameras are increasingly being integrated or adapted to be used in satellites, drones, and even smartphones (Bian et al., 2019; Petrie et al., 2019). Temperature data obtained through thermography has shown promising correlations with physiological and productivity-related parameters (Yang et al., 2019; Anda et al., 2020). Additionally, canopy temperature allows the computation of indices such as the crop water stress index (CWSI), which is the most commonly used index to quantify plant spatial and temporal variability of drought stress and to schedule precision irrigation on large irrigated fields (Khorsand et al., 2021).

The Crop Water Stress Index serves to simplify the interpretation of a plant's water status (Biju et al., 2018), providing a value ranging from 0 (indicating non-stressed conditions) to 1 (representing maximum stress conditions). These facilities and the robustness of thermography would allow farmers to make better decisions regarding irrigation. Temperature-derived indices are important for reliably estimating decreases in soybean GY (Gajić et al., 2018; Anda et al., 2020). For example, Anda et al. (2019) found that for each 0.1 increase in CWSI above 0.2, GY decreased by 434.1 g m^{-2}. However, the same authors highlighted that the relationship between the CWSI and GY should be studied for each specific climatic condition to ensure accurate and relevant results.

It was hypothesized that deficit irrigation would improve WUE in soybeans without significant yield losses. Thus, the objectives were to determine the water replacement level where soybean has no significant GY losses, to identify water stress through the canopy temperature response patterns, to verify the relationships between CWSI and GY, and between CWSI and WUE.

2. MATERIAL AND METHODS

2.1. Site characterization

The study site is located at University of São Paulo, Piracicaba-SP, in southwestern Brazil, which is consid-

ered a humid subtropical zone, Cw, according to the Koppen climate classification. The experiment was conducted under rain shelter conditions. The structure of the cover measured 5.2 meters in ceiling height and was composed of a transparent plastic cover (diffuser film) and lateral black screens, which were designed to intercept 30% of incoming radiation. The experimental area extended over 164 m^2 and was divided into 96 plots, each of which was a fiber cement box with a volume of 0.1 m^3 and had dimensions of 0.60 meters in length, 0.45 meters in width, and 0.40 meters in depth. The soil within each box was classified as red-yellow latosol with a sandy-loam texture. The plots were arranged in four rows, with 0.80 meters between rows and 0.50 meters between plots within each row.

2.2. Plant materials, experimental preparation and treatment application

Glycine max L. semi-determined habit cultivar TMG 7062 was sowed on December 16, 2019. Before initiating the sowing, a chemical analysis of the soil was conducted, and the fertilization recommendations provided by the São Paulo State Agricultural Company (IAC Nutrition Bulletin) were carefully followed. Consequently, 300 grams of monoammonium phosphate and potassium chloride were applied to the soil via fertigation. Approximately eight days after seeding (DAS), the plants were thinned to maintain a distance of twelve plants per meter (six plants per plot). Throughout the growing cycle, manual weed management was practiced, and appropriate agrochemicals were applied to address any pest or disease.

The experiment was based on a randomized block design and six replications per treatment. Soybean plants were subjected to eight irrigation replacements (L120, L100, L90, L80, L70, L60, L50, and L40), resulting in an experiment with 96 useful plots. The reference treatment (L100) was based on the water depth necessary to keep the soil profile at field capacity (Fc) every other day, whereas all other treatments were a fraction of this treatment.

The irrigation system consisted of a 500 L water reservoir, polyethylene piping, water pump, ring filter, and four watering manifolds with eight outlets each. Two emitters with a flow rate of 8 L h^{-1} were installed in each plot. For a homogeneous distribution of water on the plot, a two-way splitter was installed on each emitter. The irrigation system was managed through an *Arduino* mega microcontroller. Furthermore, the Arduino platform controlled two relays for activation of the irrigation pump and the reservoir output solenoid.

Before the beginning of the experiment, the irrigation system was evaluated to verify the emitters' flow rate. Christiansen's uniformity coefficient (CU), Distribution Uniformity (DU) and the total system flow rate were used. The performance of the irrigation system was considered excellent, as evidenced by the CU and DU values of 95.5% and 86.1%, respectively, and the total system flow rate of 1.5 m^3 h^{-1}.

Irrigation management was based on the soil water matric potential. For this purpose, tensiometers were installed at 0.15, 0.25 and 0.35 m in all repetitions of the reference treatment (L100). The matric potential was measured daily with a digital portable punction tensimeter calibrated against a mercury vacuum gauge. A spreadsheet developed in Microsoft Excel® was used for irrigation amount calculations.

Irrigation for the L100 level was computed by adding the water necessary to increase the soil water to the field capacity for all three soil layers. The amount of soil water in each layer before irrigation was estimated from the matric potential by using the van Genuchten soil water retention equation (van Genuchten, 1980), according to Equation 1:

$$\theta(\Psi_m) = \theta_r + \frac{(\theta_s - \theta_r)}{(1 + (\alpha \times \Psi_m)^n)^m} \quad (1)$$

where θ (ψm) is the soil volumetric water content (cm^3 cm^{-3}), θ_r is the soil residual volumetric water content ($cm^3\,cm^{-3}$), θ_s is the volumetric water content of the saturated soil ($cm^3\,cm^{-3}$), m and n are the regression parameters of equation (dimensionless), α is the parameter with dimension equal to the inverse of the tension (kPa^{-1}) and ψ_m is the function of the matric potential (kPa).

The physical water retention characteristics of the soil and parameters for the van Genuchten model are listed in Table 1. The criterion established to start irrigation allowed us to maintain the soil matric potential at -25 kPa prior to the initiation of irrigation throughout the entire growing cycle. This soil-based irrigation scheduling method ensures that the soybean crop achieves its potential grain yield (GY) (França et al., 2024). Before irrigation level treatments were implemented, plants were given 100% irrigation (L100) until the seedling stands were well established.

The total irrigation amount varied from 1125 mm in L120 to 375 mm in L40 (Table 2). The potential water demand (L100) in this trial (938 mm) was higher than the usual range for this crop, which commonly varies between 400 and 840 mm under field conditions (Candogan et al., 2013; Silva et al., 2017). The total number of irrigation events was 41 for all treatments.

Table 1. Physical water-retention characteristics of the soil and parameters for the van Genuchten model.

Layer m	θs $cm^3\ cm^{-3}$	θr $cm^3\ cm^{-3}$	α kPa^{-1}	m	n	θfc $cm^3\ cm^{-3}$	θwp $cm^3\ cm^{-3}$	AWC mm
0-0.20	0.095	0.422	1.346	0.1802	2.7275	0.225	0.102	24.6
0.20-0.30	0.085	0.412	1.571	0.1649	2.5001	0.226	0.098	12.8
0.30-0.40	0.123	0.375	1.128	0.2758	1.5638	0.242	0.133	10.9

Empiric parameters (α, m and n), soil residual and saturation water content (θr, θs) of the van Genuchten model, moisture at field capacity (θfc), moisture at the wilting point (θwp) and available water capacity (AWC).

Table 2. Irrigation water accumulated and number of irrigations during the soybean growing cycle.

Treatments	L40	L50	L60	L70	L80	L90	L100	L120
Accumulated irrigation (mm $cycle^{-1}$)	375.1	468.9	562.7	656.5	750.3	844.1	937.9	1125.5
Number of irrigation events	41	41	41	41	41	41	41	41

2.3. Micrometeorological monitoring, canopy temperature and crop water stress index measurements

Micrometeorological data were measured inside the greenhouse in the center of the experimental area. Measurements of air temperature, relative humidity and solar radiation flux density were recorded with a Vaissala sensor HMP45C, Vaissala barometer CS 106, and a pyranometer sensor LI200X, respectively (Campbell Scientific, Logan, Utah, USA). Micrometeorological data were integrated every 15 minutes (average values) through a CR1000 data-logger (Campbell Scientific, Logan, Utah, USA).

Infrared thermal images were taken with a FLIR One Pro thermal camera (FLIR Systems, Portland, USA) with a resolution of 160 × 120 pixels and emissivity values of 0.95. These images were acquired above the leaf canopy at a height of 1.5 m, on leaves fully exposed to the sun and with a similar insertion angle in relation to the vertical plane (Figure 1). Thermal evaluations were done three times during the growing cycle on cloudless days around noon (vegetative stage, 30 DAS; flowering, 62 DAS; and ripening, 90 DAS). Images of each plot were processed and analyzed in the software FLIR Tools, in which a representative part of the canopy was selected to calculate the average canopy temperature.

Using infrared thermal data and micrometeorological data, the CWSI was computed according to the methodology of Jackson et al. (1988), as in Equation 2:

$$CWSI = \frac{(T_c - T_{air}) - T_{wet}}{T_{dry} - T_{wet}} \quad (2)$$

T_{air} is the temperature of the air, T_c is the temperature of the canopy, T_{wet} is the non-water stressed baseline (temperature of the canopy transpiring at the potential rate), and T_{dry} is the water stressed baseline (temperature of the non-transpiring canopy). The difference between T_c and T_{air} is the canopy temperature depression (CTD).

The lower and upper temperature baselines were determined by the minimum and maximum difference between T_c and T_{air}, respectively. For CWSI calculation, (T_c - T_{air}) above 7 °C and below -10 °C were eliminated following the methodology proposed by Meron et al. (2013).

2.4. Morphological evaluations and water use efficiency

The height of the plants was evaluated in four periods during the growing cycle (20, 40, 60 and 80 DAS). Plants were harvested at physiological maturity (March 29, 2020) and divided into vegetative and reproductive components, then dried at 65° C in an oven with forced air circulation for 72 hours, and finally weighted on a precision scale. The biomass of stalks, branches, leaves, pods, and seeds resulted in the biological yield of the crop. The harvest index was calculated as the ratio of GY to biological yield, as in Equation 3:

$$HI = \frac{\text{Grain yield (kg)}}{\text{Biological yield (kg)}} \times 100 \quad (3)$$

Soybean grain yield was normalized for 13% seed water concentration. Grain yield was scaled to Mg ha^{-1} considering a useful area of 0.27 m^2 per plot. Water use

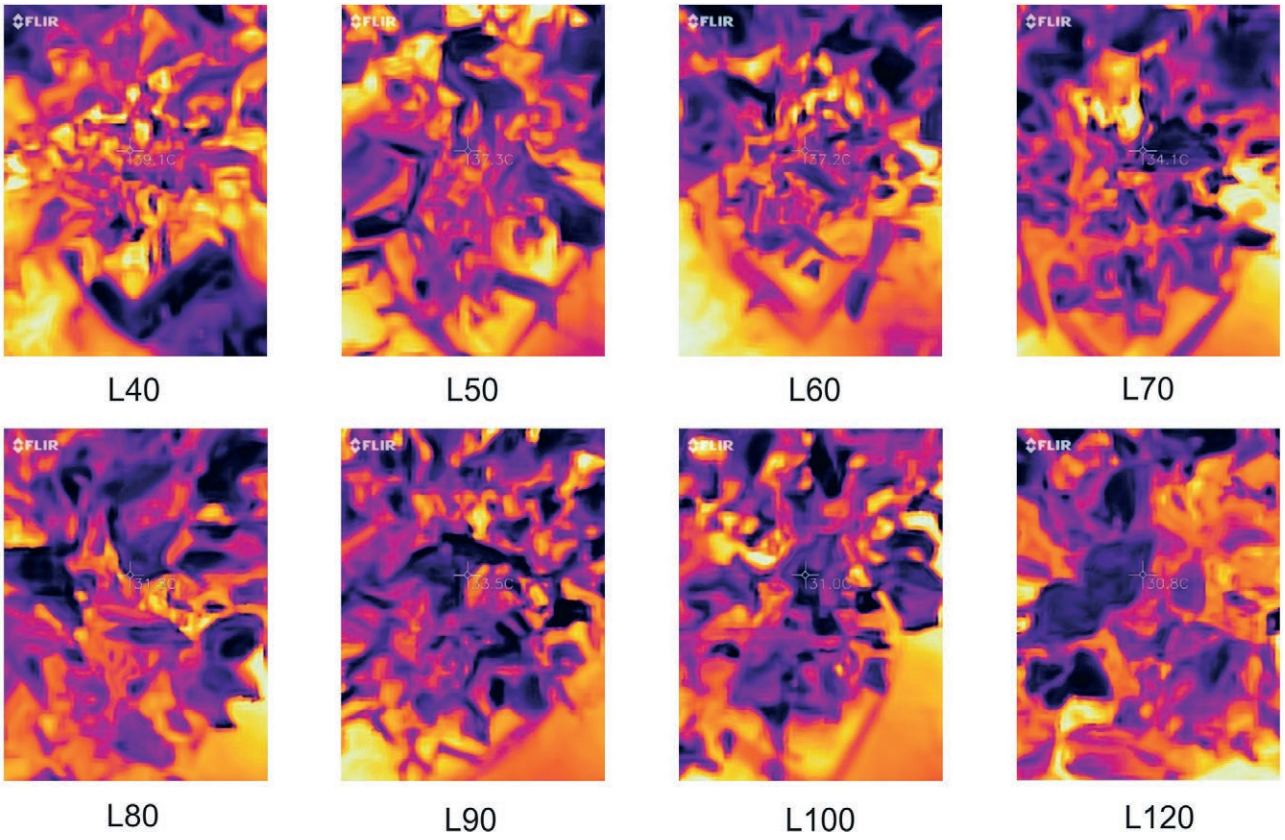

Figure 1. Infrared images from the eight water replacement levels. The darker colors in the thermal images represent cooler temperatures, while the lighter colors represent warmer temperatures.

efficiency (kg m^{-3}) was calculated as the ratio of GY to the amount of total water input, as in Equation 4:

$$WUE = \frac{\text{Grain yield (kg)}}{\text{Water consumption } (m^3)} \quad (4)$$

2.5. Statistical analysis

All the statistical analyses were performed with the R software (R Project for Statistical Computing, version 4.1.2). Exploratory data analysis was conducted to detect outliers using box-plot graphs. Analyses of variance (ANOVA) were performed after testing the homogeneity of variances and normality of the residuals by the Levene and Shapiro-Wilks tests, respectively. Variables with a significant *F* value at 5% probability were subjected to regression analysis and the post-hoc Tukey test at 5% probability. In addition, Pearson's linear correlation coefficient was performed to evaluate the relationship between the following variables: biomass of leaves, pods, stems and branches, 100-seed weight, CTD, canopy temperature, HI, irrigation amount, WUE, GY and CWSI. This coefficient and its significance level were mainly determined to illustrate how canopy temperature influences the morphological and yield variables.

3. RESULTS AND DISCUSSION

3.1. Micrometeorological data, canopy temperature and crop water stress index (CWSI)

The climatic data collected during the experimental period are presented in Figure 2. The average temperature during the growing cycle was found to be within the optimal range for soybean growth, fluctuating between 21.1 and 31 °C (Setiyono et al., 2007). The maximum temperature varied between 25.6 and 46.1 °C, while the minimum temperature ranged between 15.9 and 24.4 °C (Figure 2A). Throughout the growing cycle, the average relative humidity varied between 73.4 and 100%, while the solar radiation fluctuated between 2.8 and 22.3 MJ m^{-2} day^{-1}, with an average value of 13.7 MJ m^{-2} day^{-1} (Figure 2B).

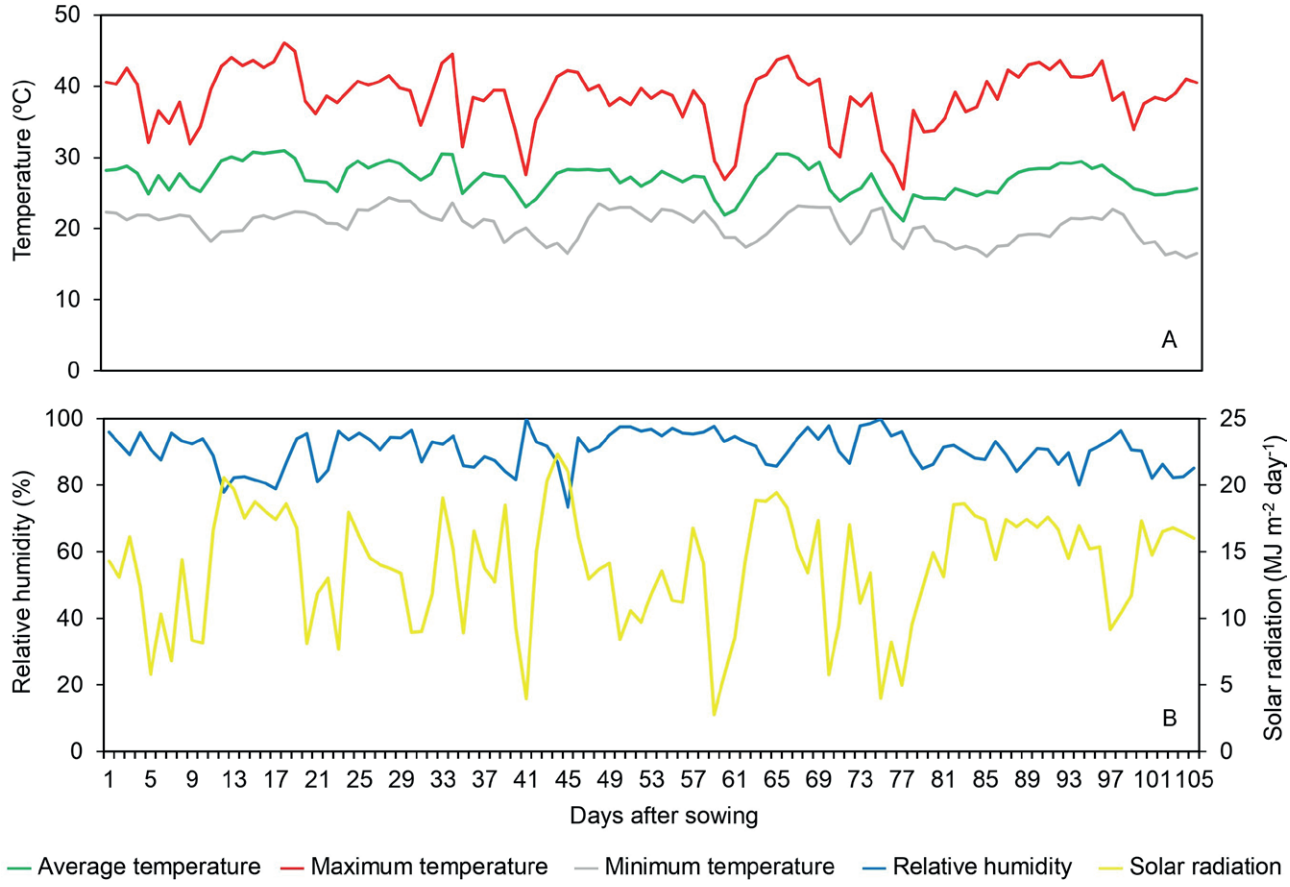

Figure 2. Maximum, minimum, and average air temperature (**A**), relative humidity and solar radiation (**B**) in the experimental area during the soybean growing cycle. 0 days after sowing (DAS): December 16, 2019 and 105 DAS: March 29, 2020.

Irrigation treatments showed a significant response in canopy temperature (T_c) and canopy temperature depression (CTD) (Table 3). The T_c was 32.9 °C for the reference treatment (L100), which was comparable to the T_c for treatments L120, L90, and L80. In contrast, the T_c of treatments L60, L50, and L40 differed from the reference irrigation treatment by an average of 4.9 °C (Figure 3A). The observed increase in canopy temperature can be attributed to the stomatal closure that contributes to a diminished capacity for transpiration cooling (Banerjee et al., 2020). Stomatal closure is a critical adaptive mechanism for plants under water stress and affects various physiological processes, including photosynthesis, transpiration, and leaf water status (Flexas and Medrano, 2002; Quiloango-Chimarro et al., 2022; Zahra et al., 2023). These changes in crop physiology also influence soybean growth and development, as discussed below.

In the present study, the variation of the CTD was about ± 2.6 °C. Under irrigation treatments L120, L100, L90, and L80, the CTD was negative, whereas under the irrigation treatments L60, L50, and L40, the CTD was positive (Figure 3B). The variation of CTD and T_c was similar, but with the increase in water supply, CTD decreased while T_c increased. CTD has been used to assess plant water status (Zia et al., 2013; Biju et al., 2018) and has been preferred in high air temperatures and low relative humidity for irrigation management (Amani et al., 1996). In addition, Singh et al. (2021) suggested that CTD and water deficit are unrelated until the soil water availability changes significantly.

Average CWSI values ranged between 0.26 in L120 and 0.66 in L40 (Figure 4). Overall, CWSI increased as irrigation levels decreased. CWSI varied between 0.18-0.25 in L120, 0.21-0.24 in L100, 0.22-0.31 in L90, 0.23-0.36 in L80, 0.33-0.50 in L70, 0.38-0.68 in L60, 0.50-0.58 in L50, and 0.61-0.71 in L40. Similar CWSI responses due to water stress have been reported in soybean. For example, in a recent study by Morales-Santos and Nolz (2023), CWSI values ranging between 0.13 and 0.23 were reported for drip-irrigated soybean. These

Table 3. Analysis of variance (ANOVA) to compare the means of the studied variables.

Source of variation	Variables	Sum of squares	Mean square	*F*
Water replacement levels	Canopy temperature (T_c) and canopy temperature depression (CTD)	212.87	30.41	18.23*
	CWSI end of the vegetative stage ($CWSI_A$)	0.90	0.13	10.28*
	CWSI flowering ($CWSI_B$)	1.55	0.22	17.76*
	CWSI ripening ($CWSI_C$)	1.03	0.15	41.33*
	Average CWSI ($CWSI_D$)	1.19	0.17	17.96*
	Plant height at 20 days after sowing (DAS)	6.52	0.93	0.31^{ns}
	Plant height at 40 DAS	75.97	10.85	1.53^{ns}
	Plant height at 60 DAS	752.70	107.53	6.48*
	Plant height at 80 DAS	2134.50	304.93	14.82*
	Dry weight of leaves	18239	2605.59	5.04*
	Dry weight of pods	15451	2350.15	10.48*
	Dry weight of stems and branches	23961	3424	15.94*
	Grain yield (GY)	33.72	4.82	7.99*
	Harvest index (HI)	144.72	20.68	1.40^{ns}
	Water use efficiency (WUE)	1.08	0.15	3.41*

^{ns}not significant; *significant at a probability level of 5%.

values closely aligned with the CWSI values obtained in the present study under the reference treatment (L100), despite the different environmental conditions (subhumid and humid subtropical). This consistency highlights the robustness of CWSI as a standard metric for irrigation scheduling, effectively isolating independent environmental factors (DeJonge et al., 2015; Kullberg et al., 2017).

3.2. Morphological responses to water deficit

Figure 5 shows the plant height response to deficit irrigation, measured four times during the growing cycle. Irrigation treatments had no effect on plant height in the first and second periods (Table 3), with average of 0.35 and 0.42 m, respectively (Figure 5A and 5B). In the third period, plant height was lower under irrigation treatments L40 and L50, with a difference of ~0.10 m compared with the L120 treatment (Figure 5C). In the fourth period, plant height was lower under the irrigation treatments L40, L50, and L60, and the greatest difference was found between L40 and L120 (~0.20 m) (Figure 5D). The final plant height under well-watered conditions was on average 0.88 m. According to Dong et al. (2019), plant height inhibition in soybeans under drought stress is more pronounced when plants are subjected to severe and long-duration stress. For example, Rosadi et al. (2005) showed that soybeans under 40% of required irrigation depth maintained plant height until the fourth week of stress, and at the end of the growing cycle, plant height was reduced by 0.26 m. Therefore, plant height is an indicator of soybean growth and development when employing water-deficit strategies.

Aerial biomass accumulation diminished as water stress increased (Figure 6). The decline in total dry matter under L40 compared with that under L100 was 48%. The biomass of leaves, pods, and stalks showed similar decreases under irrigation deficits. Thus, there was a huge difference in the biomass weight of these components in L40, L50, and L60 compared to the reference treatment (L100). When comparing the L100 and L40 treatments, there was a reduction in the biomass of the leaves, pods, and stalks by 29%, 52%, and 43%, respectively. Similar decreases in pod and leaf biomass have been observed in short-term drought stress trials (Rosales-Serna et al., 2004). However, short periods of water stress have no effect or even increase the stalk biomass (Wijewardana et al., 2018). According to Ohashi et al. (2009), drought stress at specific phenological stages induces greater partitioning of assimilates to vegetative parts (stalks) rather than reproductive parts. Thus, it is interesting to note that long-duration water deficits led to losses in all biomass components.

Grain yield decreased as the irrigation deficit increased (Table 4). Compared to the reference treatment (L100), significant reductions in GY ranged from 11% in L70 to 50% in L40. These results are comparable with those reported by Irmak et al. (2014) in which each 25.4 mm increase in water amount improved soybean yield by 0.3 Mg ha^{-1}. For example, in our study, the differences in the water amount and GY between L100 and

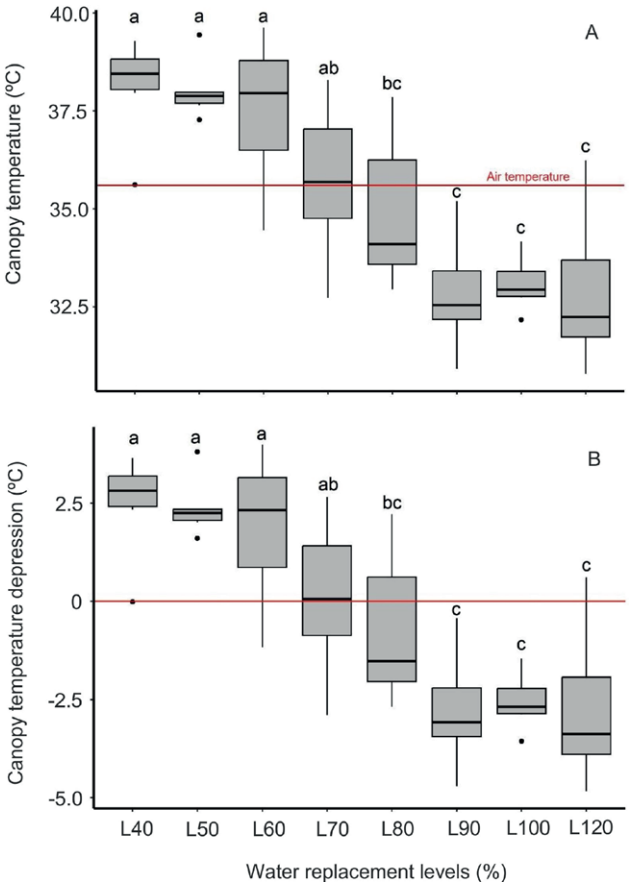

Figure 3. Boxplots of average canopy temperature derived variables. Canopy temperature (**A**), Canopy temperature depression (CTD) (**B**). Different lowercase letters indicate significant differences at 5% probability according to the Tukey test. The box represents the interquartile range (IQR) and whiskers represent the range of data. The median is depicted by a horizontal line within the box, and the outliers are illustrated by individual points outside the whiskers.

L90 were 94 mm and 1 Mg ha^{-1}, respectively. In addition, non-significant decreases under excess irrigation (L120) reflect no damage effects in soybean, which is consistent with the study of Gava et al. (2016) in soybean subjected to 50% additional irrigation. Grain yield potential (L100) in this study (4.4 Mg ha^{-1}) was superior to the Brazilian average production (3.3 Mg ha^{-1}) (Conab, 2023), confirming the benefits of irrigation in soybean. Overall, the findings indicate that GY can be sustained under extended periods of water restriction (L80), resulting in a water saving of approximately 375 mm.

Irrigation treatments had no significant effect on the average harvest index (HI), which varied from 29.9 to 33.5% (Table 3). Similar results were found by Demirtaş et al. (2010) in soybean subjected to water stress under drip irrigation. In contrast, Gajić et al. (2018) and Frederick et al. (1991) reported that the HI tended to be higher under drought stress conditions. Thus, the response of HI to drought stress could be different due to genotype–environment interactions.

Table 4. Grain yield, harvest index and water use efficiency of soybean subjected to eight water replacement levels.

Water replacement levels	Grain yield (Mg ha^{-1})	Harvest index (%)	Water use efficiency (kg m^{-3})
L120	3.3±0.5abc	29.9±1.7	0.61±0.10b
L100	4.4±0.4a	36.5±1.4	0.88±0.13ab
L90	3.4±0.5ab	33.2±2.3	0.83±0.06ab
L80	3.5±0.4ab	33.3±2.2	0.97±0.10ab
L70	3.0±0.3bcd	33.0±1.4	0.96±0.10ab
L60	2.6±0.2bcd	31.8±1.8	0.94±0.11ab
L50	2.3±0.3cd	33.2±2.5	0.99±0.08ab
L40	2.2±0.2d	33.5±1.2	1.17±0.09a

Data are Mean ± SE (n = 6). Different lowercase letters indicate significant difference according to the Tukey's test.

Significant differences in WUE were found between the irrigation treatments (Table 3). Water use efficiency ranged between 1.17 kg m^{-3} in L40 and 0.61 kg m^{-3} in L120. L40 (severe water stress) was 25% higher than L100 (reference treatment) with a water saving of 563 mm (Table 4). Gava et al. (2016) in soybean under irrigation treatments between 20 and 100% of required irrigation depth found higher values of WUE at 40-60% of water deficit (1.1 kg m^{-3}). On the other hand, lower WUE values were recorded in rainfed systems when compared with irrigated systems (Mekonnen et al., 2020), highlighting the importance of irrigation to increase the WUE of crop production. Overall, the results suggest that deficit strategies in irrigated soybean could be an option in water-scarce regions.

3.3. Correlations among studied traits

The correlation among traits is shown in Figure 7. Pearson correlation coefficients below 0.5 were marked by a "x mark" whereas positive correlations are in blue and negative correlations are in red. Grain yield was positively correlated with biomass of leaves, pods, and stalks, HI, and irrigation amount, but negatively with all derived canopy temperature variables (Canopy temperature, CTD, $CWSI_A$, $CWSI_B$, $CWSI_C$ and average $CWSI_D$). Average $CWSI_D$ was the only one closely related to GY and WUE (Pearson's R=-0.38** and 0.36*). Therefore, these relationships could be an indicator of the yield gap and allow for improved water management in irrigated soybean.

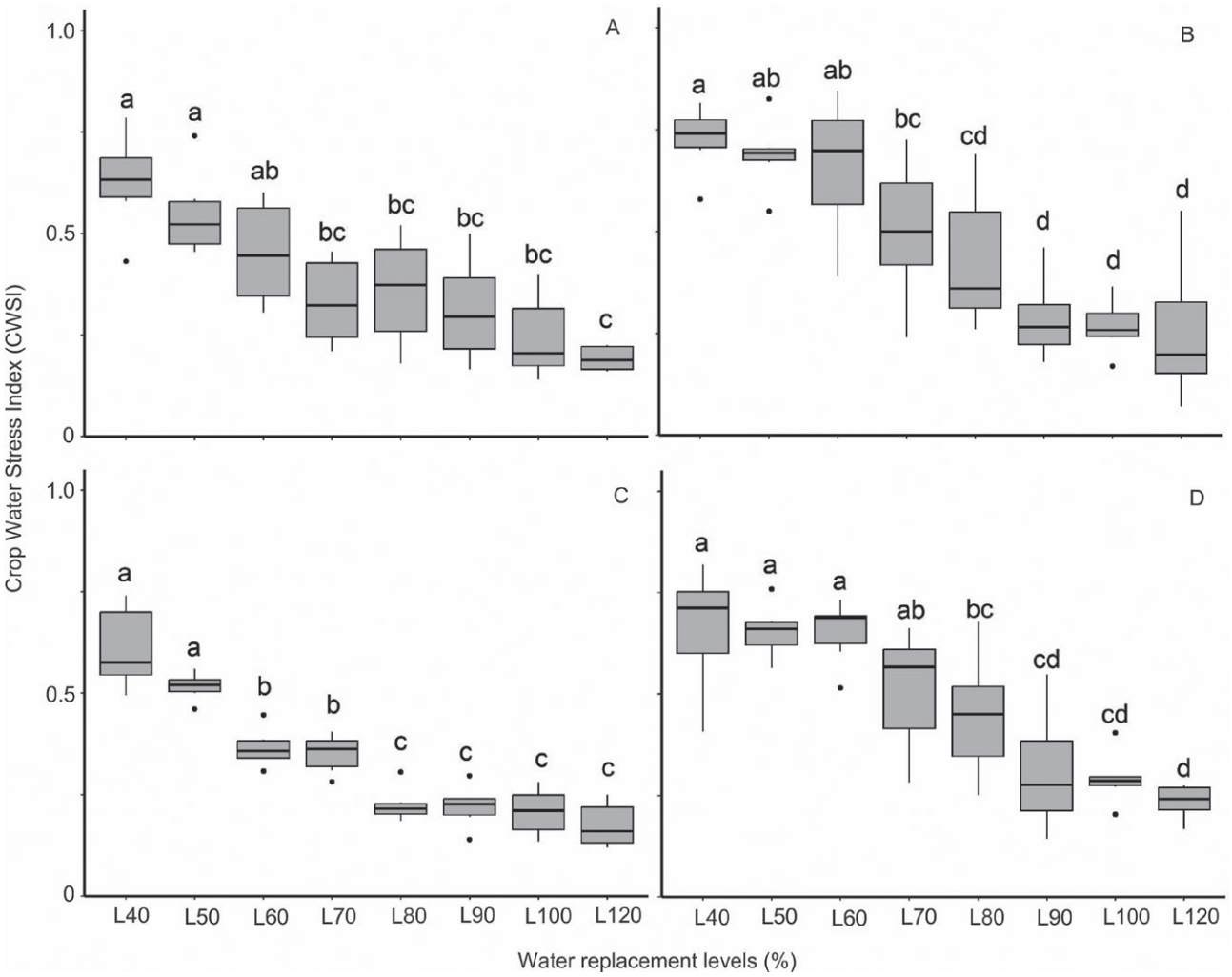

Figure 4. Crop water stress index (CWSI) throughout the growing cycle. (**A**), end of the vegetative stage; (**B**), flowering; (**C**), ripening and (**D**), average CWSI. Different lowercase letters indicate significant differences at 5% probability according to the Tukey test. The box represents the interquartile range (IQR) and whiskers represent the range of data. The median is depicted by a horizontal line within the box, and the outliers are illustrated by individual points outside the whiskers.

A second order polynomial was fitted to the average CWSI and GY (Figure 8A). A polynomial equation between CWSI-GY in soybean was also reported by Kocar et al. (2022) with a R^2=0.75. The maximum GY (4.67 Mg ha^{-1}) occurred at a CWSI of 0.34, which suggests that 80% of irrigation replacement can maintain soybean productivity similar to fully irrigated treatment (L100).

A second order polynomial was fitted to the average CWSI and WUE (Figure 8B) which is consistent with the equations found by Anda et al. (2020) and Candogan et al. (2013) in soybean deficit irrigation trials. Moreover, Dogan et al. (2007) concluded that irrigation deficit strategies in soybean improve WUE because less water is applied without great yield penalty. The maximum WUE (1.03 kg m^{-3}) occurred at a CWSI of 0.60. Overall, irrigation reduction can be conducted according to the conditions of each region.

Morales-Santos and Nolz (2023) assessed water stress indices based on canopy temperature for irrigated and rainfed soybeans in subhumid conditions, and their results indicated that the CWSI effectively reflected the different water conditions of the plant. Our findings suggest that the CWSI can serve as a basis for implementing a specific irrigation strategy in soybean cultivation. Algorithms based on Tc obtained through infrared sensors can be employed, especially in arid regions, to implement a deficit irrigation strategy that does not significantly compromise GY and enhance WUE. Fur-

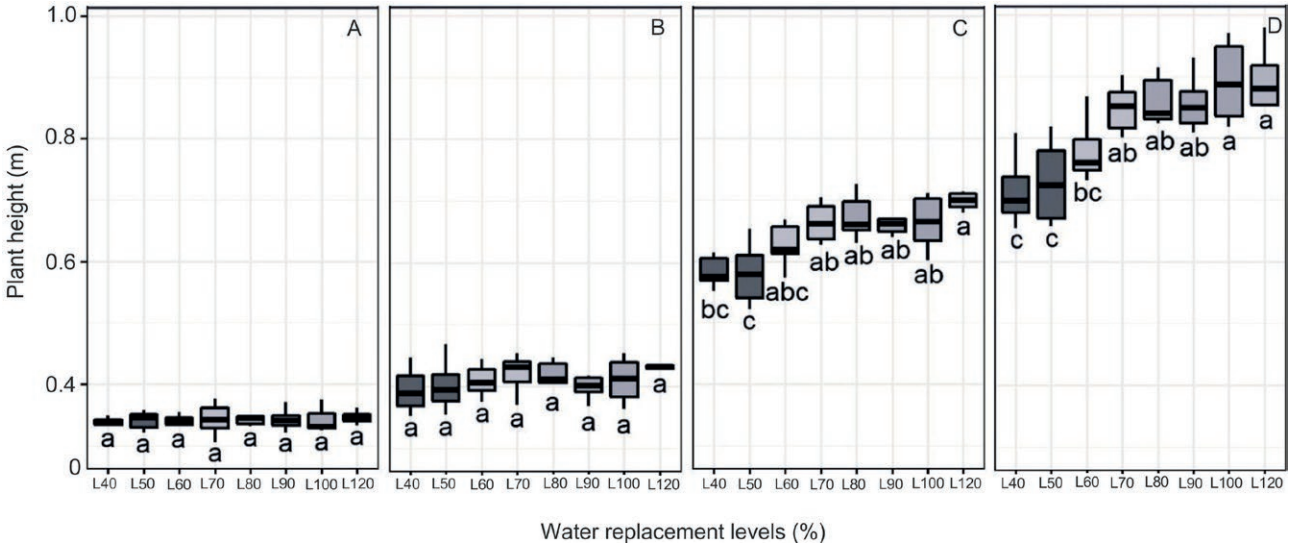

Figure 5. Growth dynamics of plant height at 20 days after sowing (DAS) (**A**), 40 DAS (**B**), 60 DAS (**C**) and 80 DAS (**D**). Different lowercase letters indicate significant differences at 5% probability according to the Tukey test. The box represents the interquartile range (IQR), whiskers represent the range of data, and the median is depicted by a horizontal line within the box.

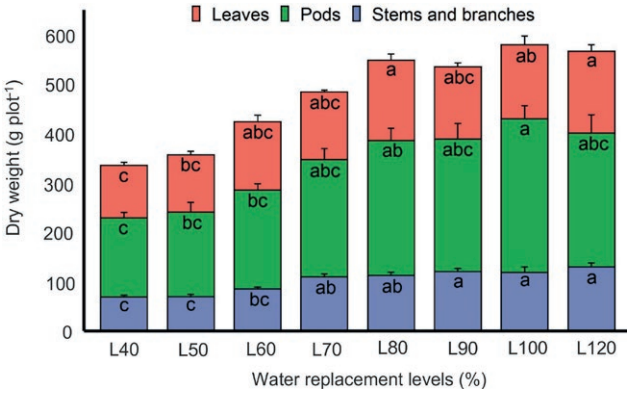

Figure 6. Average biomass allocation values of eight irrigation replacement levels. Different lowercase letters indicate significant differences at 5% probability according to the Tukey test. Bars indicate standard error of the mean.

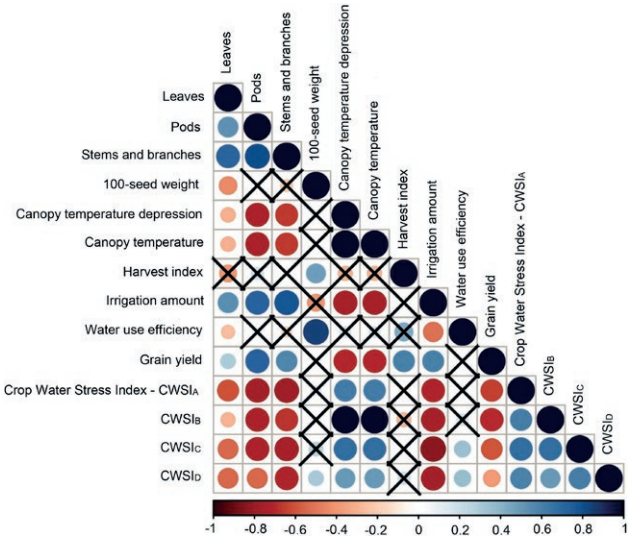

Figure 7. Relationships among studied traits. The Pearson correlation coefficients < 0.5 were marked by an "x", whereas positive correlations are in blue and negative correlations are in red.

thermore, these relationships could be applied in humid regions, where climate change impacts agricultural production by increasing crop water consumption (Singh et al., 2021). Overall, deficit irrigation managed through the use of CWSI may become a viable strategy in different environments as mentioned by Jamshidi et al. (2021).

4. CONCLUSIONS

This study reveals that the implementation of long-duration deficit irrigation strategies can maintain water use efficiency (WUE) in soybean crops at a level comparable to that of the full irrigated treatment, even under a water replacement level of 40% of required irrigation depth, which also demonstrated the highest WUE. In contrast, under the water replacement level of 120% of required irrigation depth, WUE was lower than in the other deficit irrigation treatments (from L100 to L40). These results indicate that the adoption of deficit irriga-

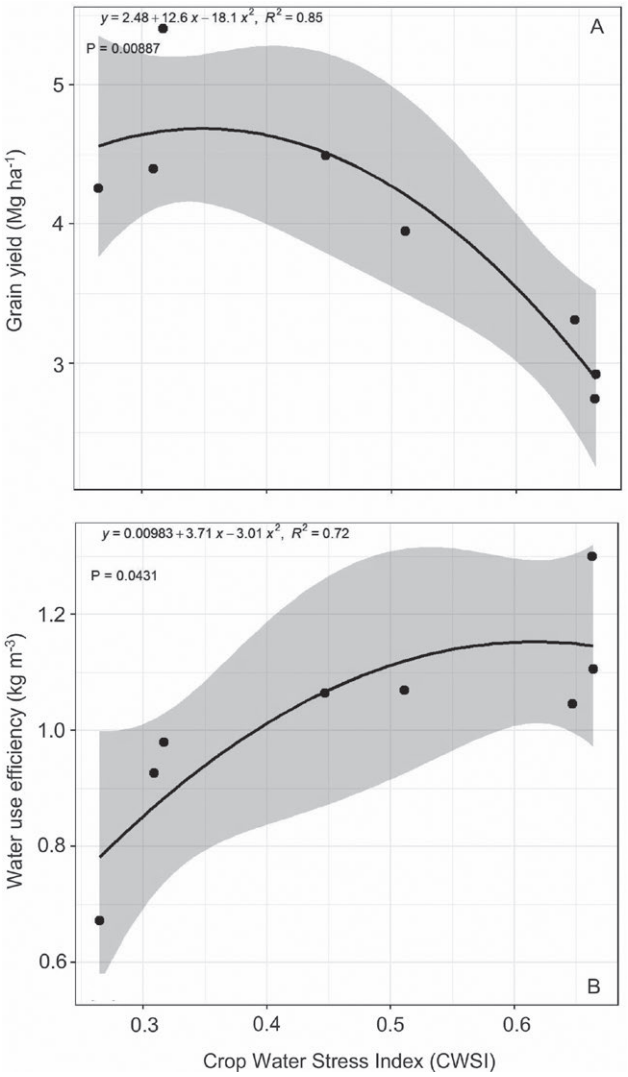

Figure 8. Relationships between (**A**) Crop water stress index (CWSI) and soybean productivity (GY) and (**B**) Crop water stress index (CWSI) and water use efficiency (WUE). The gray area indicates the 95% confidence interval.

tion strategies can lead to more sustainable and efficient water management practices in soybean production, especially in regions facing water scarcity.

The dynamics of the Crop Water Stress Index (CWSI) indicate that it can be utilized for irrigation scheduling owing to its good second-degree polynomial relationship with soybean yield and WUE. Based on the availability of water, farmers may employ distinct irrigation strategies to optimize yield or water-use efficiency, using average CWSI values as a threshold value to start irrigation.

ACKNOWLEDGEMENTS

The authors would like to thank the Brazilian Research Council - (Conselho Nacional de Desenvolvimento Científico e Tecnológico - CNPq), process number 145060/2017-9.

REFERENCES

Amani, I., Fischer, R.A., Reynolds, M.P. 1996. Canopy Temperature Depression Association with Yield of Irrigated Spring Wheat Cultivars in a Hot Climate. Journal of Agronomy and Crop Science: 176, 119–129. https://doi.org/10.1111/j.1439-037X.1996.tb00454.x

Anda, A., Simon, B., Soós, G., Kucserka, T. 2019. Crop-water relation and production of two soybean varieties under different water supplies. Theoretical and Applied Climatology: 137, 1515–1528. https://doi.org/10.1007/s00704-018-2660-9

Anda, A., Soós, G., Menyhárt, L., Kucserka, T., Simon, B. 2020. Yield features of two soybean varieties under different water supplies and field conditions. Field Crops Research: 245, 107673. https://doi.org/10.1016/J.FCR.2019.107673

Banerjee, K., Krishnan, P., Das, B. 2020. Thermal imaging and multivariate techniques for characterizing and screening wheat genotypes under water stress condition. Ecological Indicators 119: 106829. https://doi.org/10.1016/j.ecolind.2020.106829

Battisti, R., Sentelhas, P.C., Pascoalino, J.A.L., Sako, H., de Sá Dantas, J.P., Moraes, M.F. 2018. Soybean yield gap in the areas of yield contest in Brazil. International Journal of Plant Production: 12, 159–168. https://doi.org/10.1007/s42106-018-0016-0

Battisti, R., Sentelhas, P.C. 2019. Characterizing Brazilian soybean-growing regions by water deficit patterns. Field Crops Research: 240, 95–105. https://doi.org/10.1016/J.FCR.2019.06.007

Bian, J., Zhang, Z., Chen, J., Chen, H., Cui, C., Li, X., Chen, S., Fu, Q. 2019. Simplified evaluation of cotton water stress using high resolution unmanned aerial vehicle thermal imagery. Remote Sensing: 11, 267–284. https://doi.org/10.3390/rs11030267

Biju, S., Fuentes, S., Gupta, D. 2018. The use of infrared thermal imaging as a non-destructive screening tool for identifying drought-tolerant lentil genotypes. Plant Physiology and Biochemistry: 127, 11–24. https://doi.org/10.1016/j.plaphy.2018.03.005

Blum, A. 2009. Effective use of water (EUW) and not water-use efficiency (WUE) is the target of crop

yield improvement under drought stress. Field Crops Research: 112, 119–123. https://doi.org/10.1016/J.FCR.2009.03.009

Candogan, B.N., Sincik, M., Buyukcangaz, H., Demirtas, C., Goksoy, A.T., Yazgan, S. 2013. Yield, quality and crop water stress index relationships for deficit-irrigated soybean [*Glycine max* (L.) Merr.] in sub-humid climatic conditions. Agricultural Water Management 118, 113–121. https://doi.org/10.1016/j.agwat.2012.11.021

Conab, Companhia Nacional de Abastecimento. 2023. Acompanhamento da safra brasileira: grãos. Brasília: CONAB. Available in: <www.conab.gov.br>. Accessed on: March 1, 2023.

Costa, J.O., Coelho, R.D., Barros, T.H.S., Fraga Júnior, E.F., Fernandes, A.L.T. 2020. Canopy thermal response to water deficit of coffee plants under drip irrigation. Irrigation and Drainage: 69, 472–482. https://doi.org/10.1002/IRD.2429

Costa, J.O., Coelho, R.D., Barros, T.H.S., Fraga Júnior, E.F., Fernandes, A.L.T. 2018. Physiological responses of coffee tree under different irrigation levels. Engenharia Agricola: 38, 648–656. https://doi.org/10.1590/1809-4430-Eng.Agric.v38n5p648-656/2018

Craparo, A.C.W., Steppe, K., Van Asten, P.J.A., Läderach, P., Jassogne, L.T.P., Grab, S.W. 2017. Application of thermography for monitoring stomatal conductance of Coffea arabica under different shading systems. Science of the Total Environment: 609, 755–763. https://doi.org/10.1016/j.scitotenv.2017.07.158

DeJonge, K.C., Taghvaeian, S., Trout, T.J., Comas, L.H. 2015. Comparison of canopy temperature-based water stress indices for maize. Agricultural Water Management: 156, 51–62. https://doi.org/10.1016/j.agwat.2015.03.023

Demirtaş, Ç., Yazgan, S., Candogan, B.N., Sincik, M., Büyükcangaz, H., Göksoy, A.T. 2010. Quality and yield response of soybean (*Glycine max* L. Merrill) to drought stress in sub-humid environment. African Journal of Biotechnology: 9, 6873–6881. https://doi.org/10.4314/ajb.v9i41

Dogan, E., Kirnak, H., Copur, O. 2007. Effect of seasonal water stress on soybean and site specific evaluation of CROPGRO-Soybean model under semi-arid climatic conditions. Agricultural Water Management: 90, 56–62. https://doi.org/10.1016/j.agwat.2007.02.003

Dong, S., Jiang, Y., Dong, Y., Wang, L., Wang, W., Ma, Z., Yan, C., Ma, C., Liu, L. 2019. A study on soybean responses to drought stress and rehydration. Saudi Journal of Biological Sciences: 26, 2006–2017. https://doi.org/10.1016/j.sjbs.2019.08.005

Fernandes, R.D.M., de Melo, D.M., Elli, E.F., Battisti, R. 2022. Climate change impacts on rainfed and irrigated soybean yield in Brazil's new agricultural frontier. Theoretical and Applied Climatology: 147, 803-816. https://doi.org/10.1007/s00704-021-03865-w

Flexas, J., Medrano, H. 2002. Drought-inhibition of photosynthesis in C3 plants: stomatal and non-stomatal limitations revisited. Annals of Botany: 89, 183–189. https://doi.org/10.1093/aob/mcf027

França, A.C.F., Coelho, R.D., da Silva Gundim, A., de Oliveira Costa, J., Quiloango-Chimarro, C.A. 2024. Effects of different irrigation scheduling methods on physiology, yield, and irrigation water productivity of soybean varieties. Agricultural Water Management: 293, 108709. https://doi.org/10.1016/j.agwat.2024.108709

Frederick, J.R., Woolley, J.T., Hesketh, J.D., Peters, D.B. 1991. Seed yield and agronomic traits of old and modern soybean cultivars under irrigation and soil water-deficit. Field Crops Research: 27, 71–82. https://doi.org/10.1016/0378-4290(91)90023-O

Gajić, B., Kresović, B., Tapanarova, A., Životić, L., Todorović, M. 2018. Effect of irrigation regime on yield, harvest index and water productivity of soybean grown under different precipitation conditions in a temperate environment. Agricultural Water Management: 210, 224–231. https://doi.org/10.1016/J.AGWAT.2018.08.002

Gava, R., Frizzone, J.A., Snyder, R.L., de Almeida, B.M., de Freitas, P.S.L., Rezende, R. 2016. Strategies of deficit water management in irrigation of soybean crop. Revista Brasileira de Engenharia de Biossistemas: 10, 305–315. https://doi.org/10.18011/bioeng-2016v10n3p305-315

Geerts, S., Raes, D. 2009. Deficit irrigation as an on-farm strategy to maximize crop water productivity in dry areas. Agricultural Water Management: 96, 1275–1284. https://doi.org/10.1016/J.AGWAT.2009.04.009

Irmak, S., Specht, J.E., Odhiambo, L.O., Rees, J.M., Cassman, K.G. 2014. Soybean yield, evapotranspiration, water productivity, and soil water extraction response to subsurface drip irrigation and fertigation. Transactions of the ASABE: 57, 729–748. https://doi.org/10.13031/trans.57.10085

Kang, J., Hao, X., Zhou, H., Ding, R. 2021. An integrated strategy for improving water use efficiency by understanding physiological mechanisms of crops responding to water deficit: Present and prospect. Agricultural Water Management: 255, 107008. https://doi.org/10.1016/j.agwat.2021.107008

Khorsandi, A., Hemmat, A., Mireei, S.A., Amirfattahi, R., Ehsanzadeh, P. 2018. Plant temperature-based indices using infrared thermography for detecting water status in sesame under greenhouse conditions. Agricul-

tural Water Management: 204, 222–233. https://doi.org/10.1016/j.agwat.2018.04.012

Khorsand, A., Rezaverdinejad, V., Asgarzadeh, H., Majnooni-Heris, A., Rahimi, A., Besharat, S., Sadraddini, A.A. 2021. Linking plant and soil indices for water stress management in black gram. Scientific Reports: 11, 1–19. https://doi.org/10.1038/s41598-020-79516-3

Kirnak, H., Irik, H.A., Unlukara, A. 2019. Potential use of crop water stress index (CWSI) in irrigation scheduling of drip-irrigated seed pumpkin plants with different irrigation levels. Scientia Horticulturae: 256, 108608. https://doi.org/10.1016/j.scienta.2019.108608

Kocar, M.M., Josipović, M., Sudarić, A., Plavšić, H., Beraković, I., Atilgan, A., Marković, M. 2022. Environment-and genotype-dependent irrigation effect on soybean grain yield and grain quality. Applied Sciences: 13, 111. https://doi.org/10.3390/app13010111

Kullberg, E.G., DeJonge, K.C., Chávez, J.L. 2017. Evaluation of thermal remote sensing indices to estimate crop evapotranspiration coefficients. Agricultural Water Management: 179, 64–73. https://doi.org/10.1016/j.agwat.2016.07.007

Jackson, R.D., Kustas, W.P., Choudhury, B.J. 1988. A reexamination of the crop water stress index. Irrigation Science: 9, 309–317. https://doi.org/10.1007/BF00296705

Jamshidi, S., Zand-Parsa, S., Niyogi, D. 2021. Assessing crop water stress index of citrus using in-situ measurements, landsat, and sentinel-2 data. International Journal of Remote Sensing: 42, 1893-1916. https://doi.org/10.1080/01431161.2020.1846224

Li, Q., Chen, Y., Sun, S., Zhu, M., Xue, J., Gao, Z., Tang, Y. 2022. Research on crop irrigation schedules under deficit irrigation—a meta-analysis. Water Resources Management: 36, 4799-4817. https://doi.org/10.1007/s11269-022-03278-y

Meron, M., Sprintsin, M., Tsipris, J., Alchanatis, V., Cohen, Y. 2013. Foliage temperature extraction from thermal imagery for crop water stress determination. Precision Agriculture: 14, 467–477. https://doi.org/10.1007/s11119-013-9310-0

Mekonnen, M., Hoekstra, A.Y., Neale, C.M.U., Ray, C., Yang, H.S. 2020. Water productivity benchmarks: The case of maize and soybean in Nebraska. Agricultural Water Management: 234, 2–10. https://doi.org/10.1016/j.agwat.2020.106122

Morales-Santos, A., Nolz, R. 2023. Assessment of canopy temperature-based water stress indices for irrigated and rainfed soybeans under subhumid conditions. Agricultural Water Management: 279, 108214. https://doi.org/10.1016/j.agwat.2023.108214

Petrie, P.R., Wang, Y., Liu, S., Lam, S., Whitty, M.A., Skewes, M.A. 2019. The accuracy and utility of a low cost thermal camera and smartphone-based system to assess grapevine water status. Biosystems Engineering 179, 126–139. https://doi.org/10.1016/J.BIOSYSTEMSENG.2019.01.002

Quiloango-Chimarro, C.A., Coelho, R.D., Heinemann, A.B., Arrieta, R.G., da Silva Gundim, A., França, A.C.F. 2022. Physiology, yield, and water use efficiency of drip-irrigated upland rice cultivars subjected to water stress at and after flowering. Experimental Agriculture: 58. https://doi.org/10.1017/S0014479722000205

Ohashi, Y., Nakayama, N., Saneoka, H., Mohapatra, P.K., Fujita, K. 2009. Differences in the responses of stem diameter and pod thickness to drought stress during the grain filling stage in soybean plants. Acta Physiologiae Plantarum: 31, 271–277. https://doi.org/10.1007/s11738-008-0229-4

Rosadi, R.A.B., Afandi, S.M., Ito, K., Adomako, J.T. 2005. Critical water content and water stress coefficient of soybean (*Glycine max* [L.] Merr.) under deficit irrigation. Paddy and Water Environment: 3, 219–223. https://doi.org/10.1007/s10333-005-0017-3

Rosales-Serna, R., Kohashi-Shibata, J., Acosta-Gallegos, J.A., Trejo-López, C., Ortiz-Cereceres, J., Kelly, J.D. 2004. Biomass distribution, maturity acceleration and yield in drought-stressed common bean cultivars. Field Crops Research: 85, 203–211. https://doi.org/10.1016/S0378-4290(03)00161-8

Sentelhas, P.C., Battisti, R., Câmara, G.M.S., Farias, J.R.B., Hampf, A.C., Nendel, C. 2015. The soybean yield gap in Brazil - Magnitude, causes and possible solutions for sustainable production. The Journal of Agricultural Science: 153, 1394–1411. https://doi.org/10.1017/S0021859615000313

Setiyono, T.D., Weiss, A., Specht, J., Bastidas, A.M., Cassman, K.G., Dobermann, A. 2007. Understanding and modeling the effect of temperature and daylength on soybean phenology under high-yield conditions. Field Crops Research: 100, 257–271. https://doi.org/10.1016/j.fcr.2006.07.011

Silva, V.P.R., Silva, R.A., Maciel, G.F., Braga, C.C., Silva Júnior, J.L.C., Souza, E.P., Almeida, R.S.R., Silva, M.T., Holanda, R.M. 2017. Calibration and validation of the AquaCrop model for the soybean crop grown under different levels of irrigation in the Motopiba region, Brazil. Ciência Rural: 48, 1–8. https://doi.org/10.1590/0103-8478cr20161118

Singh, A. 2014. Conjunctive use of water resources for sustainable irrigated agriculture. Journal of Hydrology: 519, 1688–1697. https://doi.org/10.1016/j.jhydrol.2014.09.049

Singh, J., Ge, Y., Heeren, D.M., Walter-Shea, E., Neale, C.M.U., Irmak, S., Woldt, W.E., Bai, G., Bhatti, S., Maguire, M.S. 2021. Inter-relationships between water depletion and temperature differential in row crop canopies in a sub-humid climate. Agricultural Water Management: 256, 107061. https://doi.org/10.1016/j.agwat.2021.107061

Vale, R.L., Netto, A.M., Xavier, B.T.L., Barreto, M.L.P., Silva, J.P.S. 2019. Assessment of the gray water footprint of the pesticide mixture in a soil cultivated with sugarcane in the northern area of the State of Pernambuco, Brazil. Journal of Cleaner Production: 234, 925–932. https://doi.org/10.1016/j.jclepro.2019.06.282

van Genuchten, M.T. 1980. A Closed-form Equation for Predicting the Hydraulic Conductivity of Unsaturated Soils. Soil Science Society of America Journal: 44, 892–898. https://doi.org/10.2136/sssaj1980.03615995004400050002x

Wijewardana, C., Reddy, K.R., Alsajri, F.A., Irby, J.T., Krutz, J., Golden, B. 2018. Quantifying soil moisture deficit effects on soybean yield and yield component distribution patterns. Irrigation Science: 36, 241–255. https://doi.org/10.1007/s00271-018-0580-1

Yang, X., Wang, B., Chen, L., Li, P., Cao, C. 2019. The different influences of drought stress at the flowering stage on rice physiological traits, grain yield, and quality. Scientific Reports: 9, 1–12. https://doi.org/10.1038/s41598-019-40161-0

Zahra, N., Hafeez, M.B., Kausar, A., Al Zeidi, M., Asekova, S., Siddique, K.H., Farooq, M. 2023. Plant photosynthetic responses under drought stress: Effects and management. Journal of Agronomy and Crop Science: 209, 651–672. https://doi.org/10.1111/jac.12652

Zia, S., Romano, G., Spreer, W., Sanchez, C., Cairns, J., Araus, J.L., Müller, J. 2013. Infrared thermal imaging as a rapid tool for identifying water-stress tolerant maize genotypes of different phenology. Journal of Agronomy and Crop Science: 199, 75–84. https://doi.org/10.1111/j.1439-037X.2012.00537.x

Italian Journal of Agrometeorology
Rivista Italiana di Agrometeorologia

Firenze University Press
www.fupress.com/ijam

OPEN ACCESS

Citation: Bartolucci, M., & Veneri, F. (2024). The phenological soil water balance: a proposed model for estimating water resources for an entire watershed using crop coefficients. *Italian Journal of Agrometeorology* (1): 17-48. doi: 10.36253/ijam-2334

Received: October 16, 2023

Accepted: June 8, 2024

Published: August 2, 2024

Data Availability Statement: All relevant data are within the paper and its Supporting Information files.

Competing Interests: The Author(s) declare(s) no conflict of interest.

ORCID:
MB: 0000-0002-1972-2228
FV: 0000-0002-4881-1609

The phenological soil water balance: a proposed model for estimating water resources for an entire watershed using crop coefficients

Michele Bartolucci[1,*], Francesco Veneri[2]

[1] *Indipendent researcher, Urbino, Italy*
[2] *Dipartimento di Scienze Pure e Applicate, Università degli Studi di Urbino Carlo Bo, Campus Scientifico "Enrico Mattei", via Ca' le Suore 2/4, 61029 - Urbino (PU), Italy*
*Corresponding author. Email: michele.bartolucci1@uniurb.it

Abstract. The aim of the research was to develop a model that would allow the application, at a watershed scale, of the hydrological soil water balance model proposed by the FAO for the dosing of irrigation water in agriculture, which uses crop coefficients (K_c) for the calculation of potential crop evapotranspiration (ET_c). To be able to assess the water resources of a territory in which there are land uses other than agricultural ones, the application of the proposed model has made it necessary to determine the crop coefficients of the latter. Since crop coefficients vary according to phenological stage, this model was termed 'phenological soil water balance'. A correction factor for precipitation and potential evapotranspiration, using an acclivity coefficient (i.e., the ratio between the actual area and the projected area), has also been proposed to obtain accurate results even in non-flat areas, which allowed us to consider the actual area of the territory instead of the projected one. The model was applied daily for 7 consecutive years (from 2013 to 2019) in the Santa Maria degli Angeli watershed (Urbino, central Italy) whose area is about 14 km^2. The calibration and validation of the model were conducted by comparing the deep percolation computed by the model with baseflow values of the Santa Maria degli Angeli stream obtained by flow measurements made at the closing section of the sample watershed. The results of the model showed that the total values of deep percolation and measured baseflow only differed by 3% in the whole period considered; thus the phenological soil water balance model can be used to accurately estimate water resources and can be applied at different time intervals (daily, monthly, annual, etc.). The structure of the model makes it suitable for application in both small and large watersheds and territories.

Keywords: water resources management, watershed deficit, soil water balance, actual evapotranspiration, deep percolation.

HIGHLIGHTS

- Water scarcity due to climate change makes it necessary to better manage water resources
- Water management requires the computation of the soil water balance of a territory

- This study implemented a daily soil water balance model based on phenological stages
- Soil water balance models generally consider crop coefficients only for agricultural lands
- This model proposes crop coefficients also for non-agricultural land use

1. INTRODUCTION

Human beings use freshwater for several purposes, for drinking and other domestic uses, irrigation, energy production, industrial processes, and so forth. Freshwater is a renewable resource but the increase in the global population, growing industrialisation, growing demand for water for irrigation, soil consumption, and the use of agrochemicals in agriculture pose serious threats to its availability and quality.

Climate change is another important factor that will influence the future availability of freshwater. For each degree Celsius of global warming, approximately 7% of the global population is projected to be exposed to a decrease of renewable water resources of at least 20% (Jimenez et al., 2014). If global mean temperatures were to increase by 1°C from the 1990s, Schewe et al. (2013) estimated that about 8% of the global population would see a severe reduction in freshwater resources; this percentage would rise to 14% with a temperature increase of 2°C and to 17% with an increase of 3°C. For these reasons, proper management of water resources is indispensable to ensure water use sustainability and maintain environmental, social, and economic welfare, which must be preceded by an accurate estimation of the water resources themselves. This can be achieved through the calculation of the soil water balance using hydrological models capable of reproducing hydrological processes with a certain accuracy based on input parameters.

The inputs used by different models are representative of the geomorphological and microclimatic characteristics of the watershed. These are precipitation, air temperature, soil properties, topography, vegetation, hydrogeology, and other physical parameters. Models can be applied in very complex and large watersheds (Gayathri et al., 2015).

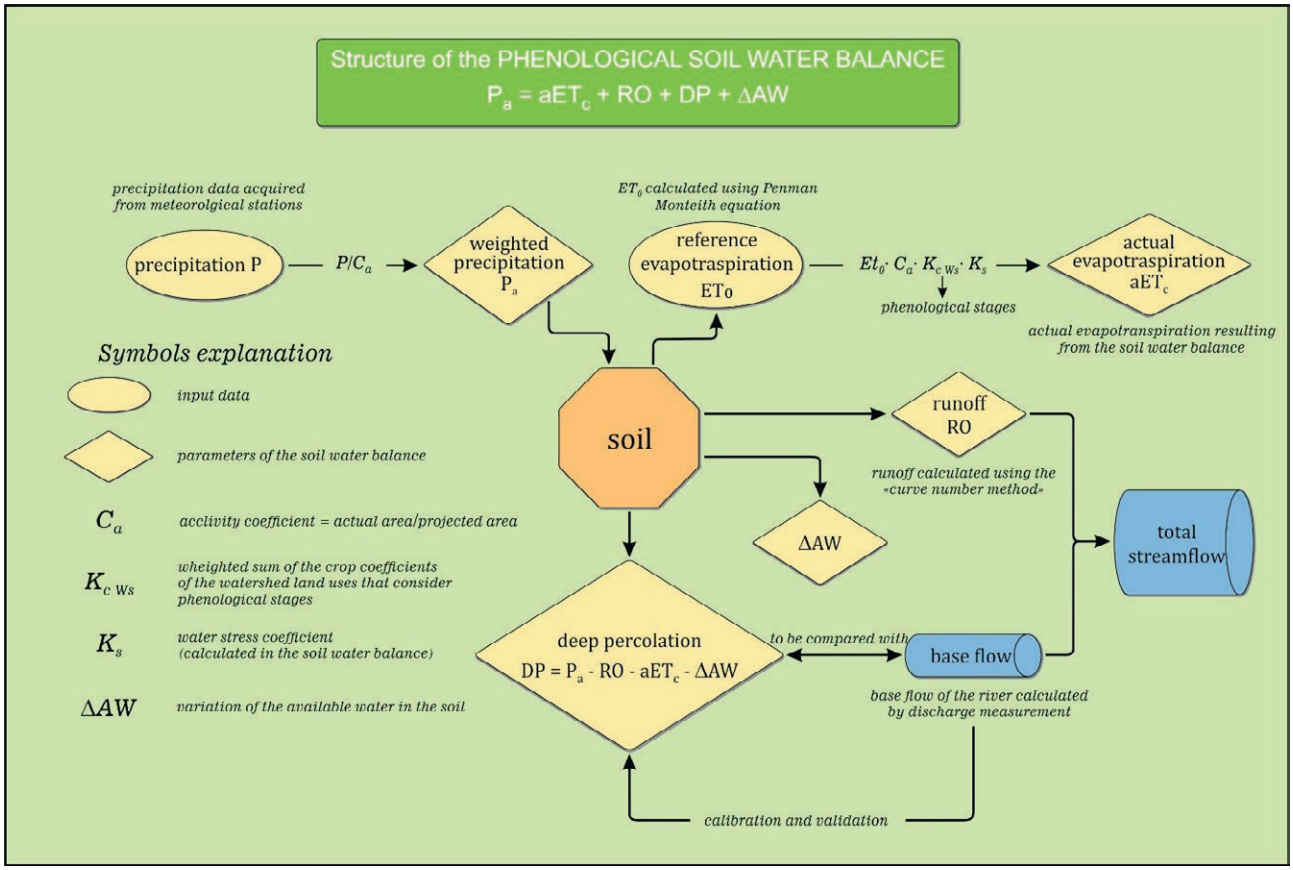

Figure 1.1. phenological soil water balance diagram.

Hydrological models can be mainly distinguished according to:

1) the structure (Gayathri et al., 2015): physically based (e.g. SWAT, Neitsch et al., 2011), empirical (e.g. the ones based on Budyko framework, Budyko, 1974), conceptual (e.g. HRU, Becker and Pfützner, 1986);
2) the spatial variability of the parameters: lumped (e.g. HEC-HMS, U.S. Army Corps of Engineers, 2013), distribuited (e.g. ATHYS, Mishra and Singh, 2003), semi-distribuited (e.g. Schumann, 1993);
3) how the output values are processed (Farmer and Vogel, 2016): deterministic, stochastic; and
4) the calculation time step: daily, monthly, annual etc.

The choice of the most suitable model to use depends on several factors such as the purpose of the study, the scale of application, the geographical region and the availability of the input parameters. Considering the spatial variability of the parameters, in theory distributed and semi-distribuited models should perform better than lumped models: this is confirmed by a study of Garavaglia et al., (2017). Anyway, this is not always the case as sometimes lumped models perform equally well or even better than distributed and semi-distributed models (Khakbaz et al., 2012, and references therein, Brirhet and Benaabidate, 2016, and reference therein). Considering calculation time step, daily time step is required for accurate recharge estimates (Dripps and Bradbury, 2007) and so is the most suitable for estimating water resources.

The purpose of our study was to develop, calibrate, apply, and validate a simple but accurate hydrological model that would allow for the accurate estimation of the water resources of a territory, specifically of a watershed.

To achieve this goal, the starting point was the United Nations Food and Agriculture Organization (FAO) Irrigation and Drainage Paper No. 56 (Allen et al., 1998; hereafter 'FAO Paper No. 56') methodology for the dosage of irrigation water for crops, which uses crop coefficients (K_c) to calculate potential crop evapotranspiration, taking phenological stages into consideration. To evaluate freshwater availability not only for cultivated areas but for a whole territory, it was necessary to extend this FAO methodology to all land uses. The result is a model that we termed 'phenological soil water balance'.

The phenological soil water balance developed in this work is:

- physically based, as it uses equations to describe the processes and calculate the values of the parameters (equations to calculate the runoff, potential evapotranspiration, etc.);
- lumped, since for each parameter it calculates a single value representative of the spatial variability of that parameter through a weighted sum (e.g. $K_{c\ Ws}$, a unique crop coefficient for the watershed used to compute potential evapotranspiration of agricultural and non-agricultural lands), or as a result of equations in the soil water balance (e.g. the actual evapotranspiration, deep percolation, etc.);
- deterministic, as it treats simulated responses as single, certain estimates of model response without considering randomness; and
- computes a daily time step.

The outline of the model structure is shown in fig. 1.1.

2. MATERIALS AND METHODS

2.1. Structure of the phenological soil water balance

The following softwares were used to calculate the phenological soil water balance:

- A spreadsheet for the calculation of the values of various parameters (potential reference evapotranspiration, climatic correction of crop coefficients, unique crop coefficient of the watershed, runoff, soil water reserve, etc.), for the processing of the results and their graphical representation.
- A Geographic Information System (GIS) for spatial data analysis and synthesis mapping.

The basic equation of the phenological soil water balance is as follows:

$$P_a = aET_c + DP + \Delta AW + RO \quad (1)$$

where:
Pa: Precipitation corrected with acclivity coefficient. The correction is indicated by the letter (a);
aET_c: actual crop EvapoTranspiration;
DP: Deep Percolation;
ΔAW: variation of soil Available Water (AW); and
RO: Runoff.

The balance equation is valid for any time interval and for the entire watershed.

For the calculation of the phenological soil water balance it is necessary to determine in advance some parameters that fall directly (e.g., P_a, RO) or indirectly (watershed unique crop coefficient $K_{c\ Ws}$, reference evapotranspiration ET_0, reference evapotranspiration corrected with the acclivity index ET_{0a}, average root depth for the calculation of soil water reserve, etc.) in the fundamental equation (eq. 1).

Deep percolation (DP) is the unknown of the balance equation, so equation 1 was solved for DP. To calibrate and validate the balance, the monthly, annual and multi-annual DP values were compared with the respective baseflow

values, measured at the closing section of the watershed since the baseflow was fed by the deep percolation water.

When comparing monthly and annual totals, the lag time between deep percolation and baseflow, due to the hypogeal path of water, must be taken into account. Deep percolation and baseflow trends were also compared in the calibration.

2.2. Flow measurement for baseflow calculation

Flow rates (or discharges) of the stream, with which to calculate the baseflow, were obtained measuring water flows weekly using surface floats (until August 2015) and a hydrometric current meter (from august 2015 to the end of 2019), according to UNI EN ISO 748 (2008). Measures were made at least waiting, after precipitation events, for the watershed runoff time (1,47 hours) before taking the measurement to prevent flow rates from including runoff or hypodermic water flow. Simultaneous measurements were sometimes made between surface floats and current meter: the regression equations found were used to revise the discharge values calculated with surface floats only. Despite this, it is possible that there are uncertainties in some flow measurements from the period up to August 2015.

2.3. Required data and step-by-step procedure

2.3.1. Required data

Table 2.1 shows the input data necessary to calculate the values of the parameters of the phenological soil water balance.

2.3.2. Step-by-step procedure

The procedure that allows the annual elaboration of the phenological soil water balance (eq. 1) consists of the following steps:

1. drafting of the land use map or updating an existing map and calculation of the related areas;
2. calculation of the value of *Curve Number* (CN) for the entire watershed;
3. calculation of daily runoff by the *curve number method;*
4. climatic correction, in the phenological stages, of the cultural coefficients (K_c) assigned to the various components of soil use;
5. calculation of the bi-weekly adjusted initial crop coefficient ($Kc_{ini\ adj}$);
6. calculation of the daily unique crop coefficient for the entire watershed ($K_{c\ Ws}$);
7. calculation of the daily reference evapotranspiration (ET_0) with the Penman–Monteith equation (Allen et al., 1998; Zotarelli et al., 2010);
8. correction for acclivity of daily ET_0 and daily P;
9. calculation of daily potential crop evapotranspiration (ET_c);
10. calculation of total available water (TAW);
11. calculation of daily rapidly available water (RAW);
12. calculation of daily water stress coefficient (K_s); and
13. calculation of deep percolation (eq. 9).

2.4. The study area and the acclivity coefficient

2.4.1. The study area

The phenological soil water balance was calibrated and validated on the little Santa Maria degli Angeli stream watershed located south of Urbino, Marche Region, central Italy (Fig. 2.1). Considering the IPCC climate classification (IPCC, 2006) the territory belongs to the 'warm temperate dry' climate zone.

The watershed is a hilly area with altitudes between 161 and 570 m a.s.l., (average 332 m a.s.l.), with a predominantly agricultural vocation (crops cover about 35% of the territory). It is a sub-watershed in the hydrographic left of the watershed of the Metauro River, which flows into the Adriatic Sea. The main waterstream is called Santa Maria degli Angeli and is 7.6 km long. The watershed has a projected area of 13.451 km^2. Soil water balance was calculated on a reduced portion of the watershed (Fig. 2.1) as the section on which the water discharges were determined is located about 1 km upstream of the closure of the watershed. This portion has a projected area of 13.098 km^2.

2.4.2. Projected area and Actual area: the acclivity coefficient

In the elaboration of data relative to a territory, the measure of the projected topographic surface (named as "projected area") is usually considered. In order not to overestimate, for example, the precipitation that effectively falls on a unit surface of soil, it is necessary to consider the actual surface area.[1] This can be obtained in a GIS environment through Digital Terrain Model (DTM) processing and make a correction. This correction can be performed introducing an acclivity coefficient (C_a), which is the ratio between the actual area and the projected area:

[1] For a more in-depth discussion of the meaning and application of the concepts "projected area" and "actual area" see supplementary material 1

Table 2.1. Input data for phenological soil water balance.

Input data	Application of input data	Source of data for case study
Daily precipitation	Soil water balance, runoff	Weather Observatory "A. Serpieri" of Urbino - meteorological stations of: Urbino, Scientific Campus "E. Mattei, Fermignano (Fig. 2.1). Civil Protection of the Marche Region
Minimum and maximum temperature, minimum and maximum relative humidity, pressure, wind speed, solar radiation (daily)	Reference evapotranspiration ET_0	Weather Observatory "A. Serpieri" of Urbino - meteorological stations of: Urbino, Scientific Campus "E. Mattei, Fermignano (Fig. 2.1). Civil Protection of the Marche Region
Base cartography	Digital Terrain Model (DTM) and Triangulated Irregular Network (TIN)	Marche Region, CTR 1:10,000 - sections 279080, 279120, 280050, 280090 https://www.regione.marche.it/Regione-Utile/Paesaggio-Territorio-Urbanistica
Geology and covers of the watershed	Soil groups for CN calculation	Geological map of Italy 1:50,000, Sheet 279 "Urbino", Sheet 280 "Fossombrone" https://www.isprambiente.gov.it/Media/carg/marche.html
	Spatialisation of the soil water reserve	PAI Marche 1:10,000 https://www.regione.marche.it/Regione-Utile/Paesaggio-Territorio-Urbanistica
	Map of infiltration/runoff propensity	Taurino (2004) Gori (2004)
Crop coefficients (K_c) of soil uses and duration of phenological stages*	Watershed unique crop coefficient ($K_{c\ Ws}$)	FAO Paper No. 56 (Allen et al., 1998) WUCOLS IV (Costello and Jones, 2014) Direct observations (phenological stages)
Depth and texture of soil	Computation of the soil water reserve	Soil profile "Mecciano" dug south of Urbino (AA.VV, 2006)
Land use	CN computation	A.G.E.A. (*AGenzia per le Erogazioni in Agricoltura*, i.e. Italian Agricultural Payments Agency) aerial orthophotos (2013, 2016)
	Attribution of phenological stages and K_c for the compution of the Watershed unique crop coefficient ($K_{c\ Ws}$)	Google Earth Pro images
	Map of infiltration/runoff propensity	

*See tab. 2.3 for values of Kc and duration of phenological stages.

$$C_a = \frac{aA}{pA} \quad (2)$$

where:
aA: actual Area; and
pA: projected Area.

The coefficient of acclivity is a function of the average slope of the watershed: the greater the average slope, the greater the coefficient of acclivity. In the considered portion of the watershed, with a projected area of 13.098 km^2 and an actual area of 13.979 km^2, the C_a is equal to 1.067. The precipitation data are corrected by multiplying them by $\frac{1}{C_a}$.

$$P_a = P \cdot \frac{1}{C_a} \quad (3)$$

where:
P: precipitation; and
P_a: precipitation corrected for acclivity.

2.5. Calculation of the potential crop evapotranspiration of the watershed (ET_c) through the watershed unique crop coefficient $K_{c\ Ws}$

2.5.1. The reference evapotranspiration corrected for acclivity (ET_{0a})

Evapotranspiration (ET) is the amount of water lost by a soil-vegetation system due to:
- evaporation from the ground and, to a lesser extent, from the surfaces of leaves, trunks, etc.; and
- transpiration of plants.

In the methodology adopted in FAO Paper No. 56 the reference evapotranspiration ET_0, calculated with

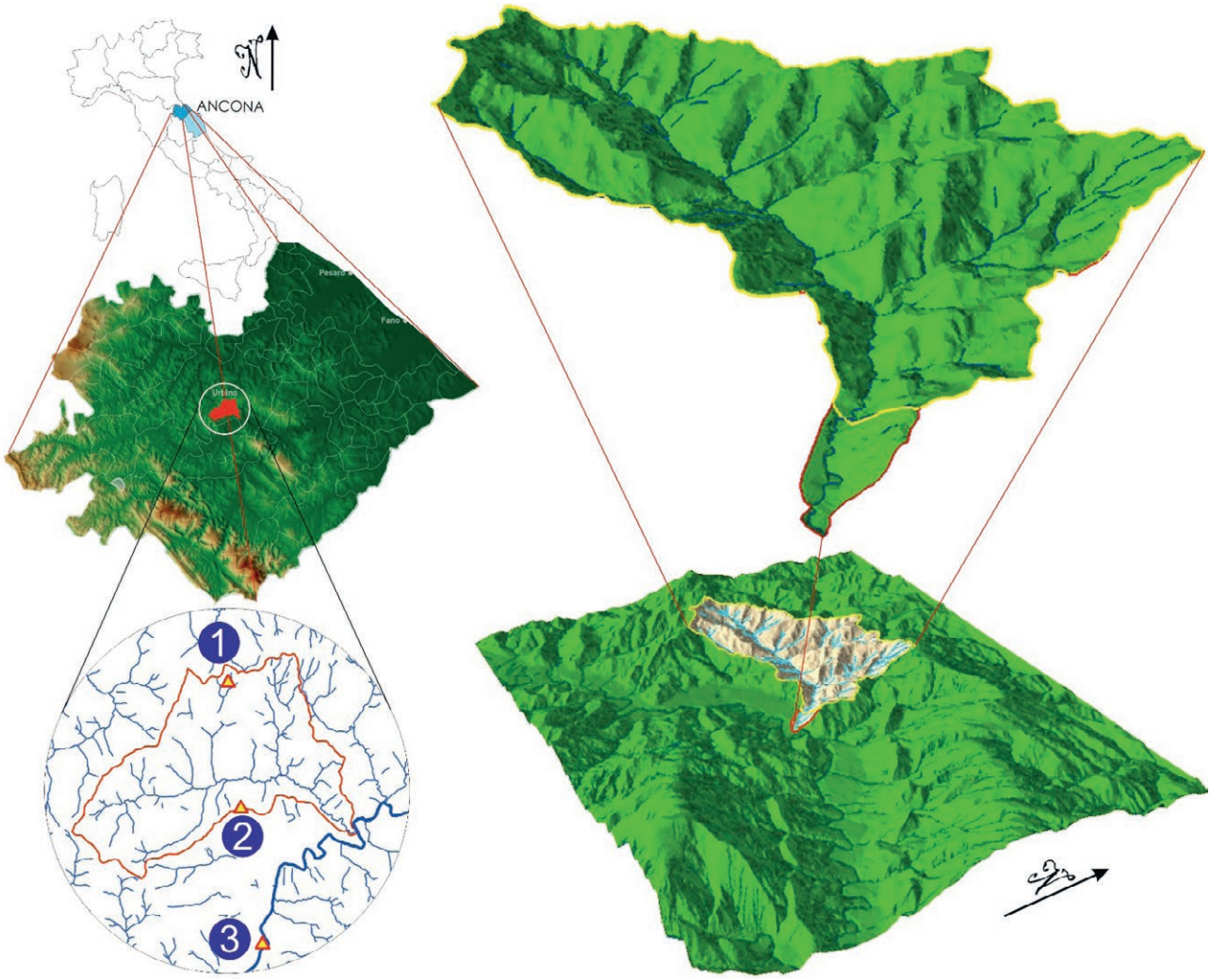

Figure 2.1. Location of the Santa Maria degli Angeli watershed study area. 1, Urbino weather station (451 m a.s.l.); 2, Scientific Campus "E. Mattei" weather station (360 m a.s.l.); 3, Fermignano weather station (235 m a.s.l.). The portion of the watershed on which the study was carried out is indicated by the yellow line.

the Penman–Monteith equation, is corrected using the crop coefficient K_c which is function of the various types of crop and their phenological stages (initial, growing, mid, late), thus obtaining crop evapotranspiration under standard conditions.

As well as for precipitation, the evapotranspiration should also be corrected for acclivity. In this case, however, the effect is the opposite: in fact, considering the projected area, this would produce an underestimation. The ET_0 therefore needs to multiplied by the acclivity coefficient (C_a).

$$ET_{0a} = ET_0 \cdot C_a \quad (4)$$

where:

ET_0: reference evapotranspiration;
ET_{0a}: reference evapotranspiration corrected for acclivity; and
C_a: acclivity coefficient.

However, to obtain an actual hydrological soil water balance, it is necessary to consider the actual evapotranspiration of the territory (aET_c). In this study, this parameter was obtained considering, besides the acclivity coefficient, a crop coefficient and a water stress coefficient, each unique to the watershed, which would consider agricultural and non-agricultural land uses.

2.5.2. Crop coefficients for agricultural and non-agricultural land use

The crop coefficient (K_c) expresses the ratio (eq. 5) between the potential evapotranspiration of a specific crop (ET_c) and the reference evapotranspiration (ET_0) calculated with the Penman–Monteith equation.

$$K_c = \frac{ET_c}{ET_0} \quad (5)$$

K_c coefficients are used for irrigation water dosing in agriculture. FAO Paper No. 56 reports the crop coefficients of different types of crops and the duration of their relevant phenological stages. Note that such values are to be considered indicative.

Through the crop coefficients the entire watershed ET_c was calculated, resulting from the values of ET_c of all the uses of the soil present in the watershed; this was necessary for the calculation of the soil water balance in the period considered.

2.5.2.1. Single crop coefficient K_c

In this study, the 'single crop coefficient' was adopted, which considers both evaporation from the soil and transpiration from plants (Allen et al., 1998).

K_c varies depending on the type of crop and its phenological stage.

For some crops in FAO Paper No. 56, the duration of the phenological stages is not indicated; in these cases, the durations were assumed based on the durations of similar crops and direct observations.

2.5.2.2. $K_{c\ ini}$ correction and calculation of $K_{c\ ini\ adj}$

In the initial stage of the vegetative cycle, for both annual crops and perennial plant species, evaporation is dominant, also considering that the beginning of the vegetative season coincides with low transpiration and with soils in high water conditions. With the advent of the growing and mid-stage, transpiration prevails, and then returns to the initial relationships at the end of the late season.

The crop coefficient for the initial stage ($K_{c\ ini}$) values, according to FAO paper n. 56, have been calculated for the duration of the initial stage by considering:

1. the time interval between precipitation (or irrigation) events;
2. evaporative power of the atmosphere; and
3. the entity of precipitation events (in relation to infiltration depth and soil texture).

The parameter thus obtained represents the value of K_c when evaporation prevails; in this study, this parameter was defined as K_c initial adjusted ($K_{c\ ini\ adj}$) and was calculated over the whole year with a two-week time interval. Two-week trends of $K_{c\ ini\ adj}$ are shown in figures 2.3, monthly trends in 2.4. It was noted that the drop in precipitation and the increase in ET_{0a} led to a sharp reduction in the $K_{c\ ini\ adj}$ in the summer months. This trend was common in all years, although with differences in terms of values such as that of December 2019 (due to low rainfall).

2.5.2.3. Land use classes of the watershed

The phenological soil water balance requires values of K_c for all uses of the soil of the watershed to calculate, for each year, a single coefficient (referred to as watershed unique crop coefficient, $K_{c\ Ws}$) that is the weighted sum of the K_c for all uses of the soil.

For this purpose, the 2013 land use classes map was created using photointerpretation of aerial orthophotos (A.G.E.A. 2013, see tab. 2.1) and satellite images. The original map is a vector type file hand-drawn and the land use classes are shown in tab. 2.2. The mapping unit was determined by the size of the spatial entities, ranging from the single building (minimal unit) to an extensive forest area (maximal unit). This map was subsequently updated for crops, as they are subject to crop rotation, in the remaining years in which the balance was drawn up (2014–2019). The update was carried out using 2016 A.G.E.A. orthophotos and satellite images, as well as field observations. Arable land (including winter wheat, sunflower, alfalfa, legumes, clover and grapes) and woodland are the most common land use classes.[2]

Land use classes are divided into single classes, consisting of a single component, and mixed classes, consisting of several components. For the latter, however, no K_c has been defined in the FAO tables. The problem was solved by breaking down these land use classes into basic components, of which the relevant K_c are given in the literature (Allen et al., 1998, Costello and Jones, 2014) or can be approximated from it. For each mixed class, the percentages of each component are indicated in table 2.2, obtained based on the photointerpretation of aerial ortophotos in the periods considered.

[2] Supplementary material 2 reports the 2013 land use map and the distribution of land use class areas within the Santa Maria degli Angeli watershed

Table 2.2. Land use classes and components of land use classes, with the percentage by which the components form the classes.

Land use classes	Components of land use classes	Percentage of components in each of the land use classes
Totally waterproof areas	Waterproof	100%
Area near built-up	Waterproof	35%
	Herbaceous species	30%
	Shrubs/small trees	15%
	Trees	20%
Arable land with wheat	Wheat	100%
Arable land with sunflower	Sunflower	100%
Arable land under fodder crops (alfalfa)	Forage (alfalfa)	100%
Arable land in legumes	Faba bean	100%
Arable land with clover	Clover	100%
Vineyard	Vineyard (vine)	100%
Set-aside land	Herbaceous species Oats	50%
	Herbaceous species Mint	50%
Uncultivated	Herbaceous species	45%
	Broom	35%
	Shrubs/small trees	10%
	Trees	10%
Sparse woods	Herbaceous species	20%
	Broom	15%
	Shrubs/small trees	15%
	Trees	50%
Woods	Herbaceous species	10%
	Broom	5%
	Shrubs/small trees	10%
	Trees	75%

2.5.2.4. Phenological stages and relative crop coefficient for all land use components

Table 2.3 shows the values of the crop coefficient for all land use components, the crop sowing period, and the start and end dates of each phenological stage, obtained by adapting the FAO Paper No. 56 values to the context of the study area or by calculating ex novo the crop coefficients of the mixed land use classes. In the notes to the table, the criteria for the attribution of the values of the K_c are shown. The crop coefficients must be corrected for average moisture and wind speed conditions, in the mid and late stages, using appropriate equations given in FAO paper No.56.

The scheme of Fig. 2.2 graphically reports the durations of the phenological stage of all the components of land use.

2.5.2.5. $K_{c\ actual}$

The daily values of K_c for each land use component (Table 2.3) were compared with the values of $K_{c\ ini\ adj}$.

K_c mainly depends on the transpiration of the plants while $K_{c\ ini\ adj}$ exclusively represents evaporation from the soil surface. In the dormancy periods, $K_{c\ ini\ adj} > K_c$, while in periods of greater vegetative development (usually the spring and summer months), $K_c > K_{c\ ini\ adj}$. To avoid underestimating the evapotranspirative demand, it is necessary to adopt the higher value of the two. This value is the $K_{c\ actual}$ and can be calculated for both single (e.g. winter wheat, Fig. 2.3) and mixed (e.g. wood) land use classes.

2.5.2.6. Watershed unique crop coefficient ($K_{c\ Ws}$) and calculation of watershed potential crop evapotranspiration (ET_c)

For each day of the year, the weighted sum of the daily values of the various $K_{c\ actual}$ of the single and mixed land use classes was calculated. In this way, a single value for the entire watershed was obtained—the unique watershed crop coefficient ($K_{c\ Ws}$)—which varies with phenological stages. The equation is as follows:

$$K_{c\,Ws} = \sum_{j=1}^{n} \frac{area_{land\ use\ j}}{area_{watershed}} \cdot K_{c\ actual\ land\ use\ j} \quad (6)$$

where:
$K_{c\ Ws}$: daily unique watershed crop coefficient;
area land use j: total area of a given land use class in the year under consideration. The values of j, from 1 to n, refer to each of the various classes identified in the watershed; and
$K_{c\ actual\ land\ use\ j}$: daily $K_{c\ actual}$ of a given land use class (see par. 2.5.2.5) based on its phenological stage. The values of j, from 1 to n, refer to each of the various classes identified in the watershed.

The value of $K_{c\ Ws}$, therefore, indicates how much the maximum daily evapotranspirative demand of the entire watershed (and not of a single crop or component or class) differs from that of reference ET_{0a}.

Figure 2.4 a and b show the monthly performance of the $K_{c\ Ws}$ in the last 2 years of the water balance. The constant value (equal to 1) of the reference coefficient ($K_{c\ ref}$), which is the value of the coefficient of the reference crop (a grass meadow/fescue maintained in optimal water conditions), is also reported. The values of $K_{c\ ini\ adj}$ and the weighted sum of the watershed land use coefficients (K_c) are also given as a comparison. It should be

Table 2.3. Components of the land use classes and K_c values adopted for each of the phenological stages. The dates of the beginning, end and duration of the phenological stages, the duration of the entire vegetative cycle, the FAO region to which the values refer (from FAO Paper No. 56, modified) are also reported. Impermeable soil: $K_c = 0$. Values of crop coefficients, in the mid and late stage, were corrected for relative humidity and wind speed as indicated by FAO Paper No. 56.

Component		Stage					Duration of vegetative cycle (days)	FAO Region FAO sowing date *Local sowing date*
		Initial	Growing[1]	Mid	Late[2]	Non vegetative stage[3]		
Winter wheat	Number of days	30	140	40	30	125	240	Mediterranean November *15 November*
	Period	15nov-14dec	15dec-03may	04may-12jun	13jun-12jul	13jul-14nov		
	K_c value	0.7	0.7→1.15	1.15	1.15→0.25	$K_{c\ ini\ adj}$		
Sunflower	Number of days	25	35	45	25	235	130	Medit./Calif. April/May *01 May*
	Period	01may-25may	26may-29jun	30jun-13aug	14aug-07sept	08sept-30apr		
	K_c value	0.35	0.35→1.05	1.05	1.05→0.35	$K_{c\ ini\ adj}$		
Legumes (faba bean)[4]	Number of days	90	55	47	43	130	235	Europe November *01 November*
	Period	01nov-29jan	30gen-24mar	25mar-11may	12may-22jun	23jun-31oct		
	K_c value	0.5	0.5→1.15	1.15	1.15→0.35	$K_{c\ ini\ adj}$		
Clover[5]	Number of days	160	41	31	22	111	254	Not present in FAO Paper No. 56 *01 November*
	Period	01nov-09apr	10apr-20may	21may-20jun	21jun-12jul	13jul-31oct		
	K_c value	0.4	0.4→1.15	1.15	1.15→0.4	$K_{c\ ini\ adj}$		
Vineyard[6]	Number of days	30	60	40	80	155	210	Mid latitudes (wine)
	Period	01apr-30apr	01may-29jun	30jun-08aug	09aug-27oct	28oct-31mar		
	K_c value	0.3	0.3→0.7	0.7	0.7→0.45	$K_{c\ ini\ adj}$		
Alfalfa[7]	Number of days	10	20	115	5	215	150 1st year 365 (successive years)	California (USA) Jan-Apr (last -4°C) *01 apr (1st year)*
	Period	01apr-10apr	11apr-30apr	01may-23aug	24aug-28aug	29aug-30mar		
	K_c value	0.4	0.4→0.95	0.95	0.95→0.9	0.4		
Oat[8]	Number of days	40	30	40	20	235	130	Not specified
	Period	05mar-13apr	14apr-13may	14may-22jun	23jun-12jul	13jul-04mar		
	K_c value	0.35	0.35→1.15	1.15	1.15→0.25	$K_{c\ ini\ adj}$		
Mint[9]	Number of days	80	40	50	40	155	365	
	Period	01jan-21mar	22mar-30apr	01may-19jun	20jun-29jul	30jul-31dec		
	K_c value	0.6	0.6→1.15	1.15	1.15→0.6	0.6		
Shrubs[10] (sp.broom or cytisus)	Number of days	75	45	75	45	125	365	
	Period	01jan-16mar	17mar-30apr	01may-14jul	15jul-28aug	29aug-31dec		
	K_c value	0.15	0.15→0.35	0.35	0.35→0.15	0.15		
Little trees/ brushes	Number of days	90	45	130	30	70	365	
	Period	01jan-31mar	01apr-15may	16may-22sept	23sept-22oct	23oct-31dec		
	K_c value	0.50	0.50→0.90	0.90	0.90→0.65	0.65→0.5		

(Continued)

Table 2.3. (Continued).

Component		Stage						
		Initial	Growing[1]	Mid	Late[2]	Non vegetative stage[3]	Duration of vegetative cycle (days)	FAO Region FAO sowing date *Local sowing date*
Trees[11]	Number of days	90	45	130	40	60	365	
	Period	01jan-31mar	01apr-15may	16may-22sept	23sept-01nov	02nov-31dec		
	K_c value	0.5	0.5→1.2÷1.3	1.2÷1.3	1.2÷1.3→0.65	0.65→0.5		

[1] The value is proportional between $K_{c\ ini}$ and $K_{c\ mid}$ (the formula is given in FAO Paper No. 56, chapter 6, equation 66).
[2] Is the final value. During the late stage the value is proportional between $K_{c\ mid}$ and $K_{c\ end}$ (the formula is given in FAO Paper No. 56, chapter 6, equation 66).
[3] For crops with a growing cycle of less than one year, the adjusted initial coefficient $K_{c\ ini\ adj}$ is applied in the months when the crop is not present.
[4] The value of $K_{c\ end}$ was increased from 0.3 to 0.35 because at harvest the *faba bean* had not yet reached the end of the vegetative cycle for climatic reasons.
[5] FAO individual cutting period. Since the clover is collected for seed in the watershed, the value of $K_{c\ end}$ of FAO Paper No. 56 was not considered suitable, as it is a pre-cut value (1.10). It was considered more correct to attribute a K_c value of 0.4.
For the clover, FAO Paper No. 56 does not indicate the phenological stage, which have been hypothesised based on direct observations.
[6] FAO grapes, wine. The vineyard is a perennial plant but in periods when there is no vegetative cycle the soil between the rows is tilled. Consequently, in the periods of the year when there is no vegetative cycle of the vine, the initial adjusted coefficient $K_{c\ ini\ adj}$ was used.
[7] The 'averaged cutting effects' typology was adopted; that is, a single cycle that averages all the cutting cycles of the crop. After the last cut, for the dormancy period, it assumed the value of $K_{c\ ini\ adj}$.
[8] Although not cultivated in the territory of study, in the wild variant it goes to form 50% of the 'grass' component of the set-aside soils. The value of $K_{c\ ini}$ was assumed here to be 0.35 by analogy with other cereals. The duration of the phenological stage was obtained from FAO Paper No. 56 without Region specification.
[9] Multiannual plant. Even if not cultivated in the territory of study, in the wild variant it goes to form 50% of the 'grass' component of the set-aside soils. The $K_{c\ end}$ of FAO Paper No. 56 is 1.10 but it is a pre-cut value; in this study, it was assumed to be 0.6 because it considers mint as a multi-annual spontaneous grass that is not harvested. The duration of the phenological stage was obtained from direct observations and by analogy with other herbaceous species reported in FAO Paper No. 56.
[10] Includes all shrubs (smoke bush, wild blackthorn, etc., except brooms) and small trees (elder, small elms, wild cherry, etc.). For the definition of the K_c values, the values of FAO Paper No. 56 were used, using the values of the crops with characteristics most like the species of this group. The duration of the phenological stage was considered to coincide with that of the trees. For the winter dormant stage, a value of 0.5 was assumed, equal to the value of the initial stage. This value is relative to the months from January to the beginning of the vegetative stage; from the end of the 'late' stage to 31 December there is a second stage ('late 2') in which K_c drops from 0.65 to 0.5, also characteristic of the component 'wood'.
[11] The duration of the phenological stage of the component 'trees' was deduced by adapting the work of Eccel et al., 2007 , which reported the trend of K_c and LAI for an alpine deciduous forest, to the context of the Santa Maria degli Angeli watershed. Values of Kc were computed using the formulas of the FAO paper No.56, chapter 9, adapted to the context of the study area. The maximum value of K_c is variable because a parameter value needs to be calculated that accounts for evaporation based on the frequency of rain events (or wet soil) during the mid-season. The symbol ÷ in this case does not represent division but is intended to signify that the value varies between 1.2 and 1.3 depending on the parameter mentioned.

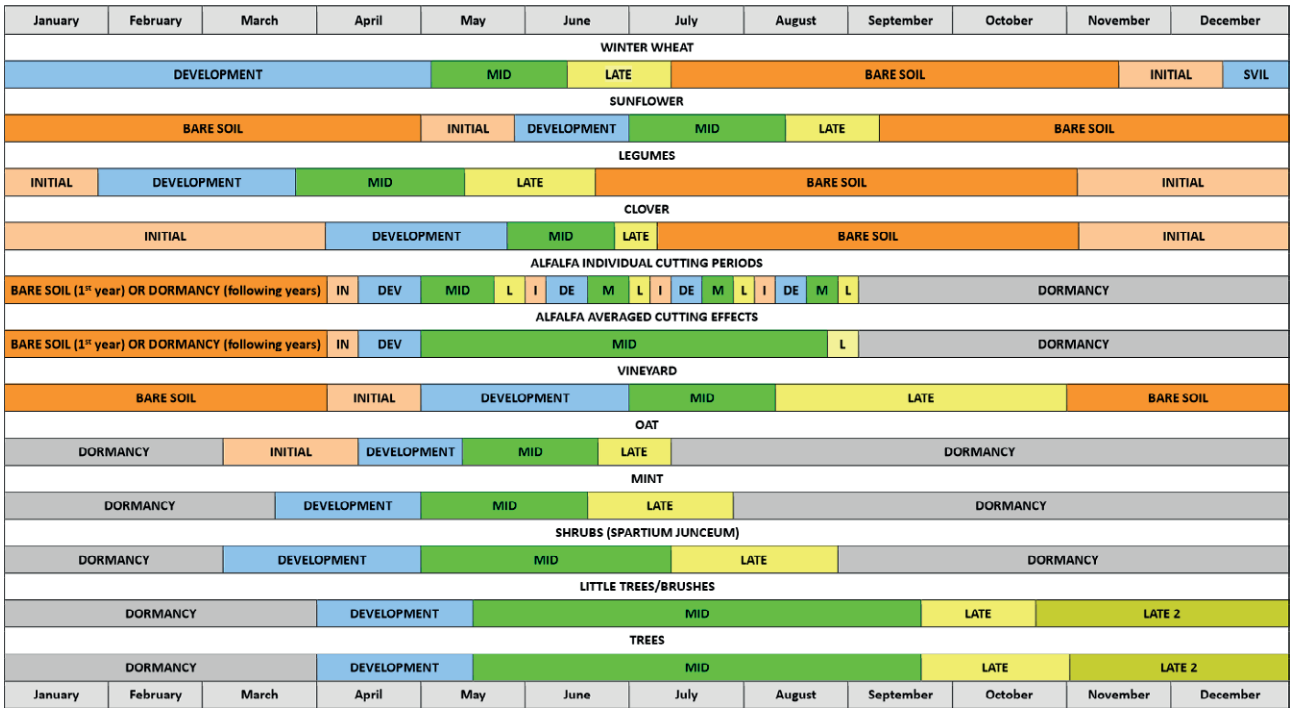

Figure 2.2. Duration of the phenological stages of the components that form the land use classes present in the Santa Maria degli Angeli watershed. The 'development' stage corresponds to the 'growing' stage in table 2.3.

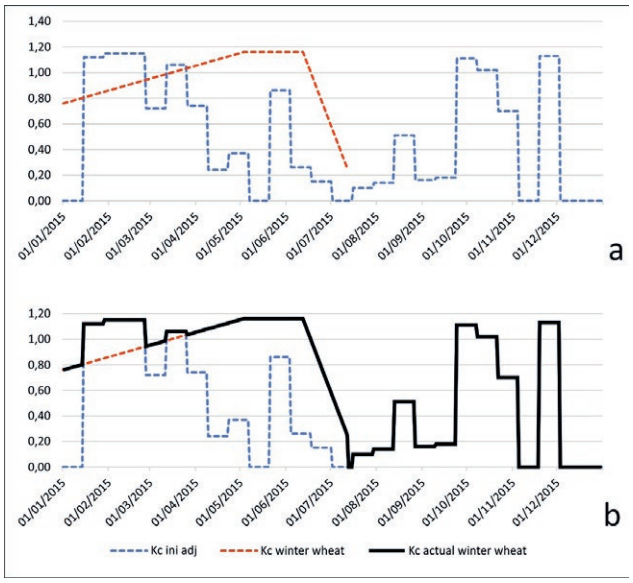

Figure 2.3. Winter wheat single land use class. a) trend of K_c and $K_{c\ ini\ adj}$ in the year 2015; b) trend of $K_{c\ actual}$ in the year 2015 obtained as the highest of the values of K_c and $K_{c\ ini\ adj}$.

noted that the parameter $K_{c\ Ws}$ assumes higher values when the value of evaporation ($K_{c\ ini\ adj}$) or transpiration (K_c) is high.

The $K_{c\ Ws}$ weights the two effects and provides a representative value of the territory from the values of the coefficients and phenological stages of all the land use classes. Although the values are different from year to year, the trends are similar. It was observed that the $K_{c\ Ws}$ almost never exceeds the $K_{c\ ref}$, so the potential evapotranspirative demand of the territory is almost always lower than the theoretical one of the reference crop.

$K_{c\ Ws}$, therefore, represents the parameter whose value is to be multiplied by the reference evapotranspiration corrected for the coefficient of acclivity (ET_{0a}) to obtain the potential crop evapotranspiration of the watershed (ET_c). The equation is as follows:

$$ET_c = ET_{0a} \cdot K_{c\ Ws} \tag{7}$$

where:
ET_c: maximum potential 'crop' evapotranspiration of the watershed (mm);
ET_{0a}: potential evapotranspiration corrected by the coefficient of acclivity (mm); and
$K_{c\ Ws}$: daily unique crop coefficient of the entire watershed.

Estimating crop evapotranspiration (ET_c) is crucial for ensuring sustainable and efficient agricultural water

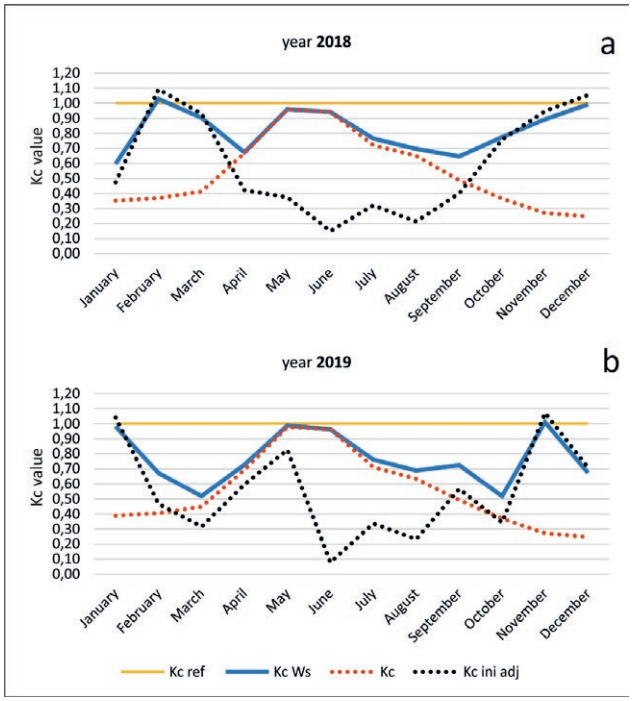

Figure 2.4. Trend of the watershed unique crop coefficient ($K_{c\ Ws}$) in the last two years of the water balance. The K_c trends obtained only from the values of Table 2.3, of the adjusted initial coefficient ($K_{c\ ini\ adj}$) and of the K_c of the reference crop ($K_{c\ ref}$) are also reported.

management (Barrera et al., 2023) and is therefore also important in water management of the whole watershed.

Finally, to obtain the actual evapotranspiration it is necessary to calculate the water stress coefficient (K_s), which is calculated inside the phenological soil water balance.

2.6. Calculation of actual evapotranspiration (aET_c)

Another parameter of the phenological soil water balance is represented by the variation of the water reserve of the soil. K_s is a coefficient denoting the state of soil water stress and is a function of total available water (TAW), rapidly available water (RAW) and soil water depletion (Dr) (Allen et al., 1998). When $K_s = 1$ there is no water stress. If $K_s < 1$ there is water stress.

These parameters were calculated based on a 'Mecciano' soil profile performed inside the watershed (AA.VV, 2006). The TAW of the 'Mecciano' soil profile was then spatially extended to consider the variability of thicknesses and soil types. This resulted in a TAW unique to the basin and used in the balance, which is the result of a weighted sum over three different conditions deriving from the crossing between land use and geology. At each of these condition a share of the TAW of the 'Mecciano' soil profile is assigned: the entire TAW value for thick soils (arable land on cover deposits), half a value for thin soils (non-arable land on rocky substrate), an intermediate value for soils of intermediate thickness (arable land on rocky substrate).

The actual evapotranspiration of the watershed of the day, aET_c, is a function of ET_c according to the coefficient of water stress K_s (Allen et al., 1998):

$$aET_c = ET_c \cdot K_s \tag{8}$$

where:
aET_c: actual watershed evapotranspiration (mm);
ET_c: potential maximum 'crop' evapotranspiration of the watershed (mm) (eq. 7); and
K_s: unique water stress coefficient for the entire watershed.

2.7. Calculation of runoff[3]

For the calculation of the daily values of the runoff parameter, which contribute to the phenological soil water balance (see eq. 1), the curve number methodology (Mockus, 1972; USDA, 2004), with its subsequent modifications (Williams et al., 2000; Williams et al., 2005; Kannan et al., 2008; Williams et al., 2012; Friuli Venezia Giulia Autonomous Region, 2018), was used.

2.8. Determination of deep percolation through soil water balance

Based on the methodology described above, the values of the parameters of the phenological soil water balance were calculated daily, excluding the deep percolation (DP) value, which remained unknown.

To derive this unknown, the equation (1) was solved as follows:

$$DP = P_a - RO - aET_c - \Delta AW \tag{9}$$

where:
DP: Deep Percolation;
P_a: daily precipitation corrected with the acclivity coefficient;
RO: daily runoff;
aET_c: daily actual crop evapotranspiration; and
ΔAW: daily variation of soil Available Water (AW).

[3] Insights into the methodology adopted, together with the calculation of runoff in significant periods of the year 2015, can be found in supplementary material 3.

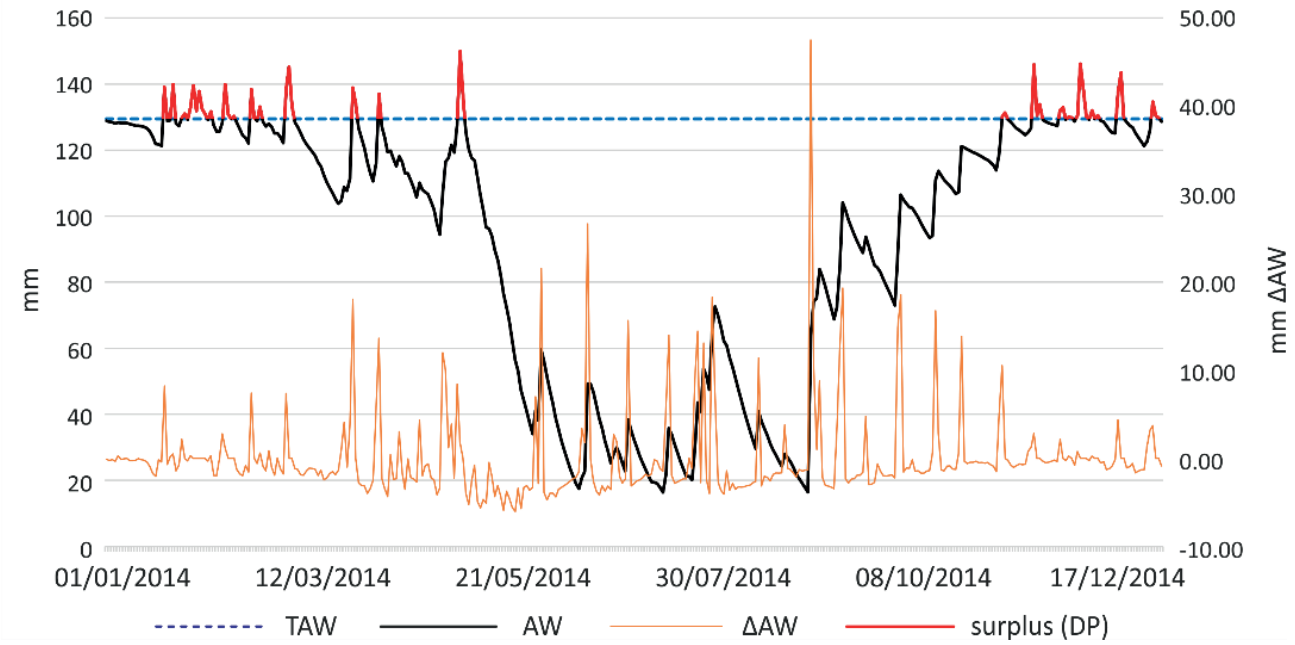

Figure 2.5. Daily trend of available water (AW), variation of available water (ΔAW) and surplus/deep percolation in the year 2014 in the soils of Santa Maria degli Angeli watershed. The total available water (TAW) value is also reported.

It should be noted that there is deep percolation only when there is surplus; that is, AW reaches the maximum value which is represented by the total available water (TAW) and then ΔAW = 0 (Fig. 2.5). The water that goes into deep percolation reaches the aquifers and hence the lower and main hydrographic network.

2.9. Calibration and validation of the model

To verify whether the model worked well, the values of deep percolation thus obtained were compared with the baseflow values deriving from flow measurements at the closing section of the watershed. The baseflow is determined by the water of the deep percolation that, after a hypogeal path, feeds the stream. The soil water balance model was calibrated in 2013 and validated in the next 3 years (2014, 2015, 2016). The last years (2017, 2018, 2019) provided further confirmation of the validity of the model.

To also make a qualitative comparison with the deep percolation, the trends in the levels of groundwater were investigated. Piezometric levels were measured in four watershed aquifers, in different hydrogeological contexts and at different depths: two shallower, and two deeper. The measurements were performed on the same dates as those of flow measurements.

Table 2.4. Values of the Pearson and KGE statistical indices for the calibration and validation period of the model.

	Pearson	Kling-Gupta Efficiency
Calibration period (2013)	0,74	0,57
Calibration + validation period (2013-2016)	0,75	0,69

Table 2.5. Totals of the baseflow and deep percolation values for the calibration and validation period of the model.

Period	Baseflow totals (mm)	Deep percolation totals (mm)	Percent change (%)
Calibration period (2013)	274	279	+2
Calibration + validation period (2013-2016)	986	877	-11

2.10. Statistical analysis on the calibration and validation of the model

The time lag between deep percolation and baseflow makes it necessary to pay attention to a statistical comparison, as deep percolation values calculated in one month may find corresponding (not equal) values one or more months later.

The sets[4] of monthly baseflow (measured/observed) and deep percolation (forecast/simulated) values for the calibration and validation period 2013-2016 were analysed using the Pearson index and KGE index (Gupta et al., 2009). The results are reported in Table 2.4.

Knoben et al. (2019) demonstrate that KGE values greater than -0.41 indicate that a model improves upon the mean flow benchmark even if the model's KGE value is negative; KGE = 1 indicates perfect agreement between observations and simulations. The values of the indices in tab. 2.4 provide a fair correlation, but as mentioned above, they are not entirely suitable for assessing the goodness of the model. Given the hydrological processes, a comparison with an index analysing multi-annual totals seems more appropriate. In Table 2.5 are the percentage changes between deep percolation and baseflow annual and multi-annual totals over the calibration and validation period.

The 11% difference, an acceptable value, between the multi-annual totals confirmed the validity of the phenological soil water balance model.

Table 3.2 in the results section shows the percent change that also considers the last years in which the balance was calculated.

3. RESULTS

Results obtained by applying phenological soil water balance, comparison with measured base flow and calculation of watershed water deficit are discussed below.

3.1. Annual values of the parameters of the phenological soil water balance

Table 3.1 gives the total annual values of deep percolation (DP) from the phenological soil water balance (eq. 9) for the seven years of the study[5].The ΔAW parameter, which indicates the changes in the amount of water available in the soil over a period of one year, had a minimal variation since the water reserve was reconstituted at the end of each year.

Table 3.1. Total annual values, expressed in mm, of the parameters of the phenological soil water balance (eq. 9), where DP = deep percolation, P_a = precipitation corrected for acclivity, RO = runoff, aET_c = actual evapotranspiration and ΔAW = variation of the available water.

$DP = P_a - RO - aET_c - \Delta AW$					
year	DP	P_a	RO	aET_c	ΔAW
2013	279.1	1022.2	144.2	599.4	-0.6
2014	245.0	1067.3	148.1	674.5	-0.3
2015	210.5	850.8	116.5	528.5	-4.7
2016	142.4	833.9	78.8	614.0	-1.3
2017	157.0	752.1	71.7	518.1	5.3
2018	251.3	857.3	74.6	537.2	-5.8
2019	113.3	803.1	60.6	625.8	3.3

3.2. Comparison of deep percolation with the measured baseflow[6]

Fig. 3.1 shows the monthly values of deep percolation, baseflow and the piezometric level of the aquifers in the 4 years of phenological soil water balance in which the calibration and validation of the model were carried out. Precipitation values are also reported.

The graph shows a correspondence between the trend of deep percolation and baseflow in both decreases and increases. However, the rise of the baseflow occurs later than the deep percolation; the observed delay time corresponds to the time needed for the hypogeous water path.

The extent of the delay depends on the characteristics of the watershed (size, geology-geomorphology, structural layout, thickness, texture and permeability of soils, slopes, land use, etc.).

The starting value of the virtual aquifer was obtained from the average of the initial levels of the four considered aquifers; its subsequent evolution was calculated based on the average of the percent changes in each aquifer.

A comparison between deep percolation and baseflow in the different years (Table 3.2) allowed for evaluation of the accuracy of the model in simulating the processes that take place in the water cycle of the territory. To annual period there is a lower correspondence between the two parameters: as previously written this is due to the delay time of the hypogeal path of the percolation water, which postpones to the first months of the following year the effect of precipitation falls in the last months of the year; in a multi-annual period the two parameters must have comparable values, otherwise the model does will not perform well. It was noted that in

[4] All monthly DP and baseflow values (2013-2019) are given in supplementary material 4

[5] An example of the application of the phenological soil water balance in significative periods of the years 2014, 2015 and 2016 is set out in supplementary material 5

[6] All monthly values of the phenological soil water balance are given in supplementary material 6

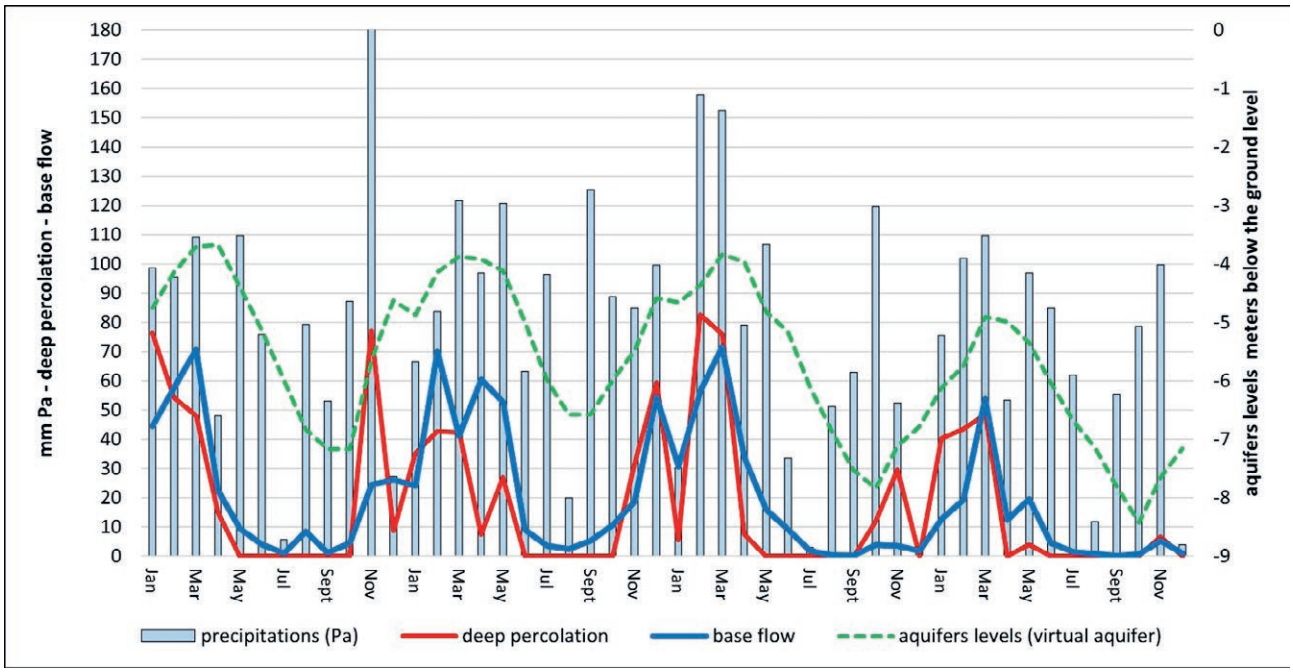

Figure 3.1. Comparison between the trends of the precipitations (P_a), deep percolation (DP), baseflow and aquifer levels (expressed through the trend of a virtual aquifer representing the trend of the levels of 4 monitored aquifers) from the years 2013 to 2016. For reasons of scale, the P_a value of november 2013 was cut (original value: 232,7 mm).

Table 3.2. Total annual values of the deep percolation derived from the phenological soil water balance model and the baseflow measured at the closing section of the watershed. Values are rounded to the nearest unit.

year	measured base flow (mm)	deep percolation (mm)	percent change (%)
2013	274	279	+2
2014	352	245	-30
2015	228	213	-7
2016	131	141	+8
2017	104	157	+51
2018	235	251	+7
2019	120	113	-6
sum	*1444*	*1400*	*-3*
mean	*206*	*200*	*-3*

some years the difference between the values could also be quite significant (in 2014 and 2017) but at a multi-annual level both the sum and the average of the values differed by a very low percentage value, signifying the good performance of the model.

The graph in Fig. 3.2 shows the average values at 10 days of runoff, deep percolation and precipitation in the period 2013–2019, useful for the estimation of the water resources of the Santa Maria degli Angeli watershed.

The mean decadal precipitation was 49 mm, resulting in a runoff of 5.4 mm (corresponding to 75970 m^3 of water) and a deep percolation of 10.9 mm (corresponding to 152995 m^3 of water).

Obviously, in the summer months there are few or no runoff and deep percolation, while the recharge of the aquifers and the rise of the baseflow (effect of the deep percolation) is maximal in the winter period.

3.3. Water deficit of the watershed

The graph in Fig. 3.3 reported the multi-annual average to 10 days time step of some parameters of the phenological soil water balance and the $K_{c\ Ws}$ throughout the study period (2013–2019).

The study allowed for quantification of the water deficit at the level of the entire watershed as the difference between ET_c and the actual evapotranspiration (aET_c), thus enabling the evaluation of the water stress during the year. Water deficit is graphically expressed by the distance between the curves representing these two parameters. The greater the distance between the two curves (indicated with a red arrow), the greater the deficit. The red arrow highlights the extent of the water deficit. The average annual value of the 2013-2019 deficit was 282 mm (about $4{\cdot}10^6$ m^3 of water).

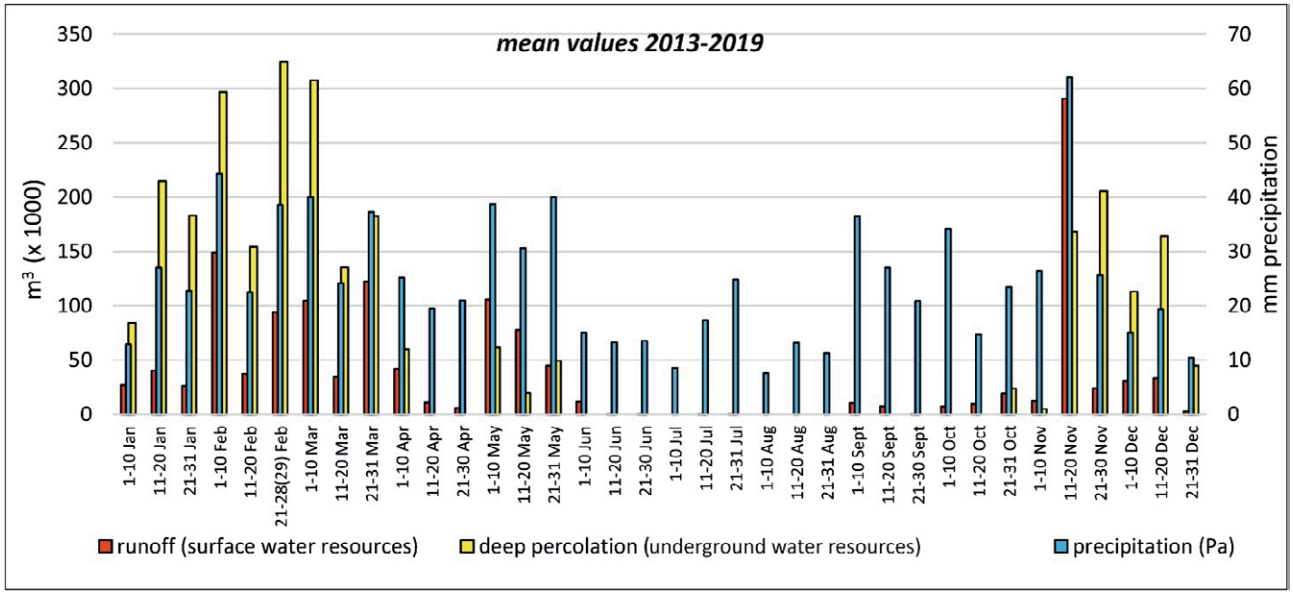

Figure 3.2. Multi-annual average to 10-day time step of the values of precipitation, runoff and deep percolation of the Santa Maria degli Angeli watershed.

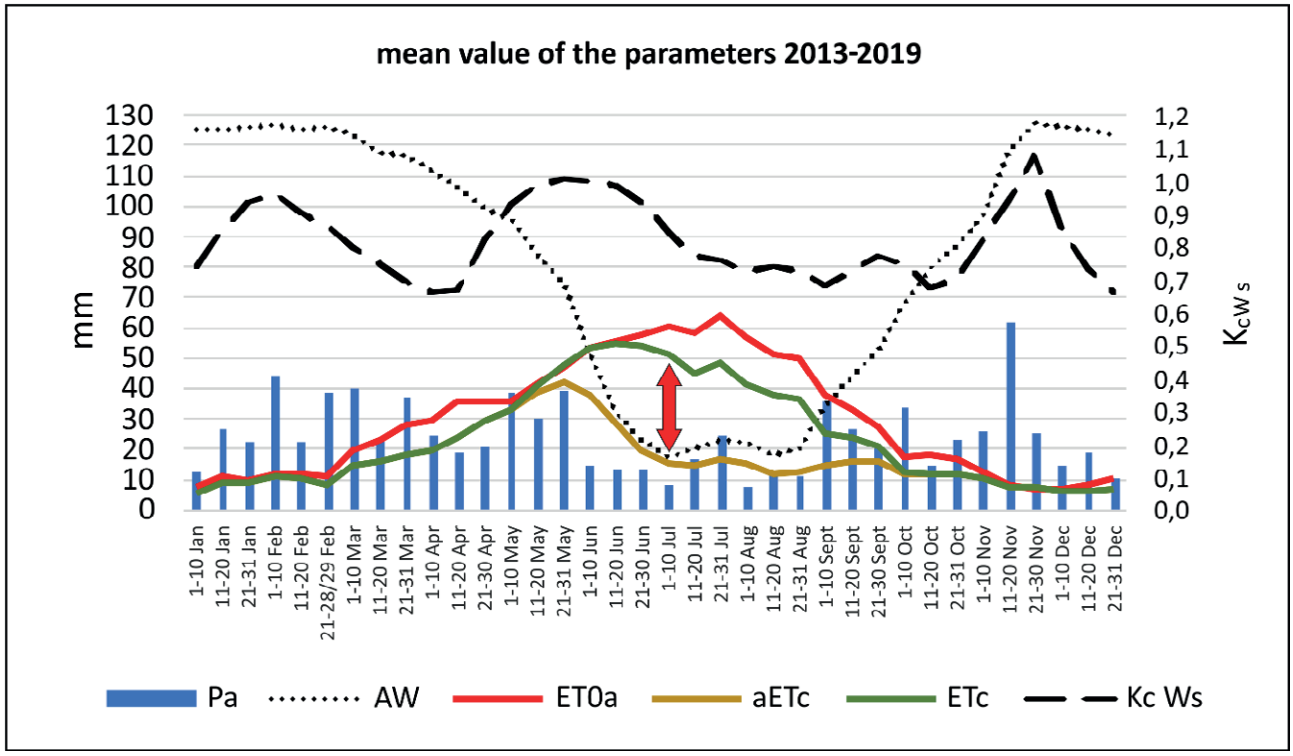

Fig. 3.3. Multi-annual mean values at 10-day time step of the parameters of the phenological soil water balance model used for the calculation of the water deficit (difference between ET_c and aET_c highlighted by the red arrow). P_a: precipitations weighted for acclivity. AW: soil water reserve. ET_{0a}: reference evapotranspiration weighted for acclivity. aET_c: actual evapotranspiration. ET_c: potential crop evapotranspiration. $K_{c\,Ws}$: unique watershed crop coefficient. All parameters are referred to the whole watershed.

During the seven years in which the phenological soil water balance was calculated, 2014 was the year with the lowest deficit (186 mm, corresponding to $2.6 \cdot 10^6$ m^3 of water while 2017 was the year with the greatest deficit (472 mm, corresponding to $6.6 \cdot 10^6$ m^3 of water;). The month for which the highest deficit value was recorded was June 2016, with a deficit of 172 mm, corresponding to $2.4 \cdot 10^6$ m^3, which almost equals the entire annual deficit of the year 2014.

4. DISCUSSION

The above results demonstrate that detailed studies of water resource management in agriculture (that use crop coefficients in the context of irrigation and applications) can also be applied at the level of the entire watershed or for an administrative entity.

The advantage of this approach that extend to whole watershed the crop coefficients methodology (and so the phenological stages of crops/plant varieties) is the accurate calculation for all land uses, through the watershed unique crop coefficient $K_{c\ Ws}$., of the parameters of maximum crop evapotranspiration (ET_c) and consequently of actual evapotranspiration (aET_c).

The latter is a key parameter in soil water balance. As a consequence of this it is possible to develop a soil water balance capable of accurately calculating deep percolation, from which the baseflow trend can be approximated, after considering the lag time between the two caused by the time taken by the water to complete its underground path. Baseflow values provides the estimate of potential water resources.

In addition, from the difference between the two evapotranspiration parameters, the deficit of the entire watershed can be calculated.

In order to achieve this type of model, the study combined the design of a theoretical hydrological model related to soil water balance with field monitoring by surveying flow rates and piezometric levels of aquifers. The monitoring of the flow rates of the main stream allowed the model to be calibrated and validated, comparing the measured baseflow values with the simulated deep percolation values.

Measures were made weekly at least waiting, after precipitation events, for the watershed runoff time before taking the measurement. This allowed baseflow to be measured excluding runoff, which was calculated by continuous CN methodology. Of course, the presence of a permanent flow measurement station would have allowed for better calibration and validation, enabling water from runoff to be monitored as well.

Another innovative aspect, and useful in achieving better performance, is the use of an acclivity coefficient to consider the actual land area when calculating the parameter values of precipitation and potential evapotranspiration, which otherwise would have been respectively overestimated or underestimated.

Given the lack of detailed data on the territory (climate, soil, etc.), we decided to create a lumped-type model of water balance of the soil, where the value of each parameter is the weighted sum of all values that the parameter assumes in the watershed. This type of model has the disadvantage of providing less information about the spatial distribution of soil water balance parameter values (especially deep percolation, the unknown calculated in the balance), information that can be useful for localised studies and applications. In any case, the aim to spatialize at least qualitatively the deep percolation values of the model was solved by creating a map of infiltration propensity, intersecting through GIS the layers of predisposing factors (supplementary material 7). In fact, infiltration is closely related to deep percolation, although the two parameters are different.

Difficulties also arose because no crop coefficients (K_c) specific to the study area were available while the model would need specific coefficients to perform better. Garofalo et al. (2011) pointed out that it is important to "calibrate" K_c for cultivars and soil and climate conditions in the growing environment, as they often differ from what is reported in FAO Paper No. 56. This can be achieved by making direct measurements of ET_c using weighing lysimeters, but this procedure is not always readily applicable, particularly for non-agricultural land uses such as uncultivated land, woods, or for orchards, vineyards, etc.

Here since direct measurements with weighing lysimeters were not possible, FAO coefficients were used, also as a basis for estimating coefficients for non-agricultural land uses. A crucial aspect of the study was indeed the determination of K_c for non-agricultural areas. FAO Paper No. 56 (chapter 9) provides equations for calculating K_c in vegetated areas. Corbari et al. (2017) used evapotranspiration measurements acquired from micrometeorological stations or through remote sensing to define the crop coefficients of vegetated natural areas, including deciduous forests, finding lower crop coefficient values than the FAO data, even though in climates other than Mediterranean. In our study the K_c values of uncultivated land and sparse and dense deciduous woods were calculated by means of a weighted sum of the K_c values of the land-use components (tab. 2.2 and 2.3), whose values are either reported in the FAO Paper or calculated from equations in the FAO Paper (which

consider local weather conditions). Given their important spatial extent in some areas, and the weight they have in the calculation of the unique watershed coefficient, the K_c of types of woods, more or less dense, should be carefully evaluated in future studies.

Another possibility for deriving crop coefficients specific to the study area is the use of the relationships between the Normalized Difference Vegetation Index (NDVI) and crop coefficients, as used by the spatially distributed SPHY model (Hunink et al., 2017). The same Authors conclude that for hydrological model applications at basin and sub-basin scale crop coefficient parameterization using satellite-based NDVI data is preferable, given the fact that sufficient long term series of NDVI data are now available for seasonal analyses at high resolution, and using literature-based crop coefficients can lead to wrong (generally under-estimated) streamflow simulations.

Considering the results, the lack of coefficient specificity and the use of FAO crop coefficients for the entire watershed does not appear to have had a significant impact on the performance of the phenological soil water balance model. Furthermore although not specific to the study area, the FAO coefficients are still reliable as demonstrated by Pereira et al. (2021), who updated the coefficients for some crop categories and found a good agreement with the K_c of FAO paper no. 56., In any case more studies should be done to evaluate these components.

The phenological soil water balance equation (eq. 9) allows calculation of the (daily, monthly, annual) unique value of deep percolation for the watershed. The most useful values of deep percolation provided by the model are not the single daily/monthly/annual totals (given the temporal discrepancy between deep percolation values and baseflow values) but the multi-annual totals or the multi-annual average value, which are really close to the true respective values of baseflow.

Future developments may improve the model by making it a distributed or semi-distributed type (for which, however, a larger amount of data would be needed) and implemented by means of a specific software. An example of software that utilises K_c (with the dual crop coefficient approach) for use in irrigation planning and scheduling and hydrologic water balances is SIMdualKc (Rosa et al., 2011, Rosa et al., 2012); a software that calculates the phenological soil water balance would have the entire watershed as its reference area. Waiting for this possible future development, a strength of the current model is that only a spreadsheet and a GIS are needed to implement it.

The model can then be improved by searching for crop coefficients specific to the study area and calibrated in watersheds with continuous flow measurements. Furthermore, up-to-date land use maps would be needed for good performance because the area extent of crop types varies from year to year. This can be obviated by considering these extents constant: the model would be less accurate but still reliable.

5. CONCLUSIONS

The need for adequate tools for evaluating the water resources of a watershed, and to understand hydrological dynamics at a deeper level, has led to the elaboration of a hydrological model to expand and improve the performance of the hydrological model proposed in FAO Paper No. 56. This model, here defined as a 'phenological soil water balance model', has innovative characteristics that enable the achievement of high levels of precision and accuracy. Firstly, it adopts a correction of the reference precipitation and evapotranspiration values, taking into account the actual area of the territory. It also applies to the whole watershed (therefore both for agricultural and non-agricultural land uses) the crop coefficients for the estimation of the maximum crop evapotranspiration, which are a function of the phenological stage. For this purpose it was necessary to research and compute crop coefficients for non-agricultural land use classes; a single daily coefficient, which is the weighted sum of the daily crop coefficients of all land use classes, was thus developed to correct the watershed potential evapotranspiration.

The model, applied for seven consecutive years (2013–2019), is lumped, physically based, deterministic and uses daily time intervals; it was calibrated and validated on a small watershed with low anthropic impact. The balance equation (Eq. 9) is valid at all time intervals (daily, weekly, monthly, annual, multi-annual). Calibration and validation were carried out by comparing the values of the deep percolation from the model with the measured baseflow at the closure section of the watershed. The consistency between the two values, which had an excellent correlation both as the trend and as multi-annual totals, demonstrated the validity of the model. Anyway further research that may lead to the determination of more suitable crop coefficients for the area under study, up-to-date land use maps, greater availability of climatic data for correcting the coefficients, making the model distributed and implementation through specific software may further improve the performance of the model.

The phenological soil water balance, which provides insights into surface and groundwater flows, allows for quantification, at different time intervals, of the potential surface and underground water resources and the water deficit for the entire watershed.

It can be a valuable technical-scientific aid for policymakers for proper water resources management, for planning the agricultural use of the watershed and also for the identification of the most suitable sites for building water collection reservoirs.

ACKNOWLEDGEMENTS

We would like to thank Drs. Piero Paolucci and Silvio Cecchini of 'A. Serpieri' meteorological observatory in Urbino for the data provided.

REFERENCES

Allen R.G., Pereira L.S., Raes D., Smith M., 1998. Crop evapotranspiration: guidelines for computing crop water requirements. In: FAO Irrigation and Drainage Paper No. 56. FAO, Rome, Italy, pp 300.

AA.VV., 2006. Suoli e Paesaggi delle Marche. ASSAM (Agency for Agro-food Sector Services of the Marche Region), Errebi Grafiche Ripesi, Falconara Marittima (Ancona, Italy), pp. 304.

Barrera Jr. W.B., Ferrise R., Dalla Marta A. (2023) Understanding trends and gaps in global research of crop evapotranspiration: a bibliometric and thematic review. Italian Journal of Agrometeorology (1): 13-35. https://doi.org/10.36253/ijam-2175

Becker A., Pfützner B., 1986. Identification and modelling of river flow reductions caused by evapotranspiration losses from shallow groundwater areas. 2nd Scientific Assembly of the IAHS, Symp. 52, Budapest, July 1986. IAHS Publ. No. 156, pp. 301–311.

Brirhet H., Benaabidate L., 2016. Comparison of two hydrological models (lumped and distributed) over a pilot area of the Issen watershed in the Souss Basin, Morocco. Eur. Sci. J. 12(18): 347-358. https://doi.org/10.19044/esj.2016.v12n18p347.

Budyko M.I., 1974.Climate and Life. Academic Press, New York, 508 pp.

Corbari C., Ravazzani G., Galvagno M., Cremonese E., Mancini M., 2017. Assessing Crop Coefficients for Natural Vegetated Areas Using Satellite Data and Eddy Covariance Stations. Sensors (Basel). Nov 18;17(11): 2664. https://doi.org/10.3390/s17112664. PMID: 29156568; PMCID: PMC5713072.

Costello L.R., Jones K.S., 2014.WUCOLS IV: Water Use Classification of Landscape Species. California Center for Urban Horticulture, University of California, Davis. http://ucanr.edu/sites/WUCOLS/

Dripps W.R., Bradbury K.R., 2007. A simple daily soil–water balance model for estimating the spatial and temporal distribution of groundwater recharge in temperate humid areas. Hydrogeol. J. 15: 433–444. https://doi.org/10.1007/s10040-007-0160-6.

Eccel E., Toller G., Ghielmi L., Salvadori C., La Porta N., 2007. Valutazione del bilancio idrico in una foresta decidua alpina. Ital. J. Agrometeorol. 12(1): 32-43.

Farmer W.H., Vogel R.M., 2016. On the deterministic and stochastic use of hydrologic models, Water Resour. Res., 52: 5619-5633. https://doi.org/10.1002/2016WR019129.

Friuli-Venezia Giulia Autonomous Region, 2018. Piano regionale di tutela delle acque. http://www.regione.fvg.it/rafvg/cms/RAFVG/ambiente-territorio/pianificazione-gestione-territorio/FOGLIA20/FOGLIA22/

Garofalo P., Vonella A.V., Maddaluno C., Rinaldi M., 2011. Verifica dei coefficienti colturali (kc) su colture erbacee in una pianura del Sud Italia. Proc. of the XIV National Congress of Agrometeorology "Agrometeorologia per l'azienda agraria". 7-9 June 2011, Facoltà di Agraria, Bologna, 15-16.

Gayathri K. Devi, Ganasri B.P., Dwarakish G.S., 2015. A review on hydrological models. Aquat. Procedia, 4: 1001–1007. https://doi.org/10.1016/j.aqpro.2015.02.126

Garavaglia F., Le Lay M., Gottardi F., Garçon R., Gailhard J., Paquet E., Mathevet T., 2017. Impact of model structure on flow simulation and hydrological realism: from a lumped to a semi-distributed approach, Hydrol. Earth Syst. Sci., 21: 3937–3952, https://doi.org/10.5194/hess-21-3937-2017

Gori S., 2004. Valutazione della pericolosità di frana attraverso l'analisi di foto aeree e in relazione alle condizioni di innesco in un'area nel comune di Urbino. Degree Diss., Università di Urbino, Italy.

Gupta H. V., Kling H., Yilmaz K. K., Martinez G. F., 2009. Decomposition of the mean squared error and NSE performance criteria: Implications for improving hydrological modelling. J. Hydrol., 377(1-2): 80–91, doi:10.1016/j.jhydrol.2009.08.003

Hunink J.E., Eekhout J.P.C., De Vente J., Contreras S., Droogers P., Baille A., 2017. Hydrological Modelling Using Satellite-Based Crop Coefficients: A Comparison of Methods at the Basin Scale. *Remote Sens. 9*(2): 174. https://doi.org/10.3390/rs9020174

Jiménez Cisneros B.E., Oki T., Arnell N.W., Benito G., Cogley J.G., Döll P., Jiang T., Mwakalila S.S., 2014. Freshwater resources. In: Climate Change 2014: Impacts, Adaptation, and Vulnerability. Part A: Global and Sectoral Aspects. Contribution of Working Group II to the Fifth Assessment Report of the Intergovernmental Panel on Climate Change [Field, C.B., V.R. Barros, D.J. Dokken, K.J. Mach, M.D. Mastrandrea, T.E. Bilir, M. Chatterjee, K.L. Ebi, Y.O. Estrada, R.C. Genova, B. Girma, E.S. Kissel, A.N. Levy, S. MacCracken, P.R. Mastrandrea, and L.L.White (eds.)].

Cambridge University Press, Cambridge, United Kingdom and New York, NY, USA, pp. 229-269.

Kannan N., Santhi C., Williams J.R., Arnold J.G., 2008. Development of a continuous soil moisture accounting procedure for curve number methodology and its behaviour with different evapotranspiration methods. Hydrol. Process. 22(13): 2114-2121. https://doi.org/10.1002/hyp.6811.

Khakbaz B., Imam B., Hsu K., Sorooshian S., 2012. From lumped to distributed via semi-distributed: Calibration strategies for semi-distributed hydrologic models. Journal of Hydrology, 418–419: 61-77. https://doi.org/10.1016/j.jhydrol.2009.02.021

Knoben W.J.M., Freer J.E., Woods R.A., 2019. Technical note: Inherent benchmark or not? Comparing NashSutcliffe and Kling-Gupta efficiency scores. Hydrology and Earth System Sciences. https://doi.org/10.5194/hess-2019-327

Mishra S.K., Singh V.P., 2003. Soil Conservation Service Curve Number (SCS-CN) Methodology. Water Sci. Technol. Library, vol 42. Springer, Dordrecht, The Netherlands, pp. 516. https://doi.org/10.1007/978-94-017-0147-1

Mockus V., 1972. Chapter 10: Estimation of Direct Runoff from Storm Rainfall. US Department of Agriculture (Ed.), Hydraulics and Hydrology — Technical References NRCS National Engineering Handbook, Part 630 Hydrology, Washington DC.

Neitsch S.L., Arnold J.G., Kiniry J.R., Williams J.R., 2011. Soil and Water Assessment Tool Theoretical documentation version 2009. Texas Water Resources Institute Technical Report No. 406, Texas A&M University System College Station, Texas 77843-2118

Pereira L.S., Paredes P., Hunsaker D.J., López-Urrea R., Mohammadi Shad Z., 2021. Standard single and basal crop coefficients for field crops. Updates and advances to the FAO56 crop water requirements method. Agricultural Water Management, Volume 243: 106466. https://doi.org/10.1016/j.agwat.2020.106466.

Rosa, R.D., Paredes, P., 2011. The SIMdualKc model. Software application for water balance computation and irrigation scheduling using the dual crop coefficient approach. CEER-Biosystems Engineering. Institute of Agronomy, Technical University of Lisbon.

Rosa, R.D., Paredes, P., Rodrigues, G.C., Alves, I, Fernando, R.M., Pereira, L.S., Allen, R.G., 2012. Implementing the dual crop coefficient approach in interactive software. 1. Background and computational strategy. Agricultural Water Management. https://doi.org/10.1016/j.agwat.2011.10.013

Schewe J., Heinke J., Gerten D., Haddeland I., Arnell N.W., Clark D.B., Dankers R., Eisner S., Fekete B., Colón-González F.J., Gosling S.N., Kim H., Liu X., Masaki Y., Portmann F.T., Satoh Y., Stacke T., Tang Q., Wada Y., Wisser D., Albrecht T., Frieler K., Piontek F., Warszawski L., Kabat P., 2013. Multi-model assessment of water scarcity under climate change. Proceedings of the National Academy of Sciences of the United States of America 111(9): 3245-3250. https://doi.org/10.1073/pnas.1222460110

Schumann A.H., 1993. Development of conceptual semi-distributed hydrological models and estimation of their parameters with the aid of GIS. Hydrol. Sci. J. 38(6): 519-528. https://doi.org/10.1080/02626669309492702.

Taurino L., 2004. Un sistema informativo territoriale per l'analisi della propensione al dissesto dei versanti dell'area urbinate. Degree Diss., Università di Urbino, Italy.

UNI EN ISO 748:2008 – Misurazione della portata di liquidi in canali aperti mediante correntometri o galleggianti. International Standards Organization (ISO), Geneva, Switzerland, 2008.

U.S. Army Corps of Engineers, 2013. Hydrologic modeling system HEC-HMS - User's Manual. Davis, CA, pp. 442. http://www.hec.usace.army.mil/software/hec-hms/.

USDA NRCS, 2004. Part 630 – Hydrology National Engineering Handbook Natural Resources Conservation Service, Washington, D.C. https://directives.sc.egov.usda.gov/viewerFS.aspx?hid=21422

Williams J.R., Arnold JG, Srinivasan R, 2000. The APEX Model. BRC Report No. 00-06. Temple, TX: Texas A&M University, Texas Agricultural Extension Service, Texas Agricultural Experiment Station, Blacklands Research Center.

Williams J.R., Izaurralde R.C., 2005. The APEX model. BREC Report No. 2005-02. Temple, Tex.: Texas A&M University, Texas Agricultural Experiment Station, Blackland Research and Extension Center.

Williams J.R., Kannan N., Wang X., Santhi C., Arnold J.G., 2012. Evolution of the SCS Runoff Curve Number and its application to continuous runoff simulation. J. Hydrol. Eng. 17(11): 1221-1229. https://doi.org/10.1061/(ASCE)HE.1943-5584.0000694

Zotarelli L., Dukes M.D., Romero C.C., Migliaccio K.W., Morgan K.T., 2010. Step by Step Calculation of the Penman-Monteith Evapotranspiration (FAO-56 Method). Doc. AE459, University of Florida. https://edis.ifas.ufl.edu/pdffiles/AE/AE45900.pdf

SUPPLEMENTARY MATERIAL 1
INSIGHT INTO THE CONCEPT OF THE COEFFICIENT OF ACCLIVITY AND ITS IMPLICATIONS IN THE PHENOLOGICAL SOIL WATER BALANCE

When calculating how much water has rained in a territory, the surface of the territory is considered as if it were flat (fig. S1/A); i.e. on the projected surface.

However, a correction should be made to distribute the precipitation over the actual surface. If it is assumed that, above the watershed line, the watershed is 'covered' by a flat surface, the precipitation water is distributed over this, which corresponds to the projected surface of the basin (fig. S1/A): for the Santa Maria degli Angeli watershed the area of this surface is 13.098 km^2.

However, the water is not distributed over this theoretical surface but is distributed over a larger, effective one (fig. S1/B), that for Maria degli Angeli watershed has an area of 13.979 km^2. The values indicated relate to the portion of watershed on which the balance was calculated, highlighted by the yellow line in figure S1/B.

The measure of the projected area was calculated using GIS, the measure of the actual area was calculated using a Digital Terrain Model.

Fig. S2 schematises this process in 2 dimensions. The broken line ABC is the ground profile. The segment BD corresponds to the projected surface of BC; we have that AB=BD, and obviously BC>AB and BC>BD.

The amount of water that falls on AB and BD is the same, but the amount that falls on BD is distributed over a larger surface, i.e. BC, resulting in a decrease in the precipitation value per unit of soil. For evapotranspiration, the effect is the opposite: the actual evapotranspirative surface is greater than the projected surface, so the losses per ET are greater. This effect is greater the greater the slope angle.

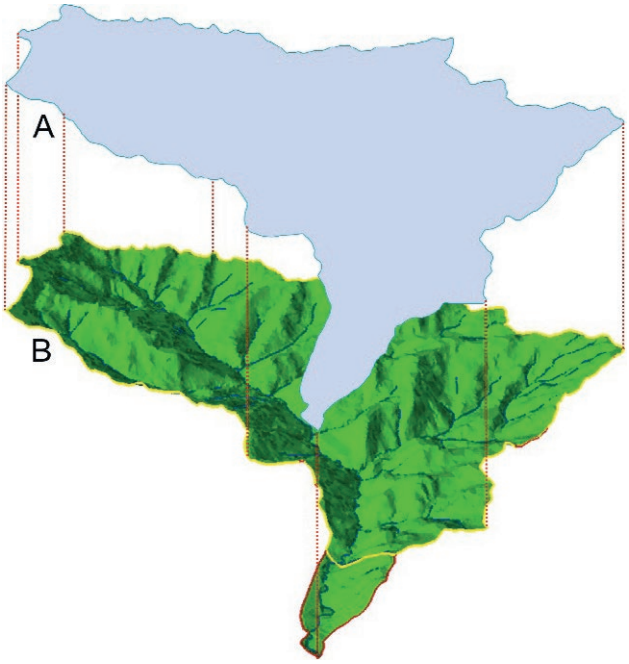

Figure S1/A. Projected surface of Santa Maria degli Angeli watershed.
Figure S1/B. Actual surface of Santa Maria degli Angeli watershed.

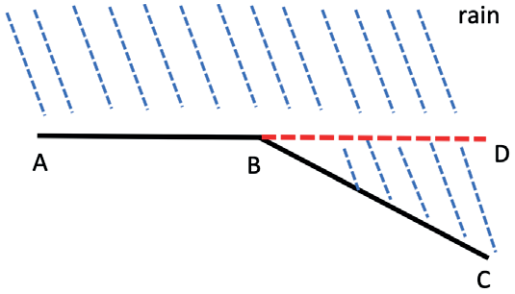

Figure S2. Schematisation of conditions for the application of the acclivity coefficient (Ca).

SUPPLEMENTARY MATERIAL 2

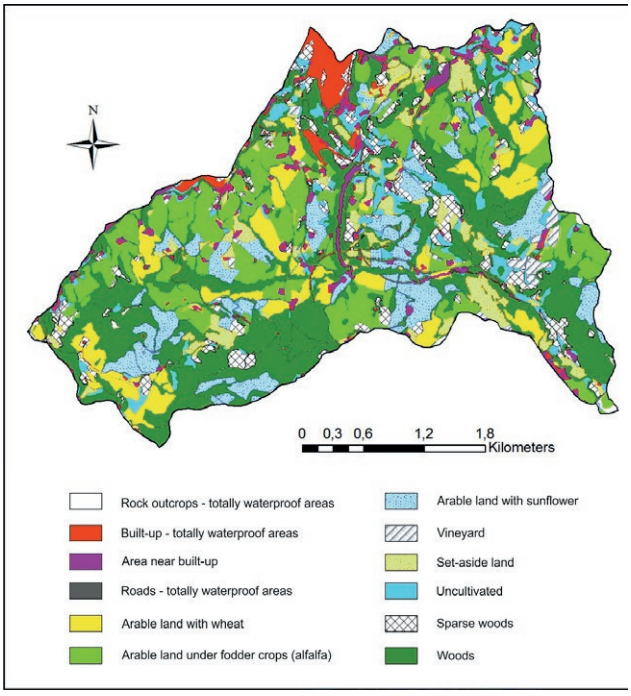

Figure S3. Land use map of Santa Maria degli Angeli watershed for the year 2013, obtained by interpretation of aerial orthophotos and processed on vector files in a GIS environment. The ' area near built-up ' land use includes mixed built-up and natural areas with low anthropogenic impact.

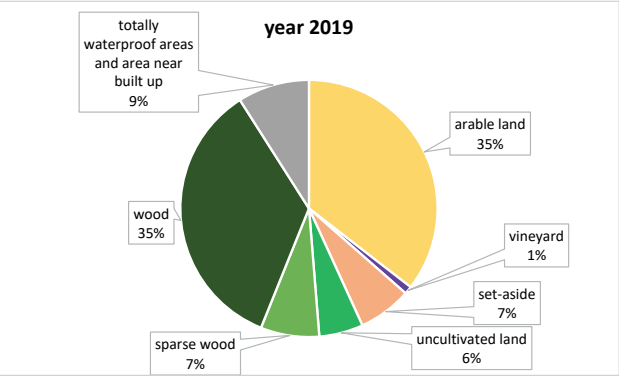

Figure S4. Percentage distribution of land use classes in the Santa Maria degli Angeli watershed, year 2019.

SUPPLEMENTARY MATERIAL 3
CALCULATION OF RUNOFF

For the calculation of the daily values of the runoff parameter, which contribute to the phenological soil water balance (see Eq. 1), the curve number methodology (Mockus, 1972; USDA, 2004), with its subsequent modifications (Williams, 2000; Kannan et al., 2008; Friuli Venezia Giulia Autonomous Region, 2018), was used.

S3.1. USDA Curve Number method

Each territory was assigned a parameter called Curve Number (CN), which has a value between 0 and 100. Each value of CN corresponds to a curve through which, based on the precipitation value, the percentage of runoff is obtained. Higher CN values correspond to higher runoff values.

The CN value of a watershed is a function of:
- land use;
- permeability of soils;
- average slope of the watershed; and
- antecedent soil moisture conditions (AMC).

Table S.1. Cumulative precipitation intervals (in mm) for each of the vegetative phases considered and corresponding classes of antecedent soil moisture conditions (AMC) and curve number (CN). The values reported in the dormancy, growing and average columns are cumulative precipitation of the 5 days before the day in which the runoff was calculated.

Dormancy	Average	Growing	AMC class	CN class
<13	<23	<36	I	CN I
13-28	23-40	36-53	II	CN II
>28	>40	>53	III	CN III

Precipitation water is initially retained by leaf interception, ground depressions and infiltration: this quantity is called 'initial abstraction' (Ia) and the runoff begins only after Ia has been saturated.

Each soil has a maximum water storage value corresponding to the potential maximum retention (S, expressed in mm). This parameter is related to the CN according to the following two equations:

$$CN = \frac{25400}{254 + S} \tag{1S}$$

$$S = \frac{25400}{CN} - 254 \tag{2S}$$

The share of water that must provide the rain to saturate the initial abstraction is equal to:

$$Ia = 0.2 \cdot S \tag{3S}$$

The value of 0.2 may vary depending on the site and other parameters but is considered to be reliable in many cases.

For a given precipitation amount, the amount of runoff (RO[7], mm) is as follows (USDA NRCS, 2004):

$$\begin{aligned} RO &= 0 && if\ P \le Ia \\ RO &= \frac{(P - Ia)^2}{P - Ia + S} && if\ P > Ia \end{aligned} \tag{4S}$$

The parameter S has a constant value depending on the CN of the territory and this implies that, even if the soils had a different degree of humidity, the share of runoff would still be the same with equal precipitation. To overcome this limit, the parameter AMC (antecedent soil moisture condition) was introduced; it is a function of the vegetative phase and the cumulative rainfall of the 5 days before the day for which the runoff is to be calculated and determines which CN value is to be used. Table S.1 shows the threshold values for each AMC and the corresponding CN.

S3.2. USDA Curve Number method using a continuous soil moisture accounting procedure: application to the case study

The ranges of cumulative rainfall values over the previous 5 days for each AMC class in the study area

[7] Note: in the original formula of the CN the runoff is indicated with the abbreviation 'Q'. To avoid confusion, the abbreviation 'RO' given in FAO Paper No. 56 and in the phenological soil water balance equation (Eq. 1) has also been used here.

Table S.2. Ranges for antecedent soil moisture conditions (AMC) for the Santa Maria degli Angeli watershed in the year 2019, corresponding to cumulative precipitation (mm) in the previous 5 days.

AMC classes		Jan	Feb	Mar	Apr	May	Jun	Jul	Aug	Sept	Oct	Nov	Dec
AMC I	<	12	12	17	22	30	32	30	31	26	22	17	12
AMC II	between	12-26	12-26	17-32	22-38	30-46	32-48	30-46	31-47	26-39	22-38	17-32	12-26
AMC III	>	26	26	32	38	46	48	46	47	39	38	32	26

Table S.3. Correspondence between USDA classes and land use classes of the Santa Maria degli Angeli watershed for the calculation of CN.

USDA class [CN values associated with the 4 soil groups]	land use class of the S.M.A. watershed
Paved parking lots, paved streets and roads [98, 98, 98, 98]	Impermeable soil
Urban districts: commercial and business (imp. 85%) [89, 92, 94, 95]	Built-up
Residential districts (imp. 65%) [77, 85, 90, 92]	Area near built-up
Small grain – contoured – good conditions [61, 73, 81, 84]	Arable land winter wheat
Row crops – contoured+crop residue cover – good conditions [64, 74, 81, 85]	Arable land sunflower
Close-seeded or broadcast legumes or rotation meadow – contoured – good conditions [55, 69, 78, 83]	Arable land alfalfa, faba bean, clover
Pasture, grassland, or range-continuous forage for grazing – good conditions [39, 61, 74, 80]	Set aside
Brush-brush-forbs-grass mixture with brush the major element – fair conditions [35, 56, 70, 77]	Uncultivated
Woods-grass combination – good conditions [32, 58, 72, 79]	sparse wood
Woods – good conditions [30, 55, 70, 77]	wood

were calculated monthly based on the vegetative phases of the components of the entire watershed land use classes. By way of example, the values for the year 2019 are given in Table S.2. Values should be recalculated if the areas of the land use class components vary.

In this study, AMC ranges were used for the calculation of parameter B of the equation 6S (Williams et al., 2000).

The procedure for determining the CN value of the watershed is reported in the Hydrology National Engineering Handbook (USDA NRCS, 2004). For this purpose, it was necessary to attribute the land use classes present in the watershed to the land use classes provided for by the method (Table S.3).

From the weighted sum of the values of the curve numbers of all uses of the soil the value of CN for the entire watershed is obtained. This value shall be corrected for the mean slope of the watershed. This is achieved by substituting, in equation 1S, the parameter S with S_{2s} (maximum soil water retention), calculated by equation 5S (Williams and Izaurralde, 2005; Williams et al., 2012).

$$S_{2s} = S_2 \cdot \left[1.1 - \frac{STP}{STP + exp(3.7 + 0.02117 \cdot STP)}\right] \qquad (5S)$$

where:
STP: average slope of the watershed (%); and
S_2: S value derived from equation 2S using the CN_2 value found.

The corrected value of CN is expressed by the abbreviation CN_{2s}.

To calculate the actual daily runoff it is necessary to replace, in equation 4S, the value of S with the daily value of retention (S_t). This value is obtained with the following equation (Williams et al., 2000; Kannan et al., 2008).

$$S_t = S_{t-1} + ET_{0t} \cdot \exp\left(\frac{-B \cdot S_{t-1}}{S_{max}}\right) - P_{t-1} + Q_{t-1} \qquad (6S)$$

where:
S_t: retention parameter of the day *t*
ET_{0t}: potential evapotranspiration of day t (the ET_c was used)
St_{-1}: retention parameter of the day t-1
B: depletion parameter.[8]
P_{t-1}: precipitation of the previous day (P_a was used)
Q_{t-1}: runoff of the previous day

[8] The value should theoretically be between 0 and 2, in practice it fluctuates between 0.5 and 1.5. In this study, the following values were assigned to B according to soil moisture conditions: with AMC I B = 0,75, with AMC II B = 1, with AMC III B = 1,25

S_{max}: maximum value of the retention parameter, corresponding to the value of S obtained by placing in equation 2S the value of CN_1.

For the first of the balance years, in the absence of data relating to previous periods, the starting value of S_t when t = 0 is obtained by placing the value of CN_{2s} in equation 2S. For subsequent years, the starting value of S_t is that of the last day of the previous year.

The parameter S_t has an upper limit, S_{max}, which is obtained by placing the value of CN_1 instead of CN in equation 2S. For the calculation of CN_1, equation 7S is used (Williams and Izaurralde, 2005; Williams et al., 2012).

$$CN_1 = CN_{2s} - \frac{20 \cdot (100 - CN_{2S})}{100 - CN_{2S} + exp[2.533 - 0.0636 \cdot (100 - CN_{2s})]} \quad (7S)$$

If the parameter S assumed the value of 0 in equation 1S, CN would assume the value of 100, which is a characteristic value of completely impermeable surfaces; this would lead to overestimation of the runoff. Consequently, following the methodology used for the realisation of the Regional Plan for the Protection of Waters of the Friuli Venezia Giulia Autonomous Region (2018), a lower limit, S_{min}, has also been established, which is obtained by placing the value of CN_3 in equation 2S.

Table S.4. Values of the CN_2 and the various types of CN in the 7 years in which the phenological soil water balance was elaborated.

Year	CN_2 Value	CN Class	Value
		CN_1	60,2
2013	73,9	CN_{2s}	77,8
		CN_3	90,3
		CN_1	60,3
2014	74,1	CN_{2s}	77,9
		CN_3	90,4
		CN_1	60,1
2015	73,9	CN_{2s}	77,7
		CN_3	90,3
		CN_1	60,0
2016	73,8	CN_{2s}	77,6
		CN_3	90,2
		CN_1	59,8
2017	73,6	CN_{2s}	77,4
		CN_3	90,1
		CN_1	59,7
2018	73,5	CN_{2s}	77,4
		CN_3	90,1
		CN_1	59,9
2019	73,7	CN_{2s}	77,5
		CN_3	90,2

For the calculation of CN_3, equation 8S is used (Williams and Izaurralde, 2005; Williams et al., 2012).

$$CN_3 = CN_{2s} exp\,[0.00673 \cdot (100 - CN_{2s})] \quad (8S)$$

The values of the three classes of CN corrected for the slope in the seven years in which the phenological soil water balance was developed are reported in Table S.4.

S3.3 Calculation of runoff: step-by-step procedure and an example of calculation of runoff in selected periods of the year 2015

The following are the steps for the calculation of runoff (the symbols are those already described in the text):

1) calculation of the values $S_{t=0}$, S_{max} and S_{min} (insertion in eq. 2S of the values of CN_{2s}, CN_1 and CN_3);
2) for each simulation day the values of the basic parameters P_a, ET_c, B are to be entered;
3) for each day, S_t is to be calculated using equation 6S; the starting value in the first balance year is $S_{t=0}$, in the following years the starting value is S_t of the last day of the previous year;
4) initial abstraction (= 0,2 · S_t) is to be calculated for each day;
5) the runoff (RO) is to be calculated for each day according to equation 4S;
6) If $S_t < S_{min}$, it poses $S_t = S_{min}$; and
7) If $S_t > S_{max}$, it poses $S_t = S_{max}$.

Below are reported some examples of the calculation of runoff in characteristic periods of the year 2015, in which S_{max} = 168,48 and S_{min} = 27,32.

First period: winter phase

For 21–22 January, it was noted that there was moderate precipitation and no runoff (RO); this was determined as P-Ia ≤ 0; in fact, there can be no runoff until the initial abstraction is not completely compensated. On January 23, the runoff (RO) started, as P-Ia > 0 and, simultaneously, S_t decreased below the value of S_{min}; in this case, the value of S_t must be replaced with S_{min}.

Second period: spring phase

In this period S_t assumes intermediate values between S_{min} and S_{max}, and with precipitation of a certain consistency, there is runoff (RO > 0). Note the drastic drop in S_t after a day of heavy precipitation and subsequent runoff. The value of S_t, however, also depends on ET_c and B (Eq. 6S).

Table S.5. Runoff calculation model - winter 2015. P_a: precipitation values corrected for acclivity coefficient; ET_c: evapotranspiration crop of the watershed; B: depletion parameter (varies between 0.75 and 1.25); S_t: day retention parameter t; Ia: initial abstraction; RO: runoff.

Date	P_a (mm)	ET_c (mm)	B	S_t (mm)	Ia (mm)	P_a-Ia (mm)	RO (mm)
21/01/2015	0.8	0.41	0.75	35.08	7.016	-6.2	0.0
22/01/2015	2.3	0.58	0.75	34.74	6.947	-4.7	0.0
23/01/2015	10.5	0.32	0.75	32.73	6.545	3.9	0.4
24/01/2015	2.2	0.70	1	27.32	5.464	-3.3	0.0
25/01/2015	0.2	1.21	1	27.32	5.464	-5.3	0.0
26/01/2015	0.0	0.98	1	27.96	5.593	-5.6	0.0
27/01/2015	0.0	0.76	1	28.61	5.721	-5.7	0.0
28/01/2015	0.0	0.83	1	29.30	5.861	-5.9	0.0
29/01/2015	1.4	1.78	0.75	30.87	6.174	-4.8	0.0
30/01/2015	7.7	1.89	0.75	31.11	6.222	1.5	0.1
31/01/2015	0.1	1.46	0.75	27.32	5.464	-5.3	0.0
01/02/2015	1.8	0.53	0.75	27.66	5.532	-3.8	0.0
02/02/2015	0.1	1.27	0.75	27.32	5.464	-5.4	0.0
03/02/2015	0.0	0.96	0.75	28.11	5.622	-5.6	0.0
04/02/2015	10.6	0.70	0.75	28.72	5.745	4.9	0.7
05/02/2015	29.2	0.44	1	27.32	5.464	23.8	11.1
06/02/2015	48.2	0.36	1.25	27.32	5.464	42.7	26.0
07/02/2015	7.7	0.43	1.25	27.32	5.464	2.3	0.2
08/02/2015	3.2	1.20	1.25	27.32	5.464	-2.3	0.0
09/02/2015	0.2	1.38	1.25	27.32	5.464	-5.2	0.0
10/02/2015	0.0	1.16	1.25	28.02	5.603	-5.6	0.0

Table S.6. Runoff calculation model - spring 2015. For explanation of symbols see table S5 legend.

Date	P_a (mm)	ET_c (mm)	B	S_t (mm)	Ia (mm)	P_a-Ia (mm)	RO (mm)
19/05/2015	0.0	6.08	0.75	96.385	19.277	-19.3	0.0
20/05/2015	0.0	4.83	0.75	99.529	19.906	-19.9	0.0
21/05/2015	0.0	4.96	0.75	102.711	20.542	-20.5	0.0
22/05/2015	66.5	1.13	0.75	103.424	20.685	45.8	14.0
23/05/2015	15.0	1.88	1.25	51.878	10.376	4.6	0.4
24/05/2015	6.2	2.16	1.25	38.760	7.752	-1.5	0.0
25/05/2015	0.1	3.95	1.25	35.476	7.095	-7.0	0.0
26/05/2015	1.6	3.31	1.25	37.960	7.592	-6.0	0.0
27/05/2015	15.9	2.34	1.25	38.168	7.634	8.3	1.5
28/05/2015	0.0	4.85	1	27.607	5.521	-5.5	0.0
29/05/2015	0.0	5.30	0.75	32.293	6.459	-6.5	0.0

Third period: summer phase

Precipitation is low and does not produce runoffs. The high values of ET_c raise S_t that exceeds S_{max}: in this case, the value of S_t is replaced with S_{max}, whose value cannot be exceeded.

Table S.7. Runoff calculation model - summer 2015. For explanation of symbols see table S5 legend.

Date	P_a (mm)	ET_c (mm)	B	S_t (mm)	Ia (mm)	P_a-Ia (mm)	RO (mm)
15/07/2015	0.0	4.98	0.75	163.122	32.624	-32.6	0.0
16/07/2015	2.9	5.06	0.75	165.572	33.114	-30.2	0.0
17/07/2015	0.0	6.07	0.75	165.603	33.121	-33.1	0.0
18/07/2015	0.0	5.27	0.75	168.122	33.624	-33.6	0.0
19/07/2015	0.0	5.99	0.75	168.475	33.695	-33.7	0.0
20/07/2015	0.0	5.53	0.75	168.475	33.695	-33.7	0.0
21/07/2015	0.0	5.22	0.75	168.475	33.695	-33.7	0.0
22/07/2015	0.0	4.75	0.75	168.475	33.695	-33.7	0.0
23/07/2015	0.0	5.43	0.75	168.475	33.695	-33.7	0.0
24/07/2015	0.1	4.47	0.75	168.475	33.695	-33.6	0.0

Table S.8. Runoff calculation model - autumn 2015. For explanation of symbols see table S5 legend.

Date	P_a (mm)	ET_c (mm)	B	S_t (mm)	Ia (mm)	P_a-Ia (mm)	RO (mm)
21/09/2015	0.0	1.99	0.75	168.475	33.695	-33.7	0.0
22/09/2015	0.0	2.09	0.75	168.475	33.695	-33.7	0.0
23/09/2015	9.4	1.77	0.75	168.475	33.695	-24.3	0.0
24/09/2015	31.6	1.26	0.75	159.638	31.928	-0.3	0.0
25/09/2015	8.2	0.79	1.25	128.241	25.648	-17.5	0.0
26/09/2015	0.3	1.35	1.25	120.578	24.116	-23.8	0.0
27/09/2015	0.9	2.68	1.25	121.329	24.266	-23.4	0.0
17/11/2015	0.1	0.20	0.75	31.429	6.286	-6.2	0.0
18/11/2015	0.0	0.35	0.75	31.609	6.322	-6.3	0.0
19/11/2015	0.3	0.74	0.75	32.252	6.450	-6.2	0.0
20/11/2015	0.0	2.87	0.75	34.456	6.891	-6.9	0.0
21/11/2015	8.9	2.67	0.75	36.747	7.349	1.5	0.1
22/11/2015	19.6	0.55	0.75	28.405	5.681	13.9	4.6
23/11/2015	10.4	0.41	1	27.319	5.464	5.0	0.8
24/11/2015	0.0	0.44	1.25	27.319	5.464	-5.5	0.0
25/11/2015	0.4	0.42	1.25	27.658	5.532	-5.1	0.0
26/11/2015	3.9	0.87	1.25	27.930	5.586	-1.7	0.0
27/11/2015	7.9	0.80	1.25	27.319	5.464	2.4	0.2
28/11/2015	0.0	0.47	1	27.319	5.464	-5.5	0.0
29/11/2015	0.1	0.52	0.75	27.783	5.557	-5.5	0.0
30/11/2015	0.0	1.44	0.75	28.993	5.799	-5.8	0.0

Fourth and fifth period: autumn phase

The last two periods shall be reported together; in the fourth period the first substantial precipitation

events do not produce runoffs (since S_t has maximum value and initial abstraction is very high), but the S_t parameter begins to drop permanently. After a couple of months, it again reaches the value of S_{min} and fluctuates around this value until the end of the year. As a result, the runoff is quite consistent.

SUPPLEMENTARY MATERIAL 4
MONTHLY VALUES OF THE DEEP PERCOLATION (SIMULATED BY THE PHENOLOGICAL SOIL WATER BALANCE) AND BASE FLOW OF THE SANTA MARIA DEGLI ANGELI STREAM (CALCULATED FROM DISCHARGE MEASUREMENTS) OVER THE PERIOD 2013-2019

Table S.9.

Year	Month	Deep percolation (mm)	Measured baseflow (mm)
2013	January	76,5	44,4
	February	54,1	57,7
	March	48,0	70,6
	April	14,8	22,6
	May	0,0	9,4
	June	0,0	4,0
	July	0,0	1,0
	August	0,0	8,4
	September	0,0	1,1
	October	0,0	4,4
	November	77,1	24,4
	December	8,6	26,0
2014	January	35,1	24,1
	February	42,6	69,9
	March	42,3	41,2
	April	7,5	60,4
	May	26,9	52,7
	June	0,0	9,1
	July	0,0	3,6
	August	0,0	2,5
	September	0,0	5,3
	October	0,0	10,6
	November	31,1	18,5
	December	59,5	54,4
2015	January	5,5	31,9
	February	82,7	58,8
	March	75,8	68,5
	April	7,8	32,1
	May	0,0	14,6
	June	0,0	9,1
	July	0,0	2,4
	August	0,0	0,8
	September	0,0	0,3
	October	11,8	3,2
	November	29,6	4,0
	December	0,0	2,6
2016	January	40,2	12,6
	February	41,8	19,9
	March	48,4	55,7
	April	0,0	13,7
	May	4,0	15,2
	June	0,0	5,1
	July	0,0	1,7
	August	0,0	1,1
	September	0,0	0,5
	October	0,0	0,5
	November	6,7	3,4
	December	0,0	1,2
2017	January	47,6	23,2
	February	33,5	24,0
	March	14,9	29,6
	April	0,0	8,7
	May	0,0	4,5
	June	0,0	0,2
	July	0,0	0,8
	August	0,0	0,9
	September	0,0	0,9
	October	0,0	0,1
	November	23,5	1,2
	December	37,4	10,2
2018	January	1,6	11,3
	February	122,5	52,5
	March	83,5	125,5
	April	0,0	21,8
	May	0,0	9,2
	June	0,0	2,2
	July	0,0	1,6
	August	0,0	0,8
	September	0,0	0,4
	October	0,0	0,0
	November	9,0	1,6
	December	34,6	7,8
2019	January	34,5	9,0
	February	10,9	16,9
	March	0,0	5,3
	April	0,0	5,0
	May	34,6	30,1
	June	0,0	25,1
	July	0,0	2,2
	August	0,0	1,1
	September	0,0	0,3
	October	0,0	2,5
	November	12,6	8,1
	December	20,8	14,4
	Totals	*1400*	*1444*

SUPPLEMENTARY MATERIAL 5

The phenological soil water balance at significant periods during the year

Table S.10. The phenological soil water balance in a phase of surplus during the year 2014 and determination of deep percolation.

			$ET_c \cdot K_s = aET_c$												
	$ET_{0a} \cdot K_{c\ Ws} = ET_c$				$TAW \cdot p = RAW$						$P_a - RO - aET_c - \Delta AW = DP$				
Date	ET_{0a}	$K_{c\ Ws}$	ET_c	K_s	TAW	p	RAW	$D_{r\ start}$	$D_{r\ end}$	AW	P_a	RO	aET_c	ΔAW	DP
18/01/2014	1.97	1.05	2.06	1.00	129.5	0.688	89.1	5.56	7.62	121.9	0.0	0.0	2.1	-2.1	0.0
19/01/2014	1.54	1.05	1.61	1.00	129.5	0.688	89.1	7.62	7.79	121.7	1.4	0.0	1.6	-0.2	0.0
20/01/2014	0.89	1.05	0.93	1.00	129.5	0.688	89.1	7.79	8.22	121.3	0.5	0.0	0.9	-0.4	0.0
21/01/2014	0.40	1.05	0.42	1.00	129.5	0.688	89.1	8.22	**(-9.57)**	**129.5**	24.2	6.0	0.4	8.2	**9.6**
22/01/2014	0.80	1.05	0.83	1.00	129.5	0.688	89.1	**0.00**	0.71	128.8	0.1	0.0	0.8	-0.7	0.0
23/01/2014	0.85	1.05	0.89	1.00	129.5	0.688	89.1	0.71	0.50	129.0	1.1	0.0	0.9	0.2	0.0
24/01/2014	0.83	1.05	0.86	1.00	129.5	0.688	89.1	0.50	**(-10.44)**	**129.5**	13.7	1.9	0.9	0.5	**10.4**
25/01/2014	1.41	1.05	1.47	1.00	129.5	0.688	89.1	**0.00**	1.41	128.1	0.1	0.0	1.5	-1.4	0.0
26/01/2014	0.72	1.05	0.76	1.00	129.5	0.688	89.1	1.41	2.17	127.3	0.0	0.0	0.8	-0.8	0.0
27/01/2014	0.83	1.05	0.87	1.00	129.5	0.688	89.1	2.17	**(-0.24)**	**129.5**	3.3	0.0	0.9	2.2	**0.2**
28/01/2014	0.43	1.05	0.45	1.00	129.5	0.688	89.1	**0.00**	**(-1.52)**	**129.5**	2.0	0.0	0.5	0.0	**1.5**

ET_{0a}: reference evapotranspiration corrected for acclivity coefficient (eq. 4 in the main article);
$K_{c\ Ws}$: unique 'crop' coefficient of the territory (eq. 6);
ET_c: crop evapotranspiration of the territory (eq. 7);
TAW: total available water (see FAO paper 56, ch.8);
p: parameter for RAW calculation (see FAO paper 56, ch.8);
RAW: rapidly available water (see FAO paper 56, ch.8);
$D_{r\ start}$: water deficit at the beginning of the day (= D_r end of the previous day)
$D_{r\ end}$: water deficit at the end of the day (= D_r start + aET_c - P_a + RO). Note: the negative values of D_r end correspond to the positive values (in bold) of water surplus that go into deep percolation. So, the next day's D_r start value is zero;
P_a: precipitation values corrected for acclivity coefficient (eq. 3);
RO: runoff (eq. 4S);
K_s: water stress coefficient (see FAO paper 56, ch.8);
aET_c: actual crop evapotranspiration (eq. 8);
AW: available water (= TAW - $D_{r\ end}$);
DP: deep percolation (eq. 9); and
ΔAW: variation of the available water with respect to the previous day.
Note: The phenological soil water balance is strictly represented by the parameters in the last 5 columns, and the equation that combines them together (shown at the top right of the table, that is the equation 9 in the main article). The other parameters are preliminary parameters to the balance.

Table S.11. The phenological soil water balance in conditions of a water stress period during the year 2014. For explanation of the symbols, see Table S10.

			$ET_c \cdot K_s = aET_c$												
	$ET_{0a} \cdot K_{c\ Ws} = ET_c$				$TAW \cdot p = RAW$						$P_a - RO - aET_c - \Delta AW = DP$				
date	ET_{0a}	$K_{c\ Ws}$	ET_c	K_s	TAW	p	RAW	$D_{r\ start}$	$D_{r\ end}$	AW	P_a	RO	aET_c	ΔAW	DP
19/05/2014	3.72	1.00	3.74	1.00	129.5	0.547	70.8	53.15	56.89	72.6	0.0	0.0	3.7	-3.7	0.0
20/05/2014	4.48	1.01	4.50	1.00	129.5	0.547	70.8	56.89	61.39	68.1	0.0	0.0	4.5	-4.5	0.0
21/05/2014	5.54	1.01	5.58	1.00	129.5	0.547	70.8	61.39	66.97	62.5	0.0	0.0	5.6	-5.6	0.0
22/05/2014	6.00	1.01	6.04	1.00	129.5	0.547	70.8	66.97	73.01	56.5	0.0	0.0	6.0	-6.0	0.0
23/05/2014	3.50	1.01	3.52	0.96	129.5	0.547	70.8	73.01	76.41	53.1	0.0	0.0	3.4	-3.4	0.0
24/05/2014	6.25	1.01	6.29	0.91	129.5	0.547	70.8	76.41	82.10	47.4	0.0	0.0	5.7	-5.7	0.0
25/05/2014	4.31	1.01	4.34	0.81	129.5	0.547	70.8	82.10	85.42	44.1	0.2	0.0	3.5	-3.3	0.0

Table S.12. Available water to the seasonal lows during the 2015. For explanation of the symbols, see Table S.10.

			$ET_c \cdot K_s = aET_c$												
	$ET_{0a} \cdot K_{c\,Ws} = ET_c$				$TAW \cdot p = RAW$					$P_a - RO - aET_c - \Delta AW = DP$					
date	ET_{0a}	$K_{c\,Ws}$	ET_c	K_s	TAW	p	RAW	$D_{r\,start}$	$D_{r\,end}$	AW	P_a	RO	aET_c	ΔAW	DP
02/08/2015	2.40	0.79	1.90	0.03	125.2	0.555	69.5	123.37	123.43	1.8	0.0	0.0	0.1	-0.1	0.0
03/08/2015	5.42	0.79	4.27	0.03	125.2	0.555	69.5	123.43	123.57	1.6	0.0	0.0	0.1	-0.1	0.0
04/08/2015	5.90	0.79	4.65	0.03	125.2	0.555	69.5	123.57	123.70	1.5	0.0	0.0	0.1	-0.1	0.0
05/08/2015	5.97	0.79	4.71	0.03	125.2	0.555	69.5	123.70	123.83	1.4	0.0	0.0	0.1	-0.1	0.0
06/08/2015	6.07	0.79	4.79	0.02	125.2	0.555	69.5	123.83	123.95	1.3	0.0	0.0	0.1	-0.1	0.0
07/08/2015	5.87	0.79	4.62	0.02	125.2	0.555	69.5	123.95	124.05	1.1	0.0	0.0	0.1	-0.1	0.0
08/08/2015	5.82	0.79	4.58	0.02	125.2	0.555	69.5	124.05	124.14	1.0	0.0	0.0	0.1	-0.1	0.0
09/08/2015	5.40	0.79	4.25	0.02	125.2	0.555	69.5	124.14	117.79	7.4	6.4	0.0	0.1	6.3	0.0
10/08/2015	3.75	0.79	2.95	0.13	125.2	0.555	69.5	117.79	113.90	11.3	4.3	0.0	0.4	3.9	0.0
11/08/2015	4.56	0.79	3.59	0.20	125.2	0.555	69.5	113.90	113.88	11.3	0.7	0.0	0.7	0.0	0.0
12/08/2015	5.61	0.79	4.41	0.20	125.2	0.555	69.5	113.88	114.78	10.4	0.0	0.0	0.9	-0.9	0.0

Table S.13. A period of the 2016 phenological soil water balance with fluctuations of the available water around the lows in the summer months. For explanation of the symbols, see Table S.10.

			$ET_c \cdot K_s = aET_c$												
	$ET_{0a} \cdot K_{c\,Ws} = ET_c$				$TAW \cdot p = RAW$					$P_a - RO - aET_c - \Delta AW = DP$					
date	ET_{0a}	$K_{c\,Ws}$	ET_c	K_s	TAW	p	RAW	$D_{r\,start}$	$D_{r\,end}$	AW	P_a	RO	aET_c	ΔAW	DP
04/07/2016	5.41	0.85	4.59	0.23	129.3	0.539	69.7	115.30	116.38	12.9	0.0	0.0	1.1	-1.1	0.0
05/07/2016	6.20	0.84	5.20	0.22	129.3	0.539	69.7	116.38	117.50	11.8	0.0	0.0	1.1	-1.1	0.0
06/07/2016	4.60	0.83	3.81	0.20	129.3	0.539	69.7	117.50	116.60	12.7	1.7	0.0	0.8	0.9	0.0
07/07/2016	6.08	0.82	4.97	0.21	129.3	0.539	69.7	116.60	117.66	11.6	0.0	0.0	1.1	-1.1	0.0
08/07/2016	6.44	0.81	5.23	0.20	129.3	0.539	69.7	117.66	118.68	10.6	0.0	0.0	1.0	-1.0	0.0
09/07/2016	6.31	0.81	5.09	0.18	129.3	0.539	69.7	118.68	119.59	9.7	0.0	0.0	0.9	-0.9	0.0
10/07/2016	5.35	0.80	4.29	0.16	129.3	0.539	69.7	119.59	120.29	9.0	0.0	0.0	0.7	-0.7	0.0
11/07/2016	6.92	0.80	5.51	0.15	129.3	0.539	69.7	120.29	121.12	8.2	0.0	0.0	0.8	-0.8	0.0
12/07/2016	8.06	0.79	6.38	0.14	129.3	0.539	69.7	121.12	122.00	7.3	0.0	0.0	0.9	-0.9	0.0
13/07/2016	6.20	0.77	4.77	0.12	129.3	0.539	69.7	122.00	113.93	15.4	8.7	0.0	0.6	8.1	0.0
14/07/2016	5.35	0.77	4.11	0.26	129.3	0.539	69.7	113.93	114.99	14.3	0.0	0.0	1.1	-1.1	0.0
15/07/2016	1.85	0.77	1.42	0.24	129.3	0.539	69.7	114.99	83.98	45.3	31.5	0.1	0.3	31.0	0.0
16/07/2016	4.74	0.75	3.56	0.76	129.3	0.539	69.7	83.98	86.59	42.7	0.1	0.0	2.7	-2.6	0.0
17/07/2016	5.64	0.75	4.23	0.72	129.3	0.539	69.7	86.59	89.62	39.7	0.0	0.0	3.0	-3.0	0.0

Table S.14. A period of the 2014 phenological soil water balance with the end of the phase of water stress. For explanation of the symbols, see Table S.10.

			$ET_c \cdot K_s = aET_c$											
	$ET_{0a} \cdot K_{c\,Ws} = ET_c$				$TAW \cdot p = RAW$					$P_a - RO - aET_c - \Delta AW = DP$				
date	ET_{0a}	$K_{c\,Ws}$	ET_c	K_s	TAW	p	RAW	$D_{r\,start}$	$D_{r\,end}$	AW	P_a	RO	aET_c	ΔAW	DP
29/08/2014	4.52	0.86	3.89	0.37	129.5	0.570	73.8	108.93	110.36	19.1	0.0	0.0	1.4	-1.4	0.0
30/08/2014	4.63	0.86	3.98	0.34	129.5	0.570	73.8	110.36	111.73	17.8	0.0	0.0	1.4	-1.4	0.0
31/08/2014	4.87	0.86	4.19	0.32	129.5	0.570	73.8	111.73	113.07	16.4	0.0	0.0	1.3	-1.3	0.0
01/09/2014	1.79	0.86	1.54	0.34	129.5	0.631	81.7	113.07	65.59	63.9	52.4	4.4	0.5	47.5	0.0
02/09/2014	1.25	0.86	1.07	1.00	129.5	0.631	81.7	65.59	55.41	74.1	11.2	0.0	1.1	10.1	0.0
03/09/2014	1.04	0.86	0.90	1.00	129.5	0.631	81.7	55.41	54.41	75.1	1.9	0.0	0.9	1.0	0.0
04/09/2014	1.29	0.86	1.11	1.00	129.5	0.631	81.7	54.41	45.62	83.9	9.9	0.0	1.1	8.8	0.0
05/09/2014	2.54	0.86	2.18	1.00	129.5	0.631	81.7	45.62	47.80	81.7	0.0	0.0	2.2	-2.2	0.0
06/09/2014	3.54	0.86	3.04	1.00	129.5	0.631	81.7	47.80	50.84	78.7	0.0	0.0	3.0	-3.0	0.0

Table S.15. A period of the 2014 phenological soil water balance; the return of the runoff and the deep percolation. For explanation of the symbols, see Table S.10.

			$ET_c \cdot K_s = aET_c$											
	$ET_{0a} \cdot K_{c\,Ws} = ET_c$				$TAW \cdot p = RAW$					$P_a - RO - aET_c - \Delta AW = DP$				
date	ET_{0a}	$K_{c\,Ws}$	ET_c	K_s	TAW	p	RAW	$D_{r\,start}$	$D_{r\,end}$	AW	P_a	RO	aET_c	ΔAW	DP
15/11/2014	1.39	1.04	1.44	1.00	129.5	0.681	88.2	4.89	4.08	125.4	2.2	0.0	1.4	0.8	0.0
16/11/2014	1.61	1.04	1.67	1.00	129.5	0.681	88.2	4.08	2.81	126.7	2.9	0.0	1.6	1.3	0.0
17/11/2014	0.53	1.04	0.55	1.00	129.5	0.681	88.2	2.81	(-16.43)	129.5	33.4	13.6	0.6	2.8	16.4
18/11/2014	1.75	1.04	1.81	1.00	129.5	0.681	88.2	0.00	(-1.00)	129.5	2.8	0.0	1.8	0.0	1.0
19/11/2014	0.78	1.08	0.85	1.00	129.5	0.681	88.2	0.00	(-4.34)	129.5	5.2	0.0	0.9	0.0	4.3
20/11/2014	0.47	1.08	0.51	1.00	129.5	0.681	88.2	0.00	0.32	129.2	0.2	0.0	0.5	-0.3	0.0
21/11/2014	0.53	1.08	0.57	1.00	129.5	0.681	88.2	0.32	0.83	128.7	0.1	0.0	0.6	-0.5	0.0
22/11/2014	0.43	1.08	0.47	1.00	129.5	0.681	88.2	0.83	1.27	128.2	0.0	0.0	0.5	-0.5	0.0
23/11/2014	0.45	1.08	0.48	1.00	129.5	0.681	88.2	1.27	1.59	127.9	0.2	0.0	0.5	-0.3	0.0
24/11/2014	0.38	1.08	0.41	1.00	129.5	0.681	88.2	1.59	1.78	127.7	0.2	0.0	0.4	-0.2	0.0
25/11/2014	0.40	1.08	0.43	1.00	129.5	0.681	88.2	1.78	2.15	127.3	0.1	0.0	0.4	-0.3	0.0
26/11/2014	0.42	1.08	0.45	1.00	129.5	0.681	88.2	2.15	(-2.58)	129.5	5.2	0.0	0.5	2.1	2.6
27/11/2014	0.43	1.08	0.46	1.00	129.5	0.681	88.2	0.00	(-3.41)	129.5	3.9	0.0	0.5	0.00	3.4
28/11/2014	0.40	1.08	0.43	1.00	129.5	0.681	88.2	0.00	0.25	129.3	0.2	0.0	0.4	-0.2	0.0

SUPPLEMENTARY MATERIAL 6 - MONTHLY VALUES OF THE PHENOLOGICAL SOIL WATER BALANCE IN THE PERIOD 2013-2019

For ease of reading, the values are shown at two-year intervals.

It should be noted that the phenological soil water balance (in bold in the tables) is valid at each time interval (daily, weekly, monthly, annual, multiannual). The relationships between the preliminary parameters are valid instead at daily intervals. For example for equation 7 in the text we have that:

$$ET_c = ET_{0a} \cdot K_{c\ Ws}$$

However, the monthly values are sums (such as $ET0_a$ and ET_c) or weighted sums (such as $K_{c\ Ws}$) and therefore the equation does not work well with these values (there is a small error). But these values are derived from daily values that are correct, values for which equation 7 is perfectly valid.

Table S.16. Monthly values of the phenological soil water balance in the period 2013-2014.

		$ET0_a$	$K_{c\ Ws}$	ET_c	**P_a - RO - aET_c - ΔAW = DP**				
					P_a	RO	aET_c	ΔAW	DP
2013	January	21,4	1,07	22,8	98,7	2,7	22,8	-3,3	76,5
	February	26,9	1,01	26,8	95,6	14,7	26,8	-0,1	54,1
	March	53,1	0,87	46,8	109,3	11,1	46,8	3,4	48,0
	April	96,0	0,68	65,0	48,1	2,5	65,0	-34,3	14,8
	May	114,5	0,95	109,5	109,6	4,3	109,5	-4,2	0,0
	June	155,3	0,98	151,8	75,9	0,9	114,7	-39,7	0,0
	July	182,2	0,84	151,9	5,7	0,0	49,6	-43,9	0,0
	August	160,2	0,80	128,5	79,2	0,0	34,1	45,1	0,0
	September	110,2	0,68	73,5	53,0	0,0	47,4	5,6	0,0
	October	52,8	0,79	41,5	87,2	4,6	41,5	41,1	0,0
	November	21,6	1,04	22,0	232,7	103,4	22,0	30,3	77,1
	December	24,7	0,79	19,2	27,3	0,1	19,2	-0,6	8,6
2014	January	26,2	0,77	21,5	66,6	9,4	21,5	0,7	35,1
	February	42,6	0,90	37,3	83,7	8,2	37,3	-4,4	42,6
	March	72,7	0,73	49,3	121,6	34,6	49,3	-4,6	42,3
	April	91,0	0,84	76,1	96,8	12,2	76,1	1,1	7,5
	May	131,5	0,99	130,9	120,6	34,8	120,7	-61,8	26,9
	June	161,4	0,98	158,1	63,2	0,1	84,4	-21,3	0,0
	July	151,9	0,80	122,2	96,4	0,0	64,9	31,5	0,0
	August	155,3	0,73	113,2	20,0	0,0	73,4	-53,4	0,0
	September	79,8	0,80	63,8	125,4	6,1	62,8	56,6	0,0
	October	56,6	0,59	33,6	88,8	10,7	33,6	44,5	0,0
	November	28,1	0,99	26,0	84,8	15,6	26,0	12,0	31,1
	December	23,1	1,06	24,5	99,5	16,4	24,5	-0,8	59,5

ET_{0a}: reference evapotranspiration corrected for acclivity coefficient;
$K_{c\ Ws}$: unique 'crop' coefficient of the territory;
ET_c: crop evapotranspiration of the territory;
$P_{a:}$ precipitation values corrected for acclivity coefficient;
RO: runoff;
aET_c: actual crop evapotranspiration;
ΔAW: variation of the available water with respect to the previous day; and
DP: deep percolation.

Table S.17. Monthly values of the phenological soil water balance in the period 2015-2016

		$ET0_a$	$K_{c\ Ws}$	ET_c	P_a - RO - aET_c - ΔAW = DP				
					P_a	RO	aET_c	ΔAW	DP
2015	January	36,3	0,72	24,6	30,2	0,5	24,6	-0,5	5,5
	February	26,6	1,04	27,5	157,7	47,8	27,5	-0,3	82,7
	March	66,3	0,84	54,2	152,5	33,5	54,2	-10,9	75,8
	April	108,5	0,68	72,3	79,1	7,6	72,3	-8,5	7,8
	May	138,1	0,93	127,5	106,8	15,9	114,5	-23,6	0,0
	June	166,2	0,97	161,0	33,6	0,0	95,6	-62,0	0,0
	July	206,0	0,83	170,5	2,9	0,0	19,5	-16,6	0,0
	August	148,3	0,78	115,9	51,2	0,0	31,0	20,2	0,0
	September	104,1	0,69	65,3	62,9	0,0	27,9	35,0	0,0
	October	41,9	0,88	37,7	119,6	2,7	37,7	67,4	11,8
	November	30,1	0,65	19,0	52,5	5,6	19,0	-1,7	29,6
	December	14,0	0,31	4,9	1,7	0,0	4,9	-3,2	0,0
2016	January	34,1	0,89	30,0	75,6	13,6	30,0	-8,1	40,2
	February	42,7	0,84	34,6	101,9	11,8	34,6	13,7	41,8
	March	62,4	0,88	51,2	109,7	21,1	51,2	-11,1	48,4
	April	102,5	0,71	72,6	53,4	2,1	72,6	-21,3	0,0
	May	129,3	1,00	129,2	96,9	17,3	127,8	-52,2	4,0
	June	151,4	0,98	147,8	84,8	4,8	104,8	-24,8	0,0
	July	176,4	0,77	136,9	62,0	0,1	51,9	10,0	0,0
	August	153,1	0,68	104,0	11,9	0,0	33,2	-21,3	0,0
	September	96,9	0,74	70,4	55,4	0,0	34,9	20,5	0,0
	October	42,3	0,93	37,9	78,6	0,0	35,8	42,8	0,0
	November	28,4	1,06	29,9	99,6	8,0	29,9	55,0	6,7
	December	24,1	0,31	8,4	4,0	0,0	8,4	-4,5	0,0

ET_{0a}: reference evapotranspiration corrected for acclivity coefficient;
$K_{c\ Ws}$: unique 'crop' coefficient of the territory;
ET_c: crop evapotranspiration of the territory;
$P_{a:}$ precipitation values corrected for acclivity coefficient;
RO: runoff;
aET_c: actual crop evapotranspiration;
ΔAW: variation of the available water with respect to the previous day; and
DP: deep percolation.

Table S.18. Monthly values of the phenological soil water balance in the period 2017-2019.

		$ET0_a$	$K_{c\ Ws}$	ET_c	P_a - RO - aET_c - ΔAW = DP				
					P_a	RO	aET_c	ΔAW	DP
2017	January	21,3	0,9	17,9	85,4	17,8	17,9	2,1	47,6
	February	38,6	0,9	33,3	82,1	13,5	33,3	1,8	33,5
	March	86,2	0,5	41,3	44,5	12,5	41,3	-24,3	14,9
	April	108,8	0,7	79,1	72,1	3,6	79,1	-10,6	0,0
	May	140,5	1,0	142,1	46,7	0,0	114,0	-67,4	0,0
	June	194,9	1,0	195,2	14,3	0,0	22,5	-8,2	0,0
	July	208,5	0,8	164,2	35,2	0,0	35,6	-0,4	0,0
	August	184,9	0,7	135,0	11,3	0,0	20,3	-9,0	0,0
	September	97,3	0,8	79,7	162,5	2,9	61,9	97,7	0,0
	October	64,3	0,5	31,0	15,4	0,0	31,0	-15,7	0,0
	November	31,3	1,0	30,5	110,4	15,6	30,5	40,9	23,5
	December	28,5	1,1	30,7	72,4	5,8	30,7	-1,6	37,4
2018	January	31,7	0,6	17,8	11,4	0,0	17,8	-8,0	1,6
	February	20,3	1,0	20,6	194,4	42,9	20,6	8,4	122,5
	March	60,7	0,9	51,0	138,4	17,6	51,0	-13,7	83,5
	April	110,4	0,7	76,5	33,1	0,1	76,5	-43,5	0,0
	May	114,8	1,0	111,0	94,9	2,6	111,0	-18,6	0,0
	June	154,4	0,9	145,4	18,0	0,0	59,9	-41,9	0,0
	July	174,1	0,8	133,1	71,0	0,0	54,6	16,5	0,0
	August	149,6	0,7	104,0	19,8	0,0	27,5	-7,7	0,0
	September	95,9	0,6	61,4	50,3	0,0	42,5	7,9	0,0
	October	48,8	0,8	39,3	76,6	0,0	37,2	39,4	0,0
	November	22,0	0,9	18,3	94,9	6,4	18,3	61,1	9,0
	December	19,9	1,0	19,6	52,5	5,1	19,6	-6,8	34,6
2019	January	24,4	1,0	24,1	68,2	2,9	24,1	6,8	34,5
	February	45,6	0,7	29,1	22,1	1,3	29,1	-19,2	10,9
	March	90,4	0,5	46,5	34,0	0,5	46,5	-12,9	0,0
	April	89,2	0,7	65,8	76,6	1,4	65,8	9,4	0,0
	May	98,0	1,0	96,4	189,1	39,6	96,4	18,5	34,6
	June	183,4	1,0	176,5	2,4	0,0	115,0	-112,6	0,0
	July	176,6	0,8	134,6	81,8	0,1	46,1	35,6	0,0
	August	155,3	0,7	106,9	29,9	0,0	63,6	-33,7	0,0
	September	103,2	0,7	74,4	79,9	0,0	51,4	28,5	0,0
	October	58,4	0,5	29,5	39,2	0,0	29,4	9,8	0,0
	November	30,1	1,0	29,9	123,7	8,8	29,9	72,4	12,6
	December	45,2	0,7	28,7	56,0	5,9	28,7	0,6	20,8

ET_{0a}: reference evapotranspiration corrected for acclivity coefficient;
$K_{c\ Ws}$: unique 'crop' coefficient of the territory;
ET_c: crop evapotranspiration of the territory;
$P_{a:}$ precipitation values corrected for acclivity coefficient;
RO: runoff;
aET_c: actual crop evapotranspiration;
ΔAW: variation of the available water with respect to the previous day; and
DP: deep percolation.

SUPPLEMENTARY MATERIAL 7

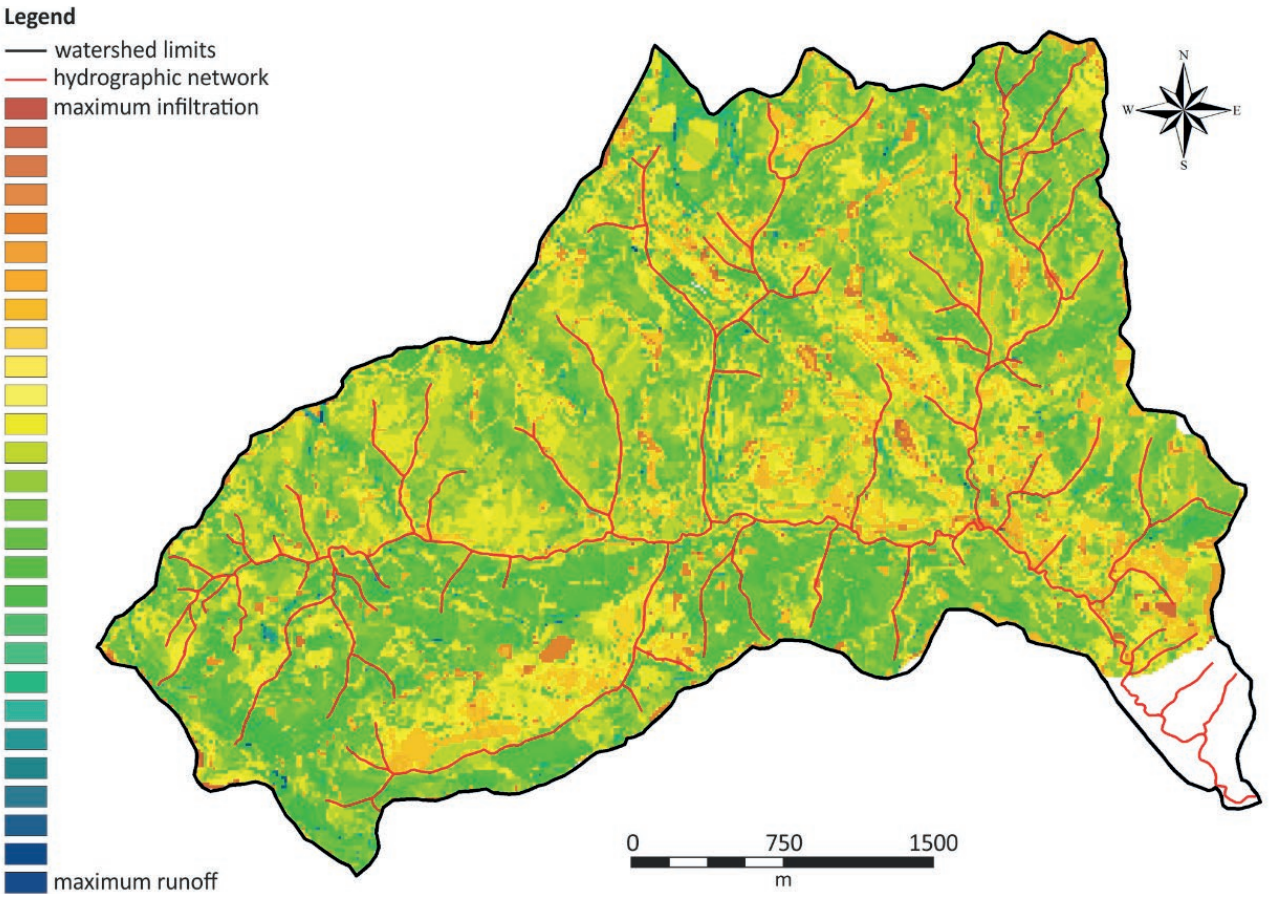

Figure S5. Map of the infiltration/runoff propensity obtained as overlapping layers of land use, hydrologic soil groups, slope and aspect. The processing was carried out up to the section in which the discharges of the Santa Maria degli Angeli stream were measured.

Italian Journal of Agrometeorology
Rivista Italiana di Agrometeorologia

Firenze University Press
www.fupress.com/ijam

OPEN ACCESS

Citation: Messeri, A., Arcidiaco, L., Bianca, E., Tiako, D., Orlandini, S., Messeri, G. & Mancini, M. (2024). Effects of air temperatures on acacia and chestnut honey yields: case study in Italy. *Italian Journal of Agrometeorology* (1): 49-58. doi: 10.36253/ijam-2296

Received: September 6, 2023

Accepted: May 31, 2024

Published: August 2, 2024

Data Availability Statement: All relevant data are within the paper and its Supporting Information files.

Competing Interests: The Author(s) declare(s) no conflict of interest.

ORCID:
AM: 0000-0001-8220-811X

Effects of air temperatures on acacia and chestnut honey yields: case study in Italy

Alessandro Messeri[1,*], Lorenzo Arcidiaco[1], Evangelista Bianca[2], Djialeu Tiako[2], Simone Orlandini[2,3], Gianni Messeri[1], Marco Mancini[2,3]

[1] *Institute of Bioeconomy, National Research Council (IBE-CNR), 50019 Florence, Italy*
[2] *Department of Agriculture, Food, Environment and Forestry (DAGRI), University of Florence, 50144 Florence, Italy*
[3] *Fondazione per il clima e la sostenibilità. Via G.Caproni. 50146, Florence, Italy*
*Corresponding author. Email: alessandro.messeri@ibe.cnr.it

Abstract. Global honey production is increasing.In Italy, the two predominant monovarietal honey types are acacia and chestnut . Climate change, with an increase in extreme weather events (including droughts, heat waves and late frosts), impacts both the phenology of melliferous species andhoneybee activity. The aim of this study was to correlate the honey yields of acacia and chestnut in five Italian climatic sub-regions with the thermal extremes during the flowering phases of the two melliferous species. The objective was to understand the impact that these parameters have on yields.The results highlighted differing impacts of thermal extremes on honey yields for acacia and chestnut, respectively . In the acacia, temperature below 4.3C° in the flowering period had a negative impact particularly in the North-West ($P<0.01$). Instead temperatures above 17.5C° impacted positively in North Italy. In contrast, for chestnut, temperatures above 23.5C° negatively affected honey yields in the North-West. Understanding the interaction between climate, melliferous species and bees is useful for beekeepers towards developing adaptation strategies to climate change with the aim of protecting the yields, income, animal welfare and ecosystem services.

Keywords: bees, climate change, agrometeorology, plant phenology, ERA5 land.

1. INTRODUCTION

Honey production is rising on a global level with an 85 % increase in the number of managed honeybee colonies reported for the 1961-2017 period (Phiri et al. 2022). In Italy honey production was 0.026Mt in 2021 and according to ISMEA (2020), the increase in the last 10 years was attributable to the growth in the number of professional and amateur beekeepers. In 2022 the recorded number of beekeepers was 72020 (Report Osservatorio nazionale del miele 2022) with 60 monovarietal honey types. However, annual production is strongly influenced by the weather conditions (Rahimi_2021, Delgado et al. 2012, Olvera et al. 2023). Acacia (*Robinia pseudoacacia L.*) and chestnut (*Castanea sativa L.*) honeys in Italy represent the two main mono-

varietal types spread over almost the national territory (Parri et al. 2014). From both observational and experimental studies, it is well established that climate change has been associated with an alteration of phenological cycles, resulting in an earlier onset of vegetation activity in spring with effects on the related leaf-out and flowering dates (Piao et al. 2019). Strong relationships were found between phenological events and early spring weather (Sparks and Carey 1995, Linderholm 2006, Richardson et al. 2013) with vegetal species respond to a rise in temperature by coming into leaf or/and flowering earlier. It is projected that in the future, leaf and flowering dates will to be 3-4 weeks earlier than present (IPCC 2023, Simpson et al. 2023). In Italy there are insufficient studies investigating the impact of meteo-climate conditions on honeybee production. Nonetheless, there have been research reports correlating the activity of bees, phenological period and resultant honey production with climatic factors (Wyver et al. 2023a, Wyver et al. 2023b, Blasi et al. 2023). It has been found (Medina 2018) from simulated bee stress conditions in the laboratory thatf high temperatures (<= 40°C) influenced on the phenotype and behavior of honey bees under heat stress, with potential consequences for colony fitness (Medina 2018). In two sites in Portugal, Fernandes et al. (2015) in Portugal showed that high rainfall and low temperatures advanced vegetative growth and early flowering in the northern study site, whereas high temperatures with no rainfall advanced growth and ripening phase of fruits in the southern site. Previous work demonstrated that the increase in average temperatures in winter and early spring accelerated the phenological development of plants by interacting with the activity of pollinators in the various ecosystems (Hung e al 2018, Villagomez et al. 2021, Hunichen et al. 2021, Mashilingi et al. 2022,). A decrease in honey production under extreme drought conditions was also observed in a case study in Cordoba, Spain (Flores et al. 2019). Zhao et al. (2021) highlighted two temperature values, 5°C and 10°C of daily minimum values, which determined the optimal start of bee activity inside and outside the hive, respectively In China an increase in temperatures and a reduction in rainfall, respectively, was shown to alter the phenology of plants in general but more specifically honey plants (Guo et al. 2013). The growing season expanded by 4.3 days per decade in Beijing region with the first flowering was advanced by high temperatures between January and June, but delayed by warm conditions during the chill accumulation phase.

Moreover, it was reported that from 1956 to 2010, the budding of many honey plants, was progressively brought forward, up to 13.5 days, with impacts on the subsequent phenological stages of many honey species (Juknys et al. 2011). This was corroborated by Visser and Both (2005), demonstrating an advance from 3 to 11 days in the manifestation of many phenological phases of cultivated species during the end of winter and the beginning of spring. Also Dalla Marta_et al. (2010) showed that the phenology of Montepulciano vine progressively advances for one day every 2 years in the budding and flowering phases. Back in 2005 (Peat amd Goulson 2005)attention was already drawn to the effects of climate change. Those authors pointed out that climate change modifies the quality and quantity of available nectar and/or pollen, limiting its collection by pollinating insects. Southern European countries, including Italy, are among the most critically affected by climate change in Europe and the situation is expected to worsen in the coming decades with an impact both temperatures and precipitation distribution (IPCC 2021). A variation in the distribution of precipitation regimes and temperatures in different Italian areas were evidenced (Brunetti et al. 2006) These variations were also highlighted by studies on a regional scale (Bartolini et al. 2014) with a decrease in precipitation during winter and spring, especially in northwestern areas. Regarding temperatures, an increase was observed during all months of the year, also associated with an increase in heat waves. More recently, Bartolini et al. (2021) demonstrated both spatial and temporal changes in dry spells in Central Italy during the 1955–2017 period. Given the climate changes and impacts on the phenology of honeybee species, the aim of the present study is to correlate the honey yields of acacia and chestnut with the thermal extremes during the flowering phases of the two species, within five Italian climatic sub-regions, in order to understand the impact of these environmental parameters on yields.

2. MATERIALS AND METHODS

2.1. Climatological dataset (Era5 Land)

Climatological data was obtained by the ERA5 reanalysis dataset from 1950 at a 0.1° resolution.The data wasstored in a tridimensional hypercube data store where the first two dimensions represented spatial dimensions (Longitude and Latitude) and the third, a time dimension. Taking into account the high heterogeneity in climate (Martinelli and Matzarakis 2017), Italy divided into 5 climatic sub-regions (North West, NW; North East, NE; Northern Central Tyrrhenian, NCT; Central Adriatic, CA; South, S) (Figure 1), each describing the different climatic zones in the April-July period. Recently a simi-

Figure 1. Italian climatic sub-regions used in the study. North West, NW; North East, NE; Northern Central Tyrrhenian, NCT; Central Adriatic, CA; South, S.

lar approach was used in studies investigating the impact of atmospheric circulations on the crop yields in specific Italian sub-areas (Central and North-East Italy) (Salinger et al. 2020, Salinger et al. 2022).

2.2. Honey production

The production of acacia and chestnut honey was obtained from the National Honey Observatory annual reports (https://www.informamiele.it/). The database reports the average production in kg/hive on a regional scale for the period 2015-2022. For each climatic sub-area, an average was calculated (Figure 2).

2.3. Phenological data

Phenological data for chestnut and acacia were acquired from the Italian PHEnology Network (IPHEN) database, a national system of monitoring based on comprehensive phenological observations for some plant species. IPHEN is a cooperative project that started in 2006 with theaim of producing nationwide maps analysis maps and forecasts for the phenological stages of plants of interest to agriculture, health, and environmental care. More details about the IPHEN dataset have been described by Mariani et al. (2012).

For acacia and chestnut, weekly IPHEN phenological maps shows the BBCH phenological stadium (Meier 2001, Meier 2018) for each vegetative season. The Day Of the Year (DOY) when 50% of flowering occurs in most of the domain was estimated for each of the Italian climatic sub-regions. DOY was considered as the Annual Zonal Peak Flowering (AZPF) in the present study. Starting from the AZPF, a temporal flowering window (FW) of 16 days (Figure 3) was derived, The FW ranges from 7 days before the AZPF to 7 days after.

2.4. Data processing and statistical analysis

For each macro-climatic area, average daily temperature data was obtained from each pixel (0.1° x 0.1°, Lat/Lon). During FW, the number of days (occurrence) for different thermal extremes were calculated. These extremes were identified with the following percentile classes: 2,10,15, 25, 75, 80, 85, 90 and 98 respectively. The occurrence was calculated during the period 1950-2022. The data obtained was than related to the honey production for the two melliferous species using a linear correlation.

Statistical analyses were carried out in the Conda 4.2 open source, using the Python 3.8 programming language, related temporal and statistical analysis (XArray, SciPy, Statistics, Numpy, Pandas) and visualization (Matplotlib) modules.

3. RESULTS AND DISCUSSION

3.1. Effects of low temperature on honey production

The effect of low temperature anomalies had a significant negative impact only on acacia honey yields in Northern Italy (Table 1).

The NW Italian area showed the highest significance ($p<0.01$) with a negative impact of low temperatures for all percentile classes except for the most extreme one (2th).

This result can be explained by the fact that during the acacia flowering period (May) the low air temperatures impacted negatively on bee activity. The present work corroborated a recent study carried out on Rho-

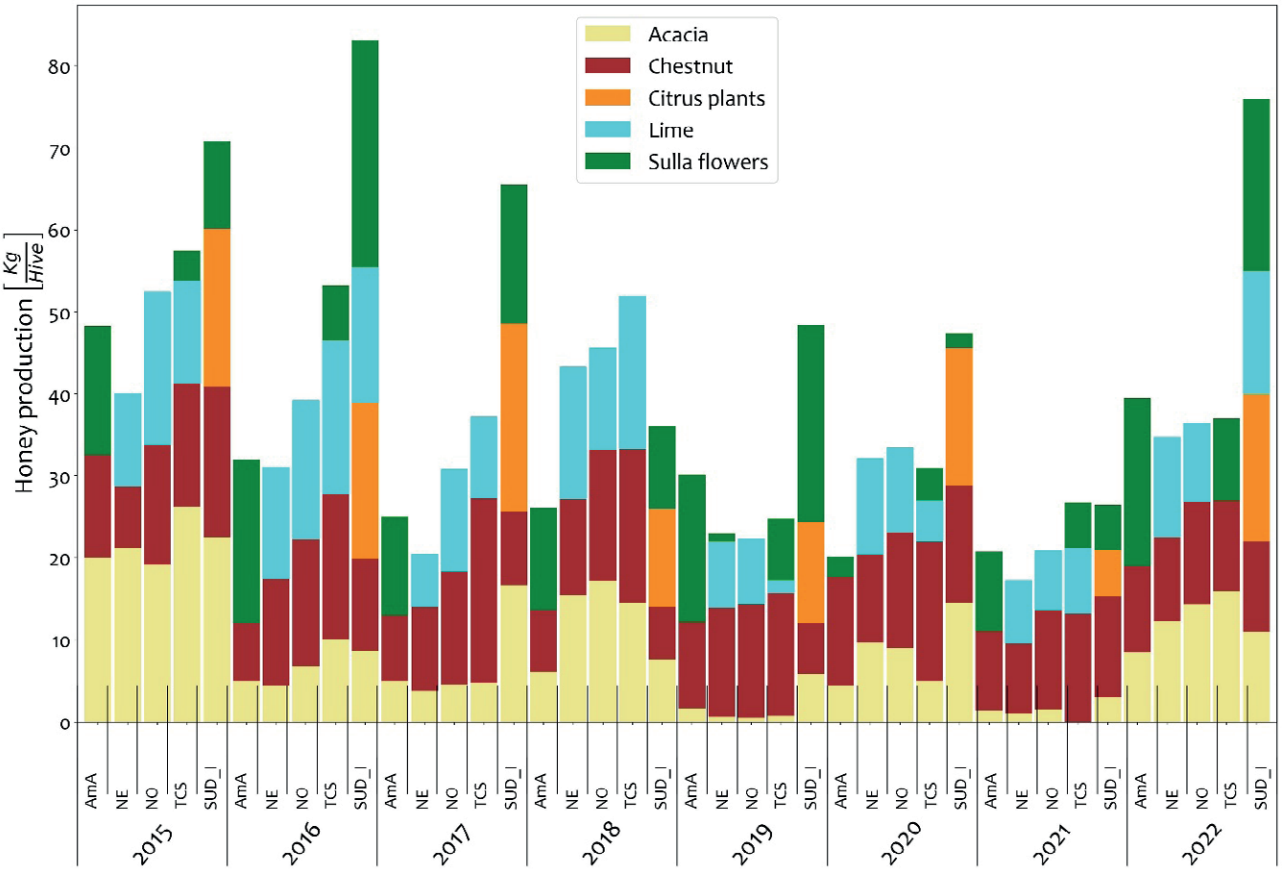

Figure 2. Production in kg/hive for each climatic sub-area in the period 2015-2022.

des Island, from 2015 to 2019, showing a link between wildflower honey production and the main microclimatic parameters (air temperature and humidity). The results showed that the optimal temperature values for the daily production of honey in spring were around 17°C, while below 14°C the balance between the honey produced and consumed became negative (Gounari et al. 2022). This was also confirmed in an earlier study demonstrating that bee foraging activity was reduced to the point of cessation at 6.5°C (Oshi and Joshi 2010). Instead, foraging activity was shown to increase at higher temperatures reaching a maximum peak around 20°C (Tan et al. 2012).

Furthermore, as is well-documented, air temperature is a determining factor of the plant species phenology (Alilla et al. 2022). *Robinia pseudacacia* was shown to be particularly damaged by late frosts which negatively impact young leaves, shoots and flowers thereby reducing the availability of food for the bee (Vítková et al. 2017). Of note, it is important to take into consideration that the low percentiles in northern Italy had lower values than the temperatures obtained in central and southern Italy.

As far as the chestnut honey yields are concerned, the analysis did not show statistical significance as regards the low temperatures. The chesnut flowering period (June) occurrs one month later than Acacia, and for this reason low temperatures are not conditioning chesnut flowering.

3.2. Effects of high temperature on honey production

The effect of positive temperature anomalies on acacia honey yields was positive in most macro-areas (Table 2) with statistical significance in NW, NE, NCT, CA.

In North Italy and in NCT, the greatest significance occurred in the less extreme percentiles. The highest significances ($P<0.001$) were observed in North Italy in the 75th percentile class.

The positive effect of high temperature is in agreement with that shown by Tan et al. (2012) who identified that the maximum bee foraging activity occurred

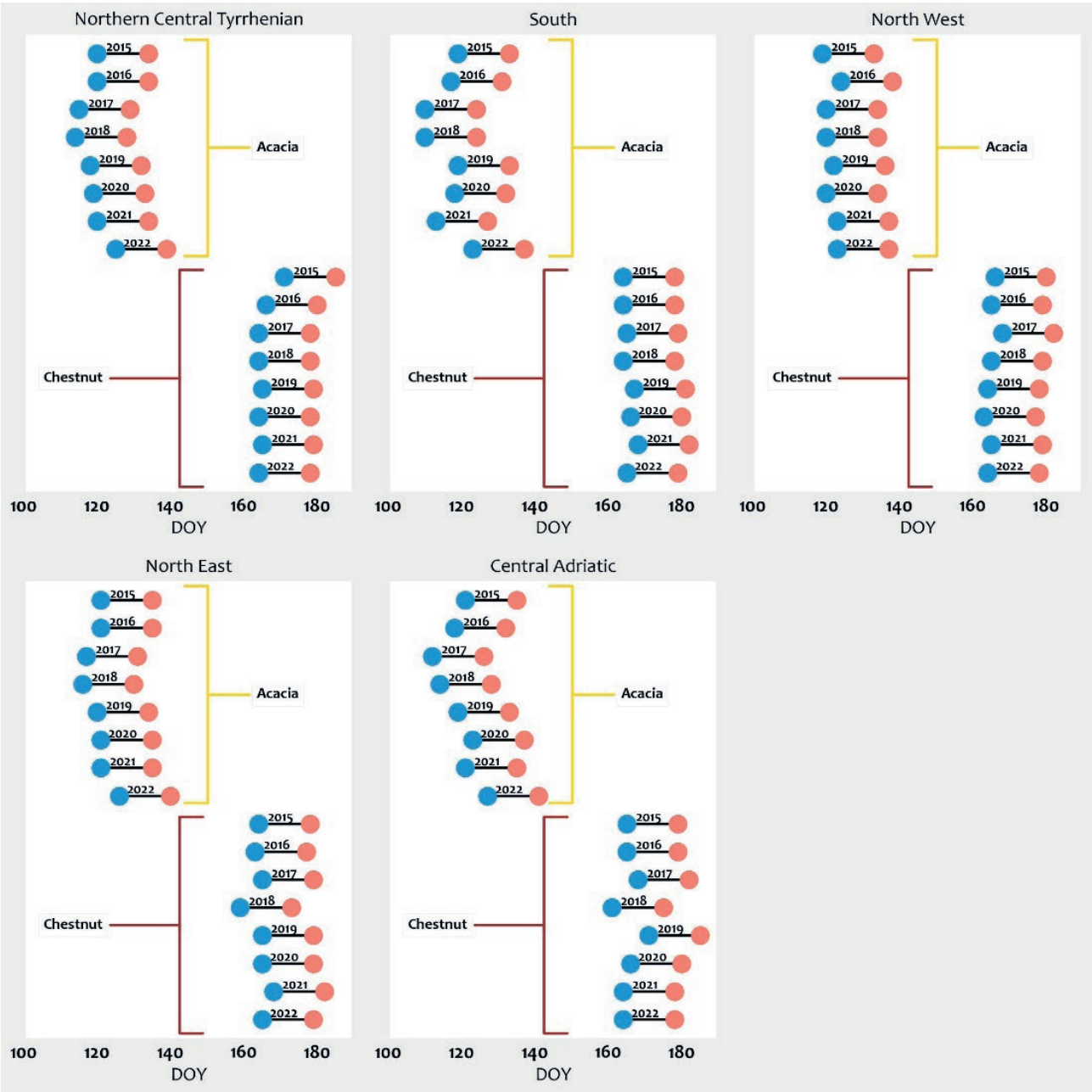

Figure 3. Acacia and chestnut flowering windows for each Italian climatic sub-region.

in the spring with temperatures close to 20°C. This temperature also has a positive effect on the nectar characteristics which becomes more available to the insects and contained a higher sugar content (Bertsch 1983, Kim et al. 2020). Furthermore, Alilla et al. (2022) found a greater nectar quantity in the advanced stages of flowering in *Robinia pseudacacia* a greater nectar quantity with maximum availability starting from the second week. The higher temperatures were also shown to allow a faster opening of the inflorescences, reducing the time period needed by the bees to obtain nectar (Giovannetti et al. 2013).

In Southern Italy, high temperatures did not have a significant effect on honey yields.

In contrast, for Chestnut honey yields, the positive temperature anomalies were generally shown to have a negative impact, significant in the NW climatic sub-region, with a reduction especially for the 85th and 90th percentile (Table 3).

Table 1. Correlation coefficient (r) and significance (sig) of the correlations between low temperatures and Acacia honey production. NS Not significant; * P<0.05; ** P < 0.01; *** = P<0.001%; NW = North West; NE = Nord East; NCT = Northern Central Tyrrhenian; CA = Central Adriatic; S =South. tt= average temperature of the percentile for each Italian climatic sub-regions.

		Climatic sub-regions														
Acacia		NW			NE			NCT			CA			S		
		r	sig	tt	r	sig	tt	r	sig	tt	r	sig	tt	r	sig	tt
percentile	2	-0.49	NS	1.0	0.00	NS	1.3	0.00	NS	4.4	0.00	NS	2.2	0.00	NS	5.2
	10	-0.70	**	2.7	-0.51	NS	3.2	-0.49	NS	6.0	-0.38	NS	4.0	-0.38	NS	6.4
	15	-0.82	**	3.3	-0.61	NS	3.8	-0.49	NS	6.4	-0.35	NS	4.5	-0.55	NS	6.9
	20	-0.79	**	3.9	-0.63	NS	4.4	-0.51	NS	6.9	-0.47	NS	5.0	-0.51	NS	7.3
	25	-0.88	***	4.3	-0.67	*	4.8	-0.60	NS	7.2	-0.58	NS	5.5	-0.56	NS	7.7

Table 2. Correlation coefficient (r) and significance (sig) of the correlations between high temperatures and Acacia honey yields. NT Not significant; * P<0.05; ** P < 0.01; *** = P<0.001%; NW = North West; NE = Nord East; NCT = Northern Central Tyrrhrenian; CA = Central Adriatic; S =South. tt= average temperature of the percentile for each Italian climatic sub-region.

		Climatic sub-regions														
Acacia		NW			NE			NCT			CA			S		
		r	sig	tt	r	sig	tt	r	sig	tt	r	sig	tt	r	sig	tt
percentile	75	0.89	***	17.5	0.93	***	18.0	0.76	*	20.2	0.66	*	19.4	0.23	NS	20.4
	80	0.84	**	18.0	0.92	***	18.5	0.83	**	20.6	0.74	*	20.0	0.16	NS	20.9
	85	0.71	*	18.5	0.89	***	19.0	0.83	**	21.0	0.69	*	20.5	0.15	NS	21.5
	90	0.78	*	19.2	0.86	**	19.7	0.84	**	21.6	0.73	*	21.2	0.01	NS	22.3
	98	0.76	*	21.2	0.63	NS	21.5	0.86	**	23.8	0.63	NS	23.4	0.08	NS	24.7

Table 3. Correlation coefficient (r) and significance (sig) of the correlations between high temperatures and Chestnut honey yields. NE = Not significant ; * P<0.05; ** P < 0.01; *** = P<0.001%; NW = North West; NE = Nord East; NCT = Northern Central Tyrrhrenian; CA = Central Adriatic; S =South. tt= average temperature of the percentile for each Italian climatic sub-region.

		Climatic sub-regions														
Chestnut		NW			NE			NCT			CA			S		
		r	sig	tt	r	sig	tt	r	sig	tt	r	sig	tt	r	sig	tt
percentile	75	-0.73	*	23.5	0.19	NS	24.2	-0.26	NS	27.1	-0.19	NS	26.2	-0.25	NS	28.3
	80	-0.72	*	24.1	0.23	NS	24.8	-0.26	NS	27.5	-0.15	NS	26.9	-0.19	NS	28.9
	85	-0.84	**	24.8	0.07	NS	25.4	-0.30	NS	28.1	-0.14	NS	27.5	-0.12	NS	29.6
	90	-0.79	**	25.6	-0.05	NS	26.2	-0.23	NS	28.8	-0.13	NS	28.4	-0.01	NS	30.3
	98	-0.508	NS	27.9	0.333	NS	28.2	-0.679	*	30.8	-0.01	NS	30.6	0.11	NS	32.7

This result can probably be explained by the change in nectar characteristics with air temperature. In a recent study on *Castanea sativa*, it has highlighted that a higher sugar content was present in the nectar with average daily air temperatures between about 22 and 25°C but that the sugar content tended to rapidly decrease with higher air temperatures (Kim et al. 2020).

In addition, studies have highlighted a positive role of high air humidity levels in the nectar characteristics. In particular, an increase in the sugar content produced by numerous herbaceous flowers, shrubby and tree species with high air humidity was reported Corbet et al. (1979). Therefore, if we consider that over the last few decades, the northern Italian areas have experienced

negative rainfall anomalies (Caloiero et al. 2021) and an increase in drought episodes (Baronetti et al. 2020), the decrease in honey production could also be explained by low air humidity.

However, this result cannot be generalized to all melliferous species. In fact, a study on the evaluation of the sugar content in the nectar of *Epilobium angustifolium* (Bertsch 1983) did not show significant differences at different air humidity rates (50%, 78%, 94%).

The main strength of the present study was to draw cognitive awareness to the complex interaction of plant, insect, man and climate. To date, correlation studies between honey production and meteorological parameters are still scarce, especially in the Mediterranean Basin.However, these correlation studies can provide a very useful tool for beekeepers to understand production dynamics. Furthermore, the use of ERA5 Land spatialized data can also be very useful in instances where ground meteorological stations are not sufficiently near apiaries.

This preliminary study must is to be considered as a starting point for understanding the dynamics correlating climate with bee activity and phenology of melliferous species. However, some limitations were shown to exist. The first limitation was the represented by the limited sample size. The number of years of production is in fact rather limited and does not allow for a sufficient comparison with the thermal extremes. Furthermore, the climatic data was calculated as an average of the macro-area, also including information from pixels of areas not suitable for the two honey species. Probably, a comparison with the Corine Land Cover could help in better defining the thermal characteristics of the areas.

Future studies are aimed at increasing the sample size, extending the study to other honey types, thereby including other melliferous species. This would also make it possible to increase the honey production window to the entire summer. In addition, overwintering conditions, effects of pests on hive health conditions should be taken into account in future studies.

Furthermore, the correlation analysis could also be extended to other meteorological parameters (e.g. wind, air humidity), which which also may play an important role in both bee activity and nectar availability. For this reason, a cross-disciplinary research in environmental sciences that make available long historical series of climatic-environmental data (for example Itineris Project,Italian Integrated Environmental Research Infrastructures System), colud be very useful in order to improve this type of research by including case studies on honey yields in specific sites.

4. CONCLUSION

Our study showed that air temperature was able to describe the trend of acacia and chestnut honey yields in Italy under many situations. Above all, high temperatures (higher percentiles) were shown to exert a positive impact on the spring acacia honey yields, especially in the more northern latitudes (North and central Italy) where cold spells are generally more likely during the spring. In contrast, the chestnut honey yields seemed to be negatively influenced by the higher air temperature which impacted on both honeybee activity and on the phenology of the melliferous species. These results, especially in the contest of climate change, could be very useful in understanding the mechanisms of interaction between climate, melliferous species and bees. In particular, the integration of the results obtained using models for estimating honey production as a function of the expected climatic conditions could allow for an early estimation of honey production in the various Italian climatic macro-areas. Moreover, the use of seasonal forecasts assist beekeepers in choosing the locations in which to carry out nomadism. The study was performed with a view to provide to beekeepers a tool that allows to adopt adaptation strategies to counteract climate change effects and consequently to protect production, income, animal welfare and ecosystem services.

ACKNOWLEDGEMENT

Activities were carried out as part of the “BEEWIN” project “Bando Miele” 2021-MASAF and ITINERIS (Italian Integrated Environmental Research Infrastructures System) PNRR project (IR0000032).

REFERENCES

Alilla R., De Natale F., Epifani C., Parisse B., Cola G., 2022. The Flowering of Black Locust (Robinia pseudoacacia L.) in Italy: A Phenology Modeling Approach. Agronomy, 12, 1623. https://doi.org/10.3390/ agronomy12071623.

Balvino-Olvera F.J., Lobo J.A., Aguilar-Aguilar M.J. et al. 2023. Long-term spatiotemporal patterns in the number of colonies and honey production in Mexico. Sci Rep 13, 1017. https://doi.org/10.1038/s41598-022-25469-8;

Baronetti A., González-Hidalgo J.C., Vicente-Serrano S.M., Acquaotta F., Fratianni S. 2020. A weekly spatio-temporal distribution of drought events over the

Po Plain (North Italy) in the last five decades. Int J Climatol 40(10), 4463–4476. https://doi.org/10.1002/joc6467.

Bartolini G., Betti G., Gozzini B., Iannuccilli M., Magno R., Messeri G., Spolverini N., Torrigiani T., Vallorani R., Grifoni D., 2021. Spatial and temporal changes in dry spells in a Mediterranean area: Tuscany (central Italy), 1955–2017. International Journal of Climatology, 42(3), 1670-1691. https://doi.org/10.1002/joc.7327.

Bartolini G., Messeri A., Grifoni D., Mannini D., Orlandini S., 2014. Recent trends in seasonal and annual precipitation indices in Tuscany (Italy). Theor. Appl. Climatol. 118, 147–157. https://doi.org/10.1007/s00704-013-1053-3.

Bertsch A.,1983. Nectar production of Epilobium angustifolium L. at different air humidities; nectar sugar in individual flowers and the optimal foraging theory. Oecologia. 59(1), 40-8. https://doi.org/10.1007/BF00388069. Epub 2004 Sep 13. PMID: 25024144.

Blasi M., Carrié R., Fägerström C., Svensson E., Persson A.S. 2023. Historical and citizen-reported data show shifts in bumblebee phenology over the last century in Sweden. Biodivers Conserv 32, 1523–1547. https://doi.org/10.1007/s10531-023-02563-5

Brunetti M., Maugeri M., Monti F., Nanni T., 2006. Temperature and precipitation variability in Italy in the last two centuries from homogenized instrumental time series. Int. J. Climatol. 26, 345–381. https://doi.org/10.1002/joc.1251.

Caloiero T., Caroletti G.N., Coscarelli R., 2021. IMERG-Based Meteorological Drought Analysis over Italy. Climate, 9, 65. https://doi.org/10.3390/cli9040065.

Corbet S.A., Willmer P.G., Beament J.W.L., Unwin D.M., Prys-jones O.E., 1979. Post-secretory determinants of sugar concentration in nectar, 2(4), 293–308. https://doi.org/10.1111/j.1365-3040.1979.tb00084.x.

Dalla Marta A., Grifoni D., Mancini M., Storchi P., Zipoli G., Orlandini S., 2010. Analysis of the relationships between climate variability and grapevine phenology in the Nobile di Montepulciano wine production area. The Journal of Agricultural Science, 148(6), 657–666. https://doi.org/10.1017/S0021859610000432.

Delgado D.L., Perez M.E., Galindo-Cardona A., Giray T., Restrepo C., 2012. Forecasting the Influence of Climate Change on Agroecosystem Services: Potential Impacts on Honey Yields in a Small-Island Developing State. Psyche: A Journal of Entomology, 2012. https://doi.org/10.1155/2012/951215.

Fernandes P., Antunes C., Correia O., Máguas, C. 2015. Do climatic and habitat conditions affect the reproductive success of an invasive tree species? An assessment of the phenology of Acacia longifolia in Portugal. Plant Ecology, 216(2), 343–355. http://www.jstor.org/stable/24557713.

Flores J.M., Gil-Lebrero S., Gámiz V., Rodríguez M.I, Ortiz M-A., Quiles F.J., 2019. Effect of climate change on honeybee colonies in a temperate Mediterranean zone assessed through remote hive weight monitoring system in conjunction with exhaustive colonies assessment. Science of the Total Environment, 653, 1111-11119, https://doi.org/10.1016/j.scitotenv.2018.11.004.

Giovanetti G., Aronne G. 2013. Honey bee handling behaviour on the papilionate flower of Robinia pseudoacacia L. Arthropod-Plant Interact, 7, 119–124. https://doi.org/10.1007/s11829-012-9227-y.

Gounari S., Proutsos N., Goras G., 2022. How does weather impact on beehive productivity in a Mediterranean island? Italian Journal of Agrometeorology 1: 65–81. https://doi.org/10.36253/ijam-1195.

Guo L., Dai J., Ranjitkar S., Xu J., Luedeling E., 2013. Response of chestnut phenology in china to climate variation and change. Agricultural and Forest Meteorology, 180, 164-172. https://doi.org/10.1016/j.agrformet.2013.06.004.

Hung K.L.J., Kingston J. M., Albrecht M., Holway D. A., Kohn J.R., 2018. The worldwide importance of honey bees as pollinators in natural habitats. Proc. R. Soc. B 285, 20172140. https://doi.org/10.1098/rspb.2017.2140.

Hünicken P.L, Morales C.L., Aizen M.A., Anderson G.K.S, García N., Garibaldi L.A., 2021. Insect pollination enhances yield stability in two pollinator-dependent crops. Agriculture, Ecosystems and Environment, 320, 107573. https://doi.org/10.1016/j.agee.2021.107573.

IPCC, 2021. Climate Change 2021: The Physical Science Basis. Contribution of Working Group I to the Sixth Assessment Report of the Intergovernmental Panel on Climate Change[Masson-Delmotte, V., P. Zhai, A. Pirani, S.L. Connors, C. Péan, S. Berger, N. Caud, Y. Chen, L. Goldfarb, M.I. Gomis, M. Huang, K. Leitzell, E. Lonnoy, J.B.R. Matthews, T.K. Maycock, T. Waterfield, O. Yelekçi, R. Yu, and B. Zhou (eds.)]. Cambridge University Press, Cambridge, United Kingdom and New York, NY, USA, In press, https://doi.org/10.1017/9781009157896.

IPCC, 2022. Climate Change 2022: Impacts, Adaptation, and Vulnerability. Contribution of Working Group II to the Sixth Assessment Report of the Intergovernmental Panel on Climate Change [H.-O. Pörtner, D.C. Roberts, M. Tignor, E.S. Poloczanska, K.

Mintenbeck, A. Alegría, M. Craig, S. Langsdorf, S. Löschke, V. Möller, A. Okem, B. Rama (eds.)]. Cambridge University Press. Cambridge University Press, Cambridge, UK and New York, NY, USA, 3056 pp., https://doi.org/10.1017/9781009325844.

ISMEA - Istituto di Servizi per il Mercato Agricolo Alimentare. Report settembre 2022. https://www.ismeamercati.it/api-miele;

Joshi, N.C., Joshi, P. 2010. Foraging behaviour of Apis spp. on apple flowers in a subtropical environment. New York Science Journal, 3(3), 71-76.

Juknys R., Sujetoviene G., Zeimavicius K., Gustainyte J., 2011. Effects of climate warming on timing of lime (Tilia cordata L.) phenology. In Environmental Engineering. Proceedings of the International Conference on Environmental Engineering. ICEE, 8, 139). Vilnius Gediminas Technical University, Department of Construction Economics & Property.

Kim Y.K., Lee S., Song J.H., Kim M.J., Yunusbaev U., Lee M.L., Kim M.S., Kwon H.W., 2020. Comparison of Biochemical Constituents and Contents in Floral Nectar of *Castanea* spp. Molecules. Sep 15; 25(18), 4225. https://doi.org/10.3390/molecules25184225.

Linderholm H.W., 2006. Growing season changes in the last century. Agricultural and Forest Meteorology, 137, 1–14. https://doi.org/10.1016/j.agrformet.2006.03.006.

Mariani L., Parisi S.G., Cola G., Failla O 2012. Climate change in Europe and effects on thermal resources for crops. Int J Biom. https://doi.org/10.1007/s00484-012-0528-8

Martinelli L., Matzarakis A. 2017. Influence of height/width proportions on the thermal comfort of courtyard typology for Italian climate zones, Sustainable Cities and Society, 29, 97–106 pp. https://doi.org/10.1016/j.scs.2016.12.004.

Mashilingi, S. K., Zhang H., Garibaldi L. A., An J. 2022. Honeybees are far too insufficient to supply optimum pollination services in agricultural systems worldwide. Agr. Ecosyst. Environ. 335, 108003. https://doi.org/10.1016/j.agee.2022.108003.

Medina R.G., Paxton R.J., De Luna E., Fleites-Ayil F.A., Medina L.A., Quezada-Euán J.J.G., 2018. Developmental stability, age at onset of foraging and longevity of Africanized honey bees (Apis mellifera L.) under heat stress (Hymenoptera: Apidae). J Therm Biol, 74, 214-225. https://doi.org/10.1016/j.jtherbio.2018.04.003.

Meier U. 2018. Growth stages of mono- and dicotyledonous plants: BBCH Monograph. Quedlinburg: Open Agrar Repositorium. https://doi.org/10.5073/20180906-074619.

Meier U., 2001. Growth Stages of Mono and Dicotyledonous Plants. BBCH Monograph, Federal Biological Research Centre for Agriculture and Forestry, Bonn.

Parri E., Lenzi A, Cifelli M, Restivo A, Degano I., Ribechini E., Zandomeneghi M., Domenici V., 2014. Studio di mieli toscani monoflorali mediante tecniche chimiche cromatografiche e spettroscopiche. Quinto Congresso di Scienze Naturali Ambiente Toscano; Edizioni ETS: Pisa, Italy, 159–169. ISBN 9788846738899.

Peat J., and Goulson D., 2005. Effects of Experience and Weather on Foraging Rate and Pollen versus Nectar Collection in the Bumblebee, Bombus Terrestris. Behavioral Ecology and Sociobiology, 58(2), 152–56. http://www.jstor.org/stable/25063598.

Phiri B.J., Fèvre D., Hidano A., 2022 Uptrend in global managed honey bee colonies and production based on a six-decade viewpoint, 1961-2017. Sci Rep, 12(1), 21298. https://doi.org/10.1038/s41598-022-25290-3. PMID: 36494404; PMCID: PMC9734161.

Piao S., Liu Q., Chen A., Janssens I.A., Fu Y., Dai J., Liu L., Lian X., Shen M., Zhu X., 2019. Plant phenology and global climate change: current progresses and challenges. Global Change Biol 25, 1922–1940. https://doi.org/10.1111/gcb.14619.

Rahimi E., Barghjelveh S., Dong P., 2021. Estimating potential range shift of some wild bees in response to climate change scenarios in northwestern regions of Iran. j ecology environ 45, 14. https://doi.org/10.1186/s41610-021-00189-8.

Report Osservatorio Nazionale del miele 2022. Il valore della terra: agricoltura e nuova ruralità, economia e sostenibilità, qualità e consumo consapevole. Rivista multimediale 1/2023. https://www.informamiele.it/wp-content/uploads/2023/03/Report-2022-Il-Valore-della-Terra-per-web.pdf.

Richardson A.D., Keenan T.F., Migliavacca M., Ryu Y., Sonnentag O., Toomey M. 2013. Climate change, phenology, and phenological control of vegetation feedbacks to the climate system, Agricultural and Forest Meteorology, 69, 156–173. https://doi.org/10.1016/j.agrformet.2012.09.012.

Salinger M., Dalla Marta A., Dalu G., Messeri A., Baldi M., Messeri,G., Vallorani R., Crisci A., Morabito M., Orlandini S., Altobelli F., Verdi L. 2020. Linking crop yields in Tuscany, Italy, to large-scale atmospheric variability, circulation regimes and weather types. The Journal of Agricultural Science, 158(7), 606–623. https://doi.org/10.1017/S0021859620001021.

Salinger M., Verdi L., Dalla Marta A., Dalu G., Baldi M., Messeri G., Messeri, A., 2022. Linking maize yields in Veneto Italy, to large-scale atmospheric variability,

circulation regimes and weather types. The Journal of Agricultural Science, 1–17. https://doi.org/10.1017/S0021859622000545.

Simpson N.P., Williams P.A, Mach K.J., Berrang-Ford L., Biesbroek R., Haasnoot M, Segnon A.C., Campbell D., Musah-Surugu J.I, Joe E.T., Nunbogu A.M., Sabour S., Meyer A.L.S, Andrews T.M., Singh C., Siders A.R., Lawrence J., van Aalst M., Trisos C.H., 2023. Adaptation to compound climate risks: A systematic global stocktake. iScience, 26(2), 105926. https://doi.org/10.1016/j.isci.2023.105926.

Sparks H.T., Carey P.D., 1995. The Responses of Species to Climate Over Two Centuries: An Analysis of the Marsham Phenological Record, 1736-1947. Journal of Ecology, 83(2), 321–329.

Tan K., Yang S., Wang, Z.W., Radloff, S.E., Oldroyd B.P., 2012. Differences in foraging and broodnest temperature in the honey bees Apis cerana and A. mellifera. Apidologie, 43(6), 618–623. https://doi.org/10.1007/s13592-012-0136-y.

Villagomez G., Nurnberger F., Requier F., Schiele S., Steffan-Dewenter I., 2021. Effects of temperature and photoperiod on the seasonal timing of Western honey bee colonies and an early spring flowering plant. Ecology and Evolution, 11(12), 7834–7849. https://doi.org/10.1002/ece3.7616.

Visser M.E and Both C., 2005. Shifts in phenology due to global climate change: the need for a yardstick-Proc. R. Soc. B.2722561–2569. http://doi.org/10.1098/rspb.2005.3356.

Vítková M., Müllerová J., Sádlo J., Pergl J., Pyšek P. 2017. Black locust (Robinia pseudoacacia) beloved and despised: a story of an invasive tree in Central Europe. For Ecol Manage. 15; 384, 287–302. https://doi.org/10.1016/j.foreco.2016.10.057. PMID: 30237654; PMCID: PMC6143167.

Wyver C., Potts S.G., Edwards M., Edwards R., Roberts S., Senapathi D. 2023a. Climate-driven phenological shifts in emergence dates of British bees. Ecology and Evolution 13(7)- https://doi.org/10.1002/ece3.10284.

Wyver C., Potts S.G., Edwards M., Edwards R., Roberts S., Senapathi D. 2023b. Climate driven shifts in the synchrony of apple (Malus x domestica Borkh.) flowering and pollinating bee flight phenology. Agricultural and Forest Meteorology 329, 109281. https://doi.org/10.1016/j.agrformet.2022.109281.

Zhao H., Li G., Guo D. et al. 2021. Response mechanisms to heat stress in bees. Apidologie 52, 388–399. https://doi.org/10.1007/s13592-020-00830-w.

Italian Journal of Agrometeorology
Rivista Italiana di Agrometeorologia

Firenze University Press
www.fupress.com/ijam

OPEN ACCESS

Citation: Babakos, K., Papamichail, D., Pisinaras, V., Tziachris, P., Demertzi, K. & Aschonitis, V. (2024). Using a random cross-validation technique to compare typical regression vs. Random Forests for modelling pan evaporation. *Italian Journal of Agrometeorology* (1): 59-72. doi: 10.36253/ijam-2043

Received: February 10, 2023

Accepted: December 7, 2023

Published: August 2, 2024

Data Availability Statement: All relevant data are within the paper and its Supporting Information files.

Competing Interests: The Author(s) declare(s) no conflict of interest.

ORCID:
KB: 0000-0003-0771-7816
DP: 0000-0002-3214-1348
VP: 0000-0001-6094-7659
PT: 0000-0002-3454-4132
KD: 0000-0003-4842-1974
VA: 0000-0003-4852-5992

Using a random cross-validation technique to compare typical regression vs. Random Forests for modelling pan evaporation

Konstantinos Babakos[1,2], Dimitris Papamichail[2], Vassilios Pisinaras[1], Panagiotis Tziachris[1], Kleoniki Demertzi[3], Vassilis Aschonitis[1,*]

[1] *Soil and Water Resources Institute, Hellenic Agricultural Organization - Dimitra, Thessaloniki 57001, Greece*
[2] *Department of Hydraulics, Soil science and Agricultural Engineering, Faculty of Agriculture, Forestry and Natural Environment, Aristotle University of Thessaloniki, Thessaloniki 54124, Greece*
[3] *Goulandris Natural History Museum, Greek Biotope/Wetland Centre, Thermi-Thessaloniki 57001, Greece*
*Corresponding author. Email: v.aschonitis@swri.gr

Abstract. Pan evaporation (E_{pan}) of class A pan evaporimeter under local semi-arid conditions was modelled in this study based on meteorological observations as input data using an integrated regression approach that includes three steps: a) first step: appropriate selection of transformations for reducing normality departures of independent variables and ridge regression for selecting variables with low collinearity based on variance inflation factors, b) second step (RCV-REG): regression (REG) of the final model with selected transformed variables of low collinearity implemented using an iterative procedure called "Random Cross-Validation" (RCV) that splits multiple times the data in calibration and validation subsets considering a random selection procedure, c) robustness control of the estimated regression coefficients from RCV-REG by analyzing the sign (+ or -) variation of their iterative solutions using the 95% interval of their Highest Posterior Density Distribution (HPD). The iterative procedure of RCV can also be implemented on machine learning methods (MLs) and for this reason, the ML method of Random Forests (RF) was also applied with RCV (RCV-RF) as an additional case in order to be compared with RCV-REG. Random splitting of data into calibration and validation set (70% and 30%, respectively) was performed 1,000 times in RCV-REG and led to a respective number of solutions of the regression coefficients. The same number of iterations and random splitting for validation was also used in the RCV-RF. The results showed that RCV-REG outperformed RCV-RF at all model performance criteria providing robust regression coefficients associated to independent variables (constant signs of their 95% HPD interval) and better distribution of validation solutions in the iterative 1:1 plots from RCV-RF (RCV-RG: R^2=0.843, RMSE=0.853, MAE=0.642, MAPE=0.081, NSE=0.836, Slope(1:1 plot)=0.998, Intercept(1:1 plot)=0.011, and RCV-RF: R^2=0.835, RMSE=0.904, MAE=0.689, MAPE=0.088, NSE=0.818, Slope(1:1 plot)=1.120, Intercept(1:1 plot)=-1.011, based on the mean values of 1,000 iterations). The use of RCV approach in various modelling approaches solves the problem of subjective splitting of data into calibration and validation sets, provides a better evaluation of the final modelling approaches and enhances the competitiveness of typical regression models against machine learning models.

Keywords: Class A pan evaporation, random cross validation, regression model, random forest model, machine learning, Highest Posterior Density Distribution of solutions.

1. INTRODUCTION

Evaporation is among the leading components of the hydrologic cycle since it transforms liquid water into gas form, which is diffused into the atmosphere enriching the clouds that regulate precipitation. For this reason, it is always a hot research topic especially during the last years when the analysis of climate change has become a crucial component in developing water resources management plans (Konapala et al., 2020; Althoff et al., 2020). The evaporative water flow rate from large water bodies is significant and the simulation of this loss is prerequisite to understand the contribution of evaporation to hydrologic cycle under varying climatic conditions.

The most common experimental procedure for measuring water evaporation is the pan evaporation (E_{pan}) method. This method is based on measurements of water level fluctuations in evaporimeter tanks (pans), which have specific properties. The most common evaporimeter types are the class A and the Colorado sunken pans (Doorenbos and Pruitt, 1977; Allen et al., 1998). Although, pan evaporation observations are not equivalent to evaporation rates of large water bodies (e.g. lakes), their values are highly correlated and can be useful in understanding the mechanisms that take place between the water surface and the atmosphere, helping to find transition methods between the magnitudes of the two different evaporation types (i.e. pan, lake evaporation) (Finch and Hall, 2001).

Evaporation measurements are extremely useful for researchers and water resources planners, but the installation and the preservation of evaporation pans exhibits a lot of difficulties since their employment cannot be fully automated (e.g. water filling, cleaning of pan etc). For this reason, pan evaporimeter is not a basic instrument of a meteorological station and this led to many efforts for modelling pan evaporation by using meteorological parameters (Finch and Hall, 2001). The first models that were developed are transformations of energy balance equations in combination with terms of water vapor removal (Penman, 1948, 1956; Brutsaert and Lei Yu, 1968). Later, more comprehensive models were developed, which considered more processes involved in the procedure of evaporation, through the evaluation of existing energy balance models (Xu and Singh, 1998; Molina et al., 2006; Valiantzas, 2006). Other models were simply based on regression analysis using measurements from typical meteorological stations and evaporation pans under various climates that differ in the number of required input variables and their form (Irmak and Haman, 2003; Konvoor and Nandagiri, 2007; Almedeij, 2012).

The last years, artificial intelligence has become very popular in many research fields, as well as in hydrology and agrometeorology, and the derived machine learning (ML) algorithms have significantly improved the performance of modelling efforts. Machine learning models do not consist of mathematical equations, which describe physical processes, but they are data driven models, so called black-box models, and their parameterization and performance depends on the attributes of the available data. Since the beginning of 2000, the first Machine Learning implementation approaches have been implemented to calculate daily E_{pan}, mainly using artificial neural network (ANN) methods and, in general, performed better compared to regression models (Bruton et al., 2000; Keskin and Terzi, 2006; Piri et al., 2009; Rahimikhoob, 2009; Shirsath and Singh, 2010; Tabari et al., 2010; Kim et al., 2012; Alsumaiei, 2020). Except for the ANN models, at that time, researchers had developed models using fuzzy logic to estimate E_{pan} (Keskin et al., 2004; Kisi et al., 2005) and other artificial intelligence methods (genetic programming, regression trees), along with ANN, with adequate performance and in some cases with limited available data (Chang et al., 2013; Shiri et al., 2014; Kim et al., 2015). Later, many researchers attempted to calculate E_{pan} by developing models combining machine learning and numerical analysis (hybrid models). The developed hybrid models, in general, further improved the accuracy of the estimations of E_{pan} compared to the machine learning models (Pammar and Deka, 2015; Deo and Samui, 2017; Wang et al., 2017; Ashrafzadeh et al., 2018; Ghorbani et al., 2018; Seifi and Soroush, 2020; Wang et al., 2020). ML models generally show better performance than regression models, but they are highly dependent on the way the data set is split into training and test set and consequently they are prone to fitting the possible noise of the data set (overfitting) (Dietterich, 1995).

A recently published work by Babakos et al. (2020) provided a new approach for assessing the robustness of regression model coefficients but also for comparing the predictive power of regression and machine learning models. The specific approach was a combination of

bootstrap and cross-validation techniques that allowed to assess the predictive power during the validation procedure considering the probabilistic range (based on highest posterior density distribution) of regression coefficients, statistical metrics (R^2, RMSE) and the slope and intercept of linear trend line from 1:1 plots between observed vs. predicted values. The analysis was based on pan evaporation measurements for assessing reference crop evapotranspiration. The results of the analysis showed that a Random Forest model (machine learning model) showed slightly better statistical metrics (R^2, RMSE) from a regression model, but it was not balanced showing worse slope and intercept values of the trend line than the regression model.

The aim of this study is to develop a regression model for simulating pan evaporation at local conditions by using only meteorological parameters based on the approach of Babakos et al. (2020) and to compare its strength versus a machine learning approach (Random Forests). The steps presented in this paper could be used as example to investigate and compare the proposed regression method against machine learning methods that use only meteorological data for the simulation of pan evaporation.

2. DATA AND METHODS

2.1. Data

Daily meteorological data of precipitation (P), temperature (T), solar radiation (R_s), relative humidity (RH) and wind speed at 2 m above ground (u_2) covering the warm-dry periods (May to September) of 2008 and 2009 were obtained from the meteorological station located in the Aristotle University Farm (~1 m a.s.l., 40°32'08" N, 22°59'18" E) in Thessaloniki (Greece). The daily values of the meteorological parameters were calculated as mean values of hourly observations of a 24-h period. Moreover, a class A pan evaporimeter made by Monel metal with fetch distance F = 1 m (green upwind fetch - Case A) was used for obtaining daily E_{pan} measurements during the same periods of 2008 and 2009. The climate and evaporation data are representative of the warm-dry season conditions of the Thessaloniki Plain in Greece, where the climate is considered as semi-arid Mediterranean environment (Hastie et al., 2009). The 5-month period of May–September is the period for cultivating summer crops, and it is responsible for more than 70% of the annual reference evapotranspiration in the study area (Aschonitis et al., 2018). The meteorological data were used in this study for building models that estimate daily E_{pan}. The records of rainfall days (P > 0) during May–September were excluded from the analysis, leading to a final number of 212 daily records of meteorological and E_{pan} data. The statistical properties and distribution characteristics of the data are given in Table 1 and in Figs. 1,2.

2.2. Methods of analysis

The methodological steps that are going to be followed are provided in the following subsections and in the flowchart presented in Fig. 3.

Table 1. Statistical properties and distribution characteristics of daily measured Class A pan evaporation (E_{pan}), temperature (T), incident solar radiation (R_s), relative humidity (RH), and wind speed at 2 m above ground surface (u_2) after excluding rainfall days.

Parameter	T (°C)	R_s (MJ m^{-2} d^{-1})	RH (%)	u_2 (m s^{-1})	E_{pan} (mm d^{-1})
Minimum	16.70	7.41	31.55	0.85	2.53
Lower quartile	23.79	21.46	47.94	1.20	6.80
Average	25.56	23.87	54.91	1.43	8.14
Median	26.07	24.91	54.99	1.36	8.45
Upper quartile	27.75	27.26	62.10	1.50	9.33
Maximum	31.01	30.04	81.14	3.34	14.85
Range	14.32	22.63	49.58	2.49	12.32
Standard deviation	2.95	4.30	9.65	0.43	2.15
Coeff. of variation	11.56%	18.03%	17.56%	30.32%	26.42%
Stnd. skewness	-3.95	-6.56	0.05	15.26	-0.12
Stnd. kurtosis	0.26	3.66	-1.07	23.09	1.24
Kolmogorov-Smirnov Norm. Test (p-value)*	0.099	<0.05	0.93	<0.05	0.14
Shapiro-Wilk Norm. Test (p-value)*	<0.05	<0.05	0.82	<0.05	<0.05

* p-values <0.05 indicate that data do not follow a normal distribution at 95% confidence level (for both normality tests).

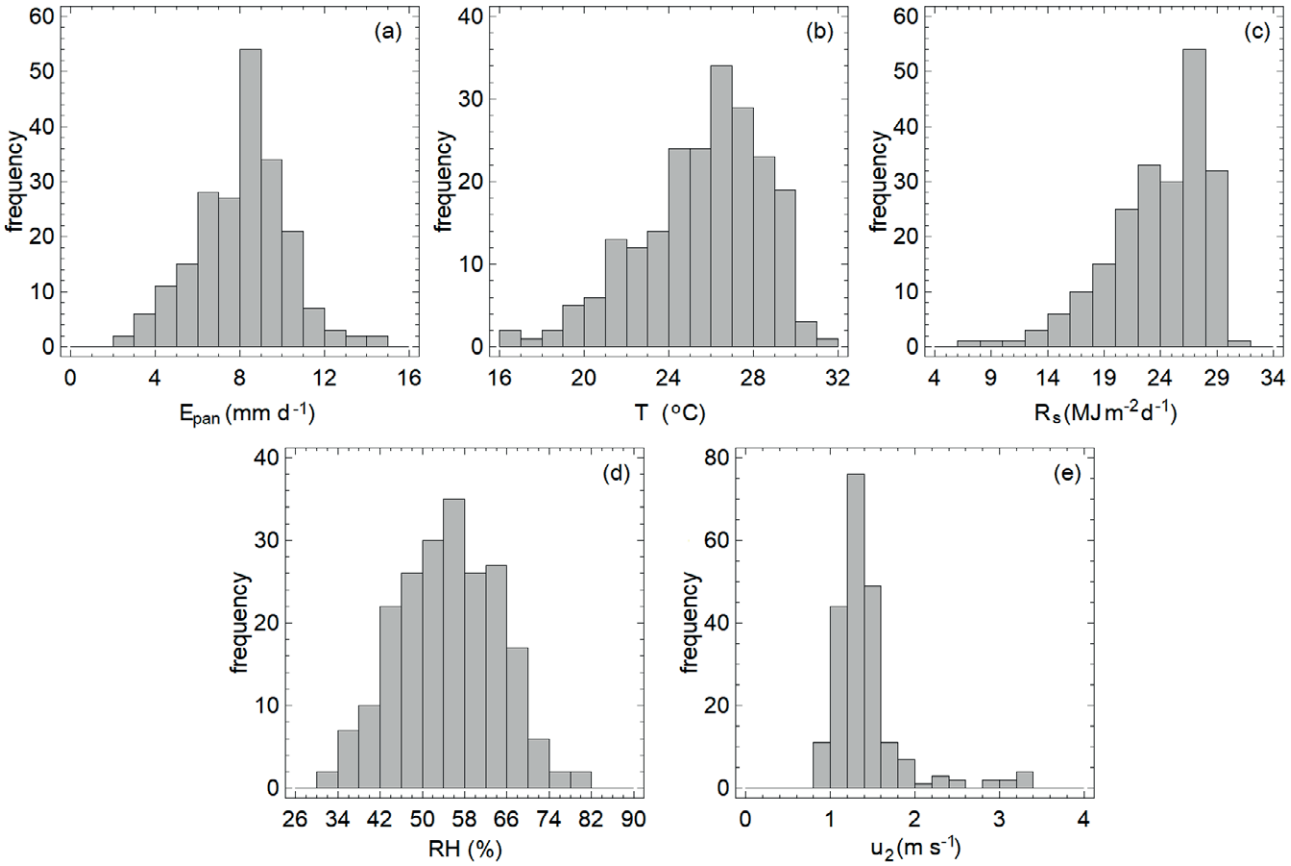

Figure 1. Frequency histograms for daily class A pan evaporation (E_{pan}) data and for daily meteorological parameters of temperature (T), incident solar radiation (R_s), relative humidity (RH) and wind speed at 2 m above ground (u_2).

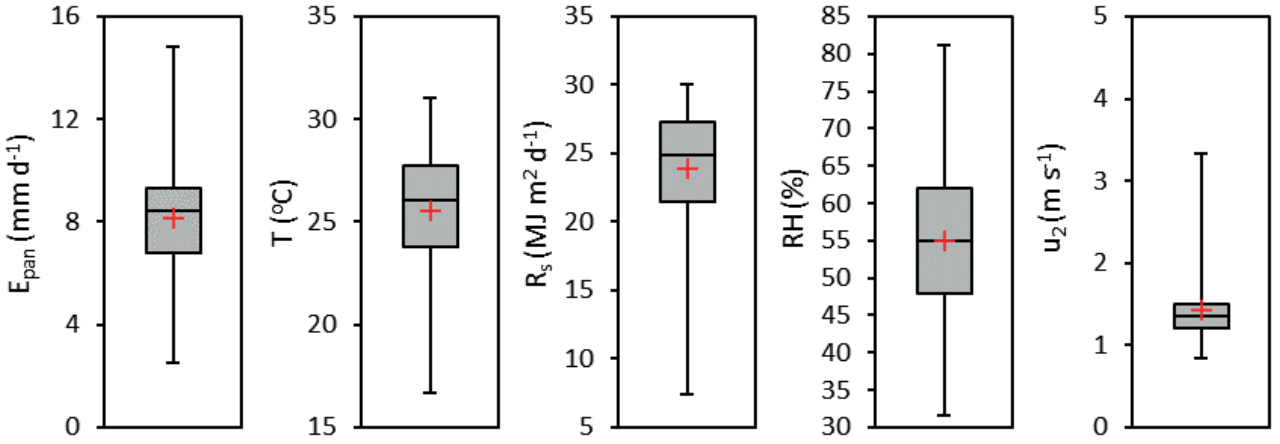

Figure 2. Box-Whisker plots for daily class A pan evaporation (E_{pan}) data and for daily meteorological parameters of temperature (T), incident solar radiation (R_s), relative humidity (RH) and wind speed at 2 m above ground (u_2).

2.2.1. Transformation of variables and Ridge regression

A common problem when building models based on meteorological parameters is the high multicollinearity that may appear among some parameters (e.g. temperature and solar radiation). High multicollinearity among independent variables leads to imprecise estimates of the regression model coefficients using ordinary

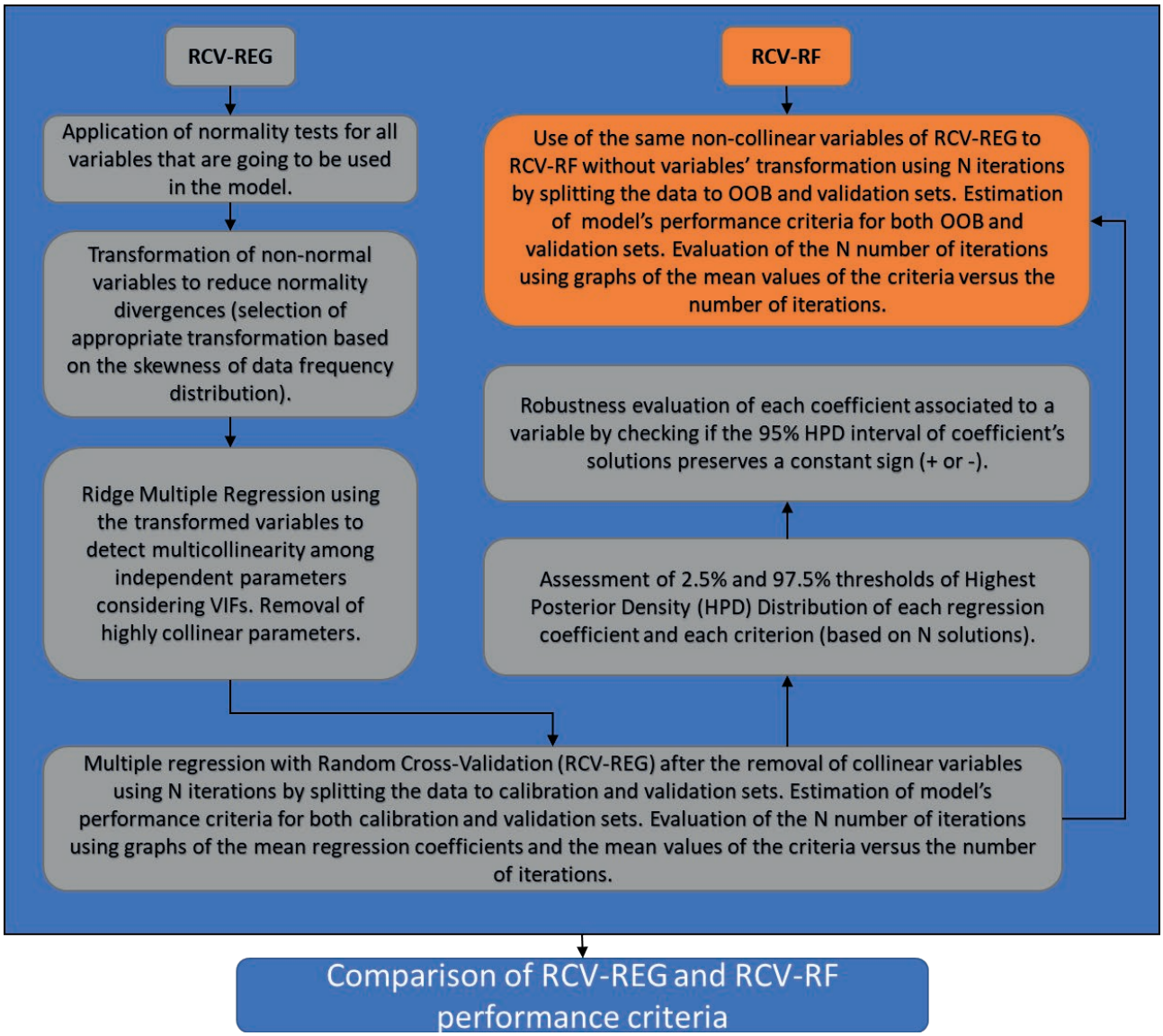

Figure 3. Flowchart of the methodological steps.

least squares, whereas the final model tends to overfit the data. A solution to this problem is the use of Ridge regression analysis, which is based on the idea that the variance of the slope estimates can be greatly reduced by introducing some bias into them. Ridge regression analysis also includes the estimation of the variance inflation factor (VIF) of each independent variable, which is a valuable indicator of multicollinearity among them. A large VIF has not been universally defined, but it is commonly considered large when exceeds the threshold value 10; however, some use 4 as threshold value (Kutner et al., 2004; O'brien, 2007; Vatcheva et al., 2016; Helsel et al., 2020).

Considering the above, ridge regression to fit the E_{pan} data using the T, R_s, RH and u_2 parameters was considered a crucial step to detect if multicollinearity exists among the independent variables. Before ridge regression, the normality tests of Shapiro-Wilk and Kolmogorov-Smirnov (STATGRAPHICS Centurion XV software, StatPointTechnologies Inc.) were used to identiy normality divergences of E_{pan}, T, R_s, RH and u_2 data for $p<0.05$ (Table 1). R_s and u_2 data failed to pass both normality tests, T and E_{pan} succeeded to pass only the test o Kolmogorov-Smirnov while RH succeeded to pass both tests. To reduce normality divergences, different transformations were employed according to the rules of Hel-

sel (2020) that are based in data skewness. T and R_s data were negatively skewed (Fig.1b,c) and for this reason the square transformation (x^2) was used. On the other hand, u_2 data were positively skewed (Fig.1e) and for this reason the logarithmic transformation ln(x+1) was used. E_{pan} was not transformed because different tested transformations did not improve the results of the normality tests. Thus, the final form of the ridge regression model with transformed variables was the following:

$$E_{pan} = a + b \cdot T^2 + c \cdot R_s^2 + d \cdot RH + e \cdot \ln(u_2 + 1) \quad (1)$$

where E_{pan} is the measured evaporation from the evaporimeter (mm d^{-1}), T is the mean daily air temperature (°C), R_s is the incident solar radiation (MJ m^{-2} d^{-1}), u_2 is the mean daily wind speed at 2 meters height (m s^{-1}), RH is the mean daily relative humidity (%), u_2 is the mean daily wind speed at the height of 2 m (m s^{-1}). The ridge regression is used as a preliminary control procedure to assess multicollinearity before proceeding to the modelling approach of RCV-REG, which is described in the next section. In case of high multicollinearity, the indipedent variables of Eq. 1 are reduced in order to reach an acceptable VIF value of the remaining parameters before their use in RCV-REG.

2.2.2. Regression with Random Cross-Validation (RCV-REG)

The E_{pan} model (Eq. 1) contains non-linear transformations of the independent variables and its predictive power was investigated using a random cross-validation regression (RCV-REG) analysis based on the concept of Babakos et al. (2020). The RCV-REG analysis performs a random splitting of the initial dataset into a calibration set (70% of the records) and a validation set (30% of the records). This random splitting is performed 1000 times (number adusted by the user), leading to a respective number of calibration and validation pairs of datasets. The calibration procedure leads to 1000 estimations of the regression coefficients of Eq. 1. The estimated coefficients of each calibration set were used to validate the model based on the respective validation set. The RCV-REG was built in R software using the "nls.lm" function of the {minpack.lm} package (Guan et al., 2020), which includes the Levenberg-Marquardt nonlinear least-squares algorithm. The range of 1000 solutions of each regression coefficient from calibration and validation procedures was respectively defined by the 95% confidence interval of the highest posterior density (HPD) distribution. The 2.5% and 97.5% thresholds (HPD thresholds) containing the central 95% interval of the HPD distribution were estimated in R software using the "p.interval" function of the {LaplacesDemon} package (Majhi et al., 2020). This function returns unimodal or multimodal HPD intervals depending on the form of the probability distributions. The HPD intervals are extremely valuable since they can provide information about the robustness of regression coefficients, the robustness of the independent variables associated to them and consequently the robustness of the overall model. The following robustness rule was suggested by Babakos et al. (2020) based on the results of the complete RCV-REG procedure: "a model is robust only when the 95% HPD intervals of all its regression coefficients associated to independent variables preserve a constant sign (+ or -)". When a 95% HPD interval of a regression coefficient contains positive and negative values, then it indicates a non-robust coefficient (non clear effect of the indipedent variable) that can significantly affect the robustness of the model.

2.2.3. Random Forests with Random Cross-Validation (RCV-RF)

Random forests (RF) is among the most important machine-learning methods (Breiman, 2001), which is an improvement of the Classification and Regression Trees (CART) method (also called decision trees). RF employs a modification of the bootstrap aggregating technique (bagging), where a large collection of decorrelated, noisy, approximately unbiased trees are constructed and averaged in order to minimize the model variance and instability problems (Hastie et al., 2009). RF is an ensemble method where the aggregation of multiple trees increases the prediction accuracy, with results described by both low bias and low variance (Breiman, 2001; Diaz-Uriarte and De Andres, 2006). Advantages of RF are the ability of modeling high-dimensional nonlinear relationships with few user-defined parameters, relative robustness with resistance to overfitting and estimation of importance of the variables (Dietterich, 1995; Breiman, 2001; Hastie et al., 2009; Diaz-Uriarte and De Andres, 2006; Strobl et al., 2009).

The hyperparameters of the RF model significantly affect model's performance. The hyperparameters that were considered in this study are the number of the regression trees (num.trees), the proportion of train set that was used for building the model (sample.fraction), the number of candidate predictors that were randomly sampled (mtry), and the minimum number of points in the terminal nodes of the regression trees (min.node.size). Different combinations of various values of hyperparameters was built, and by executing the

"ranger" package (Wright et al., 2020), their optimal set of values was determined (mtry = 2, num.trees = 1000, sample.fraction = 0.7, and min.node.size = 5). The validation set was set to 30% of the initial dataset in order to be comparable with the RCV-REG. RF also includes an iterative process (Out-Of-Bag - OOB) during training (calibration) by using different sets of the training dataset (the rest 70%), which is used to reduce the variance without changing the bias of the complete ensemble. RF also estimates the predictor variables' importance, which is calculated as the mean-across all trees-decrease (%) of accuracy, expressed by the % change in Mean Squared Error - MSE (%) of the Out-of-Bag (OOB) sample when the variable is not considered by permuting its values randomly and maintaining the others as they were.

The internal random procedures in RF lead every time to different solutions using constant optimal values of hyperparameters (Hastie et al., 2009). For this reason, 1000 RF iterations (RCV-RF) were also made in order to make comparisons with the RCV-REG model (Eq. 1). RF is not restricted by the limitations of a predefined nonlinear form and can be used as a benchmark model for evaluating the predictive accuracy of typical regression models but, also, for assessing the relative importance of the predictor meteorological variables to affect E_{pan}. The main reason for selecting the Random Forests approach is that it does not consider assumptions regarding normality, linearity, homoscedasticity, and collinearity. It also does not demand a high sample-to-predictor ratio, it is very suitable to interaction effects (including nonlinearity) and it is recognized as one of the state-oftheart methods in terms of prediction accuracy (Flach 2012; Geurts et al., 2009; Golino and Gomes, 2016). The RCV-RF analysis was performed using all the same predictor variables of RCV-REG without transforming the variables since RF does not consider assumptions of normality.

2.2.4. Models' performance criteria and evaluation of required number of iterations used in RCV-REG and RCV-RF

The models' performance criteria of R^2, the root mean square error (RMSE), the mean absolute error (MAE), the mean absolute percentage error (MAPE), and the Nash–Sutcliffe efficiency were estimated: a) for each calibration and validation dataset of the RCV-REG analysis for Eq. 1, and b) for the OOB and validation dataset of the RCV-RF analysis; leading to 1000 respective estimations of their values for each model. Moreover, the 1000 estimations of slope and intercept of the trend line in the 1:1 plot of observed vs. predicted E_{pan} models only using the validation sets were also made (for both RCV-REG or RCV-RF) as complementary criteria. The 1000 estimations of the criteria were also analyzed through the computation of HPD intervals.

The evaluation of the selected number of iterations (i.e. 1000) used in RCV-REG and RCV-RF was performed using individual graphs of the mean regression coefficients (only for RCV-REG) and of the mean criteria values (for both RCV-REG and RCV-RF) versus the number of iterations. Based on these graphs, it was assumed that the required number of iterations is succeeded when the mean value of a regression coefficient or a criterion reaches a stablized plateau.

3. RESULTS

Ridge regression analysis was performed on the transformed variables of Eq. 1 to detect any multicollinearity among them and the VIF results of the variables are shown in Table 2. The VIF values of all the variables were below the threshold value 4, suggesting low multicollinearity degree and low overfitting effects by their combined use. For this reason, indipedent variables were not removed from Eq. 1 and it was used as it is in the RCV-REG approach.

The mean, standard error, minimum, maximum and 2.5% and 97.5% HPD quantiles of the coefficients of the RCV-REG approach for Eq. 1 are given in Table 3. The statistical metrics and the robustness rule of Babakos et al. (2020) based on the 1000 iterations (Table 3) showed that the form of Eq. 1 is robust considering that all the estimated coefficients associated to independent variables have stable sign between 2.5% and 97.5% HPD thresholds. Only the regression coefficient of intercept (coefficient a in Eq. 1) does not follow the rule of robustness, but it is not associated to an independent variable. The regression model's performance is described by the statistical criteria given in Table 4 for both the calibration and validation subsets.

Table 2. VIF values of Ridge regression analysis on transformed data.

	Value of the coefficient	VIF
Constant	-0.51	-
T^2	0.005	1.54
$\ln(u_2+1)$	4.03	1.63
RH	-0.027	1.87
R_S^2	0.006	1.47
R^2 of the regression	0.852	

Table 3. Highest posterior density distributions of 1000 estimations of coefficients of independent variables for the RCV-REG model (Eq. 1).

	a	b	c	d	e
Mean	-0.458	0.005	4.019	-0.028	0.006
St.Error	0.022	0.000	0.012	0.000	7.14E-06
Min	-2.542	0.003	2.611	-0.048	0.005
HPD thres. 2.5%	-1.995	0.004	3.131	-0.040	0.005
median	-0.453	0.005	4.018	-0.028	0.006
HPD thres. 97.5%	0.788	0.006	4.707	-0.017	0.006
Max	1.970	0.006	5.272	-0.008	0.006

Table 5. Importance indicators of indipedent variables based on the RCV-RF approach.

Imp. Indicator	T	u_2	RH	R_s
Mean	75.992	84.319	88.730	204.366
St.Error	0.395	0.418	0.412	0.529
Min	36.362	49.824	50.894	152.022
HPD thres. 2.5%	51.118	60.887	63.887	170.893
median	76.208	84.023	87.980	204.772
HPD thres. 97.5%	98.923	111.048	113.947	234.927
Max	111.194	132.797	142.721	264.168

The mean, standard error, minimum, maximum and 2.5% and 97.5% HPD thresholds of the importance indicator of the variables from the RCV-RF method are given in Table 5, where the importance of independent variables showed the following ranking R_s>RH>u_2>T.

As regards the implementation of RCV-RF approach, the statistical metrics for both the OOB set and the validation set are given in Table 6.

Considering the mean values of metrics for the validation datasets (1,000 iterations) of RCV-REG and RCV-RF (Table 4 and 6), it is observed that RCV-REG outperformed RCV-RF in all criteria indicating that the proposed regression approach can compete the accuracy of machine learning methods for building evaporation models.

Finally, for the evaluation of the selected number of iterations (i.e. 1000) used in RCV-REG and RCV-RF, the individual graphs of the mean regression coefficients (only for RCV-REG) and of the mean criteria values from the validation procedure (for both RCV-REG and RCV-RF) versus the number of iterations are given in Fig. 4 and 5. Based on these graphs, it is evident that the all the regression coefficients and perfromance criteria reached a stablized plateau even after 500 iterations. Thus, the number of 1000 iterations is considered more than enough for assuming a robust analysis using both approaches.

4. DISCUSSION

4.1. Performance of the models

The most possible reason to justify why RCV-REG showed better performance from RCV-RF in the external validation (metrics denoted as pred. in Tables 4 and 6) is probably due to the normality improvement of the data based on proper selection of transformations used in RCV-REG. Transformed variables were not used in

Table 4. Performance criteria for the RCV-REG model.

Criterion		Mean	St.Error	Min	HPD thres. 2.5%	Median	HPD thres. 97.5%	Max
Calibration	R^2	0.854	0.000	0.801	0.827	0.854	0.880	0.893
	RMSE	0.817	0.001	0.715	0.746	0.822	0.887	0.914
	MAE	0.615	0.001	0.544	0.571	0.616	0.669	0.692
	MAPE	0.078	0.000	0.068	0.072	0.078	0.084	0.088
	NSE	0.854	0.000	0.801	0.827	0.854	0.880	0.893
Validation	R^2	0.843	0.001	0.675	0.777	0.845	0.907	0.926
	RMSE	0.853	0.003	0.570	0.703	0.846	1.020	1.073
	MAE	0.642	0.002	0.456	0.526	0.640	0.751	0.850
	MAPE	0.081	0.000	0.057	0.067	0.081	0.096	0.110
	NSE	0.836	0.001	0.660	0.770	0.838	0.903	0.919
	Intercept*	0.011	0.015	-1.493	-0.853	0.005	1.059	1.288
	Slope*	0.998	0.002	0.836	0.875	0.998	1.116	1.197

*Estimated only for the validation set.

Table 6. Performance criteria for the RCV-RF model.

	Criterion	Mean	St.Error	Min	HPD thres. 2.5%	Median	HPD thres. 97.5%	Max
OOB	R2	0.823	0.001	0.761	0.791	0.824	0.852	0.881
	RMSE	0.902	0.001	0.788	0.842	0.903	0.968	1.002
	MAE	0.685	0.001	0.599	0.636	0.684	0.737	0.758
	MAPE	0.088	0.000	0.076	0.081	0.088	0.094	0.097
	NSE	0.821	0.001	0.760	0.790	0.823	0.851	0.880
Validation	R2	0.835	0.001	0.673	0.775	0.838	0.896	0.910
	RMSE	0.904	0.003	0.649	0.744	0.896	1.093	1.267
	MAE	0.689	0.002	0.481	0.564	0.687	0.820	0.918
	MAPE	0.088	0.000	0.061	0.071	0.088	0.107	0.117
	NSE	0.818	0.001	0.663	0.759	0.821	0.881	0.892
	Intercept*	-1.011	0.020	-3.236	-2.299	-1.021	0.120	0.657
	Slope*	1.120	0.002	0.898	0.963	1.121	1.260	1.378

*Estimated only for the validation set.

Random forest method because this approach overcomes problems of normality, linearity, homoscedasticity and collinearity (Flach 2012; Geurts et al., 2009; Golino and Gomes, 2016) since it doesn't use metric distances between data points but applies splits along a tree. Another possible reason is the difference in the degrees of freedom of the two models (associated to the number of coefficients that are free to vary) in combination with the number of records used in this study. Models that have low degrees of freedom (e.g. linear or non linear regression such as RCV-REG) are not usually so flexible to fit the data. Thus, the lower the degrees of freedom of a model the lower is the effect of the noise/bias in the data included in the final model (e.g. noise/bias in the data may come from other sources such as errors associated to the observer). Moreover, when the number of data records to calibrate the model is low, the larger is the effect of the noise/bias included in the final calibration. Based on the above, machine learning models that are generally used to solve problems using Big Data and they have much more degrees of freedom, may not be the proper choice for typical modelling applications, where the number of data is small, because they "absorb" a large portion of the data noise. This may lead to a lower performance of a machine learning model compared to a regression model during external validation. In this study, the number of records were 212 and they are not in the category of Big Data but they are enough for the typical regression analysis. This was an additional reason for including the RCV approach of iterations in both modelling approaches.

4.2. Limitations of RCV-REG approach

The RCV-REG iterative procedure in combination with the preliminary analyses of the Ridge regression and the tranformation of variables can be considered a complete methodology that takes into account all the nessecary elements for building a robust model. On the other hand, the final form of the model is based on the experience of the user, which may not be adequate to achieve the maximum potential of the methodology. Moreover, RCV-REG approach is limited to provide a graphical representation of the results. For example, it is typical in modelling approaches to provide 1:1, quantile:quantile (Q:Q) plots of observed vs. predicted data, 2D plots of the respective joint probability distribution etc. The problem of the RCV-REG is that there are 1,000 iterations that neither can be plotted seperately (due to the large number) nor to merge the results of all iterations in one graphic type. The second case is feasible for 1:1 plot but leads to clouds of points that come from different 30% of the initial data.

4.3. Reasons for excluding records of cold season and rainfall days

The reason for not including pan evaporation measurements of the cold season and of the rainy days was because these measurements have a lot of bias. During the six-month cold season in this location, E_{pan} is low and generally falls in the range 0-2 mm/day not only due to the lower temperature but also due to high relative humidity with a lot of foggy days and condensed moisture (dew) in the leaves of the surrounding vegetation

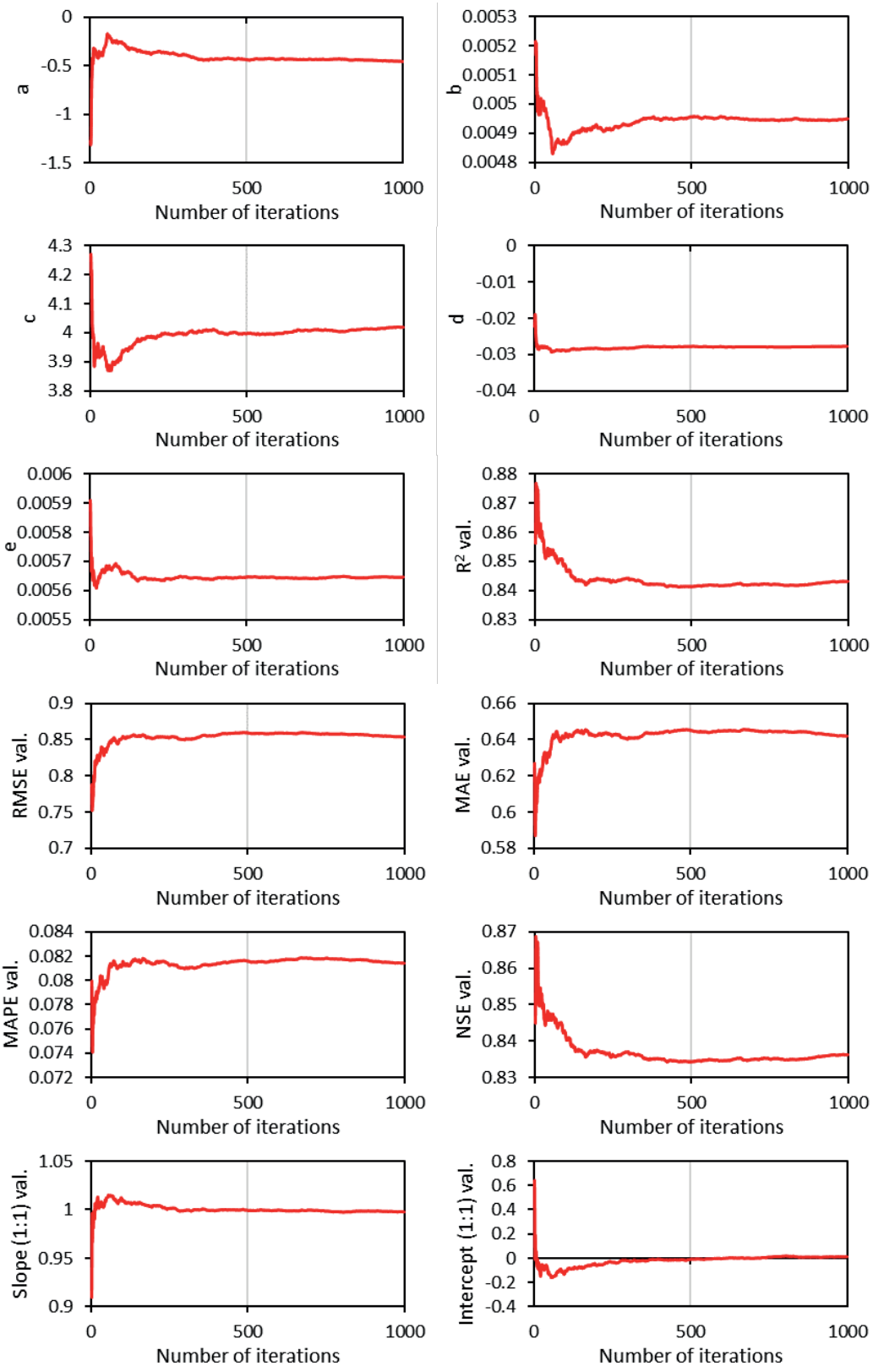

Figure 4. Variation of mean values of regression coefficients of Eq. 1 and performance criteria from the validation procedure versus the number of iterations for RCV-REG.

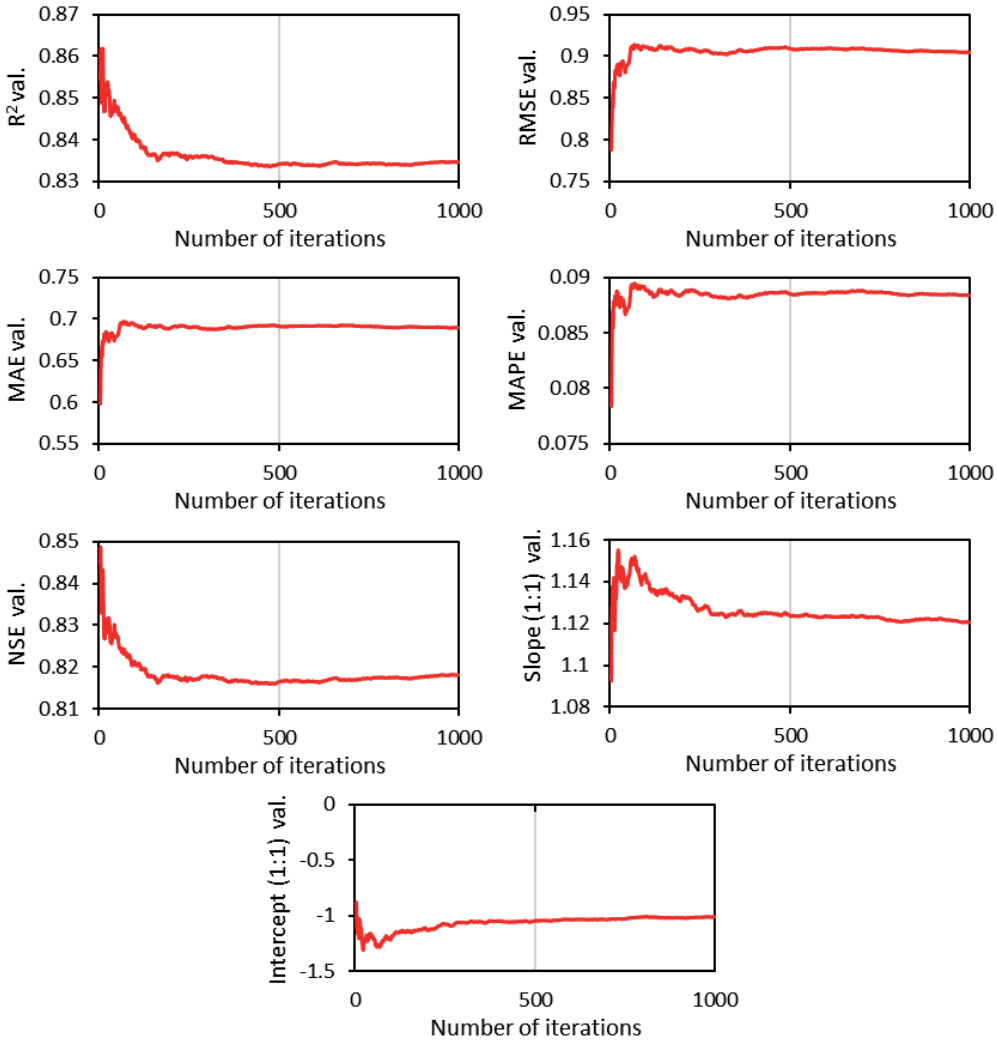

Figure 5. Variation of mean values of performance criteria from the validation procedure versus the number of iterations for RCV-RF.

during the morning. During these months, even during April or October, it was observed the occurrence of negative E_{pan} measurements due to condensed dew input in the pan. The rainfall days during the warm season were also excluded because the temperature of rainfall is quite different from the water temperature in the pan (even 10°C) and their mixing changes the evaporative energy demand. The records of rainfall days could only be used in the case of deterministic modelling approaches based on energy budget where the water temperature is used as input parameter.

Another reason for not including the data from the six-month cold season is that the seasonal variation of temperature and solar radiation between summer and winter leads the two variables to be collinear and thus the one should be removed from the modelling approach. Using only the data of the warm season, the two variables present lower collinearity that allows their combined use in the models.

The general concept and methodological steps presented in this study are valid for all areas that have distinct warm and cold seasons. If cold season does not exist (e.g. tropical environments), data from all seasons can be included. Rainfall days can also be included but it is expected to lead to a reduction in the predictive accuracy of the final model. The larger the proportion of the rainfall days in the final record, the larger is expected to be the reduction of the predictive accuracy. For the inclusion of rainfall days, it is proposed the inclusion of rainfall variable in Eq. 1 or the use of a categorical variable for splitting the records in rainfall and no-rainfall days. The second case is considered as categorical regression.

5. CONCLUSIONS

The implementation of the RCV-REG method, which includes regression with transformed variables of low collinearity and analysis of the 95% HPD of regression coefficients, was found to be an extremely powerful approach for E_{pan} analysis that can compete machine learning methods and can provide a complete evaluation of the regression coefficients robustness. As it was shown from the results of this study for modelling E_{pan} using meteorological variables, the specific method succeeded to outperform RCV-RF in all performance criteria. Moreover, RCV-REG gave a better aspect and evaluation of the robust effect of the indipedent variables (through the HPD analysis on the regression coefficients associated to the indipedent variables) in comparison to RCV-RF that is able to provide only a relative ranking of indipedent variables' importance.

Moreover, the use of the RCV data splitting approach in various modelling approaches solves the problem of subjective splitting of data into calibration and validation sets, provides a better evaluation of the final modelling approaches and enhances the competitiveness of typical regression models against machine learning models. Despite the fact that machine learning methods are more advanced in comparison to typical regression methods, mostly by handling better Big Data, they still face the problem of transferability from the developer to the user for various reasons, such as non-availability of the calibrated code or its form (since it is a black box) and lack of users's expertise to handle such models. On the other hand, the resulting models through typical regression approaches do not require advanced skills and can be used in other studies either by adopting the entire calibrated model or by adopting the general form of the model.

Future studies should focus on (a) the investigation of E_{pan} models with the inclusion of records of rainfall days and (b) the investigation of new graphical methods for representing different elements of the results of the RCV-REG method.

REFERENCES

Allen R.G., Pereira L.S., Raes D., Smith M., 1998. Crop Evapotranspiration: Guidelines for Computing Crop Water Requirements. Irrigation and Drainage Paper 56, Food and Agriculture Organization of the United Nations: Rome.

Almedeij J., 2012. Modeling Pan Evaporation for Kuwait by Multiple Linear Regression. The Scientific World Journal, Ar. ID 574742: 1-9. https://doi.org/10.1100/2012/574742

Alsumaiei A.A., 2020. Utility of artificial neural networks in modeling pan evaporation in hyper-arid climates. Water (Switzerland), 1508: 1-12. https://doi.org/10.3390/w12051508

Althoff D., Rodrigues L.N., da Silva D.D., 2020. Impacts of climate change on the evaporation and availability of water in small reservoirs in the Brazilian savannah. Climatic Change, 159: 215–232. https://doi.org/10.1007/s10584-020-02656-y

Aschonitis V., Diamantopoulou M., Papamichail D., 2018. Modeling plant density and ponding water effects on flooded rice evapotranspiration and crop coefficients: critical discussion about the concepts used in current methods. Theoretical and Applied Climatology, 132: 1165-1186. https://doi.org/10.1007/s00704-017-2164-z

Ashrafzadeh A., Malik A., Jothiprakash V., Ghorbani M.A., Biazar S.M., 2018. Estimation of daily pan evaporation using neural networks and meta-heuristic approaches. ISH Journal of Hydraulic Engineering, 26(4): 421-429. https://doi.org/10.1080/09715010.2018.1498754

Babakos K., Papamichail D., Tziachris P., Pisinaras V., Demertzi K., Aschonitis V., 2020. Assessing the robustness of pan evaporation models for estimating reference crop evapotranspiration during recalibration at local conditions. Hydrology, 7(3): 62. https://doi.org/10.3390/hydrologfy7030062

Breiman L., 2001. Random forests. Machine Learning, 45: 5-32. https://doi.org/10.1023/A:1010933404324

Bruton J.M., McClendon R.W., Hoogenboom G.,. 2000. Estimating daily pan evaporation with artificial neural networks. Transactions of the American Society of Agricultural and Biological Engineers, 43(2), 491-496. https://doi.org/10.13031/2013.2730

Brutsaert B., Lei Yu S., 1968. Mass Transfer Aspects of Pan Evaporation. Journal of Applied Meteorology and Climatology, 7: 563–566. DOI:10.1175/1520-0450(1968)007<0563:MTAOPE>2.0.CO,2

Chang F.J., Sun W., Chung C.H., 2013. Dynamic factor analysis and artificial neural network for estimating pan evaporation at multiple stations in northern Taiwan. Hydrological Sciences Journal, 58(4): 813-825. https://doi.org/10.1080/02626667.2013.775447

Deo R.C., Samui P., 2017. Forecasting evaporative loss by least-square support-vector regression and evaluation with genetic programming, gaussian process, and minimax probability machine regression: Case study of Brisbane city. Journal of Hydrologic Engineering, 22(6), art. no. 05017003. https://doi.org/10.1061/(ASCE)HE.1943-5584.0001506

Díaz-Uriarte R., De Andres S.A., 2006. Gene selection and classification of microarray data using random forest. BMC bioinformatics, 7: 1-13. https://doi.org/10.1186/1471-2105-7-3

Dietterich T.G., 1995. Overfitting and undercomputing in machine learning. ACM Computing Surveys, 27(3): 326-327. https://doi.org/10.1145/212094.212114

Doorenbos J., Pruitt W.O., 1977. Guidelines for Predicting Crop Water Requirements. Irrigation and Drainage Paper No. 24, 2nd ed., Food and Agriculture Organization of the United Nations: Rome.

Finch J.W., Hall R.L., 2001. Estimation of open water evaporation–a review of methods. R&D Technical Report W6–043/TR. Environment Agency, Rio House, Waterside Drive, Aztec West, Almondsbury, Bristol.

Flach, P. 2012. Machine Learning: The Art and Science of Algorithms that Make Sense of Data. Cambridge: Cambridge University Press.

Geurts P., Irrthum A., Wehenkel L., 2009. Supervised Learning with Decision Tree-based Methods in Computational and Systems Biology. Molecular Biosystems, 5(12), 1593-1605. https://doi.org/10.1039/b907946g

Ghorbani M.A., Deo R.C., Yaseen Z.M., Kashani M.H., Mohammadi B., 2018. Pan evaporation prediction using a hybrid multilayer perceptron-firefly algorithm (MLP-FFA) model: case study in North Iran. Theoretical and Applied Climatology, 133: 1119-1131. https://doi.org/10.1007/s00704-017-2244-0

Golino H.F., Gomes C.M.A., 2016. Random forest as an imputation method for education and psychology research: its impact on item fit and difficulty of the Rasch model. International Journal of Research and Method in Education, 39(4): 401-421. https://doi.org/10.1080/1743727X.2016.1168798

Guan Y., Mohammadi B., Pham Q.B., Adarsh S., Balkhair K.S., Rahman K.U., Linh N.T.T., Tri D.Q., 2020. A novel approach for predicting daily pan evaporation in the coastal regions of Iran using support vector regression coupled with krill herd algorithm model. Theoretical and Applied Climatology, 142: 349-367. https://doi.org/10.1007/s00704-020-03283-4

Hastie T., Tibshirani R., Friedman J., 2009. The elements of statistical learning. 2nd ed. Springer, New York.

Helsel D.R, Hirsch R.M, Ryberg K.R, Archfield S.A, Gilroy E.J., 2020. Statistical Methods in Water Resources. In Book 4, Hydrologic Analysis and Interpretation, U.S. Geological Survey, U.S., 4–A3, pp. 460.

Irmak S., Haman D., 2003. Evaluation of Five Methods for Estimating Class A Pan Evaporation in a Humid Climate. Horttechnology, 13: 500-508. https://doi.org/10.21273/HORTTECH.13.3.0500

Keskin M.E., Terzi Ö., Taylan D., 2004. Fuzzy logic model approaches to daily pan evaporation estimation in western Turkey / Estimation de l'évaporation journalière du bac dans l'Ouest de la Turquie par des modèles à base de logique floue. Hydrological Sciences Journal, 49: 1001-1010. https://doi.org/10.1623/hysj.49.6.1001.55718

Keskin M.E., Terzi Ö., 2006. Artificial neural network models of daily pan evaporation. Journal of Hydrologic Engineering, 11: 65-70. https://doi.org/10.1061/(ASCE)1084-0699(2006)11:1(65)

Kim S., Shiri J., Kisi O., 2012. Pan Evaporation Modeling Using Neural Computing Approach for Different Climatic Zones. Water Resources Management, 26: 3231-3249. https://doi.org/10.1007/s11269-012-0069-2

Kim S., Shiri J., Singh V.P., Kisi O., Landeras G., 2015. Predicting daily pan evaporation by soft computing models with limited climatic data. Hydrological Sciences Journal, 60(6): 1120-1136. https://doi.org/10.1080/02626667.2014.945937

Kisi O., Keskyn E.M., Terzy Ö., Taylan D., 2005. Discussion of "Fuzzy logic model approaches to daily pan evaporation estimation in western Turkey". Hydrological Sciences Journal, 50(4): 727-730. https://doi.org/10.1623/hysj.2005.50.4.727

Konapala G., Mishra A. K., Wada Y., Mann M. E., 2020. Climate change will affect global water availability through compounding changes in seasonal precipitation and evaporation. Nature Communications, 11, art. no. 3044. https://doi.org/10.1038/s41467-020-16757-w

Kovoor G.M., Nandagiri L., 2007. Developing regression models for predicting pan evaporation from climatic data - A comparison of multiple least-squares, principal components, and partial least-squares approaches. Journal of Irrigation and Drainage Engineering, 133: 444-454. https://doi.org/10.1061/(ASCE)0733-9437(2007)133:5(444)

Kutner M., Nachtsheim C., Neter J., 2004. Applied Linear Regression Models, 4rd ed., McGraw Hill Irwin, pp. 495.

Majhi B., Naidu D., Mishra A.P., Satapathy S.C., 2020. Improved prediction of daily pan evaporation using Deep-LSTM model. Neural Computing and Applications, 32: 7823-7838. https://doi.org/10.1007/s00521-019-04127-7

Molina J.M., Martínez V., González-Real M.M., Baille A., 2006. A simulation model for predicting hourly pan evaporation from meteorological data. Journal of Hydrology, 318: 250–261. https://doi.org/10.1016/j.jhydrol.2005.06.016

O'brien R.M., 2007. A Caution Regarding Rules of Thumb for Variance Inflation Factors. Qual-

ity & Quantity, 41: 673-690. https://doi.org/10.1007/s11135-006-9018-6

Pammar L., Deka P.C., 2015. Forecasting daily pan evaporation using hybrid model of wavelet transform and support vector machines. International Journal of Hydrology Science and Technology, 5: 274-294.

Penman H.L., 1948. Natural evaporation from open water, bare soil and grass. Proceedings of the Royal Society of London. Series A, Mathematical and Physical Sciences, 193: 120–145. https://doi.org/10.1098/rspa.1948.0037

Penman H.L., 1956. Evaporation: an introductory survey. Netherlands Journal of Agricultural Science, 4: 9–29. https://doi.org/10.4236/jss.2016.43010

Piri J., Amin S., Moghaddamnia A., Keshavarz A., Han D., Remesan R., 2009. Daily pan evaporation modeling in a hot and dry climate. Journal of Hydrologic Engineering, 14: 803-811. https://doi.org/10.1061/(ASCE)HE.1943-5584.0000056

Rahimikhoob A., 2009. Estimating daily pan evaporation using artificial neural network in a semi-arid environment. Theoretical and Applied Climatology, 98: 101-105. https://doi.org/10.1007/s00704-008-0096-3

Shirsath P.B., Singh A.K., 2010. A Comparative Study of Daily Pan Evaporation Estimation Using ANN, Regression and Climate Based Models. Water Resources Management, 24: 1571-1581. https://doi.org/10.1007/s11269-009-9514-2

Seifi A., Soroush F., 2020. Pan evaporation estimation and derivation of explicit optimized equations by novel hybrid meta-heuristic ANN based methods in different climates of Iran. Computers and Electronics in Agriculture, 173, art. no. 105418. https://doi.org/10.1016/j.compag.2020.105418

Shiri J., Marti P., Singh V.P., 2014. Evaluation of gene expression programming approaches for estimating daily evaporation through spatial and temporal data scanning. Hydrological Processes, 28(3): 1215-1225. https://doi.org/10.1002/hyp.9669

Strobl C., Malley J., Tutz G., 2009. An introduction to recursive partitioning: rationale, application, and characteristics of classification and regression trees, bagging, and random forests. Psychological Methods, 14(4): 323-348. https://doi.org/10.1037/a0016973

Tabari H., Marofi S., Sabziparvar A.-A., 2010. Estimation of daily pan evaporation using artificial neural network and multivariate non-linear regression. Irrigation Science, 28: 399-406. https://doi.org/10.1007/s00271-009-0201-0

Valiantzas J.D., 2006. Simplified versions for the Penman evaporation equation using routine weather data. Journal of Hydrology, 331: 690–702. https://doi.org/10.1016/j.jhydrol.2006.06.012

Vatcheva K.P, Lee M, McCormick J.B, Rahbar M.H., 2016. Multicollinearity in Regression Analyses Conducted in Epidemiologic Studies. Epidemiology, 6(2): 227-246. https://doi.org/10.4172/2161-1165.1000227

Wang L., Niu Z., Kisi O., Li C., Yu D., 2017. Pan evaporation modeling using four different heuristic approaches. Computers and Electronics in Agriculture, 140: 203-213. https://doi.org/10.1016/j.compag.2017.05.036

Wang H., Yan H., Zeng W., Lei G., Ao C., Zha Y., 2020. A novel nonlinear Arps decline model with salp swarm algorithm for predicting pan evaporation in the arid and semi-arid regions of China. Journal of Hydrology, 582, art. no. 124545. https://doi.org/10.1016/j.jhydrol.2020.124545

Wright M.N., Wager S., Probst P., Package 'ranger': 2020. A Fast Implementation of Random Forests,. Available online: https://github.com/imbs-hl/ranger (accessed on 1/5/2020)

Xu C.-Y., Singh V.P., 1998. Dependence of evaporation on meteorological variables at different timescales and intercomparison of estimation methods. Hydrological Processes, 12: 429–442. https://doi.org/10.1002/(sici)1099-1085(19980315)12:3<429::aid-hyp581>3.0.co,2-a

Italian Journal of Agrometeorology
Rivista Italiana di Agrometeorologia

Firenze University Press
www.fupress.com/ijam

OPEN ACCESS

Citation: Habibi, B., Meddi, M. & Abdelkader, M. (2024). The frequency distribution and stochastic analysis of the hydrological drought in northern Algeria. *Italian Journal of Agrometeorology* (1): 73-94. doi: 10.36253/ijam-1730

Received: July 4, 2022

Accepted: December 15, 2023

Published: August 2, 2024

Data Availability Statement: All relevant data are within the paper and its Supporting Information files.

Competing Interests: The Author(s) declare(s) no conflict of interest.

The frequency distribution and stochastic analysis of the hydrological drought in northern Algeria

Brahim Habibi[1,*], Mohamed Meddi[2], Mohamed Abdelkader[3]

[1] *Faculty of Natural and Life Sciences, Hassiba Benbouali University of Chlef and GEE Laboratory, Blida, Algeria*
[2] *National School of Hydraulics and GEE Laboratory, Blida, Algeria*
[3] *Department of Civil, Environmental, and Ocean Engineering (CEOE), Stevens Institute of Technology, Hoboken, NJ, USA*
*Corresponding author. Email: habibibrahime7@gmail.com

Abstract. The objective of this study was to examine drought using the Streamflow Drought Index (SDI) at various time scales and its temporal evolution using monthly streamflow data from 1973 to 2009. Streamflow records were collected from a network of 14 hydrometric stations distributed throughout the study area. The Akaike Information Criterion (AIC) and the Bayesian Information Criterion (BIC) were used to assess the quality of the adjustment. According to these criteria, the gamma law better suited the time scales of 3, 6, and 12 months, whereas the log-normal law was better suited to the scale of 9 months. The analysis of the Streamflow Drought Index in the three study basins (Middle and Upper Cheliff, Lower Cheliff, and the Mina) revealed that different classes of drought among 3, 6, 9, and 12-month time scales in the period of 1973 to 2009 had occurred, notably beginning in 1980. The frequency of 19 to 54% was found at all stations and in years marked by a mild drought. The moderate years had a frequency of 6 to 19%, while the severe and extreme years had a lower percentage (about 3 to 6%) in the study area. Two consecutive years of drought (D-D) were more likely in the Middle and Upper Cheliff basins (> 60%) for the 6, 9, and 12-month time scales, according to the transition of probability of first-order non-stationary Markov chain. On a three-month time scale, the transition probabilities (D-D) were greater than 50% in the Coastal basin and Lower Cheliff basin, as well as the Mina basin, and less than 50% in the Middle and Upper Cheliff basins.

Keywords: monthly stream flow, hydrological drought, frequency, Markov chain, North of Algeria.

INTRODUCTION

Climate change in arid and semi-arid regions is marked by a decrease in precipitation as well as a deprivation due to drought; this phenomenon is one of the most extreme climate conditions, affecting more people than any other natural disaster (Wilhite, 2000). Algeria is one of the countries in the Mediterranean basin that suffers from water scarcity from

one season to the next and year to year. Water runoff is characterized by significant seasonal and interannual irregularities, as well as the severity and rapidity of the floods. In addition, the climate is characterized by lengthy periods of drought and irregular precipitation patterns in terms of both time and space. The lack of precipitation has resulted in evaporation deficits ranging from 37 to more than 70% from the east to the west of the country (Meddi and Hubert, 2003). Algeria, like the rest of the North African region, has been suffering from a persistent drought for more than three decades (Meddi and Meddi, 2009; Ghenim et al., 2013). The hydrological drought is the reduction of surface flow in watercourses and, consequently, it leads to a decrease in the volume stored in hydraulic structures and a natural drop in the water level in underground wetlands (Bergaoui and Alouini, 2001). The economic impact of hydrological drought on a country can be significant. For example, higher average temperatures in winter than in summer, has an impact on snow and ice tourism in particular (Yuan et al., 2022). Hydrological drought is defined by reduced river flow, dam fill rates, and groundwater recharge (Soro et al., 2011). Drought is a prolonged dry period in the natural climate cycle that can occur anywhere in the world. It is a slow on-set phenomenon caused by a lack of rainfall (WMO, 2014). Meteorological drought is characterized by the absence of precipitation or lower precipitation heights than those generally recorded in the same period and signaled by a lack of precipitation over time (WMO, 2014). Between 1970 and 2012, severe African droughts caused nearly 680,000 deaths (OMM, 2014). Thierry (2020) and Faye et al. (2015) defines agricultural drought as the influence of meteorological or hydrological droughts on crop yield. There are several indices for assessing the hydrological and meteorological drought at different scales (3, 6, 9 and 12 months), including the Palmer Drought Severity Index (PDSI, Palmer, 1965), The Standard Precipitation Index (SPI, McKee et al.,1993), the Standardized Stream Flow Index (SSFI, Modarres, 2007), the Standardized Runoff Index (SRI, Shukla and Wood, 2008), the Surface Water Supply Index (SWSI, Shafer and Dezman, 1982) and the Streamflow Drought Index (SDI, Nalbantis and Tsakiris, 2009) . The SPI, SDI and SSFI indices were used to generate drought intensity at time scales of 3, 6, 9 and 12 months. According to the time scale, the 3-month SPI index provides a seasonal estimate of precipitation; the 6- and 9-month SPIs indicate the medium-term precipitation trend. As for SPIs of 12 months and more, they reflect the long-term trend. They are generally related to stream flows, reservoir filling rates and even static groundwater levels (Khan et al., 2008). Modarres (2007), the SSFI provides the benefit of controlling hydrological drought and/or water supply on a short, medium, and long term basis. Standardized streamflow index (SSFI) was utilized by Hosseinzadeh Talaee et al. (2014) to characterize hydrological drought in the west of Iran for the hydrological years of 1969/1970 to 2008/2009 through 29 rainfall stations.

Nalbantis and Tsakiris (2009) proposed the Streamflow Drought Index (SDI) method, which is used to evaluate dryness over time. The SDI method, developed by Nalbantis and Tsakiris (2009), includes a similar calculation to the Standardized Precipitation Index (SPI) method (McKee et al. 1993). Zamani et al. (2015) determined the hydrological droughts through the SDI index in the Karkheh river basin in southwest Iran at time scales of 3, 6, 9, and 12 months. Several researchers around the world have used the SDI index to analyze hydrological drought, for example, Tabari et al.,2013; Rezaeian-Zadeh and Tabari (2014); Yeh et al.,2015; Hong et al., 2015; WMO and GWP , 2017; Kavianpour et al., 2018 ; Akkurt Eroğluer and Apaydin, 2020 ; Jahangir and Yarahmadi, 2020; Zaki, 2020; Zhao et al., 2020 ;Koffi et al.,2020 ; Tareke and Awoke, 2022 ; Elbeltagi et al., 2023). Meteorological and hydrological droughts have been analyzed by many researchers around the world on the basis of SPI and SDI indices (Sardou and Bahramand, 2014; Arya Akbari et al., 2015; Pathak et al., 2016; Koudamiloro Olivier et al., 2017; Dabanli, 2018 ;Melhaoui et al., 2018; Boudad et al., 2018; Zulfiqar et al., 2019; González-López et al., 2020; Benlabiod et al., 2020; Sun et al., 2020; Zhong et al., 2020; Jiang et al., 2020; Minea et al., 2021; Ngoc Quynh Tram et al., 2021; Prajapati et al., 2022). Bartczak et al. (2015) applied the Box-Cox transformation to identify drought events through the Standardized Precipitation Index (SPI) and Streamflow Drought Index (SDI).

In Algeria, there are researchers who have used the SDI index and the SSFI index to analyze and characterize hydrological drought. Filali (2004) investigated medium and long-term dryness using (SPI) and (SSFI) over two time scales of 6 and 12 months. Ghenim and Megnounif (2011) used the SPI and SSFI indices between September 1946 to August 2009 to study drought variability. The results showed that the drought severity values by SPI -12 for the two sub-basins vary within the same range [-2.24; 1.79], i.e. from extreme drought to severe humidity. On the other hand, the drought severity of the SSFI index over 12 months varied between -2.3 (extreme drought) and 1.8 (severe humidity) in Meffrouche and Beni Bahdel from -1.99 (severe drought) at 2.39 (extreme humidity). Ghenim and Megnounif (2013)

used two indices, SSFI and SPI, to show that the Meffrouche sub-basin in northwestern Algeria had experienced periods of moderate humidity and drying, with a drying trend. Meddi et al. (2013) used the Streamflow Drought Index (SDI) to study drought in the Tafna river basin during periods of 3, 6, 9, and 12 months in the northeast of Algeria between 1941 and 2010. In this regard, some researchers have applied the Standardized Streamflow Index (SSFI) and the SDI Index in Algeria, such as Bendjema (2019) and Atallah et al (2021). They discovered that precipitation decreased by 26% in the Tafna basin after 1975, with a notable reduction in runoff of around 62%. In comparison, the three basins of Middle and Upper Cheliff, Lower Cheliff , and the Mina, which belong to the grand basin of Cheliff-Zahrez, have had severe and moderate droughts since 1980 (Habibi et al., 2018; Habibi and Meddi, 2021).

The Markov chain methodology may be used to determine the likelihood of having a dry year following a dry year. This procedure expresses conditional probabilities of transiting from the previous year's state to the current year's state. Because the stochastic process X_n (n = 0, 1, 2...) is a Markov chain (Medhi, 1994), the probabilities of transitions are only dependent on the current and future states (Meddi and Meddi, 2009; Meddi et al., 2013; Tokarczyk and Szaliska, 2014; Meddi et al., 2014; Tabari et al., (2015) :Lazri et al., 2015; Merabti and Meddi, 2016;Tettey et al., 2017; Habibi et al., 2018; Santos et al., 2019; Sattar et al., 2020).

The aim of this study is to provide quantitative information on hydrological drought (SDI) in semi-arid climatic conditions in northern Algeria using random Markov chain models and to

obtain probabilistic hydrological information. The SDI index was chosen to describe hydrological drought. The SDI (Nalbantis and Tsakiris, 2009) index has been widely used to describe and characterize hydrological drought. It is also simple in its use and allows a good description of this type of drought, which has been shown by several researchers around the world (Jahangir and Yarahmadi, 2020; Zhang et al., 2022; Katipoğlu, 2023). We have chosen this indicator for the efficient service and management of surface water (dams) and for the control of groundwater levels in the Cheliff-Zahrez basin, which is considered as an important agricultural area in the north of Algeria. The information on the probability of occurrence of drought is an important challenge for making short- and long-term decisions on water management.

This research motivates researchers and policymakers to use the most accurate and representative temporal characterization of drought risk in a semi-arid region.

STUDY AREA

The study area is located in the midwest of northern Algeria which includes three hydrographic basins (Lower Cheliff and the Mina, Middle and Upper Cheliff, and Coastal Dahra) (Figure 1). These three basins extend over 132,411 km^2. Lower Cheliff and the Mina, and Middle and Upper Cheliff are crossed by the Cheliff River. These basins have a very dense hydrographic network (Figure 2) with around 2, 2 km of permanent wadis and 5,600 km of temporary wadis. The Cheliff River's main watercourse of 349 km long results from the junction of the two large wadis of Nahr Touil and Nahr Ouassel (ABH CZ, 2004). The drainage density varies between 0.57 and 1.54 km/km^2. The low values characterize low-pitched terrain, which is mainly located on the high plains and results from low rainfall on permeable formations.

Data and methodology

The data used in this study is made up of a series of monthly flows. The characteristics of hydrometric stations, in terms of geographical location and observation periods, are summarized in Table 1. The largest moving sub-basin is that of El Abtal, which covers 5,400 km2 (Table 1), while the second largest sub-basin is that of Ammi Moussa, which covers 1,890 km2, and they are followed by the sub-basin of Takhemaret, which covers 1,550 km2. The fourteen stations in the study area are not regulated by the dam waters. We chose 14 sites to cover the study area completely. The operating period of the selected stations was 37 years, beginning with the hydrological year 1973/74 and ending with the year 2009/10. September is considered the beginning of the hydrological year in Algeria.

Hydrometric data relating to monthly flows was collected from the National Agency for Hydraulic Resources (ANRH) Algeria.

Streamflow Drought Index (SDI)

Nalbantis (2009) developed the SDI method for the detection of the onset of hydrological drought in two river basins in Greece. The SDI is calculated using several time scales. Furthermore, according to Nalbantis (2008), the calculation of SDI is based on monthly flows, which are then accumulated based on the duration k. For a k-year hydrological period, the cumulative flow volume is obtained. It is necessary to understand the circumstances, magnitude, extent, and frequency of the drought (Tabari et al., 2013). Other researchers used the

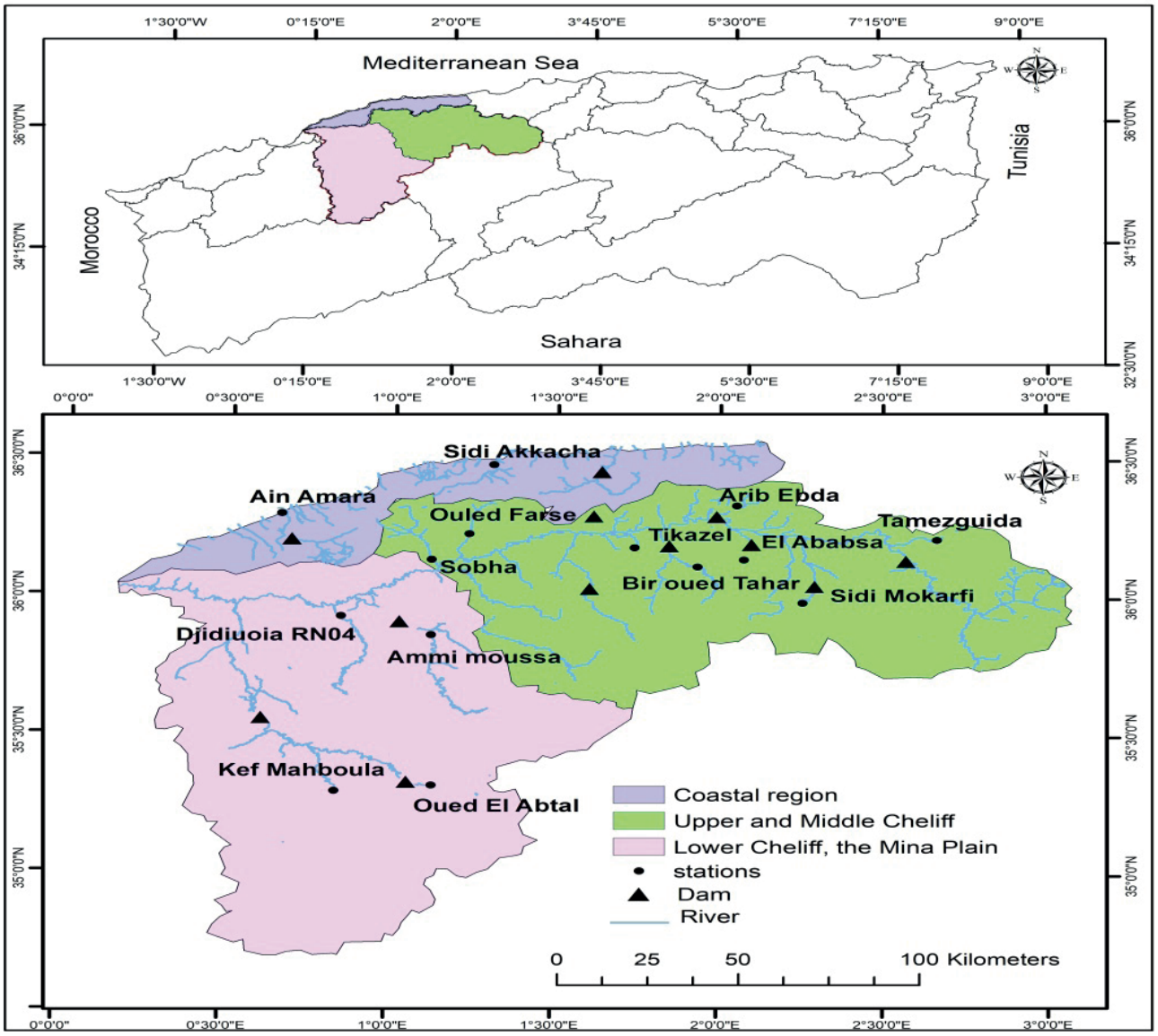

Figure 1. Geographical location of the study area.

SDI index to calculate hydrological drought (e.g., Tabari et al., 2013; Manikandan and Tamilmani, 2015; Yeh et al., 2015). According to the impact studied, SDI values of 3 months or less are useful for routine drought monitoring, SDI values of 6 months or less are useful for agricultural impact monitoring, and SDI values of 12 months or more are useful for hydrological impact detection (WMO, 2012).

The SDI is calculated as follows using the cumulative flow $V_{i,k}$, in which *i* denotes the hydrological year and *j* the month within that hydrological year (j = 1 for September et j = 12 for August), $V_{i,k}$ can be obtained based on Equation (1):

for the i-th hydrological year and the reference period k:

$$V_{i,k} = \text{Sum}\,(Q_{i,j})\ i=1, 2..T, J=1, 2, ...12, k=1, 2, 3, 4 \quad (1)$$

Q_{ij} is the monthly flow, and $V_{i,k}$ is the cumulative streamflow volume for the i-th hydrological year and the k-th reference period, k = 1 is used for the period of September to November, k = 2 is used for the period of November to February, k = 3 is used for the period of September to May, and k = 4 is used for the period of September to August.

After calculating $V_{i,k}$, the SDI is calculated for each reference period k of i years:

Table 1. Characteristics of the hydrometric stations studied.

Name	Basin	X (m)	Y (m)	Z (m)	Observation period
Sidi Akkacha	Coastal Dahra	375000	354300	120	1973-2009
Ain Amara		316450	335120	775	1973-2009
Tamesguida	Middle and Upper Cheliff	497000	323899	490	1973-2009
El Ababsa		443950	318050	313	1973-2009
Arib Ebda		439600	335600	280	1973-2009
Bir Oued Tahar		431000	313250	245	1973-2009
Tikazel		413668	320905	215	1973-2009
Ouled Fares		368100	326650	370	1973-2009
Sobha		357649	316399	375	1973-2009
Ammi Moussa	Lower Cheliff and the Mina	357400	286150	140	1973-2009
Djidiuoia RN04		332600	293899	550	1973-2009
Kef Mahboula		330500	223800	620	1973-2009
Sidi Mokarfi		463000	302600	425	1973-2009
Oued El Abtal		357350	225849	490	1973-2009

$$SDI_{i,k} = \frac{V_{i,k} - V_k}{S_k} \quad i=1, 2\ldots. \quad k=1, 2, 3, 4. \tag{2}$$

where
$\overline{V}_k$ and S_k are the long-term average and standard deviation of the cumulative flow volumes of the reference period k, respectively. In this definition, the truncation level is set to $\overline{V}_k$, although other values based on rational criteria can also be used (Nalbantis and Tsakiris, 2009).

In general, flow data for small basins does not follow a normal distribution and has an asymmetric probability distribution. In accordance with Nalbantis and Tsakiris (2009), Tabari et al. (2013), and Zamani et al. (2015), a log-normal distribution is used as follows to fit the flow data for the SDI calculation:

$$SDI_{i,k} = \frac{y_{i,k} - \bar{y}_k}{S_{y,k}} \quad i=1, 2\ldots. \quad k=1, 2, 3, 4. \tag{3}$$

In such case:

$$y_{i,k} = \ln(V_{i,k}) \quad i=1, 2\ldots,T \quad k=1, 2, 3,4. \tag{4}$$

where
$\overline{y}_k$ and $S_{y,k}$ represent the mean and standard deviation values of V_i, and T is the number of years. According to Nalbantis and Tsakiris, 2009, hydrological drought classification using SDI is shown in Table 2.

The first-order Markov process

Hydrological drought and Markov chains have been studied by many authors, we can cite among them Nalbantis and Tsakiris (2009) ; Meddi and Meddi, 2009; Meddi et al., 2013; Tabari et al., (2015); Lazri et al., 2015; Merabti and Meddi, 2016; Tettey et al., 2017; Habibi et al., 2018; Santos et al., 2019; Sattar et al., 2020 and recently Rahmouni et al., (2021).

Table 2. Hydrological drought based on the SDI (Nalbantis and Tsakiris, 2009).

State description	Criterion	Probability (%)
Non-drought	≤ 0.0	50
Mild drought	-1.0 ≥ SDI <0.0	34.1
Moderate drought	-1.5 ≥ SDI <-1.0	9.2
Severe drought	-2.0 ≥ SDI <-1.5	4.4
Extreme drought	SDI <-2.0	2.3

Markov chains are the simplest example of stochastic processes, when in the study of a series of random variables, one abandon the assumption of independence. It is a non-memory discrete time process.

The first order Markov Chain takes into account only the actual state (present) of the process and not the previous states (past).

Formally, we model with Homogeneous Markov chains the evolution over time of quantities X which can take a finite number of states $X = x_1$, $X = x_2$,… $X = x_n$, and which pass from the state i at time t at state j at the next time t + 1 with a given probability p_{ij}.

$p_{ij} = P(X_{T+1} = x_j/X_t = x_i$ therefore satisfy $0 \leq p_{ij} \leq 1$ and $\sum_{j=0}^{n} p_{ij} = 1$ (since if the chain is in state xi at a time, it will necessarily be in one of the possible states x1,…, xn the next instant and therefore $p_{i1} + p_{i2} + \ldots + p_{in} = 1$; The expression $P(X_{t+1} = j/X_t = i)$ is called a conditional probability and represents the "probability that the quantity X will be j at time t + 1 knowing that it is i at time t".

To define a Markov chain, two basic ingredients are therefore needed:

1. The state space S:=$\{x_1 \ldots x_n\}$ known that we will assume finite
2. The transition (or passage) matrix

$$P=(p_{ij})_{1\leq i\leq n, 1\leq j\leq n}=\begin{matrix} \\ x_1 \\ \\ \\ \end{matrix}\begin{matrix} x_2 \cdots x_n \\ \\ \\ \end{matrix}\begin{pmatrix} p_{11} & p_{12} \cdots p_{1n} \\ \vdots & \\ p_{n1} & p_{n2} \quad p_{nn} \end{pmatrix} \tag{5}$$

Two-state, first-order Markov chain

A two state-, first-order Markov chain is illustrated schematically in figure 2. The two states wet ("1") and dry ("0"). were considered in this study as at each time t, the random variable X can be in one state. First order time dependence implies that there are $2^2 = 4$ transition

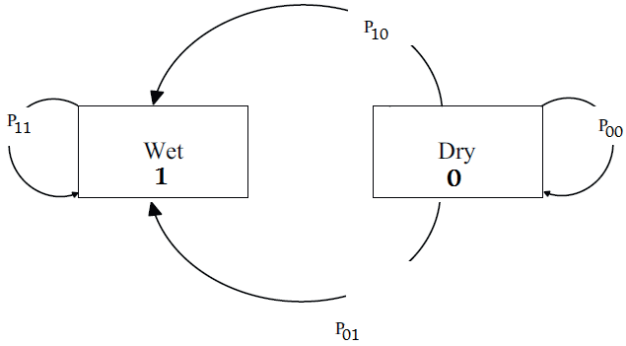

Figure 2. Transitions diagram of two-state, first-order Markov chain.

probabilities, p_{ij}, with $p_{i1} + p_{i2} = 1$ with i = 1, 2. Estimation of the transition probabilities for two-state Markov chains are obtained from the conditional relative frequencies of the transition counts (n_{ij}):

$$\hat{p}_{ij} = \frac{n_{ij}}{\sum_{k=0,1} n_{ik}}, i, j = 0,1. \quad (6)$$

We used the following hypothesis: the model is non-stationary order lag-one Markov chain, i.e $P(X_n=0)$ is not constant over time. Furthermore, it was assumed that transition probabilities were constant across time.

The transition from one state to another at any moment was determined by a P transition matrix of size nxn with the following properties:

$$P = \begin{bmatrix} P_{00} & P_{01} \\ P_{10} & P_{11} \end{bmatrix} \quad (7)$$

In order to calculate the probabilities of a higher-order transition, we used the Chapman-Kolmogorov (Ross, 2014; Lakshmi and Manoj, 2020). equations given by the following matrix product:

$P^{k+1} = P^k P$, where k = 1, 2 ... n.

The limit law of the steady state (which is stationary) exists and is unique because the Markov chain is aperiodic and irreducible in the space of finite states, and it is invariant in determining the limit equation:

$$\begin{bmatrix} 1- p & p \end{bmatrix} \begin{bmatrix} P_{00} & P_{01} \\ P_{10} & P_{11} \end{bmatrix} = \begin{bmatrix} 1- p & p \end{bmatrix}: \quad (8)$$

Let $p_0 = P(X_0 = 1)$. Here p_0 is the probability that the initial year was wet year in our data.

Solving equation 7 gives the following solution:

$$p = \frac{P_{01}}{1 - (P_{11} - P_{01})} \quad (9)$$

p is the probability of remaining in state "1," and $1/p$ is the average time to return to that state.

The law of probabilities of sojourn time in the state "1: Wet" noted by W, which follows the geometric law of a parameter (P_{11}), i.e.

$$P(W = k) = (1 - P_{11})\, P_{11}^{K-1} \quad (10)$$

As a result, the transition probabilities of Wet sequences of lengths greater than k are:

$$P(W > k) = \sum_{t=k+1}^{\infty} P(W = t) = P_{11}^{K} \quad (11)$$

Similarly, the probability of a dry episode of a length m is

$$P(D = m) = (1 - P_{00})\, P_{00}^{m-1} \quad (12)$$

and the probability of dry sequences of lengths greater than "m" is:

$$P(D > m) = (P_{00})^m \quad (13)$$

The criteria for comparison

The Akaike Criteria (AIC) was proposed by Akaike (1974) and the Bayesian Criteria (BIC) was proposed by Schwarz (1978). Akaike's Information Criterion (AIC) and Bayesian Information Criterion (BIC) are two of the most widely used criteria for model selection and performance measures (Qi et al., 2001). Lower AIC and BIC values indicate better model fit. Akaike (1974) formula is given in equation (14):

$$AIC_c = \left[\frac{2n}{n-k-1}\right] k - 2\ln[L_{\max}] \text{ (for n>≈40).} \quad (14)$$

The Bayesian Criteria (1978) is defined by equation (15) as follows:

$$BIC = \ln[n]k - 2\ln[L_{\max}] \quad \text{(for n>≈20)} \quad (15)$$

DISCUSSION AND RESULTS

The frequency analysis of flows at different scales was carried out on data from 14 hydrometric stations from 1973 to 2009. The laws used are: gamma, Gumbel, log-normal and Halphen type A. According to Nalbantis 2008; Shukla and Wood 2008 the log-normal distribution is the most adequate distribution for flow adjustment. In our work, we adapt the flow series to both the gamma law and the log-normal distribution and we determine the validity of the law by the criteria of AIC and BIC.

The analysis of the results showed that the log-normal is better adjusted with the Coastal Dahra stations at different scales of 3, 6, 9 and 12 months according to the AIC and BIC criteria. On the other hand, the Gamma law appears better with the stations Middle and Upper Cheliff and Lower Cheliff and the Mina for the scale 6, 9 and 12 (tables 3 and 4).

Knowledge of SDI classes for different time scales plays an important role in drought identification. It then allows better control of the water supply which generates the proper functioning of the system of forecasting and management of water resources in the short, medium and long term.

The results of an SDI analysis for 14 sites for the period from 1973 to 2009 (September-October-November) showed that three basins had experienced a variety of droughts, with the most severe occurring during the 1980s.

The duration of drought episodes (Fig. 3) showed that variations were occurring from one time scale to another and from one station to another. The Coastal basin had a longer period of non-drought (six years) from 1996 to 2001, and the same class was recorded in the basins of the Lower Cheliff and the Mina from 1992 to 1995, 1999 to 2001, and 2006 to 2008. In the meantime, the Middle and Upper Cheliff basins faced

Table 3. Results of the AIC and BIC criteria (3 months).

Basin	Station names	Criteria	Gamma	Log-normal
Coastal Dahra	Ain Amara	AIC	319.2	301.3
		BIC	323.8	305.9
	Sidi Akacha	AIC	65.8	64.8
		BIC	69	68
Middle and Upper Cheliff	Tamezghuida	AIC	176.7	172.8
		BIC	179.9	176.1
	El Ababsa	AIC	157.1	119.4
		BIC	150.3	122.6
	Arib Ebda	AIC	129.4	127.1
		BIC	132.6	130.3
	Bir Ouled Tahar	AIC	176.3	175.1
		BIC	179.6	178.3
	Tikazel	AIC	136.4	125
		BIC	139.6	128.3
	Ouled Fares	AIC	54.7	52.8
		BIC	57.9	56
	Sobha	AIC	74.5	70.9
		BIC	77.8	74.2
Lower Cheliff and the Mina	Ammi Moussa	AIC	172.7	175.1
		BIC	175.9	178.3
	Djediouia RN 04	AIC	37.6	39.9
		BIC	40.8	43.1
	Kef Mahboula	AIC	79.2	84.3
		BIC	82.4	87.5
	Oued El Abtal	AIC	236.3	284.7
		BIC	239.5	287.9
	Sidi Mokarfi	AIC	90.3	91
		BIC	93.5	94.3

Table 4. Results of the AIC and BIC criteria (12 months).

Basin	Station names	Criteria	Gamma	Log-normal
Coastal Dahra	Ain Amara	AIC	227,4	226,6
		BIC	230,6	229,8
	Sidi Akacha	AIC	197,3	193,5
		BIC	200,5	196,8
Middle and Upper Cheliff	Tamezghuida	AIC	272,1	277,9
		BIC	275,3	281,2
	El Ababsa	AIC	86,5	91,6
		BIC	89,7	94,8
	Arib Ebda	AIC	277,2	279,9
		BIC	280,5	283,1
	Bir Ouled Tahar	AIC	173,6	175,3
		BIC	176,8	178,5
	Tikazel	AIC	93,6	106,1
		BIC	96,8	109,3
	Ouled Fares	AIC	238,1	248,5
		BIC	241,3	246,8
	Sobha	AIC	188,1	189,9
		BIC	191,3	193,2
Lower Cheliff and the Mina	Ammi Moussa	AIC	296	297,5
		BIC	299,2	300,7
	Djediouia RN 04	AIC	200	200.6
		BIC	203,8	203,8
	Kef Mahboula	AIC	137,8	140,3
		BIC	141	143.6
	Oued El Abtal	AIC	262,2	263,2
		BIC	265,1	266,5
	Sidi Mokarfi	AIC	239,1	242,5
		BIC	236,3	248,7

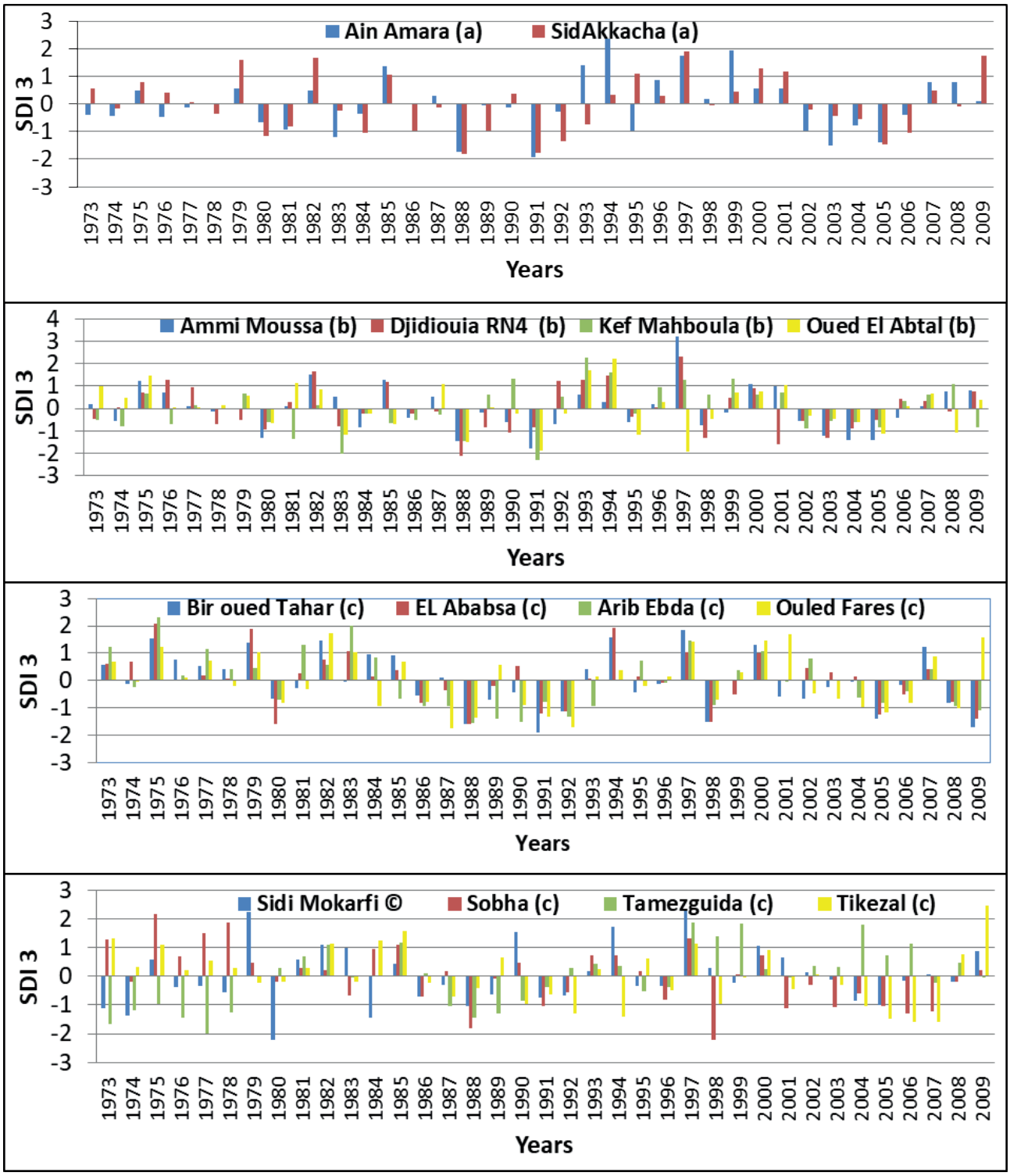

Figure 3. The evolution of the 3-month SDI for (a) Coastal, (b) Lower Cheliff and the Mina, and (c) Middle and Upper Cheliff.

wet periods from 1974 to 1978 and from 1981 to 1984 in the months of September, October, and November. On a three-month scale, the hydrological drought in the Coastal basin consisted of a number of mild episodes between 13 to 14, 2 to 5 moderate episodes, 2 to 3 severe episodes and 0 extreme episodes with a maxi-

mum intensity of -1 .9. In terms of the Lower Cheliff and the Mina basins, they recorded 10 to 15 mild episodes, 2 to 5 moderate episodes, 0 to 2 severe episodes, and 1 to 2 extreme episodes with a maximum intensity of -2.3. Furthermore, hydrometric stations in the Middle and Upper Cheliff basins recorded 9 to 17 mild episodes, 2 to 6 moderate episodes, 1 to 4 severe episodes, and 0 to 1 extreme episode with a maximum intensity of -2.2.

The three basins are distinguished by different types of drought based on a six-month analysis of the SDI. The results are depicted in the figures below.

During the 6-month period (September, October, November, December, January, and February), the three basins (Fig. 4) experienced extreme drought with maximum intensities of -2.2 (Coastal), -2.2 (Lower Cheliff and the Mina), and -2.4 (Middle and Upper Cheliff). They were observed between 1988 and 1989, and between 1990 and 1991. A mild drought of flow supplies ($-1.0 < SDI < 0.0$) was noted at most of study sites between 1980 and 1985. A mild drought was marked by the occurrence of 13 to 15 episodes in the Coastal basin, 9 to 12 episodes in the Middle Cheliff and the Mina basins, and 9 to 20 episodes in the Upper Cheliff basin. However, from September to February, the Coastal and Lower Cheliff faced moderate droughts of 2 to 4 episodes, while the Mina experienced moderate droughts of 2 to 6 episodes. The Middle and Upper Cheliff basins faced 2 to 7 Moderate drought episodes.

During a 6-month period, the basins of Lower Cheliff and the Mina recorded 2 to 3 severe episodes and 0 to 2 extreme episodes. Furthermore, the hydrometric stations in the Middle and Upper Cheliff basins recorded 0 to 4 severe episodes and 0 to 1 extreme episode. And the Coastal basin recorded 2 to 3 severe drought episodes and 1 extreme episode.

Considering all the study stations, the evolution of the 9-months SDI in Figure 5 shows successive occurrences of moderate, mild, and severe droughts, which were observed between 1980 and 1986, 1985 and 1993, and 1995 and 2006. For instance, a 9-month drought was recorded in 1983 at Oued El Abtal (-2.2) and Kef Mahboula (-2.2), in 1988 at Kef Mahboula (-2.6), in 1991 at Bir Oued Tahar (-2.2), in 1992 at Arib Ebda (-2.3), and in 2006 at Tikazel (-2.9).

In terms of mild drought episodes, 13 episodes were observed in the Coastal basin, 9 to 12 episodes in the Lower Cheliff and the Mina basins, and 9 to 18 episodes in the Middle and Upper Cheliff basins. Comparable moderate droughts of 9 months duration are counted in the order of 5 to 7 sequences in the Coastal basin. The Bas Chéliff and Mina basin recorded 2 to 6 drought sequences and the Middle and Upper Chéliff 3 to 5 sequences. On the other hand, in terms of severe drought episodes, 0 to 2 episodes were observed in the Coastal basin, 0 to 3 episodes in the Lower Cheliff and the Mina basins, and 1 to 4 episodes in the Middle and Upper Cheliff basins. In addition, the 9-month evolution of droughts revealed 5 extreme episodes in three study basins: Arib Ebda, Bir Oued Tahar, Kef Mahboula, Oued El Abtal, and Tikazel.

The variability of the evolution of the 12-month SDI in Figure 6 was studied, and it was discovered that it varied in terms of both time and region. The results of a 12-month SDI analysis (from September to August) are depicted in the figures, which show the various classes, and they particularly occurred in the 1980s. It is also noted that the driest years during the study period were recorded from 1999 to 2006 at the stations of Sidi Akkacha and Ain Amara and from 1985 to 1990 at the stations of Bir Oued Tahar, El Ababsa, Arib Ebda and Ouled Fares. On the same time scale, the stations in the Coastal basin had 13 episodes of mild drought with a maximum intensity of -0.5. From 1973 to 2009, 9 to 12 mild drought episodes were observed in the Lower Cheliff and the Mina basins, and 9 to 18 mild drought episodes were observed in the Middle and Upper Cheliff basins, based on 12-month records. In the three study basins, a 12-month moderate drought was observed with a number of episodes between from 2 to 7, with maximum intensities of -1.4 (Coastal), -2 (the Lower Cheliff and the Mina), and -2 (the Middle and Upper Cheliff). Severe and extreme drought episodes occurred in two basins (the Lower Cheliff and the Mina, and the Middle and Upper Cheliff), with the number of episodes ranging from 0 to 3. The maximum intensity was recorded at the Middle and Upper Cheliff basins (e.g. -2.9 (Tikazel), -2.4 (Arib Ebda)) as well as at two stations in the Lower Cheliff and the Mina basins (Kef Mahboula (-2.4) and Oued El Abtal (-2.4)).

Comparison of the number of episodes in each of the three basins at various time scales

The graphs below show the number of extreme, severe, and moderate drought sequences that occurred in three basins in northern Algeria between 1973 and 2009. The analysis revealed that the number of episodes varied from one time scale to another and from one station to another.

The number of drought episodes in each of the three basins was determined using the SDI (shown in Figure 7) at various time scales, allowing us to identify the periods of extreme drought (ED), severe drought (SD), and moderate drought (MD) in the Middle and

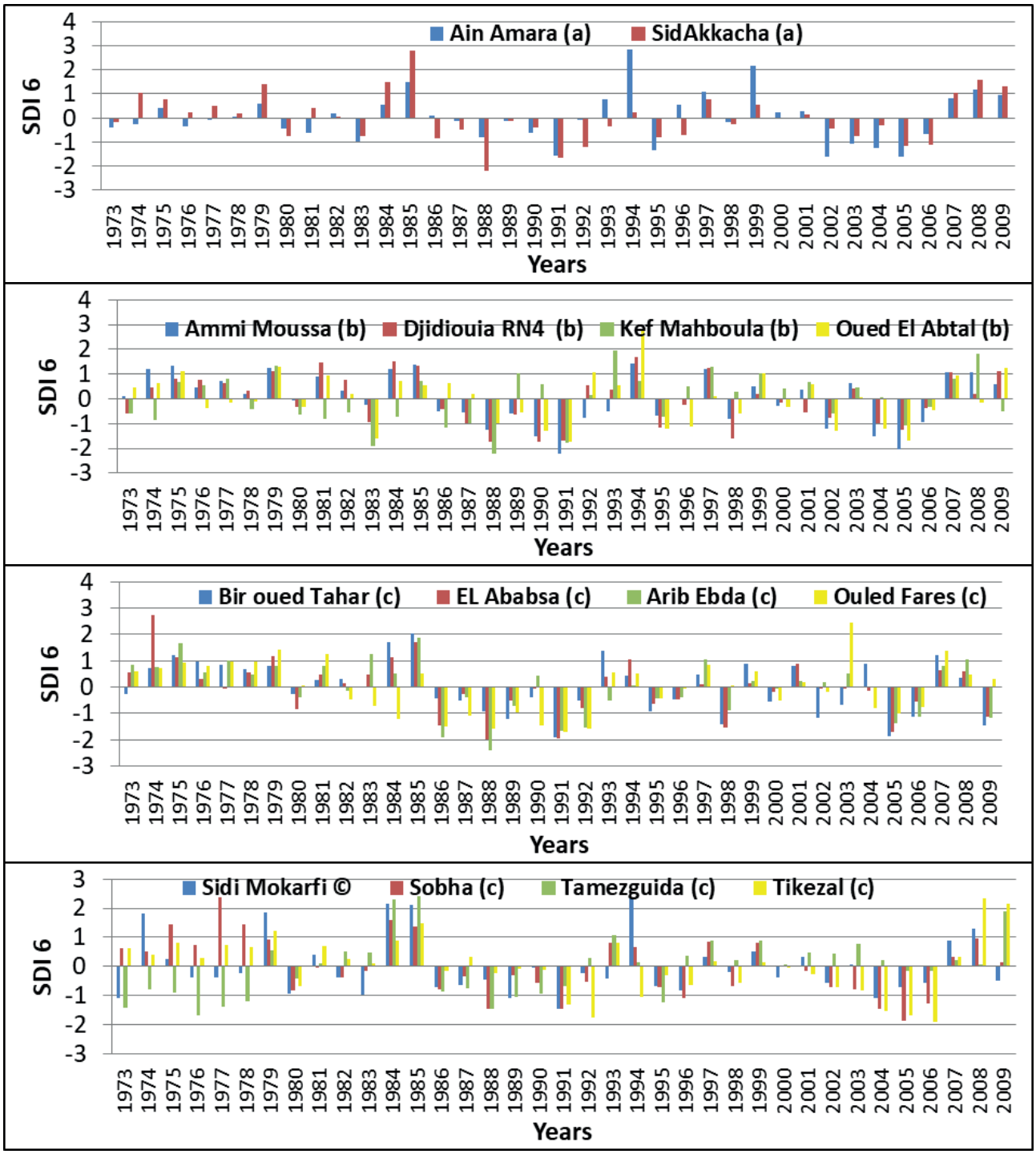

Figure 4. The evolution of the 6-month SDI for (a) Coastal, (b) Lower Cheliff and the Mina, and (c) Middle and Upper Cheliff.

Upper Cheliff basins, the Lower Cheliff basin, and the Mina basin. Extreme drought episodes were observed at 14 hydrometric stations across the study area, with episodes ranging from 1 to 2 months in length. On the other hand, the four stations of the Bas Cheliff and Mina basins were confronted with two extreme episodes of drought on a time scale of 9 months. Ammi Moussa (Lower Cheliff and the Mina), Bir Oued Tahar,

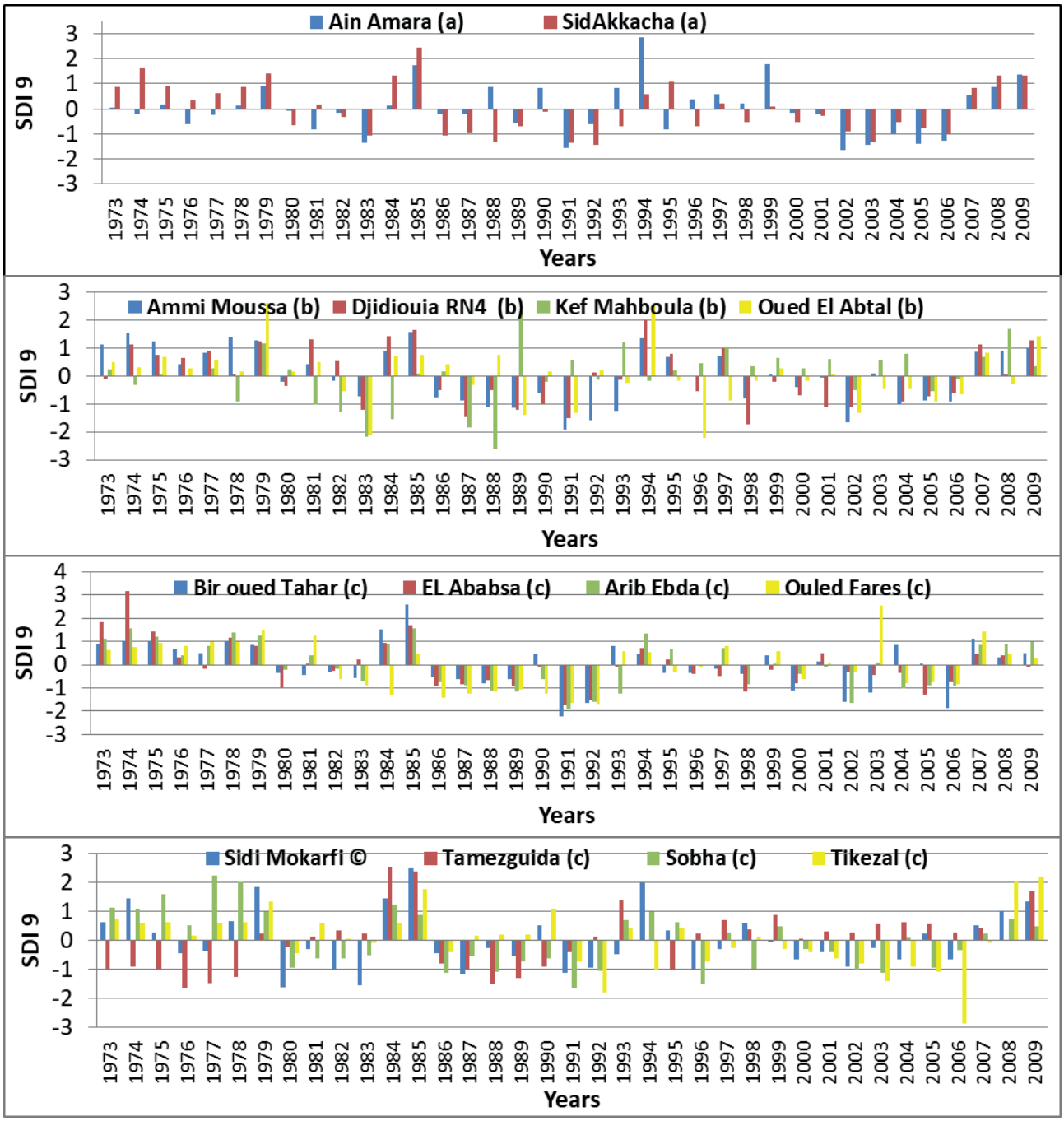

Figure 5. The evolution of the 9-month SDI for (a) Coastal, (b) Lower Cheliff and the Mina, and (c) Middle and Upper Cheliff.

El Ababsa, and Tikazel (Middle and Upper Cheliff) had all experienced severe drought, with a maximum of four episodes. The obtained results suggest that moderate drought periods can be classified into three main categories. Each category can be distinguished by the length and frequency of the drought event occurrence. This condition is the result of the dry climate trend that has been seen in northern Algeria since the 1980s (Meddi and Meddi, 2009).

Frequency mapping of the SDI

We used a histogram that represents through a bar the frequency of drought classes at each interval for the

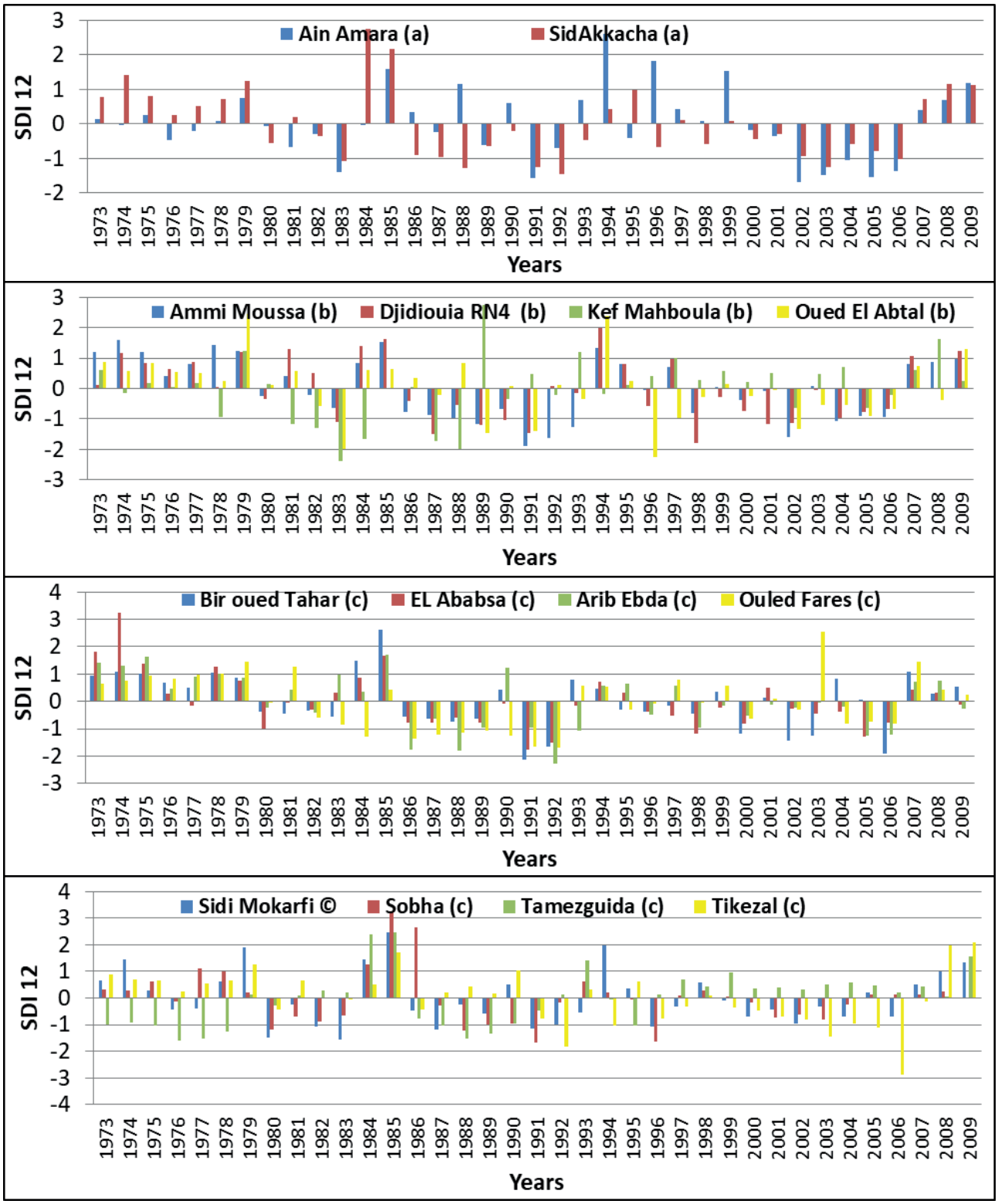

Figure 6. The evolution of the 12-month SDI for (a) Coastal, (b) Lower Cheliff and the Mina, and (c) Middle and Upper Cheliff.

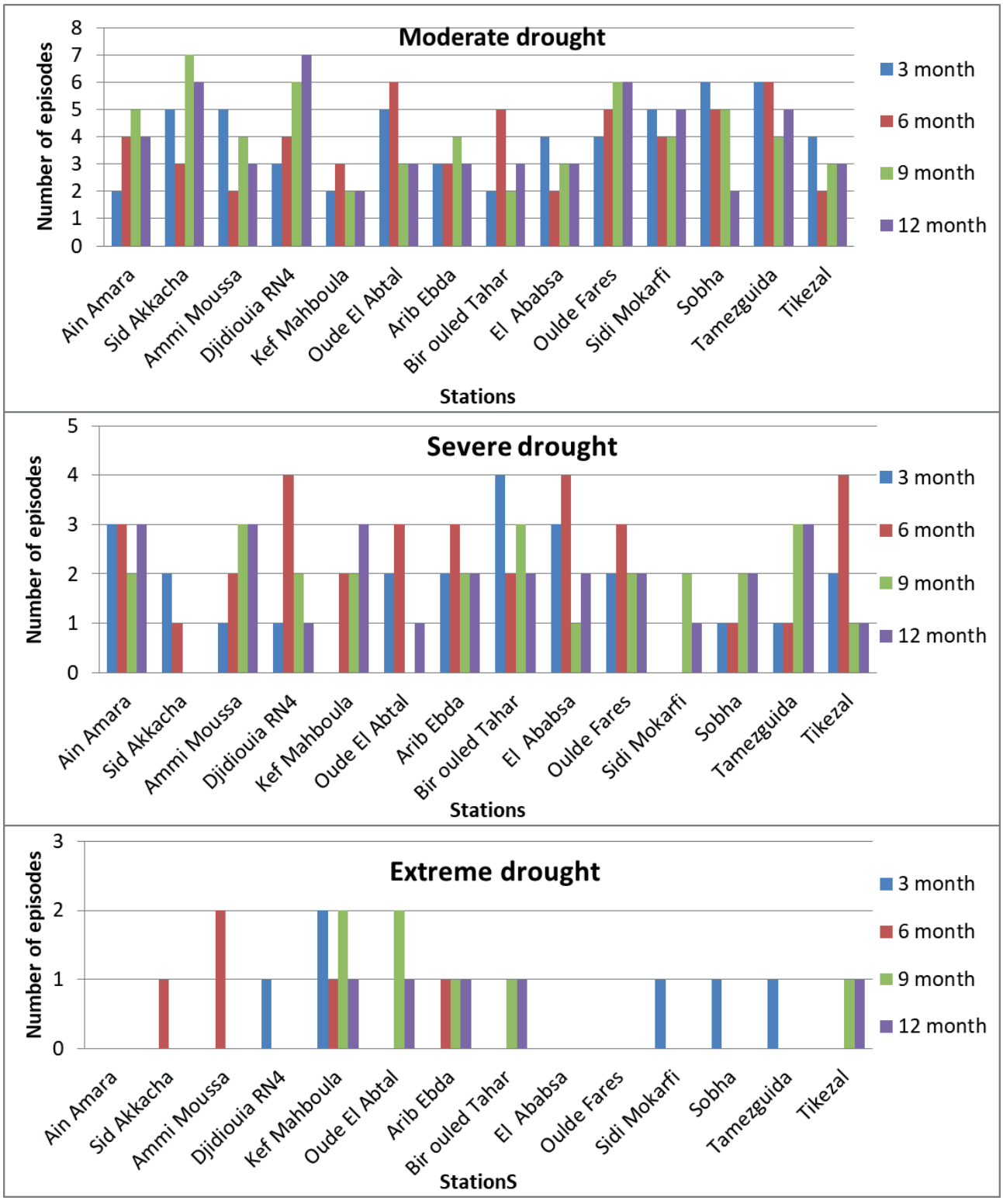

Figure 7. the number of episodes in each of the three basins at various time scales.

description and analysis of the variability of relative frequencies at different time scales in the three basins. Figure 8 shows the frequency distribution, which takes into account the continuous nature of variables and the fact that the classes have different amplitudes. In the meantime, the relative frequency provides the percentage for each drought class in a range of 0 to 1. The distribution of drought classes for all three basins was represented by projecting the results of the SDI frequencies onto the map of the studied region. This type of representation makes the distribution of frequencies of stations in the study area more visible.

Figure 8 depicts the spread of five different kinds of hydrological drought throughout the whole catchment basin. The non-drought class (ND) was found at all the stations in the study area, with a peak at El Ababsa (62%), and a nadir at Oued El Abtal, Tamesguida, and Ferme-Farhat (45%). At Ferme-Farhat, a mild drought (MLD) with a maximum trend (17%) was recorded. And then, 15% frequency was recorded at the levels of Sidi Mokarfi, Kef Mahboula, Bir Oued Tahar, and Djidiuoia RN04. A minimum mild drought (MLD) of 7% was recorded at the El Ababsa station. The maximum frequency of moderate drought (MD) was observed at the stations of Ammi Moussa and Sobha, which reached 27%. Except for the station at Bir Oued Tahar, which recorded an 11% frequency of severe (SD) and extreme (ED) droughts, the whole study area was characterized by very low values ranging from 0% to 8%.

The non-drought frequency (6-month) of the fourteen hydrometric stations was found to be between 62 % and 44%, and they are shown in Figure 8. The repetition of the mild drought (MLD) of high frequency at the level of three basins (Middle and Upper Cheliff basin, Coastal and Lower Cheliff basin, and the Mina basin) was of the order of Sidi Mokarfi (54.1%), Sobha (37.8%), Sidi Akkacha (40.5%), and Ferme-Farhat (29.7%).

Analysis of the 9-months frequency distribution map (Fig. 9) of the study basin shows that the non-drought (ND) frequency was between 45% and 60% in all hydrometric stations such as Tamesguida (56.8%), Kef Mahboula (59.6%), Ferme-Ferhat (54.1%), and Sidi Akkacha (46%). In addition, the mild drought was quite strong in the Middle and Upper Cheliff basins with a maximum value at the station of Sobha (32.4%). Moreover, stations in the Coastal and Lower Cheliff basins were marked by a rather low frequency (Ammi Moussa (32.4%), and Kef Mahboula (24.3%). Severe drought (SD) was recorded in the upper part of Tamesguida (8.1%) and in the upper part of Ferme-Farhat (10.8%). Extreme drought (ED) was detected at the stations of Kef Mahboula (5.4%) and Oued El Abtal (5.4%).

Between 1973 and 2009, the 12-month non-drought class frequencies (Fig.9) reflected the most significant trend in the study area, ranging between 59 % and 38%. The highest non-drought (ND) frequency was discovered in the east and southeast. In the mild class (MLD), the sub-basin of Lower Cheliff had relatively low frequencies, averaging 32.4%, whereas the other basins had quite high frequencies, ranging from 48% to 19%. In the whole study basin, frequencies ranging from 11% to 0 were found for the two severe and extreme drought classes.

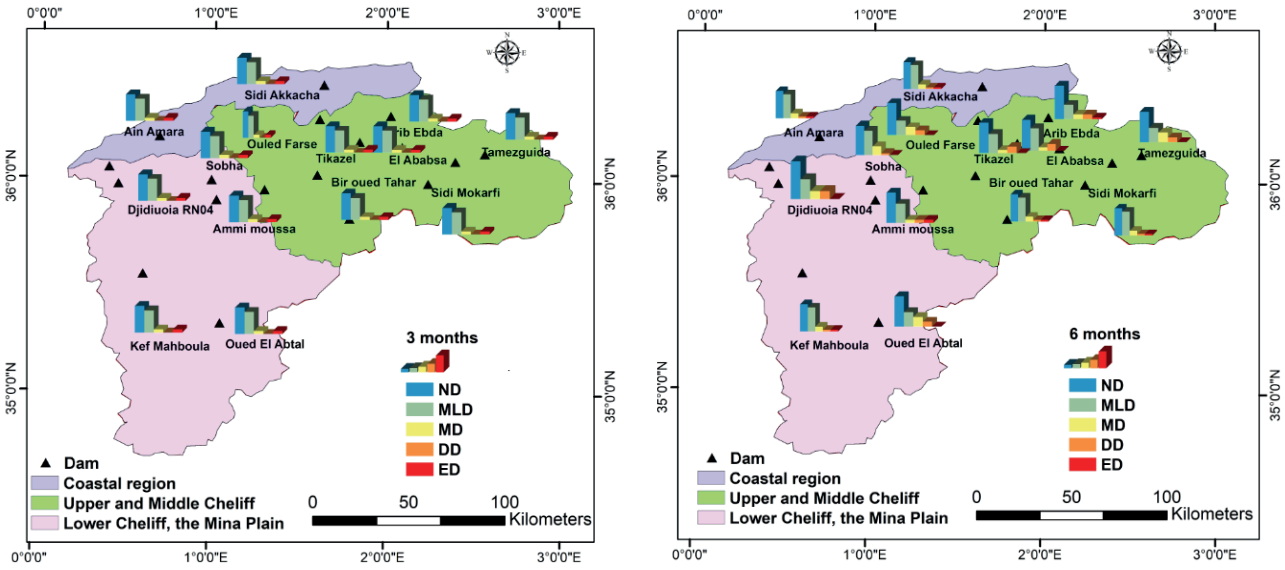

Figure 8. Frequency distribution of the SDI-3 (left) and SDI-6 (right).

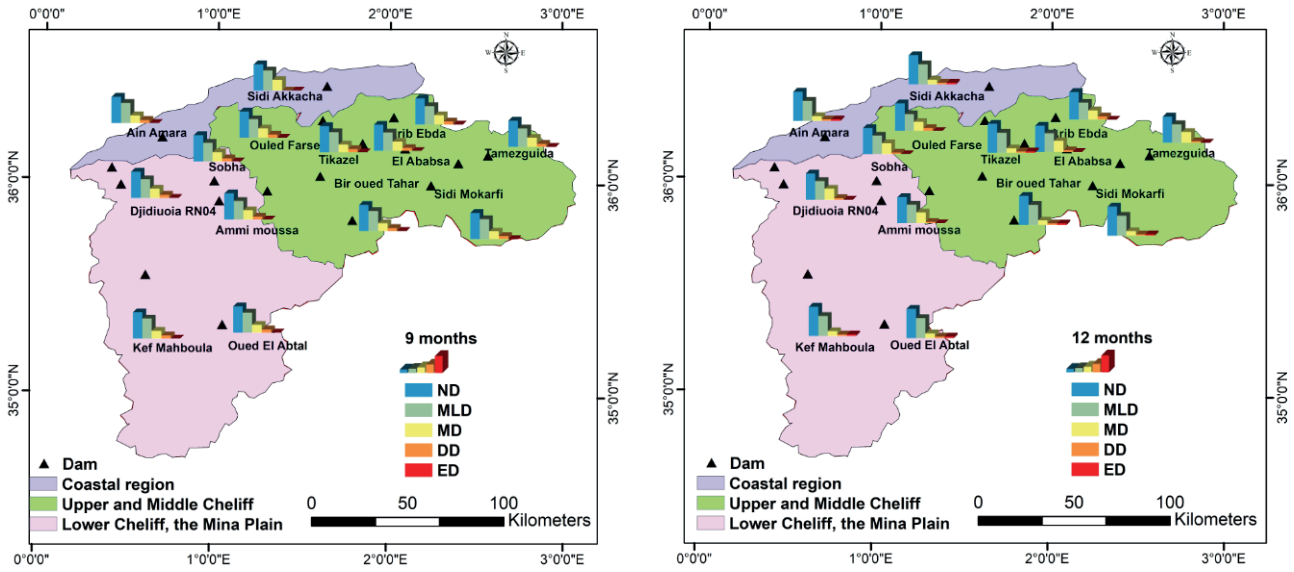

Figure 9. Frequency distribution of the SDI-9 (left) and SDI-12 (right).

First-order Markov chain

In this study, we used the stochastic first-order Markov chain model and the SDI to investigate hydrological drought episodes at various time scales (3, 6, 9, and 12 months) and during a period spanning from 1973 to 2009. To better visualize the variability of hydrological drought, we represented the probabilities of transitions using a histogram. A first-order Markov chain was used to generate probability histograms for three basins (Coastal, Middle and Upper Cheliff, as well as Lower Cheliff and the Mina).

The analysis of these histograms of probability of transition from one dry hydrological year to another dry hydrological year (D-D, Figure 10) over a three-month period (September-October-November) revealed a north-south gradient of 75% to 50%, indicating a strong trend of hydrological drought in the north. In the Middle and Upper Cheliff basins, however, the probability of transition on a 6-month scale (September, October, November, December, January, and February) recorded high values (about 80%). The Lower Cheliff and the Mina basins had the lowest transition probabilities for D-D (40%-45%). In the Middle and Upper Cheliff basins, and in the Coastal basin, the probability of transition from one dry hydrological year to another dry hydrological year (D-D) over 12-month and 9-month periods was fairly similar, rang-

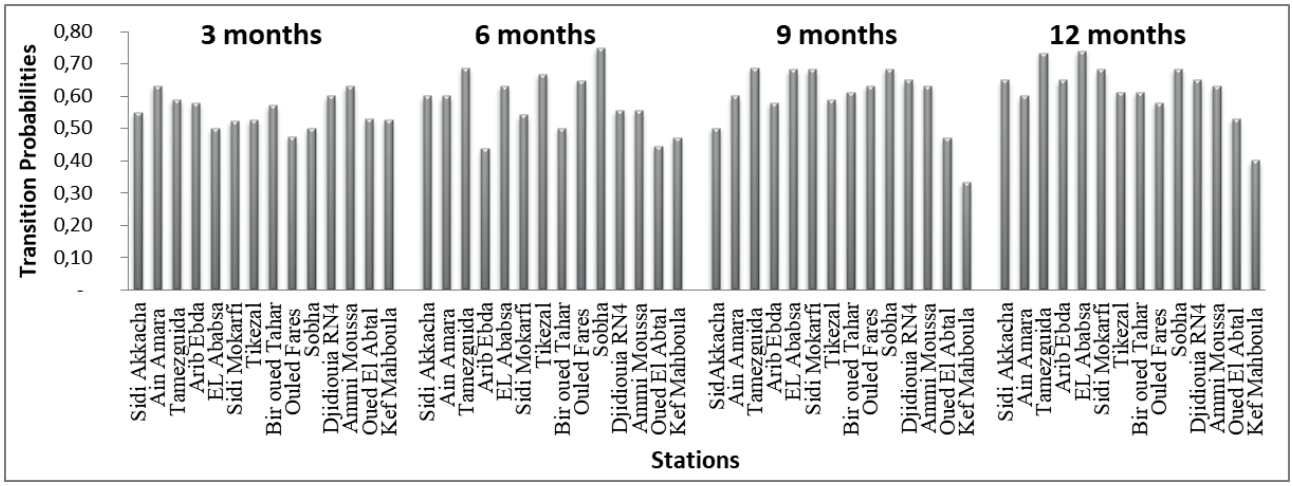

Figure 10. Transition Probabilities (D-D) for the First-Order.

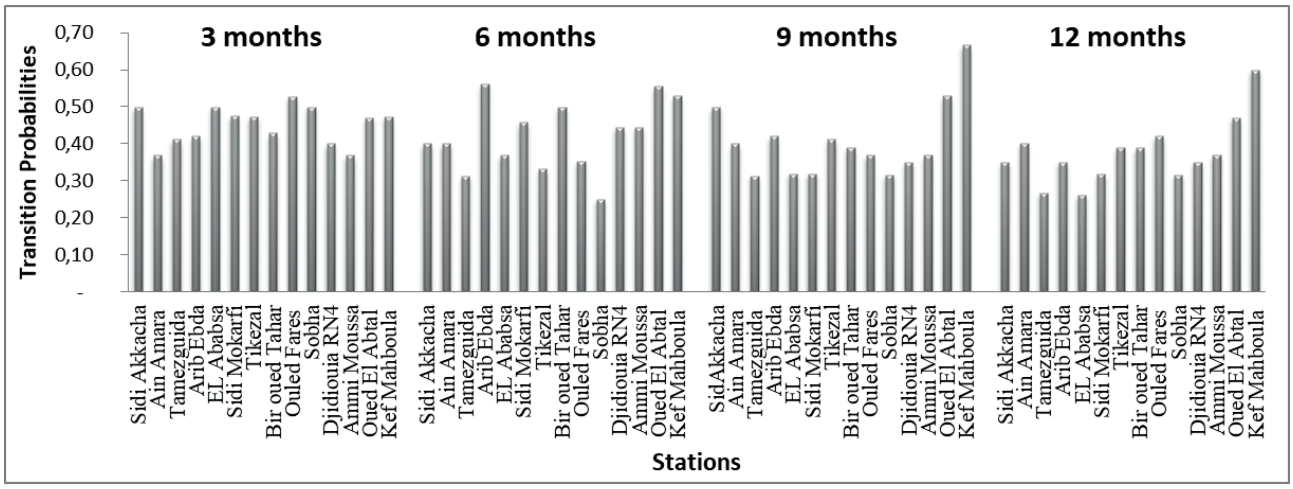

Figure 11. Transition Probabilities (D-W) for the First Order.

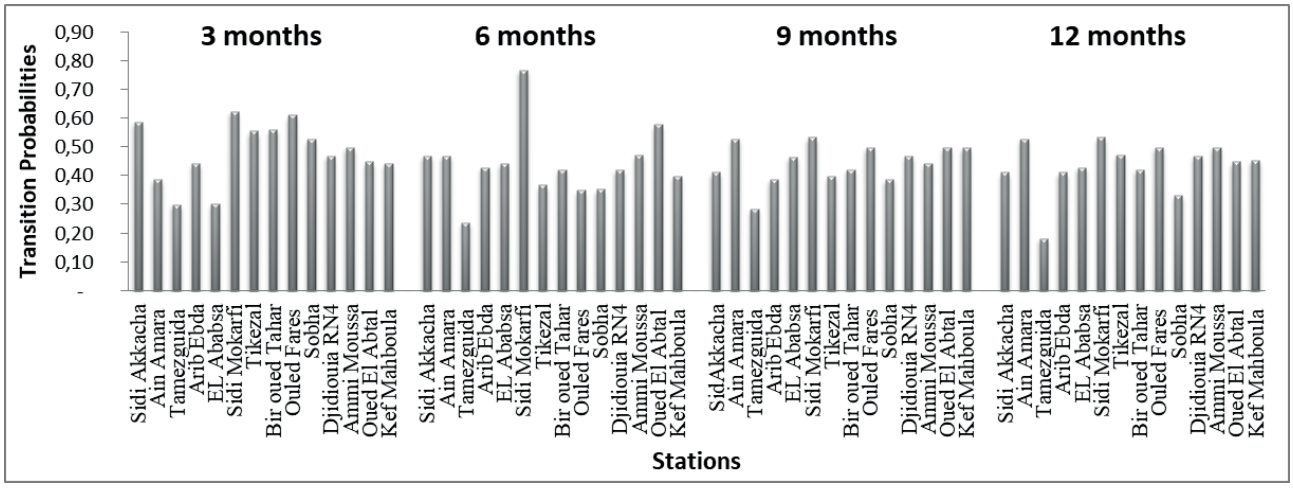

Figure 12. Transition Probabilities (W-D) for the First Order.

ing between 50% and 69%. In the Lower Cheliff and the Mina basins, however, it ranged between 33% and 65%.

For the 3-month scale, the probability of a dry year followed by a wet year (D-W, Fig. 11) revealed a decreasing east-west gradient of 53% (Ouled Fares) to 37% (Ammi Moussa). However, for the same stations, the 6-month transition probability was 31% to 0.56% (Middle and Upper Cheliff), 40% (Coastal), and 44% to 56% (Lower Cheliff and the Mina). The transition probabilities for D-W on a 9-month time scale showed a high probability at the Kef Mahboula station (67%). On the other hand, probabilities of between 31% and 0.41% were found in the Middle and Upper Cheliff basins. In the Coastal basin, the probabilities (D-W) were rather high (> 40%). The probability of transition (D-W) of 14 stations showed a north-south trend of 35% to 60% during a 12-month time scale, with minimum values recorded at the levels of El Ababsa (26%) and Tamesguida (27%).

The transition probability of a wet state followed by a dry state (W-D, Fig. 12) was revealed by an east-west gradient from 63% to 30%.

In the Middle and Upper Cheliff basins, the probabilities (W-D) on a 6-month time scale ranged from 30% to 63%. In the meantime, the remaining stations in these basins ranged from 32% to 58%. It's also worth noting that the study's stations had nearly identical transition probabilities (W-D) for the two scales, 9-month and 12-month (between 18 and 53%).

On a 3-month scale, the probability of transiting through two wet years in a row (W-W, Fig.13) ranged

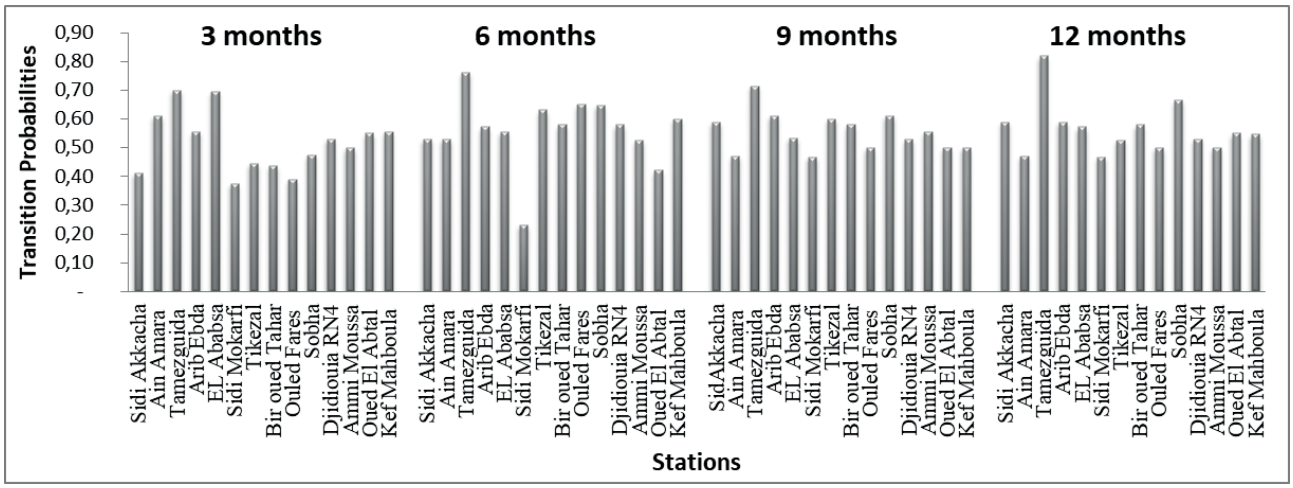

Figure 13. Probability of transition W-W for the first-order.

from 38% to 70%. For example, the two stations Sidi Mokarfi and El Ababsa in the Middle and Upper Cheliff basins were determined by probabilities of 38% (W-W) and 70% (W-W), respectively, and the station Ain Amara in the Coastal basin was determined by a probability of 70% (W-W). The two stations in the Coastal basin recorded the same probability of transition during a 6-month period (53%). In the Middle and Upper Cheliff basins, however, the probability of transition varied between 76% (W-W, Tamesguida) and 23% (W-W, Sidi Mokarfi).

Comparatively, the stations in the Lower Cheliff and the Mina basins recorded probabilities ranging from 40% (W-W, Oued El Abtal) to 60% (the Mina) (W-W, Kef Manboula). In the Lower Cheliff and the Mina basins' and in the Coastal basin's 12-month time scale, probabilities corresponding to 47%-59% were recorded for the two consecutive years (1st order Markov chain, W-W). The stations of the Middle and Upper Cheliff basins, on the other hand, had values ranging from 47% in Sidi Mokarfi to 82% in El Ababsa.

Comparison with previous studies

The balance between resources and needs is an important indicator that guides us in correcting the future of water policy to mitigate the effects of the deficit in all sectors. It is clear that the North African country of Algeria is experiencing a severe resource shortage at a time when demand is growing and the available water supply is shrinking. This is due to a variety of natural and human-caused issues that affect water catchment sites (siltation of dams (3%), or 34 million m3/year in 2000).

Northern Algeria has been exposed to hydrological drought (Nekkache et Megnounif Abdessalem, 2011; Rahmouni et al., 2022). During the different periods 3, 6, 9 and 12 months, the Lower Cheliff and the Mina, Middle and Upper Cheliff, and Coastal Dahra basins were subjected to severe drought with maximum intensity as high maximum values were recorded for example (-2.42) and observed between 7519 and 1995. These results are confirmed by several research works in northern Algeria, for example Meddi et al 2014, showed by a hydrological analysis of drought based on SDI that almost all stations in the Tafna basin (northern Algeria) have suffered from drought during the study period and especially after 1975. Additionally, extreme droughts occurred most frequently after 1975. Bendjemaa et al (2019) showed by the SSFI index that the Bouchegouf station is the most affected by continuous drought conditions in the periods 1987/1988 to 2001/2002 and 2005/2006 to 2009/2010. Nekkache and Megnounif (2011) showed by Standardized Streamflow Index (SSFI) that the two basins of Meffrouche and Béni Bahde (northern Algeria) experienced extreme drought which reached -2.30. Nekkache and Megnounif (2013) showed a deficit of 30% for precipitation after 1970 which caused a drop in flow of more than 60% da in the supply basin of the Meffrouche dam (North-West of Algeria. The driest hydrological years were 1991-1993 and 2005-2006, and that a time scales of 12 months was the most appropriate for developing an effective drought mitigation strategy (Atallah et al., 2022). Brouziyne et al., 2020, the Bouregreg watershed (Marocco) exhibited several dry years with a higher frequency and a significant decrease in annual water inflows were simulated during dry years, ranging from -45.6 %. Tareke and Awoke (2022) showed by SDI

index that 1984/85, 1986/87, 2002/03 and 2010/11 were the most severe and extreme drought years in the river basins of Tekeze, Abbay and Baro.

Hydrological drought and Markov chains have been studied by many researchers, e.g. Nalbantis and Tsakiris (2009); Tabari et al.,2015; Yeh et al., 2015 and Rahmouni et al., 2021 ; Hasan et al., 2021. Our results by the SDI drought index and the transition probabilities indicate that the study area is sensitive to hydrological drought. On the other hand, Meddi et al 2009 and Habibi et al 2018 showed that northern Algeria experienced severe drought by SPI index and Markov chains.

CONCLUSION

This study used statistical methods to investigate hydrological drought in three semi-arid basins (the Coastal basin, the Middle and Upper Cheliff basins, and the Lower Cheliff and the Mina basins). The statistical treatment of hydrological data allowed researchers to investigate drought frequency and persistence using a first-order Markov chain for the period of 1973-2009. The study area consisted of 14 hydrometric stations distributed across three basins.

Different time scales (3, 6, 9, and 12 months) were examined to fully understand the hydrological drought. The results obtained from the SDI values in this study showed that the frequency of drought episodes varied significantly in terms of both time and region. Meanwhile, since 1980, most of the stations have experienced increased hydrological drought.

The results obtained by the SDI index at different time scales showed that hydrological drought was dominant over the entire study area. Mild drought, on the other hand, was defined by a frequency of greater than 5% but less than 21%. Moderate drought episodes had a frequency of between 5% and 18%, whereas severe and extreme drought years had a low percentage (about 4% to 1%). Furthermore, the SDI calculation for periods of 3, 6, 9, and 12 months revealed that almost all the stations experienced moderate-to-mild drought throughout the study period.

For the time scales of 6, 9, and 12 months, the transition probability of first-order non-stationary Markov chains showed that two years of drought (D-D) were more likely in the Middle and Upper Cheliff basins (> 60%). On a three-month scale, the transition probabilities (D-D) were greater than 50% in the Coastal basin and in the Lower Cheliff and the Mina basins, and less than 50% in the Middle and Upper Cheliff basins.

This research highlighted the relevance of studying hydrological drought and how it affects water resource management. The organizations and managers of water resources are responsible for monitoring and controlling the indicators of drought. In the meantime, the interventions to consider: optimization of water resource management, improvement of irrigation techniques to reduce losses and maximize the use of water resources and then structural works (dams, etc.)

REFERENCES

Agence du Bassin Hydrographique Cheliff-Zahrez (ABH CZ)., 2004. Cadastre hydraulique du bassin hydrographie du Cheliff—Aval du barrage de Boughzoul. Première partie: Haut et Moyen Cheliff. (p. 62).

Akbari H., Rakhshandehroo G. R., Sharifloo A. H., Ostadzadeh E., 2015. Drought Analysis Based on Standardized Precipitation Index (SPI) and Streamflow Drought Index (SDI) in Chenar Rahdar River Basin, Southern Iran. Watershed Management, Conference: EWRI Watershed Management Symposium 2015At: ASCE Headquarter, Reston, VA, USA.

Akkurt Eroğluer T., Apaydin H., 2020. Estimation of Drought by Streamflow Drought Index (SDI) and Artificial Neural Networks (ANNs) in Ankara-Nallihan Region. Turkish Journal of Agriculture - Food Science and Technology, 8(2), 348. https://doi.org/10.24925/turjaf.v8i2.348-357.3045.

Atallah M., Djellouli F., Bouanani A., Hasan K., 2022. Assessment of Catchment Behavior of the Wadi Louza in NW-Algeria Under Hydrological Drought Conditions. Earth Systems and Environment. DOI:10.1007/s41748-022-00325-x.

Bendjema L., Baba-Hamed K., Bouanani A., 2019. Characterization of the climatic drought indices application to the Mellah catchment, North-East of Algeria. Journal of Water and Land Development, 43(1), 28-40. https://doi.org/10.2478/jwld-2019-0060.

Benlabiod D., Medjerab A., Mega N., 2020. Characterization of Drought Events in South Oran and South Algiers Steppes in Algeria. International Journal of Ecology & Development, 35(1).

Bergaoui M., Alouini A., 2001. Caractérisation de la sécheresse météorologique et hydrologique: Cas du bassin versant de Siliana en Tunisie. Sécheresse, 12, 215-213.

Boudad B., Sahbi H., Mansouri I., 2018. Analysis of meteorological and hydrological drought based in SPI and SDI index in the Inaouen Basin (Northern Morocco). Journal of Materials and Environmental Sciences, 9(1), 219-227. https://doi.org/10.26872/jmes.2018.9.1.25.

BrouziyneY., Abouabdillah A., Chehbouni A., Hanich L., Bergaoui K., McDonnell R., Benaabidate L., 2020 Assessing Hydrological Vulnerability to Future Droughts in a Mediterranean Watershed: Combined Indices-Based and Distributed Modeling Approaches. Water, 12(9), 2333. https://doi.org/10.3390/w12092333

Dabanli I., 2018. Drought hazard, vulnerability, and risk assessment in Turkey. Arabian Journal of Geosciences, 11(18), 538. https://doi.org/10.1007/s12517-018-3867-x.

Elbeltagi A., Kumar M., Kushwaha N. L., Pande C. B., Ditthakit P., Vishwakarma D. K., Subeesh A., 2023. Drought indicator analysis and forecasting using data driven models: Case study in Jaisalmer, India. Stochastic Environmental Research and Risk Assessment, 37(1), 113-131. https://doi.org/10.1007/s00477-022-02277-0.

Faye C., Sow A. A., Ndong J. B., 2015. Étude des sècheresses pluviométriques et hydrologiques en Afrique tropicale: Caractérisation et cartographie de la sècheresse par indices dans le haut bassin du fleuve Sénégal. Physio-Géo, 9, 17-35. https://doi.org/10.4000/physio-geo.4388.

Filali B. A., 2004. Enjeux stratégiques et défis majeurs de l'irrigation dans les pays du Maghreb. H.T.E, 129, 2-7.

Ghenim A. N., Megnounif A., 2011. CARACTÉRİSATİON DE LA SÉCHERESSE PAR LES İNDİCES SPI ET SSFI (NORD-OUEST DE L'ALGÉRİE). LJEE, 18.

Ghenim A. N., Megnounif A., 2013. Ampleur de la sécheresse dans le bassin d'alimentation du barrage Meffrouche (Nord-Ouest de l'Algérie). Physio-Géo, 7, 35-49. https://doi.org/10.4000/physio-geo.3173

Ghenim A. N. e, Megnounif A., i Seddini A., Terfous A., 2010. Fluctuations hydropluviométriques du bassin-versant de l'oued Tafna à Béni Bahdel (Nord-Ouest algérien). Sécheresse, 21(2).

González-López, N., Carvajal-Escobar, Y., & Universidad del Valle, Cali, Colombia. (2020). Caracterización de sequías hidrológicas en el río Cauca en su valle alto. Tecnología y ciencias del agua, 11(1), 235-265. https://doi.org/10.24850/j-tyca-2020-01-06.

Habibi B., Meddi M., 2021. Meteorological drought hazard analysis of wheat production in the semi-arid basin of Cheliff–Zahrez Nord, Algeria. Arabian Journal of Geosciences, 14(11), 1045. https://doi.org/10.1007/s12517-021-07401-y.

Habibi B., Meddi M., Torfs P. J. J. F., Remaoun M., Van Lanen H. A. J., 2018. Characterisation and prediction of meteorological drought using stochastic models in the semi-arid Chéliff–Zahrez basin (Algeria). Journal of Hydrology: Regional Studies, 16, 15-31. https://doi.org/10.1016/j.ejrh.2018.02.005.

Hasan H. H., Mohd Razali S. F., Muhammad N. S., Asmadi A., 2021. Hydrological Drought across Peninsular Malaysia: Implication of Drought Index. Natural Hazards and Earth System Sciences. https://doi.org/10.5194/nhess-2021-249.

Hong X., Guo S., Zhou Y., Xiong L., 2015. Uncertainties in assessing hydrological drought using streamflow drought index for the upper Yangtze River basin. Stochastic Environmental Research and Risk Assessment, 29(4), 1235-1247. https://doi.org/10.1007/s00477-014-0949-5.

Hosseinzadeh Talaee P., Tabari H., Sobhan Ardakani S., 2014. Hydrological drought in the west of Iran and possible association with large-scale atmospheric circulation patterns: hydrological drought in the west of Iran. Hydrological Processes, 28(3), 764-773. https://doi.org/10.1002/hyp.9586.

Jahangir M. H., Yarahmadi Y., 2020. Hydrological drought analyzing and monitoring by using Streamflow Drought Index (SDI) (case study: Lorestan, Iran). Arabian Journal of Geosciences, 13(3), 110. https://doi.org/10.1007/s12517-020-5059-8.

Jiang H., Khan M. A., Li Z., Ali Z., Ali F., Gul, S., 2020. Regional drought assessment using improved precipitation records under auxiliary information. Tellus A: Dynamic Meteorology and Oceanography, 72(1), 1-26. https://doi.org/10.1080/16000870.2020.1773699.

Khan S., Gabriel H. F. Rana T., 2008. Standard precipitation index to track drought and assess impact of rainfall on watertables in irrigation areas. Irrig Drainage Syst 22, 159-177.

Kavianpour M., Seyedabadi M., Moazami S., 2018. Spatial and temporal analysis of drought based on a combined index using copula. Environmental Earth Sciences, 77(22), 769. https://doi.org/10.1007/s12665-018-7942-0.

Koffi B., Kouadio Z. A., Kouassi K. H., Yao A. B., Sanchez M., Kouassi K. L., 2020. Impact of Meteorological Drought on Streamflows in the Lobo River Catchment at Nibéhibé, Côte d'Ivoire. Journal of Water Resource and Protection, 12(06), 495-511. https://doi.org/10.4236/jwarp.2020.126030.

Lakshmi G., Manoj J., 2020. Application of Markov Process for Prediction of Stock Market Performance. International Journal of Recent Technology and Engineering (IJRTE), 8(6), 1516-1519. https://doi.org/10.35940/ijrte.F7784.038620

Lazri M., Ameur S., Brucker J. M., Lahdir M., Sehad M., 2015. Analysis of drought areas in northern Algeria using Markov chains. Journal of Earth System Sci-

ence, 124(1), 61-70. https://doi.org/10.1007/s12040-014-0500-6.

Manikandan M., Tamilmani D., 2015. Assessing Hydrological Drought Charactertics: A Case Study in a Sub Basin of Tamil Nadu, India. Scientific Journal Agricultural Engineering, 71-83.

McKee TB., Doesken NJ., Kleist J., 1993. The relationship of drought frequency and duration to time scales. Preprints Eighth Conf on Applied Climatology Anaheim CA. Amer Meteor Soc, pp. 179–184.

Meddi H., Meddi M., 2009a. Etude de la persistance de la secheresse au Niveau de sept plaines Algeriennes Par utilisation des chaines de Markov (1930-2003). Courrier du Savoir N°09, Mars 2009, 39-48.

Meddi H., Meddi M., 2009b. Variabilité des précipitations annuelles du Nord-Ouest de l'Algérie. Sécheresse, 20(1), 57-65. https://doi.org/10.1684/sec.2009.0169.

Meddi H., Meddi M., Assani A. A., 2014. Study of Drought in Seven Algerian Plains. Arabian Journal for Science and Engineering, 39(1), 339-359. https://doi.org/10.1007/s13369-013-0827-3.

Meddi M., Hubert P., 2003. Impact de la modification du régime pluviométrique sur les ressources en eau du nord-ouest de l'Algérie. Proceedings of an International Symposium «Hydrology of the Mediterranean and Semiarid Regions», Montpellier, Montpellie.

Meddi M., Toumi Samir., Mehaiguene M., 2013. Hydrological drought in Tafna Basin-northwest of Algeria. https://doi.org/10.13140/2.1.2598.2245.

Medhi J., 1994. Stochastic Processes. New Age International Publishers, New Delhi, India.

Melhaou M., Mezrhab A., Mimouni J., 2018. Evaluation et cartographie de la secheresse meteorologique dans les hauts plateaux de l'oriental du Maroc (zone du projet PDPEO). Rev. Microbiol. Ind. San et Environn. 12(19, 71-92.

Merabti A., Meddi M., 2016. Etude de la persistance de la secheresse au niveau de sept plaines dans le nord-est algerien. 4 eme Colloque International Terre & Eau 2016. Annaba 16, 17 & 18 Mai2016.

Minea I., Iosub M., Boicu D., 2022. Multi-scale approach for different type of drought in temperate climatic conditions. Natural Hazards, 110(2), 1153-1177. https://doi.org/10.1007/s11069-021-04985-2.

Modarres R., 2007. Streamflow drought time series forecasting. Stochastic Environmental Research and Risk Assessment, 21(3), 223-233. https://doi.org/10.1007/s00477-006-0058-1.

Nalbantis I., 2008. Evaluation of a Hydrological Drought Index. European Water 23/24, 67-77.

Nalbantis I., Tsakiris G., 2009. Assessment of Hydrological Drought Revisited. Water Resources Management, 23(5), 881-897. https://doi.org/10.1007/s11269-008-9305-1.

Ngoc Quynh Tram V., Somura H., Moroizumi T., 2021. Evaluation of drought features in the Dakbla watershed, Central Highlands of Vietnam. Hydrological Research Letters, 15(3), 77-83. https://doi.org/10.3178/hrl.15.77.

Olivier K., Wilfrid V. E., Jean-Marie D., 2017. Caractérisation Des Risques Hydroclimatiques Dans Le Bassin Versant De L'Ouémé A L'exutoire De Bétérou Au Bénin (Afrique De L'ouest). European Scientific Journal, ESJ, 13(15), 101. https://doi.org/10.19044/esj.2017.v13n15p101.

Ozkaya A., Zerberg Y., 2019. A 40-Year Analysis of the Hydrological Drought Index for the Tigris Basin, Turkey. Water, 11(4), 657. https://doi.org/10.3390/w11040657.

Palmer, W.C. (1965). Meteorological Drought. Weather Bureau Research Paper No. 45. Washington, DC: US Department of Commerce.

Pathak A. A., Channaveerappa., Dodamani B. M., 2016. Comparison of two hydrological drought indices. Perspectives in Science, 8, 626-628. https://doi.org/10.1016/j.pisc.2016.06.039.

Prajapati V. K., Khanna M., Singh M., Kaur R., Sahoo R. N., Singh D. K., 2022. PCA–based composite drought index for drought assessment in Marathwada region of Maharashtra state, India. Theoretical and Applied Climatology. https://doi.org/10.1007/s00704-022-04044-1.

Qi M., Zhang G. P., 2001. An investigation of model selection criteria for neural network time series forecasting. European Journal of Operational Research, 132(3), 666-680. https://doi.org/10.1016/S0377-2217(00)00171-5.

Rahmouni A., Meddi M., Hamoudi Saaed A., 2022. Hydrological Drought Response to Meteorological Drought Propagation and Basin Characteristics (Case Study: Northwest of Algeria). Russian Meteorology and Hydrology 47, 708-717.

Rezaeianzadeh M., Tabari H., Arabi Yazdi A., Isik S., Kalin L., 2014. Flood flow forecasting using ANN, ANFIS and regression models. Neural Computing and Applications, 25(1), 25-37. https://doi.org/10.1007/s00521-013-1443-6.

Ross Sheldon M., 2014. "Chapter 4.2: Chapman–Kolmogorov Equations". Introduction to Probability Models (11th ed.). p. 187.

Santos E. A. B. dos., Stosic, T., Barreto I. D. de C., Campos L., Silva A. S. A. da., 2019. Application of Markov chains to Standardized Precipitation Index (SPI) in São Francisco River Basin. Ambiente e Agua - An

Interdisciplinary Journal of Applied Science, 14(3), 1. https://doi.org/10.4136/ambi-agua.2311.

Sattar M. N., Jehanzaib M., Kim J. E., Kwon H.-H., Kim T.-W., 2020. Application of the Hidden Markov Bayesian Classifier and Propagation Concept for Probabilistic Assessment of Meteorological and Hydrological Droughts in South Korea. Atmosphere, 11(9), 1000. https://doi.org/10.3390/atmos11091000.

Shafer B. A., Dezman L. E., 1982. Development of a surface water supply index (SWSI) to assess the severity of drought conditions in snowpack runoff areas. Proceedings of the Western Snow Conference, 164-175.

Shukla S., Wood A.W., 2008. Use of a standardized runoff index for characterizing hydrologic drought. Geophys. Res. Lett., 35(2008), L02405.

solaimani sardou, F, Bahramand A., 2014. Hydrological drought analysis using SDI index in Halilrud basin of Iran. Environmental Resources Research, 2(1). https://doi.org/10.22069/ijerr.2014.1678.

Soro T. D., Soro N., Oga Y. M.-S., Lasm T., Soro G., Ahoussi K. E., Biémi J., 2011. La variabilité climatique et son impact sur les ressources en eau dans le degré carré de Grand-Lahou (Sud-Ouest de la Côte d'Ivoire). Physio-Géo, 5, 55-73. https://doi.org/10.4000/physio-geo.1581.

Sun X., Wang M., Li G., Wang Y., 2020. Regional-scale drought monitor using synthesized index based on remote sensing in northeast China. Open Geosciences, 12(1), 163-173. https://doi.org/10.1515/geo-2020-0037.

Tabari H., Nikbakht J., Hosseinzadeh Talaee P., 2013. Hydrological Drought Assessment in Northwestern Iran Based on Streamflow Drought Index (SDI). Water Resources Management, 27(1), 137-151. https://doi.org/10.1007/s11269-012-0173-3.

Tabari H., Zamani R., Rahmati H.,Willems P., 2015. Markov Chains of Different Orders for Streamflow Drought Analysis. Water Resources Management 29(9): 3441-3457. https://doi.org/10.1007/s11269-015-1010-2.

Tareke K.A., Awoke A.G., 2022. Hydrological drought analysis using streamflow drought index (SDI) in Ethiopia. Advances in Meteorology . 4/22/2022, p1-19. 19p. Volume 2022. https://doi.org/10.1155/2022/7067951.

Tettey M., Oduro F. T., Adedia D., Abaye D. A., 2017. Markov chain analysis of the rainfall patterns of five geographical locations in the south eastern coast of Ghana. Earth Perspectives, 4(1), 6. https://doi.org/10.1186/s40322-017-0042-6.

Thierry T. N., 2020. Evaluation et impact de la sécheresse sur une région agricole: Cas de la plaine irriguée de la Beqaa. Université d'Orléans.

Tokarczyk T., Szalińska W., 2014. Combined analysis of precipitation and water deficit for drought hazard assessment. Hydrological Sciences Journal, 59(9), 1675-1689. https://doi.org/10.1080/02626667.2013.862335.

Wilhite D., 2000. Drought as a natural hazard: Concepts and definitions. Environmental Science, 1-18.

World Meteorological Organization. (2012). Standardized Precipitation Index User Guide (WMO-No.1090), Geneva.http://www.droughtmanagement.info/literature/WMO_standardized_precipitation_index_user_guide_ en_2012.pdf.

World Meteorological Organization (WMO) and Global Water Partnership (GWP)., 2014: National Drought Management Policy Guidelines: A Template for Action (D.A. Wilhite). Integrated Drought Management Programme (IDMP) Tools and Guidelines Series 1. WMO, Geneva, and GWP, Stockholm, http://www.droughtmanagement.info/literature/IDMP_NDMPG_en.pdf.

World Meteorological Organization (WMO),. Global Water Partnership (GWP)., 2017. Handbook of drought indicators and indices (M. Svoboda and B.A. Fuchs). Integrated Drought Management Program (IDMP), Integrated Drought Management Tools and Guidelines Series 2. Geneva. ISBN 978–92–63-11173-9.

Yuan D., Lu E., Dai W., Chao Q., Wang H., Li, S., 2022. The Ice-and-Snow Tourism in Harbin Met Its Waterloo: Analysis of the Causes of the Warm Winter with Reduced Snowfall in 2018/2019. Atmosphere, 13(7), 1091. https://doi.org/10.3390/atmos13071091.

Yeh C.-F., Wang J., Yeh H.-F., Lee C.-H., 2015. SDI and Markov Chains for Regional Drought Characteristics. Sustainability, 7(8), 10789-10808. https://doi.org/10.3390/su70810789.

Zaki N. A., 2020. The role of agriculture expansion in water resources depletion in central Iran. https://doi.org/10.13140/RG.2.2.31754.90566.

Zamani R., Tabari H., Willems P., 2015. Extreme streamflow drought in the Karkheh river basin (Iran): Probabilistic and regional analyses. Natural Hazards, 76(1), 327-346. https://doi.org/10.1007/s11069-014-1492-x.

Zhang Q., Shi R., Xu C.-Y., Sun P., Yu H., Zhao, J., 2022. Multisource data-based integrated drought monitoring index: Model development and application. Journal of Hydrology, 615, 128644. https://doi.org/10.1016/j.jhydrol.2022.128644.

Zhao C., Brissette F., Chen J., Martel J.-L., 2020. Frequency change of future extreme summer meteorological and hydrological droughts over North America. Journal of Hydrology, 584, 124316. https://doi.org/10.1016/j.jhydrol.2019.124316.

Zhong F., Cheng Q., Wang P., 2020. Meteorological Drought, Hydrological Drought, and NDVI in the Heihe River Basin, Northwest China: Evolution and Propagation. Advances in Meteorology, 2020, 1-26. https://doi.org/10.1155/2020/2409068.

Zulfiqar A., Ijaz H., Muhammad F., 2019. Annual Characterization of Regional Hydrological Drought using Auxiliary Information under Global Warming Scenario [Preprint]. Hydrological Hazards. https://doi.org/10.5194/nhess-2018-373.

Italian Journal of Agrometeorology
Rivista Italiana di Agrometeorologia

Firenze University Press
www.fupress.com/ijam

OPEN ACCESS

Citation: Wawo, A., Lestari, P., Setyowati, N., Syarif, F., Juhaeti, T., & Kartika, K. (2024). The influence of temperature on germination and seedling growth of sorghum. *Italian Journal of Agrometeorology* (1): 95-107. doi: 10.36253/ijam-1828

Received: September 16, 2022

Accepted: June 6, 2042

Published: August 2, 2024

Data Availability Statement: All relevant data are within the paper and its Supporting Information files.

Competing Interests: The Author(s) declare(s) no conflict of interest.

ORCID:
AHW: 0000-0001-8996-8402
NS: 0000-0002-4980-2333
TJ: 0000-0002-9256-5249
PL: 0000-0002-5596-9850
KK: 0000-0002-7116-7014
FS: 0000-0003-0158-3415

The influence of temperature on germination and seedling growth of sorghum

Albertus Husein Wawo[1,*], Peni Lestari[2], Ninik Setyowati[1], Fauzia Syarif[3], Titi Juhaeti[1], Kartika Kartika[2]

[1] *Research Center for Applied Botany, National Research and Innovation Agency (BRIN), Indonesia*
[2] *Research Center for Holticulture, National Research and Innovation Agency (BRIN), Indonesia*
[3] *Research Center for Environmental and Clean Technology Research Center, Biological and Environmental Research Organization, National Research and Innovation Agency (BRIN), Indonesia*
*Corresponding author. Email: wawoal@gmail.com

Abstract. The extensification of agricultural activities to suboptimal areas, including dryland, is being considered. Sorghum as a drought-tolerant crop is usually cultivated in dryland areas in Indonesia. However local farmers are having difficulty in choosing quality seeds suitable for the specific area temperature condition. This study evaluated the physical quality of commonly used sorghum cultivars in Indonesia and their responses to several germination temperatures. The three sorghum cultivars used were Strong Brown (SB) Sorghum known as the local cultivar, Pale yellow (PY), and Light Brown (LB). The result revealed that each sorghum cultivar has specific seed characteristics, especially in the color, shape, and size of the seeds. The seeds of the Light Brown sorghum had the highest quality, followed by Strong Brown sorghum and PaleYellow sorghum cultivars based on both the tetrazolium test and the direct germination test. The optimum temperature for sorghum seed germination ranged from 25 to 35°C. Each sorghum cultivar has its specific temperature requirement for germination. Low temperature (20°C) potentially reduces the percentage of germination and delays the seed germination time of these three cultivars. LB cultivar has the highest relative growth rate (RGR) from the first week to the second week (R1), while the RGR from the first week to the third week (R2), LB sorghum cultivar is in the second position after the PY cultivar. Cultivar LB is suggested for cultivating in elevations 300-500 m asl, moreover cultivar SB elevations 50-250 m asl.

Keywords: germination, RGR, sorghum, seed characteristics, temperature.

HIGHLIGHT

- Sorghum cultivar can be differentiate based on their color, size, and shape.
- Specific sorghum cultivars require specific temperature for their germination.
- The suitable cultivation area for each sorghum cultivar affected by environmental condition, including temperature.

INTRODUCTION

Drylands in Indonesia cover about 13.3 million hectares. Most of the dry lands in Indonesia have been underutilized or utilized for agriculture using poor cultivation practices. Drylands are the area where average rainfall is lower than the potential moisture loss through evapotranspiration (FAO, 2004). Drylands are characterized by high surface temperature and light intensity, low humidity, and low soil nutrients. Drylands are extremely sensitive to global climate change (Huang *et al*., 2017). Climate change has increased the annual mean temperature in Indonesia by 0.36-0.46ºC since 1990 (Mariah, 2010). Drylands are defined as suboptimal land but have the potential for agricultural development. Stewart (2016) suggested that a successful dryland farming system requires 3 components, i.e retaining the precipitation, reducing evapotranspiration, and utilizing drought tolerance crops.

Drought tolerance is a combination of molecular, physiological, and morphological traits in plants (Chaniago, Syarif and Riviona, 2017). Akinseye *et al.* (2020) suggested selecting a suitable cultivar for raising crop production in a certain area. Sorghum (*Sorghum bicolor* [L] Moench) has been reported for a high tolerance of many unfavorable environmental conditions, including drought, salinity, heat, chilling and flooding (Maiti and Satya, 2014). Compared to other cereal crops, sorghum has a higher ability to adapt well under limited water conditions (Bibi *et al*., 2012; Badigannavar *et al*., 2018; Widiyono *et al*., 2020). Schlegel *et al*., 2018 reported that the cultivation of sorghum in dryland resulted in a higher yield than corn. Aerial part biomass of sorghum in the flowering phase has the potential to reach 28.34 t ha^{-1} by 504 mm of water consumption (Garofalo *et al*., 2020). The development of sorghum cultivation in the drylands of Indonesia is potential as an alternative food resource. Queiroz *et al.* (2015) reported that sorghum contains 55.2-75.2% carbohydrates, 8.6-18.9% proteins, 1.7-4.9%lipids, 9.3-25.2% fibers and 1.1-2.4% ash. Sorghum contains many amino acids which are valuable to be consumed as a functional food (Abah *et al*., 2020). Moreover, sorghum biomass is also beneficial as biofuel, sugar, and animal feed industry (Hu *et al*., 2022).

In order to obtain high productivity and produce high-quality seeds, the utilization of superior varieties is one of the important technological components. Seed quality is complex and can be determined by four key quality attributes, including genetic, physiological, physical and health (Bishaw, Makkawi and Niane, 2007). Genetic quality is defined as the potential for resulting higher productivity with better quality and greater tolerance to biotic or abiotic stresses. Physiological quality shows the potential of germination and vigor leading to subsequent seedling emergence and crop establishment in the field. Physical quality can be seen by the free from contamination from other crops and weed seeds, mechanical damage, discoloration, and uniformity of weight and size. Health quality shows the absence of infection of seed-borne pests.

The availability of quality seeds of sorghum in Indonesia is still limited. The farmers usually utilized the seeds harvested from the previous growing season. A higher number of seeds (4-5 seeds per hole) is required in anticipation of failure to grow due to the information unavailability of seed quality. Consequently, sorghum cultivation requires a high number of seeds the wasting of planted seeds was unavoidable. Therefore, this study was conducted to evaluate the physical quality of commonly used cultivars in Indonesia and their responses to several germination temperatures. This result is proposed to motivate the farmers to choose sorghum seeds that are suitable for the daily temperature of field cultivation, especially in drylands.

MATERIALS AND METHOD

Plant materials

Seeds of three sorghum cultivars were used in this study. The cultivars used differed based on the grain color, which were Strong Brown (SB), Pale Yellow (PY), and Light Brown (LB). These cultivars were commonly cultivated during dry seasons in Pajarakan Village, Buleleng, West Bali, Indonesia. SB originated from West Bali, PY from Thailand and LB from China. All seeds were obtained from a farmer in Pajarakan village, Grokgak, West Bali. The seeds were stored in the farmers' storage room for 6 months and carried to Plant Physiology Laboratory, Research Center for Biology, Indonesian Institute of Sciences (LIPI), now BRIN, Cibinong, West Java, Indonesia for experimenting. The experiment site was located at 6°29'52.9"S 106°50'43.4"E, 250 m above sea level with a daily temperature of 30-33°C and air humidity around 70-80%.

Seed characterization

The seeds characterization was performed by the bulk method covering the color, shape, size and weight of 100 seeds. The sample seeds samples were obtained from the top, middle, and bottom of the seed lot. Measurement of seed diameter was conducted using a manual

caliper with an accuracy of 0.01 mm. The weight of 100 sorghum seeds was measured using digital analytical scales with an accuracy 0.001 g. Each measurement was replicated 4 times. The seeds' color was observed qualitatively under natural light conditions using RHS Color Chart EditionVI (Royal Horticulture Society, America). Each seed was placed at the bottom of each hole from fully saturated to the less saturated color chart of RHS until matched the most exact color.

Moisture content and conductivity test

Seed moisture content was measured using the oven drying method. A total of 50 fresh seeds were weighed using analytical scales, then dried at a temperature of 105°C for seventeen hours 2 times and reweighted until reaching the constant weight. The moisture content was counted following ISTA (1976) equation. The ion leakage was observed using conductometer CG 855 (Gebrauchsanleitungcompany, German). Seeds were rinsed 3-5 times using the distilled water and soaked in a flask filled with distilled water (50 ml g^{-1} seed) for 24 hours at ambient temperature. The flask filled with distilled water without seed was used as a control (blank). The ion leakage of the blank flask must be < 5 $uS.cm^{-1}$. The measurement was taken at 25°C temperature. The ion leakage was identified as conductivity values through the following equation:

$$CV = \frac{(S-A)x\ B\ x\ K}{W}$$

Notes:
CV = Conductivity values
S = Measurement result for sample
A = Measurement result for blank
B = Bereich scale (20/200/2000 μScm^{-1})
K = Constant (0.91 cm^{-1})
W= Sample weight (gram).

Tetrazolium test

Tetrazolium test refers to Masullo *et al.* (2017). Ten sorghum seeds per replication were soaked in distilled water for 24 hours. The seeds were split into two parts until the embryo was visible, and then they were soaked with 0.5 % tetrazolium solution for 4 hours. A solution of 0.5% tetrazolium in 100 ml of buffer (pH 6.5-7) was carried out by dissolving 0.5 g of powdered 2,3,5-triphenyl tetrazolium chloride (TTC) into 100 ml of buffer (pH 6.5-7). The buffer solution was prepared using 2 solutions. Solution 1 was prepared by dissolving 0.908 g of Na_2HPO_4 thoroughly in some distilled water, then filling up the distilled water to 100 ml. Solution 2 was prepared by weighing 1.1876 g of Na_2HPO_4 powder, putting it in a certain amount of distilled water, and tera up to 100 ml. Both solutions were mixed (40 ml of solution 1 + 60 ml of solution 2) to make 100 ml of a buffer solution with a pH of 6.5-7. The seeds were categorized as viable seeds when the embryo was bright red. If the color of the embryo was pale red or white, the seeds were categorized as dead.

Vigor test and germination value

Seed and seedling vigor was measured using a direct viability test, namely: the germination test and seedling relative growth (Hartmann *et al.*, 2011). During the germination test, seeds were sowed at three germination facilities, i.e seed incubator, nursery (with a waterproof roof and gauze wall) and germination chamber. The temperature in germination facilities were 20 ± 3°C, 25-35°C and 30 ± 3°C, respectively.

This experiment was conducted using the Nested Design (Completely Randomized Group Design) with three replications. The first factor was the germination facilities (the nursery, incubator, and germination chamber). Meanwhile, the second factor was sorghum cultivars, namely PY (Pale Yellow), LB (Light Brown), and SB (Strong Brown). The SB was local cultivar sorghum form Bali, Indonesia; while PY and LB was introduced cultivar from Thailand dan China, respectively. The sorghum seeds were sown in a germination tray with the hilum facing down. Each tray was filled with 5cm height growing media and each tray was planted with 30 seeds. A tray with the seeds of each cultivar was placed in each germination facility. The media was kept in a moist condition by watering twice a day. The number of germinated seeds was recorded daily for ten days. The seed viability evaluation included the percentage of germination (%) and the average number of days to germination. The percentage of germination was calculated based on the percentage of the total number of seeds germinated on day 10 to the total number of seeds planted (Queiroz *et al.*, 2019). The average number of days to germination was counted following Hartmann *et al.* (2011). Germination value (GV) was obtained by multiplying Peak Value (PV) and Mean Daily Germination (MDG). PV is defined as the peak point of increase in percentage germination on the graph of percent germination before sloping down (Hartmann *et al.*, 2011); while the MDG (%) was calculatted by dividing the highest total of percentage of germination by number of days to reach the value.

Seedling growth

The vigor of the seedling phase was observed by measuring the Relative Growth Rate (RGR). The study used a Completely Randomized Design with three replications. The treatments were three sorghum cultivars. Two seeds were sown in each polybag (40×40 cm) containing a mixture of soil and sand (1:1 v/v). After one seed grew, another seed was removed. Thus, there was only one seedling for observation. Each cultivar maintained 30 seedlings for three weeks.

Observation of seedlings' vigor was carried out by destructively observing three seedlings per replication every week starting from the first until the third week after planting (WAP). The seedlings were gently taken out of the media and cleaned with tap water. Shoot height (cm), number and length of leaves, length of root (cm), fresh weight (g), and dry weight (g) were measured. The fresh and dry weight of sorghum seedlings is the accumulation from both the aerial part and the root. The dry weight was measured after the sample was dried in an oven at 105°C until the sample reach the constant weight. RGR of seedling (R) was calculated with the following Whitehead and Myerscough (1962):

$$R = \frac{LogW2 - LogW1}{Tn - T1}$$

Notes:
W1= dry weight of 1 wap
W2 = dry weight of 2 wap
W3 = dry weight of 3 wap
wap = week after planting
Tn = week-nth
T1 = the first week

Microclimate measurement

Environmental parameters consist of temperature (°C), air humidity (%), and light intensity (Lux). The temperature and humidity of the incubator and germination chamber were stable, with temperatures of 20 ± 3°C and 30 ± 3°C, respectively, and RH of 50-53%, in total darkness. While, the environmental parameters at nursey were observed every day at the morning, afternoon, and evening for ten days. The air temperature and humidity were measured with a Thermo-hygro meter (AS ONE Th-321, Corona), while the light intensity was measured with a lux meter (LUXOR). The average microclimate conditions at the nursery are presented in Table 1.

Table 1. Microclimate condition in the nursery.

Observation time	Light intensity (lux)	Temperature (˚C)	Humidity (%)
Morning	5069	28.51	69.4
Afternoon	10318.0	32.31	63.0
Evening	2964. 3	29.65	61.8

Data analysis

All data on seed germination and seedling growth were displayed in graph, documentation and table. Collected data were analyzed using the statistical analysis software (SAS portable 9.0, SAS Institute Inc., Cary, North Carolina, US) and microsoft excel 2013 (Microsoft Office Home and Student 2019, Redmond, Washington, USA).

RESULT AND DISCUSSION

Seed characters

The current study emphasizes the main characteristics of the seeds. The three sorghum cultivars used in this study have different characteristics, such as shape, color, and size (Figure 1). PY cultivar characterized by flat round shape, pale yellow color, with a diameter of 4.06 mm and the weight of 100 seeds of 3.36 g. SB cultivar has an ovate shape, strong brown color, 3.05 mm in diameter and the weight of 100 seeds of 1.84 g. While LB cultivar has an ellipse shape, brownish orange color, 3.51 mm in diameter and a weight of 100 seeds of 2.65 g.

Seeds characters are commonly used to distinguish genera, species, and even varieties since the characters are categorized as high heritability and are readily used in sorghum plant breeding programs (Slamet *et al.*, 2020). According to UPOV (2014) on sorghum identification, there are variations in the shape, size, and color of seeds. Sorghum has color variations ranging from white, pale yellow, red, brown, and purplish brown, while the shape were varies from flat, ovate, and ellipse. The size of the seed varies between 4-8 mm in diameter with 10-60 mg in weight. Queiroz *et al.*, (2019) describe that the differences in seed size affect the amount of amylum and other nutrients in the seeds. Furthermore, it can affect germination and seedling growth.

Seed viability

The sorghum seeds' viability was detected through three tests, namely tetrazolium test, ion leakage, and

Seeds Parameter	Sorghum Cultivars		
	Pale Yellow (PY)	Strong Brown (SB)	Light Brown (LB)
Fresh weight	3.36 g	1.84 g	2.65 g
Diameter	4.06 mm	3.05 mm	3.51 mm
Shape	Flat round	Ovate	Ellipse
Color	Pale Yellow 161 D Greyed-Yellow Group	Strong Brown 172 A Greyed-Orange Group	Brownish Orange 165B Greyed-Orange Group

Figure 1. The seed characteristics of PY, SB and LB sorghum cultivars.

moisture test. All three tests are frequently used to estimate seed quality quickly in many species. These tests are very useful for post-harvest handling of large numbers of seeds in a short time in many species. As well as handling the storage and marketing process. Among the three tests, the tetrazolium test is the most popular, due to its simplicity and doesn't require special equipment.

The tetrazolium test was categorized the viable seed is based on the red color that forms in the seed tissue, especially the embryonic part. The intensity of the red color in the tissue indicates the viability of the tissue (Subantoro & Prabowo, 2013). The test result showed that SB and LB cultivars had a 100% bright red color. Meanwhile, the PY cultivar resulted in 90% red color (Figure 2). It indicates that the viability of SB and LB cultivars was 100%, while PY cultivar was 80-90%. Based on the tetrazolium test, it can be concluded that the viability of all three sorghum cultivars qualified based on the ISTA (1976) standard since the result of tetrazolium test was more than 80%. The principle of this test is to distinguish between living and dead seeds based on the rate of respiration in wet conditions (Whitehouse *et al.*, 2020), however, this test is disabled to detect abnormalities of the seed. In order to complete the tetrazolium test data, moisture content measurement and conductivity tests (ion leakage) of sorghum seeds were also performed (Table 2). Both ion leakage and moisture tests are able to

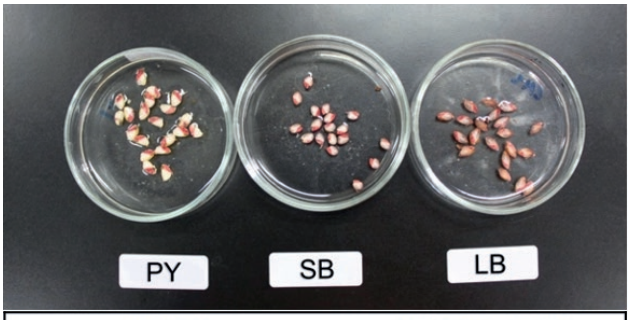

Cultivars	Tetrazolium Test (%)
Pale Yellow (PY)	90%
Strong Brown (SB)	100%
Light Brown (LB)	100%

Figure 2. Tetrazolium test result of sorghum seed.

detect seed damage due to mechanical damage or pests. The measurement of seed moisture content is important to consider the speed of seed deterioration by the increase of moisture content, meanwhile, ion leakage from the seed to the water indicates a symptom of seed damage due to membrane damage.

The highest moisture content was obtained by the LB cultivar of 11.32%, followed by PY and SB cultivars of 10.45% and 9.17%, respectively. Seed moisture content is affected by harvest time, drying process, and storage

conditions (Surki *et al*., 2012). However, in the present study, all cultivars were treated equally during the post-harvest handling: drying, packing and storing. Thus, the difference in seed moisture content was affected by each cultivar's characteristics. The ion leakage value of PY, SB and LB cultivars were 0.67 μScm^{-1}, 0.12 μScm^{-1} and 0.06 μScm^{-1}, respectively. A higher ion leakage value indicates lower seed viability in sorghum (Fatonah *et al*., 2017). Ion leakage occurs because the cell membrane function related to ion exchange between inside and outside the cell is being interrupted. The ions coming out of the cell membrane accumulate in the seed immersion water and are identified as electrical conductivity values (Brunei-Muguet *et al*., 2015). A higher ion leakage value indicates more ions released from the seeds into immersion water and greater damage to the cell membrane. de Carvalho Miguel & Filho (2002) explains that the electrical conductivity test is one of the best tests for the evaluation of the loss of cell membrane integrity by the concentration of electrolytes released by seeds during imbibition.

Sorghum seeds are grouped as orthodox seeds (Solberg *et al*., 2020). The recommended moisture content for orthodox seeds is 5% in low humidity conditions storage. However, if the seeds are handled traditionally, the moisture content should be around 13-16% (FAO, 2018). The moisture content of seeds after drying and stored in the storage room fluctuates depending on the humidity of the storage room. If the humidity increases, the moisture content of the seeds will increase, and vice versa (Awosanmi *et al*., 2020; Mbofung, 2012). In this study, the handling of the three sorghum cultivars was equal. The difference in seed moisture content is affected by the genetic traits, especially the thickness of the seed coat of each cultivar. The difference in ion leakage values was also suspected to be affected by differences in genetic traits. Based on ion leakage, it showed that PY cultivar is more susceptible to environmental fluctuations compared to SB and LB cultivars. In addition to the effect of genetic traits, ion leakage is also affected by temperature in storage room. (Wawo *et al*., 2019) reported an increase of ion leakage when *Inocarpus fagiferus* seeds with high moisture content are stored at room temperature (25-27°C) for four weeks. We suggest that sorghum seeds at farmer's storage in this study, without temperature and humidity control, are likely to have fluctuated seed moisture levels in accordance with temperature and humidity fluctuations. High-temperature conditions in the room will stimulate the respiration rate in the seeds, which will deplete the food reserves in the seeds and decrease the energy for germination. Sorghum cultivars that are susceptible to high temperatures will experience a rapid decline in viability compared to those that are tolerant of high temperatures. The temperature of Grokgak district (where the seed was stored) during the dry season (September-November) was 40°C, with rainfall of 7.4-91.4 mm (BPS Kabupaten Buleleng, 2018).

Table 2. Moisture content and ion leakage values of three sorghum cultivars

Cultivars	Moisture Content (%)	Ion Leakage (μScm^{-1})
Pale Yellow (PY)	10.45	0.67
Strong Brown (SB)	9.17	0.12
Light Brown (LB)	11.32	0.06

Seed vigor

Each plant requires a certain temperature range (minimum, optimum, and maximum) for each stage of its growth, which is called the cardinal temperature (Salisburry and ross, 1995). Sampayo-Maldonado *et al.* (2019) affirmed that the cardinal temperature is the condition that drives at least 50% germination of the total sample during the test period, while Shaban (2013) stated that the optimum temperature is the temperature that enables to produce of the highest percentage of germination of seeds in one lot in a short time. Shaban (2013) also reported that many types of cereal germinate optimally at 15-30°C with a maximum temperature of 30-40°C.

This study revealed that higher temperature resulted in a higher germination percentage and faster germination time (Table 3). The temperature requirement for sorghum germination was occurred range at 25-30°C. This range of temperature value was tighly related to sorghum temperature requirement for growth stage, ranged from 25-32°C (Garofalo *et al*., 2020). Each sorghum cultivar had its specific temperature for germination. The highest germination percentage for LB cultivar (93.33%) occurred at 30°C, while for SB (98.89%) and PY (67.78%) cultivars occurred at 25-35°C. It indicated the optimum temperature of SB and PY cultivars is in the range of 25-35°C, while the LB cultivar sorghum is around 30°C.

Germination at 20°C tended to take a longer time (6-9 DAS) and resulted in a lower final germination percentage value than at 25-35°C temperatures (4-5 DAS; >80% germination percentage) (Table 4). The SB cultivar requires a longer time to reach the highest germination percentage compared to LB and PY cultivars. The difference in germination time was influenced by base-moisture content in the seed of each sorghum cultivar. In general, the seed water content of cereal crops must reach

Table 3. Interaction between cultivars and temperature of germination facilities on final germination percentage.

Sorghum cultivars	Temperature (°C)			Means cultivars
	20	30	25-35	
PY	28.89 e ± 1.95	60.00 d ± 2.49	67.78 cd ± 1.53	52.21 b
SB	73.33 cd ± 5.74	74.44 cd ± 3.33	98.89 a ± 0.98	82.22 a
LB	87.78 bc ± 1.26	93.33 ab ± 1.79	86.67 bc ± 0.81	89.26 a
Means Temperature	63.70 b	75.56 a	84.44 a	

Note: Numbers that are followed by the same letter in one column mean that they are not significantly different based on the Duncan test with 5% levels. The number after ± means standard deviation.

Table 4. Interaction between cultivars and temperature of germination facilities on germination mean per day.

Sorghum cultivars	Temperature (°C)			Means cultivars
	20	30	25-35	
PY	8.00 ab ± 2.00	4.33 c ± 1.15	4.33 c ± 0.58	5.55 b
SB	9.00 a ± 2.08	7.67 ab ± 1.73	5.00 c ± 1.00	7.22 a
LB	6.00 bc ± 0.00	5.00 c ± 1.73	4.00 c ± 1.00	5.00 b
Means Temperature	7.22 a	6.11 a	4.44 b	

Note: Numbers that are followed by the same letter in one column mean that they are not significantly different based on the Duncan test with 5% levels. DAS = days after sowing. The number after ± means standard deviation.

at least 35 to 45% of seed dry mass to occur during the germination process (Queiroz *et al.*, 2019). The fact that the handling of the three sorghum cultivars was similar led the author to suggest that the difference in seed moisture content is affected by the character of each cultivar, such as the thickness of the seed coats. Thicker the seed coat need the more time to absorb water from the seed surrounding environment. The present study did not observe chemical changes during the germination process, but Benincasa *et al.* (2019) stated that the chemical and biophysical composition of seeds control the germination process, and the process was driven by environmental conditions, including temperature. At constant high temperatures, the growth enzyme activity will be stimulated and triggers germination (Gardner *et al.* 1991).

A previous study proved that at low temperatures, sorghum seeds consistently reduce the germination percentage (Solberg *et al.*, 2020). Furthermore, each cultivar had a different tolerance to low-temperature germination. LB cultivar was more tolerant to low temperature, while SB and PY cultivars were susceptible (Table 4). Solberg *et al.* (2020) explained that the germination response was influenced by several factors, including species, variety, the mother tree's condition, and both duration and condition of seed storage. The cultivars used in this study originated from different countries. The genetic basis of each cultivar might strongly influence the optimum germination temperature requirement. Thus, SB and PY cultivars which are originated from the equator are more susceptible to low temperatures. In contrast, the LB cultivar has a wider temperature adaptation because it has adapted to a temperate climate, characterized by higher monthly temperature fluctuations.

In accordance with FAO (2018) standard that quality seeds must have a germination percentage of at least 80%. In this study, SB cultivar (82.22%) and LB cultivar (89.26%) can be categorized as the quality seed. While the highest germination in PY cultivar was less than 80%. The low percentage of germination is closely related to the high value of ion leakage (Marcos-Filho, 2015).

One of the important characteristics of seed quality observation is the uniformity of seed germination. The information on the germination process is generally shown by the peak value, mean daily germination, and germination value. The peak value is the time when an increase in germination percentage happened in a short time that can be signed with a sharper increase in the curve simultaneously with an increase in germination percentage which is signed with the slighter increase in the curve and horizontal (Hartmann *et al.*, 2011). The Peak Value (PV) of all three cultivars is strongly affected by germination temperature (Figure 3). The peak value (PV) at 20°C (3-6 DAS) was slower than at 30°C and 25-35°C (2-3 DAS). This value is related to the final germination, when the germination percentage is high, the

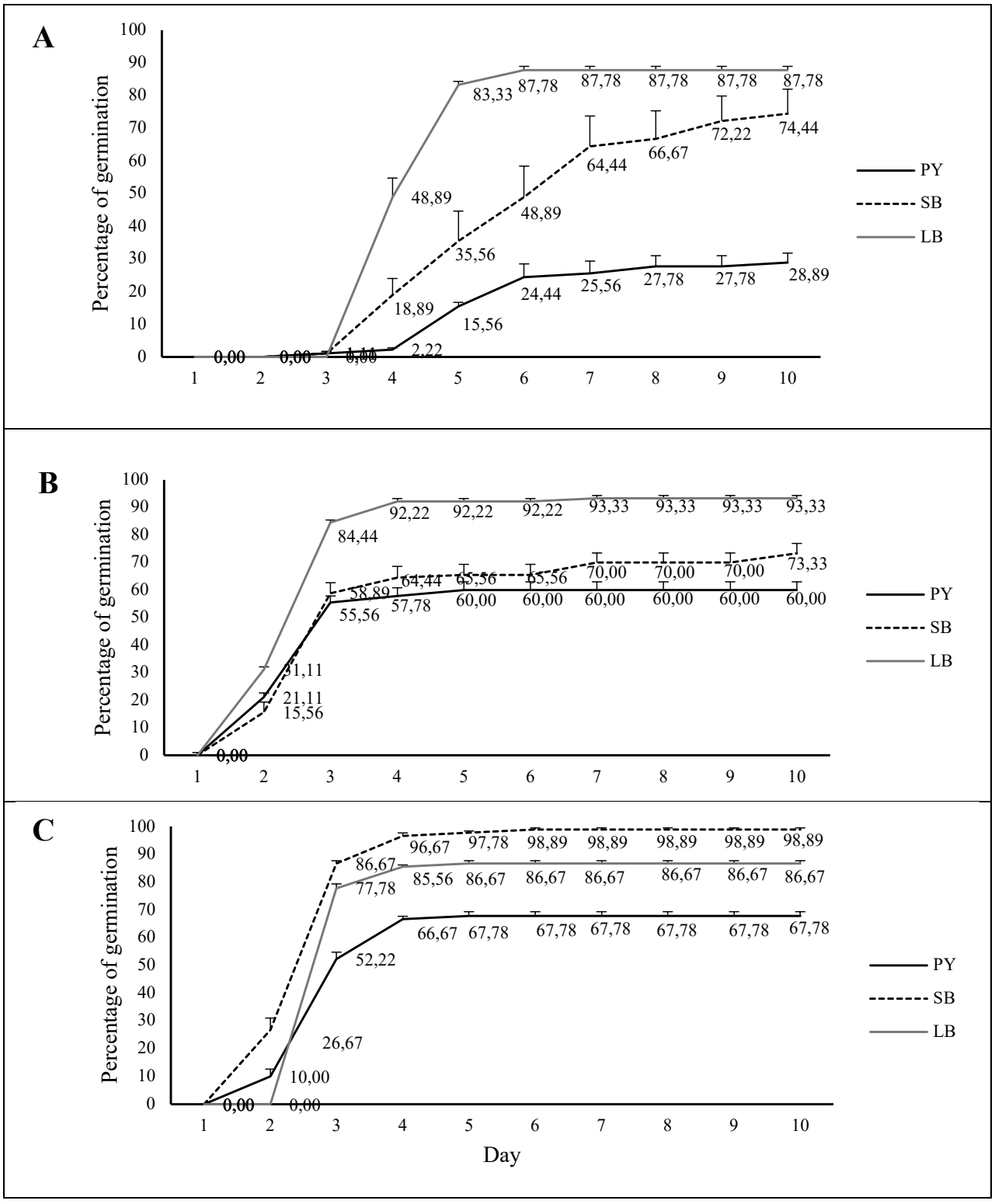

Figure 3. Daily germination percentage of PY, SB and LB sorghum cultivars at 20ºC (A), 30ºC (B) and 25-35ºC (C). vertical bars indicated standard deviation.

Table 5. Peak Value (PV), Mean Germination Day (MDG), and Germination Value (GV) of PY, SB and LB sorghum cultivars at 20°C, 30°C and 25-35°C.

Sorghum cultivars	Temperature (°C)		
	20	30	25-35
	Peak Value (PV)		
PY	4.07	18.52	17.41
SB	8.15	19.63	28.89
LB	16.67	28.89	25.93
	Mean of Germination Day (MDG)		
PY	2.50	12.00	13.56
SB	7.44	7.33	16.48
LB	14.63	23.06	17.33
	Germination Value (GV)		
PY	11.80	222.24	236.08
SB	60.64	143.89	467.11
LB	243.88	649.14	449.37

PV value also showed the same trend. LB and PY cultivars showed a similar trend of PV (Table 5). The PV of both cultivars was lowest at 20°C and highest at 30°C, while SB cultivar had a linear trend related to the raising of germination temperature.

Mean Daily Germination (MDG) values of the three cultivars are varied depending on the germination temperature (Table 5). The MDG of LB cultivar was constantly higher than other cultivars at any germination temperature. The MDG values were found lowest when seeds germinated at 20°C and then increase at 30°C and 25-35°C. The PV and MDG will strongly affect germination value. The highest germination value indicates strong seed vigor to germinate under certain conditions, especially at a specific temperature. The result of this study showed that the LB seeds required 30°C to obtain the highest germination value while the SB and PY seeds required 25-35°C to reach the highest germination value. The specific temperature that is required by each cultivar to reach the highest germination value is called optimum temperature. Shaban (2013) explained the optimum temperature is the temperature that enables to the production of the highest percentage of germination in a short period of time.

Seedling growth

The quality of seeds is also determined by seedling growth. Seedling is defined as a complete germination process after the release of radicle and plumules through the seed coat and grows into young plants with roots and leaves. This process was driven by soil nutrition and light. Dubey et al (2018) confirmed that each phase of plant growth requires different environmental conditions to achieve maximum growth. Plant performance during its life is an interaction between plant genetic potential and the environment. Therefore, the growth of seedlings in the nursery was observed without any control of environmental temperature and light.

The plant characteristics that were observed at the seedling phase included plant height, number of leaves, root length and plant biomass. The sorghum seedling height showed a sigmoid pattern. The curve experiences a rapid increase from the first week to the second week of observation, then sloping in the third week. Overall, the LB cultivar showed the tallest and highest growth rate, followed by PY and SB cultivars (Figure 4a). The highest number of leaves during the 1st and 2nd weeks were found in LB cultivar, followed by SB and PY cultivars. However, in the 3rd week, all cultivars had the same number of leaves (Figure 4b).

The root length was observed for three weeks and experienced a different increase. LB cultivars have the longest roots at 1 WAP (17.2 cm), followed by SB cultivars (12.3 cm) and PY cultivars (10.2 cm). The root length increased along with the age of the plant. The successive increase of the length of the root was 12.7 cm for LB cultivar, 4.1 cm for SB cultivar, and 22.8 cm for PY cultivar. In the third week, the length of the root of PY cultivar decreased by 6.5 cm. It is suspected that a part of the root was broken off during root sampling. The length of the root of SB and LB cultivars increased by 4.9 cm and 0.2 cm from the previous week (Figure 4c).

By all the plant growth parameters, the biomass measurement showed that SB cultivar had lower fresh weight compared to PY and LB cultivars at each seedling age (Figure 4d). The seedling growth rate of LB cultivar was higher compared to the other two cultivars, which started from the beginning of their growth until the third week. The growth rate was drawn from a higher number of leaves and taller ones since the first week of observation. which results in higher fresh weight and dry weight of the seedlings compared to PY and SB cultivars Timotiwu et al (2017) state that seedlings that have high vigor will have longer seedling roots and greater dry weight.

Thai cultivars seemed higher in early growth, but the growth rate gets slow in the second week. The production of leaves is also lower than that of SB cultivars. The seedling growth rate has a significant impact on the fresh weight and dry weight of seedlings. Queiroz *et al.* (2019) state that the seeds of each plant have a different amount of starch and other nutrients. This difference in

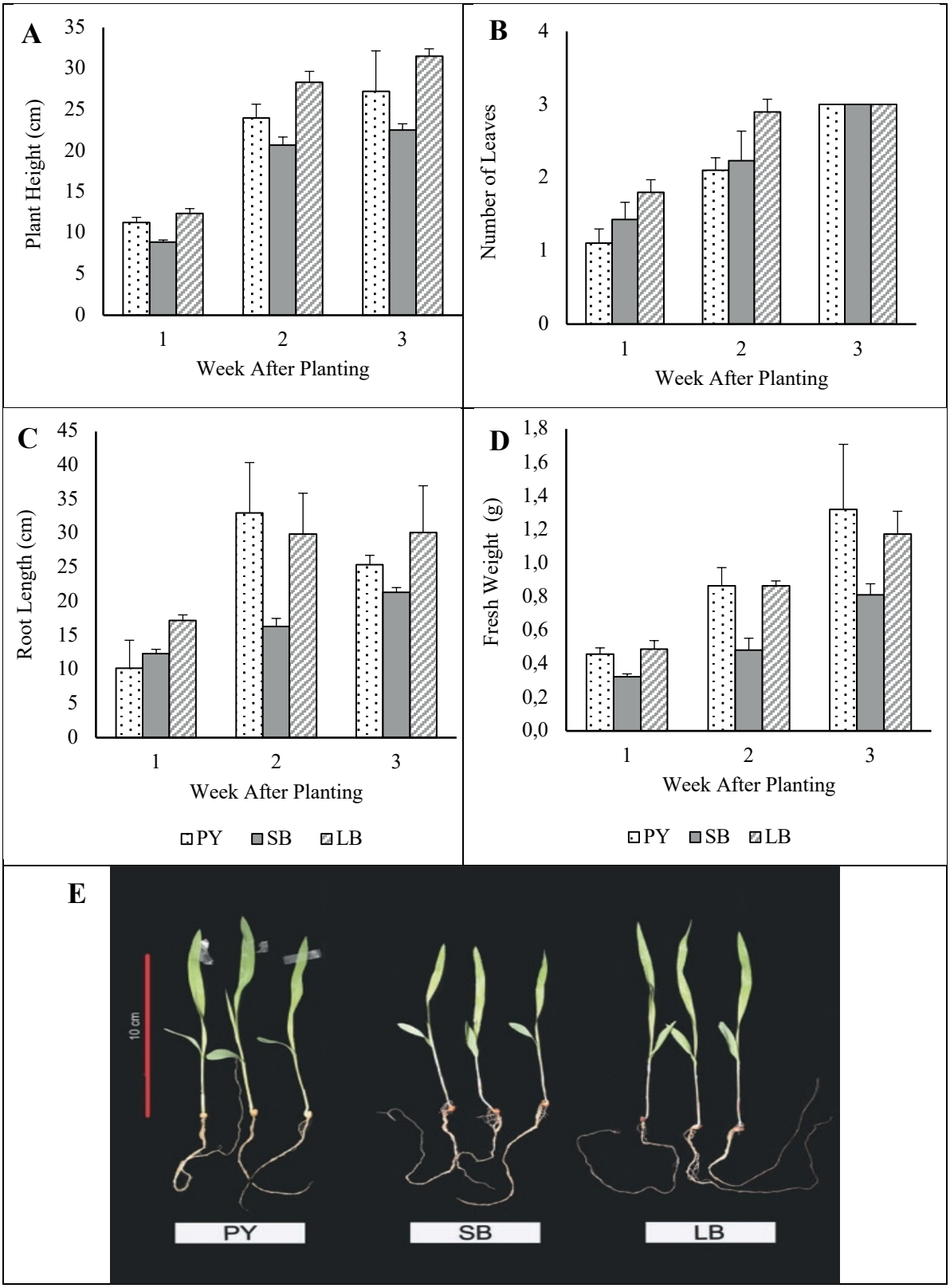

Figure 4. The seedling growth of 3 sorghum cultivars: plant height (A), number of leaves (B), root length (C), fresh weight (D), and Pictures of sorghum seedlings at the third week (E).

the amount of starch and nutrients is one of the major factors affecting seedling growth. Sorghum seeds of SB cultivars have smaller sizes compared to LB and PY cultivars, possibly because of genetic factors of the cultivar and the size of the seeds that affect the seedling growth.

Relative Growth Rate (RGR)

The relative growth rate of seedlings in each cultivar was different (Table 6). It showed that each cultivar has a different growth ability. The relative growth rate in the second week reached 0.321 g week^{-1} for LB cultivar, 0.289 g week^{-1} for PY cultivar, and 0.239 g week^{-1} for SB cultivar. The growth rates of LB and SB cultivars in the third week decreased to 0.261 g week^{-1} and 0.224 g week^{-1}, respectively. Meanwhile, PY cultivar increased to 0.304 g week^{-1} from the previous week. The distribution of biomass to aerial parts of plants appears to be more influenced by genetic factors (plant cultivars) because environmental conditions were homogeneous.

The relative growth rate of each cultivar tends to be higher at R1 (first-second week) than R2 (first-third week). The higher R value indicates faster growth, while lower R values indicate slower plant growth. LB cultivar was thought to be early maturing sorghum, which is characterized by rapid vegetative growth and starts the generative phase quickly. On the other hand, the slower-growing SB and PY cultivars showed both were deep-aged sorghum.

Based on the results and discussion of the research, it can be concluded that the quality of sorghum seeds can be varied, depending on the germination temperature. Therefore, it is important to choose a sorghum cultivar that is suitable for the daily temperature range. Generally, the distribution of temperature and light intensity depends on the altitude above sea level. Considering the cardinal temperature range of sorghum germination, this commodity is suitably cultivated in areas with temperatures below 40ºC with full light intensity for optimal growth. Regarding the three sorghum cultivars tested in this experiment, the LB cultivar was recommended to be cultivated at an altitude of 300 – 500 m above sea level. This area is identical with less fluctuation in daily temperature, around 30ºC, corresponding to the optimum temperature for LB cultivar germination, but the light intensity is quite high, and the humidity is low. SB cultivar, which has higher germination temperatures, seems to be more suitable for cultivation in lower areas, between 50 – 250 m above sea level. Such areas have more fluctuating daily temperatures due to sea breezes, with low humidity and high light intensity. Sopandie (2013) explained that temperatures above the optimum temperature will reduce plant physiological activities, especially the inactivity of several enzymes, and disrupt the balance between photosynthetic activity and respiration. Conductivity test values in this study had a similar trend to the tetrazolium test, also in line with the direct germination test and moisture test. We consider that the conductivity test can be used by local farmers in assessing the quality of the seeds. This test is simple and requires an inexpensive tool. Conductivity tests can also solve the problem of subjectivity in the color-based assessment of the tetrazolium test. At the seedling level, the relative growth rate measurement based on the growth rate of the plumule can be utilized to assess seed vigor.

Table 5. Relative growth rate (R) of sorghum seedlings.

Cultivars	Dry Weight (g)			Relative Growth Rate (g week^{-1})	
	1 WAP	2 WAP	3 WAP	R1(g)	R2(g)
PY	0.019	0.037	0.077	0.289	0.304
SB	0.015	0.026	0.042	0.239	0.224
LB	0.021	0.044	0.070	0.321	0.261

Notes: WAP= Weeks after planting, R1= first-second week, R2= second-third week.

ACKNOWLEDGMENTS

Highly appreciated from the authors to Research Center For Biology (Indonesian Institute of Sciences), Now BRIN, for facilitating the research and to Fitri Uswatun Khasanah (Student of FMIPA, Sebelas Maret University, Solo) for all her support and dedication during this research.

REFERENCES

Abah, C. R., Ishiwu, C. N., Obiegbuna, J. E., &Oladejo, A. A. (2020). Sorghum Grains: Nutritional Composition, Functional Properties and Its Food Applications. *European Journal of Nutrition & Food Safety*, 101–111. https://doi.org/10.9734/ejnfs/2020/v12i530232

Akinseye, F. M. (2020). Improving sorghum productivity under changing climatic conditions: A modelling approach. *Field Crops Research*, 246, 107685. https://doi.org/10.1016/J.FCR.2019.107685

Badigannavar, A. *et al.* (2018) 'Physiological, genetic and molecular basis of drought resilience in sorghum

[Sorghum bicolor (L.) Moench]', *Indian Journal of Plant Physiology*, 23(4), 670–688. Available at: https://doi.org/10.1007/s40502-018-0416-2.

Benincasa, P., Falcinelli, B., Lutts, S., Stagnari, F., & Galieni, A. (2019). *Sprouted Grains: A Comprehensive Review*. https://doi.org/10.3390/nu11020421

Bibi, A. *et al.* (2012) 'Screening of sorghum (sorghum bicolor var moench) for drought tolerance at seedling stage in polyethylene glycol', *Journal of Animal and Plant Sciences*, 22(3), 671–678.

Bishaw, Z., Makkawi, M. and Niane, A.A. (2007) 'Seed Quality and Alternative Seed Delivery Systems', *Lentil: An Ancient Crop for Modern Times*, (March 2019), 350–367. Available at: https://doi.org/10.1007/978-1-4020-6313-8.

BPS Kabupaten Buleleng. (2018). *Average rainfall and rainy days in Buleleng Regency Year 2017*.

Brunei-Muguet, S., D'Hooghe, P., Bataillé, M. P., Larré, C., Kim, T. H., Trouverie, J., Avice, J. C., Etienne, P., &Dürr, C. (2015). Heat stress during seed filling interferes with sulfur restriction on grain composition and seed germination in oilseed rape (Brassica napus L.). *Frontiers in Plant Science*, 6(APR). https://doi.org/10.3389/fpls.2015.00213

Chaniago, I., Syarif, A. and Riviona, P. (2017) 'Sorghum seedling drought response: In search of tolerant genotypes', *International Journal on Advanced Science, Engineering and Information Technology*, 7(3), 892–897. https://doi.org/10.18517/ijaseit.7.3.1303.

de Carvalho Miguel, M. V., & Filho, J. M. (2002). *Potassium leakage and maize physiological potential potassium leakage and maize seed physiological potential*. 315–319.

Dubey, A. N., Goswami, S., &Devedee, A. K. (2018). *Effect of Temperature on Different Growth Stages and Physiological Process of Rice crop-a Review*. https://www.researchgate.net/publication/330254231

Emmanuel AWOSANMI, F., & Adesola AJAYI Emmanuel Ewere BAFFOE, S. (2020). Influence of Seed Moisture Content on Short Term Storage of Cowpea (Vigna unguiculata L. Walp) Seeds. *Agric. Conspec. Sci*, 85(1), 37–42.

FAO (2004). Carbon sequestration in dryland soils, *Journal of Environmental Quality*, p. 108.

FAO. (2018). *Seed Toolkit-Module 6: Seed storage*. The Food and Agriculture Organization of the United Nations.

Fatonah, K., Suliansyah, I., &Rozen, N. (2017). Electrical conductivity for seed vigor test in sorghum (Sorghum bicolor). *Cell Biology and Development*, 1(1), 6–12. https://doi.org/10.13057/cellbioldev/v010102

Garofalo, P. *et al.* (2020) 'Italian Journal of Agrometeorology climate change management', *Italian Journal of Agrometeorology*, 1, 49–62. https://doi.org/10.13128/ijam-855.

Hartmann, H. T., Kester, D. E., Davies, F. T., & Geneva, R. L. (2011). *Plant Propagation. Principles and Practices* (8th ed.). Prentice Hall. https://www.semanticscholar.org/paper/Hartmann-and-Kester%27s-Plant-Propagation%3A-Principles-Davies-Geneve/e1989dacd70fdff19db2112f38e1c9883755a3b3

Hu, W., Zhou, L., & Chen, J. (2022). Conversion sweet sorghum biomass to produce value-added products. *Biotechnology for Biofuels and Bioproducts* 15(1), 1–11. https://doi.org/10.1186/S13068-022-02170-6

Huang, J. *et al.* (2017) 'Dryland climate change: Recent progress and challenges', *Reviews of Geophysics*, 719–778. https://doi.org/10.1002/2016RG000550.

ISTA. (1976). *III. Seed Moisture Content*. https://www.bioversityinternational.org/fileadmin/bioversity/publications/Web_version/188/ch05.htm

Juhaeti, T., Utami, N. W., Syarif, F., & Lestari, P. (2014). *Prospek dan Teknologi Budi DayabeberapaJenisSayuranLokal* (T. Juhaeti & N. Hidayati, Eds.). LIPI Press. http://penerbit.lipi.go.id/data/naskah1431490288.pdf

Maiti, R.K. and Satya, P. (2014) 'Research advances in major cereal crops for adaptation to abiotic stresses', *GM crops & food*, 259–279. Available at: https://doi.org/10.4161/21645698.2014.947861.

Marcos-Filho, J. (2015). Seed vigor testing: An overview of the past, present and future perspective. *Scientia Agricola* 72(4), 363–374. https://doi.org/10.1590/0103-9016-2015-0007

Mariah, M. (2010). Indonesia: A Vulnerable Country in the Face of Climate Change, *Global Majority E-Journal*, 1(1), 46–56.

Masullo, L. S., Piña-Rodrigues, F. C. M., Figliolia, M. B., &Américo, C. (2017). Otimização do teste de tetrazólio para avaliação da qualidade de sementes de Platymiscium floribundum, Lonchocarpusmuehlbergianus e Acacia polyphylla DC. *Journal of Seed Science*, 39(2), 189–197. https://doi.org/10.1590/2317-1545v39n2167534

Mbofung, G. Y. (2012). *Effects of maturity group, seed composition and storage conditions on the quality and storability of soybean (Glycine max L. Merrill) seed Recommended Citation* [Seed Science, Iowa State University]. https://lib.dr.iastate.edu/etd/12596

Queiroz, V.A.V. *et al.* (2015) 'Nutritional composition of sorghum [sorghum bicolor (L.) Moench] genotypes cultivated without and with water stress', *Journal of Cereal Science*, 65, 103–111. https://doi.org/10.1016/j.jcs.2015.06.018.

Queiroz, M. S., Oliveira, C. E. S., Steiner, F., Zuffo, A. M., Zoz, T., Vendruscolo, E. P., Silva, M. v., Mello, B. F.

F. R., Cabral, R. C., &Menis, F. T. (2019). Drought Stresses on Seed Germination and Early Growth of Maize and Sorghum. *Journal of Agricultural Science*, 11(2), 310. https://doi.org/10.5539/JAS.V11N2P310

Sampayo-Maldonado, S., Ordoñez-Salanueva, C. A., Mattana, E., Ulian, T., Way, M., Castillo-Lorenzo, E., Dávila-Aranda, P. D., Lira-Saade, R., Téllez-Valdéz, O., Rodriguez-Arevalo, N. I., & Flores-Ortíz, C. M. (2019). Thermal Time and Cardinal Temperatures for Germination of Cedrela odorata L. *Forests*, 10(10). https://doi.org/10.3390/f10100841

Scariot, M. A., Tiburski, G., Reichert Júnior, F. W., Radünz, L. L., &Meneguzzo, M. R. R. (2017). Moisture Content at Harvest and Drying Temperature on Bean Seed Quality. *Pesquisa Agropecuaria Tropical*, 47(1), 93–101. https://doi.org/10.1590/1983-40632016v4743135

Schlegel, A. J., Lamm, F. R., Assefa, Y., & Stone, L. R. (2018). Dryland corn and grain sorghum yield response to available soil water at planting. *Agronomy Journal*, 110(1), 236–245. https://doi.org/10.2134/agronj2017.07.0398

Shaban, M. (2013). Effect of water and temperature on seed germination and emergence as a seed hydrothermal time model. In *International journal of Advanced Biological and Biomedical Research* (Vol. 1). http://www.ijabbr.com

Slamet, A., Hisra, H., & Rajab, R. (2020). The Characteristics of the Morphological Genotypes of Local Sorghum [Sorghum bicolor (L.) Moench] from Buton Selatan. *Scientiae Educatia*, 9(1), 87. https://doi.org/10.24235/sc.educatia.v9i1.6120

Solberg, S. Ø., Yndgaard, F., Andreasen, C., von Bothmer, R., Loskutov, I. G., &Asdal, Å. (2020). Long-Term Storage and Longevity of Orthodox Seeds: A Systematic Review. *Frontiers in Plant Science*, 11. https://doi.org/10.3389/fpls.2020.01007

Sopandie, D. (2013). *FisiologiAdaptasiTanamanterhadapCekamanAbiotik pada AgroekosistemTropika*. IPB Press.

Stewart, B.A. (2016) *Dryland Farming*, *Reference Module in Food Science*. Elsevier. https://doi.org/10.1016/b978-0-08-100596-5.02937-1.

Subantoro, R., & Prabowo, R. (2013). *PengkajianViabilitasBenihdengan Tetrazolium Test pada Jagung dan Kedelai.*

Surki, A. A., Sharifzadeh, F., &Afshari, R. T. (2012). Effect of drying conditions and harvest time on soybean seed viability and deterioration under different storage temperature. *African Journal of Agricultural Research*, 7(36), 5118–5127. https://doi.org/10.5897/ajar12.060

Timotiwu, P. B., Pramono, E., -, A., &Asih, N. W. A. S. (2017). Effect of Storage Periods on Physical Quality and Seed Vigor of Four Varieties of Sorghum (Sorghum Bicolor [L.] Moench). *Research in Agriculture*, 2(2), 29. https://doi.org/10.22158/ra.v2n2p29

UPOV. (2014). *International Union for the Protection of New Varieties of Plants: Sorghum*. www.upov.int

Wawo, A. H., Setyowati, N., Utami, N. W., & Lestari, P. (2019). *Mengenalgayam, Tanaman multi manfaat*. LIPI Press.

Whitehead, F. H., & Myerscough, P. J. (1962). Growth Analysis of Plants. The Ratio of Mean Relative Growth Rate to Mean Relative Rate of Leaf Area Increase. *New Phytologist* 61(3). https://www.jstor.org/stable/2429812

Whitehouse, K. J., Hay, F. R., & Lusty, C. (2020). Why seed physiology is important for genebanking. *Plants* 9(5). MDPI AG. https://doi.org/10.3390/plants9050584

Widiyono, W., Nugroho, S., Rachmat, A., Syarif, F., Lestari, P., &Hidayati, N. (2020). Drought tolerant screening of 20 indonesian sorghum genotypes through leaf water potential measurements under water stress. *IOP Conference Series: Earth and Environmental Science*, 439, 012033. https://doi.org/10.1088/1755-1315/439/1/012033

Italian Journal of Agrometeorology
Rivista Italiana di Agrometeorologia

Firenze University Press
www.fupress.com/ijam

OPEN ACCESS

Citation: Ferreira Palheta, L., Oliveira Simões, P.H., Prado Neves, R.L., da Silva Ataíde, W.L., de Paula, M.T., Carvalho Dornelas, K., Santiago, A.V., & Pereira de Carvalho, J.O. (2024). Influence of meteorological variables on the development in plantation of Tachigali vulgaris L.G. Silva & H.C. Lima (tachi-branco). *Italian Journal of Agrometeorology* (1): 109-117. doi: 10.36253/ijam-2136

Received: May 8, 2023

Accepted: June 21, 2024

Published: August 2, 2024

Data Availability Statement: All relevant data are within the paper and its Supporting Information files.

Competing Interests: The Author(s) declare(s) no conflict of interest.

ORCID:
LFP: 0000-0003-4727-7990
WLSA:0000-0002-2275-0887
PHOS: 0000-0003-1395-0374
KCD: 0000-0003-3780-913X
JOPC: 0000-0001-9396-2417
AVS: 0000-0002-6636-2595
RLPN: 0000-0002-0997-4851
MTP: 0000-0002-8795-8830

Influence of meteorological variables on the development in plantation of *Tachigali vulgaris* L.G. Silva & H.C. Lima (tachi-branco)

Lenilson Ferreira Palheta[1,*], Pedro Henrique Oliveira Simões[2], Raphael Lobato Prado Neves[3], Wander Luiz da Silva Ataíde[1], Manoel Tavares de Paula[3], Karoline Carvalho Dornelas[2], Alailson Venceslau Santiago[5], João Olegário Pereira de Carvalho[4]

[1] *Secretary of Environment and Sustainability of the State of Pará - Av. Nª Sra.de Nazaré, 130, 66040170, Belém, PA, Brazil*
[2] *University Federal of Mato Grosso, University Campus of Sinop, 78550728, Sinop, MT, Brazil*
[3] *State University of Pará, Highway PA-125, angelim, 68625-000, Paragominas-PA, Brasil*
[4] *University Federal Rural of the Amazon, Avenida Presidente Tancredo Neves, 66.077-830, Belém, PA, Brasil*
[5] *Embrapa Amazônia Oriental, Tv. Dr. Enéas Pinheiro, s/n - Marco, Belém - PA, 66095-903 Belém, PA, Brazil*
*Corresponding author. Email: eng.lenilson@gmail.com

Abstract. The objective of this work was to evaluate the influence of meteorological variables on height and diameter increment in a Tachigali vulgaris plantation fertilized with NPK. The meteorological data were recorded by the agroclimatological station of Embrapa Amazônia Oriental, located in Igarapé-Açu, in the period from March 2016 to June 2018. The monitoring of the increment rate in height and diameter of the plants was done. The data collected were: monthly temperature, average maximum temperature, average minimum temperature andprecipitation. The maximum quarterly periodic increment in height occurred in the June-September 2017 quarter, while the highest diameter increment occurred in the June-September 2016 quarter. Principal component analysis showed that the first three factors together explained 94% of the total variance of the species' growth, where the unfolding analysis of the first two principal components showed that the variables that contributed most to explain the species' stand development correlated with the climate measures observed in this study, were mean and maximum temperatures and precipitation, followed by height, diameter and minimum temperature. It was concluded that the weather variables positively influenced the increment in height and diameter of plants Tachi, with precipitation being the variable with the greatest contribution to predicting tree growth.

Keywords: rainfall, plant incremente, seasonality, forestry, bioenergy.

STUDY IMPLICATIONS

The global demand for forest products, although with different rates by segment, in general, has consistently grown in recent years, which has increased the demand for raw materials, resulting in an increase in new forest plantations. However, most of the reforestations are implemented in areas of weathered and leached soils, that is, they have low availability of nutrients, which generates variations in productivity, and the implementation of forestry projects may be economically unfeasible in some cases. In this way, understanding forest production in this context is necessary, since it can be expressed as the result of a function that considers the availability of edaphoclimatic resources, the amount of these absorbed by the plant and the efficiency with which it uses them, to fix atmospheric CO_2 and transform it into biomass. The study of growth trends of forest plantations in different meteorological variations is important in the sense of helping decision-making regarding places where there is little knowledge about adaptation and performance of forest species to be planted. Among the reforestation species is *Tachigali vulgaris* L.G.Silva & H.C.Lima (white tachi), considered an Amazonian species, promising for bioenergetic production. So, providing information on its cultivation under a given microclimate becomes necessary for the establishment of this crop in similar regions, which plays an important economic and ecological role for its region of origin.

INTRODUCTION

Seasonality is the first description of the behavior of the system over time. The difference in the seasonal pattern of functioning of a biological system, which can be more or less stable, is due to both biotic factors and environmental impacts. The Amazon is an example of a highly seasonal environment, with its diverse arboreal component (Silva et al., 2017).

Tree growth is defined by the genetic composition of the species and can be influenced by its characteristics, interacting with the environment. Environmental influences include climatic factors (temperature, precipitation, wind, and sun exposure) (Kanieski et al., 2012). In this context, works have been carried out in order to evaluate the influence of meteorological variables on the growth of tropical and subtropical species. Many studies report that the influence of meteorological variables (precipitation and average temperature) on the increment in diameter of some forest species show positive correlations (Soares & Cruz, 2016, Kanieski et al., 2017, De Jesus et al., 2019, Bertolini et al., 2020).

The excess or insufficiency of available water in the soil causes a decrease in the photosynthetic rate reflecting in the decrease of plant growth. The influence of temperature and precipitation on the distribution and growth of forests is demonstrated by the high correlation between these aspects and climate classifications, such as those made by Merriam, Köppen and Thornthwaite (Zanon & Finger, 2010).

The distribution of forest stands is closely related to the microclimatic conditions of a given region. The climatic elements, such as temperature, relative humidity, precipitation, wind and solar exposure, can influence the growth, development and even the survivability of plants (Santos Neto, 2014). In this context, the study of the growth trends of from forest plantations in different types of soil and on the variation of the water regime is important in order to help decision making regarding the places where there is little knowledge about the adaptation and performance of the forest species to be planted (Santos et al., 2017). Although plants adapted to low nutrient availability can develop naturally (Camargo et al., 2004, Rosim et al., 2016), the adoption of management practices and correction of soil fertility in areas cultivated with species of rapid growth in order to raise the productivity of forest sites, or at least maintain it for future rotations (Pinkard, 2003).

Management practices planit and soil must take into account the use of nutrient sources through mineral or organic fertilization (Vogel, 2005, Silva et al., 2021), ensuring that the soil supplies all nutrients in quantities necessary to obtain the desired growth for plants (Forrester et al., 2006, Smethurst, 2010). The elements nitrogen, phosphorus and potassium stand out, which are essential macronutrients for plant development (Zhang et al., 2010, Biagiotti et al., 2017). Where effects of fertilization with these nutrients on both plant growth and leaf chemical content have been extensively studied in forests such as eucalyptus (Graciano et al., 2006, Rosim et al., 2016, Santos et al., 2017). Thus, the objective of this work was to evaluate the influence of meteorological variables on the increment in height and diameter of planting *Tachigali vulgaris* L. G. Silva & H. C. Lima fertilized with NPK.

MATERIAL AND METHODS

Study área: The study was carried out at the Fazenda Escola de Igarapé Açu - FEIGA of the Universidade Federal Rural da Amazônia - UFRA, in the municipality of Igarapé-açu, Pará State, Brazil.

The municipality belongs to the Northeast Paraense mesoregion and the Bragantine microregion. The municipal seat has the geographical coordinates 01°07'33" South latitude and 47°37'27" West Greenwich longitude. The climate of the municipality is Am type by Köppen classification (Costa et al., 2013), with an average temperature around 25°C throughout the year. The annual precipitation of the region is high, reaching 2,853 mm, with a strong concentration in the months from January to June and less rainy from July to December. The predominant soil in the region is yellow Latosol (Rousseau et al., 2014).

Meteorological data

The meteorological data for this study were obtained from the Embrapa Amazônia Oriental agroclimatological station, located in Igarapé-Açu, Pará, Brazil, situated at latitude 01°07'33"S, longitude 47°37'27" W and altitude 45 m, distant 28 km from the study area.

The meteorological data such as air temperature, maximum and minimum temperature, and precipitation were analyzed in the period from March 2016, when planting was performed, until June 2018.

Experimental design and evaluations

A stand of *Tachigali vulgaris* L. G. Silva & H. C. Lima was established in 2016, whit area of 1.44 hectare (14,400 m2), containing 1728 trees, distributed in four plots with a distance of five meters, to facilitate the implantation of future experiments, with the use of fertilizers applied to the soil surface, thus avoiding contamination between treatments by rainfall, with plants spacing 2 × 3 m (plants × rows), as recommended by Sousa et al. (2016). The planting was submitted to different levels of fertilization, which were applied in grams per plant, which constituted the treatments, of two doses of nitrogen-N (0, 26.67 g), two doses of phosphorus-P (0, 19.56 g) and two doses of potassium-K (0, 30 g). The commercial formulations of urea, triple superphosphate and potassium chloride respectively were used, combined according to the fractional factorial 2k, which totals 8 treatments randomly distributed, with 4 plants grouped in the planting plots, whit 4 replications, namely: T0 (control, no fertilization), T1 (30 g of K), T2 (19.56 g of P), T3 (19.56 g of P + 30 g of K), T4 (26.67 g of N), T5 (26.67 g of N + 30 g of K), T6 (26.67 g of N + 19.56 g of P), T7 (26.67 g of N + 19.56 g of P + 30 g of K). Fertilizations were performed in 2016, right after planting and repeated twelve months later in 2017. Being used as a *parameter of* comparison with the climatic data, the average data of growth in height and diameter of all treatments.

To follow the periodicity and the rate of increment in height and diameter of the plants, measurements were made every three months during the 2-year period, corresponding to the months of March 2016 to March 2017 in the first year and from June 2017 to June 2018 in the second year, thus providing a quarterly analysis of the increment in height and diameter of the plants. The diameter evaluations during the two years were divided into two forms of measurement, due to the fact that the plants only presented measurable DBH (diameter at breast height at 1.3 m from the ground) at 15 months of age, which corresponded to the measurement in June 2017.

In the first year, the diameter was measured at the height of the basal diameter (BD), using a digital caliper, as the plant heights were less than 1.3 m. In the second year, the diameter measurement was made at DBH (Diameter at breast height - 1.3 m), using a diametric tape graduated in centimeters. The total height of the plants was measured with a ruler graduated in centimeters. Periodic quarterly increments (IPT) of plant diameter and height were calculated to express the growth of *Tachigali vulgaris* every three months (equation 1).

$$IPT = Y(t + n) - Y_t \quad (1)$$

where: IPT = quarterly periodic increment
Y = considered dimension
t = age
n = time period

Statistical analysis

The data were submitted to the normality test, and subsequent statistical analysis. In order to verify the associations between the growth variables of *Tachigali vulgaris* L. G. Silva & H. C. Lima and the climatic variables, a multivariate statistical analysis of Principal Components – PCA and Pearson's correlation was performed. For that, the software R studio was used.

RESULTS

The average results found for the quarterly periodic increase in height of the forest stand of *Tachigali vulgaris* L. G. Silva & H. C. Lima showed (Table 1 and Figure 1) that the species maintained its growth rate until September 2017 (94.4 cm overall average), when 76.3 mm of rain was recorded, which was reduced in the fol-

Table 1. Periodic quarterly increase in height and diameter of *T. vulgaris* plants subjected to N, P and K fertilization, and the variation during the period of the meteorological variables of temperature (average, maximum and minimum) and precipitation.

Increments / Treatments		2016			2017			2018	
		Mar.-June	June-Sept.	Sept.-Dec.	Dec.-Mar.	June-Sept.	Sept.-Dec.	Dec.-Mar.	Mar.-June
Height (cm)	0	18.7	37.1	23.3	43.8	77.1	44.4	57.7	76.6
	n:26.67	30.8	45.3	34.3	49.9	96.2	61.1	69.2	69
	p:19.56	19.6	42.9	26.8	48	82.3	47.8	66.3	65.7
	k:30	20.4	44.4	35	46.8	92.6	54.2	70.3	82
	n:26.67, p:19.56	30.7	47.5	32.8	53.4	94.6	55.9	75.3	76.4
	n:26.67, k:30	24.5	45.7	38.7	47	103.3	59.7	68.5	60.3
	p:19.56, k:30	21.3	44.9	41.1	52.6	108.1	54.4	80.2	78.8
	n:26.67, p:19.56, k:30	26.4	48.3	32.9	51.5	100.9	54.5	60.9	71.2
	Average treatments	24	44.5	33.1	49.1	94.4	54	68.6	72.5
Diameter (cm)	0	0.36	1.09	0.78	0.82	1.05	0.73	1.2	0.97
	n:26.67	0.6	1.65	0.74	1.27	1.43	1.01	1.15	0.95
	p:19.56	0.38	1.47	0.63	1.01	1.44	0.69	1.04	0.93
	k:30	0.41	1.31	0.76	0.85	1.31	0.83	1.2	1
	n:26.67, p:19.56	0.54	1.71	0.82	1.2	1.45	0.75	1.01	0.9
	n:26.67, k:30	0.58	1.58	0.83	0.84	1.54	0.81	1.2	0.97
	p:19.56, k:30	0.49	1.45	0.89	1.3	1.82	0.86	1.4	1.09
	n:26.67, p:19.56, k:30	0.58	1.47	0.84	1.05	1.33	0.73	0.96	0.81
	Average treatments	0.49	1.47	0.79	1.04	1.42	0.8	1.15	0.95
Meteorological variables	Temperature-T. °C	27.7	27.5	28	27.5	28.7	28.6	27.5	27.3
	T. maximum °C	32.5	33	33.7	32	33.8	34.1	32	31.9
	T. minimum °C	23	22	22.3	23.1	23.6	23.1	22.9	22.8
	Precipitation (mm)	321.2	120.5	78.9	384.7	76.3	32.6	262.5	310.1

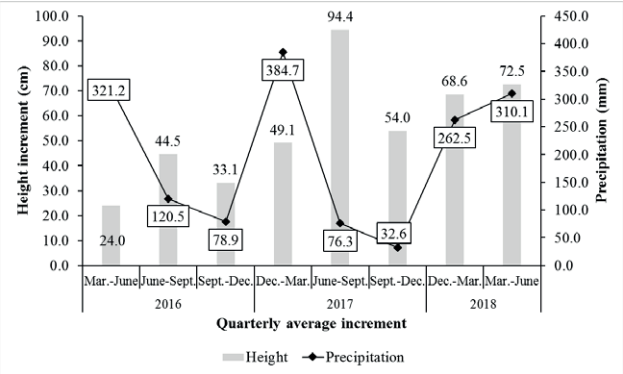

Figure 1. Average quarterly increase in height (cm) of T. vulgaris plants subjected to N, P and K fertilization, and rainfall (mm) during the studied period.

lowing quarter (54.0 cm), which had the lowest rainfall observed during the study, 32.6 mm of rain. The results found indicate that there is a gradual proportionality for the vertical increment of the plants and the precipitation, being able to infer that the planting presented good elasticity regarding the low precipitations, while the temperature was stable over the years, not having great variation (Table 1), keeping within a range of approximately 1°C.

The maximum quarterly periodic increase in height occurred in the quarter from June to September 2017, where treatments with fertilization of nitrogen + potassium, phosphorus + potassium and NPK (nitrogen, phosphorus and potassium) presented values of 103.3, 108.1 and 100.9 cm, respectively (Table 1). And the second largest increase in planting corresponded to the quarter from March to June 2018, where the treatment without fertilization obtained dendrometric accumulation at a height similar to that with the addition of nitrogen plus potassium (76 cm). This growth rate in height is outside the expected patterns, since normally the greatest increases occur in the rainy season, which was not observed in the present study.

Unlike growth in height, the largest increase in diameter occurred in the first year of planting (2016), with 1.47 cm in June-September (Table 1 and Figure 1). The second largest increase (1.42 cm) also occurred in June-September, but in the following year (2017). Pre-

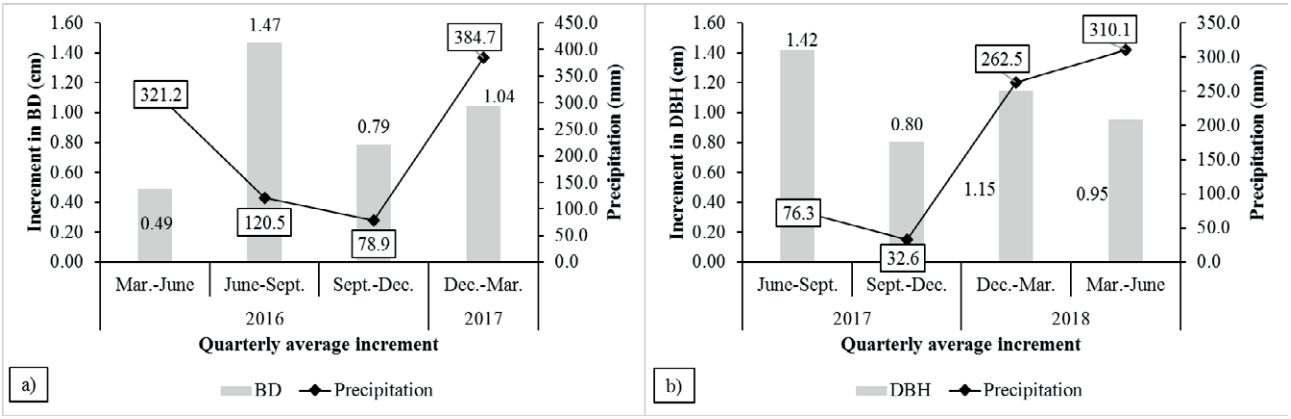

Figure 2. Average increment of basal diameter (BD) (cm), corresponding to the first year of planting (a), diameter at breast height (DBH) (cm), corresponding to the second year of planting (b), and rainfall (mm) during the periods studied.

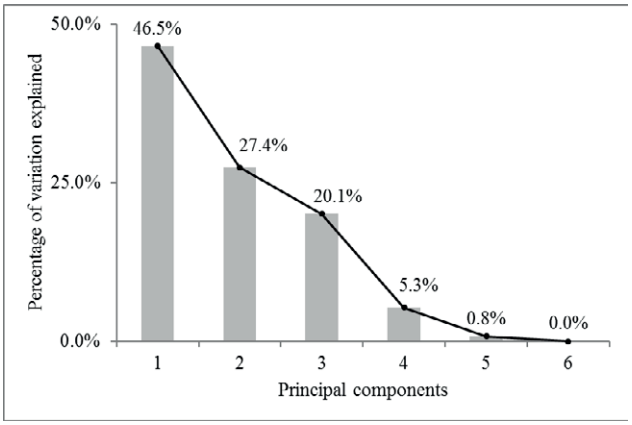

Figure 3. Result of the analysis of principal components of the variables of growth (height and diameter) of *T. vulgaris* plants and meteorological variables (temperature and precipitation).

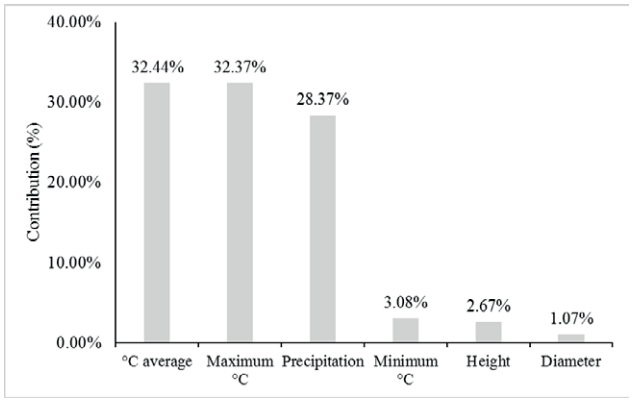

Figure 4. Contribution of the variables of height, diameter, temperature (minimum, average and maximum temperatures) and precipitation, for the first principal component, in a *T. vulgaris* plantation submitted to fertilization with N, P and K.

cipitation in these periods of greatest increase was only 120.5 mm in Jun-Sep 2016 and 76.3 mm in Jun-Sep 2017 (Figure 2).

Among the treatments with the highest mean increments, those with the addition of nitrogen + phosphorus (1.71 cm), nitrogen (1.65 cm) and nitrogen + potassium (1.58 cm) stand out (Table 1).

The reduction in the increase in tree diameter and height in the quarter from December to March 2017, despite the high level of precipitation (384.7 mm), can be partially attributed to the greater number of cloudy days affecting respiration and nutrient translocation. by the roots and photosynthesis, with reflection in the increase of the dendrometric variables.

The principal component analysis showed that the first three factors have eigenvalues, which correspond to 46.5%, 27.4% and 20.1% of the variance (Figure 3), explained by the model's eigenvalues, that is, they explain together 94 % of the total variance of species growth, with a stabilization of the curve after the fourth component. Thus, the first three components were considered, considering that the other components present a low explanation.

The breakdown of the analysis of the first two main components shows that the variables that most contributed to explain the development of the population of the species, correlated with the meteorological variables observed in this study, were the average and maximum temperatures and precipitation (Figure 4), followed by the height, diameter and minimum temperature (Figure 5). For the third main component, only the minimum temperature contributed to explain the data variance (Table 2). This demonstrates that the temperature variation and the amount of rain were the first variables to

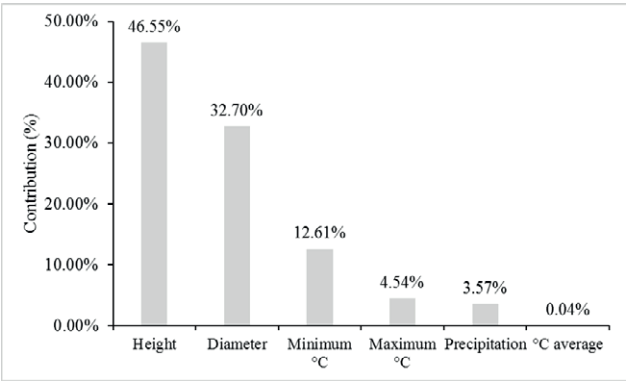

Figure 5. Contribution of height, diameter, temperature (minimum, average and maximum) and precipitation variables to the second principal component in a *T. vulgaris* plantation subjected to N, P and K fertilization.

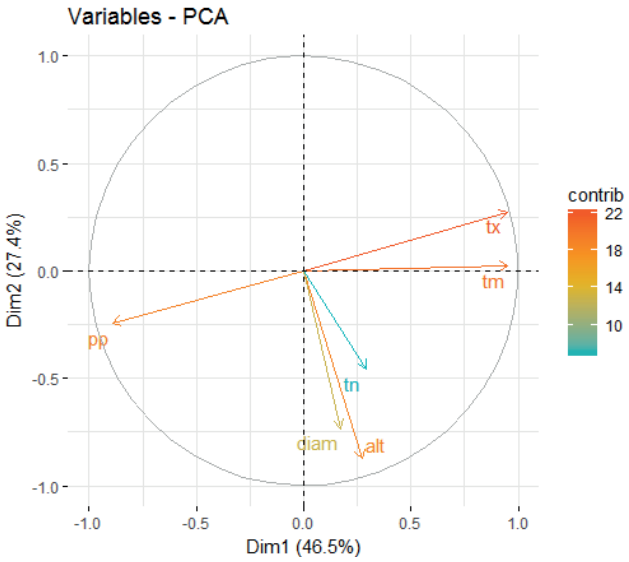

Figure 6. Ordering diagram of the original variables of the six Principal Components, extracteds from the analyzed growth and meteorological variables, in a *T. vulgaris* plantation fertilized with N, P and K.

Table 2. Contribution of growth and meteorological variables to the first three Principal Components extracted, in a *T. vulgaris* plantation fertilized with N, P and K.

Variable	Principal Components		
	1	2	3
Height	2.67%	46.55%	0.63%
Diameter	1.07%	32.70%	25.16%
Average temperature	32.44%	0.04%	7.03%
Maximum temperature	32.37%	4.54%	0.90%
Minimum temperature	3.08%	12.61%	56.74%
Precipitation	28.37%	3.57%	9.53%

predict the development of the plantation, followed by the dendrometric indicators.

In the ordering diagram of the original variables of the six principal components, it can be seen that some dendrometric and climatic variables are superimposed (right side of the circle), which demonstrates that they have similar representation (Figure 6). It can also be observed that the environmental variables are close to the unit circle, denoting a strong relationship with the increase in height and diameter.

Pearson's correlation showed that the variables that most correlated were precipitation with mean and maximum temperatures, with correlation values close to 1 (100%) (Table 3). The height and diameter variables had a low (R=0.3) to moderate (R=0.6) correlation with precipitation. In planting of *Tachigali vulgaris* with spacing (4 × 2 m).

Table 3. Pearson correlation matrix for the growth and meteorological variables studied, in a *T. vulgaris* plantation fertilized with N, P and K.

Variables	Pearson's correlation matrix					
	Height	Diameter	Average T.	Maximum T.	Minimum T.	Precipitation
Height	1					
Diameter	,	1				
Average T.	-	-	1			
Maximum T.	-	-	B	1		
Minimum T.	-	.	.	-	1	
Precipitation	-	.	*	B	-	1

Legend: "-" 0.3, "." 0.6, "," 0.8, "*" 0.95, "B" 1, correlation level.

DISCUSSION

For Brienen et al. (2017), growth can vary intra and interspecifically according to the size class of the trees, in the case of the study they were still in the initial phase of growth, therefore, the association of factors with the climate is important. determinant in the dynamics of growth combined with carbon gain, since larger trees have greater monthly growth, disregarding the point at which age can be limiting (Lyra et al., 2017).

Dias & Marenco (2016) evaluated the effect of rainfall seasonality on tree growth of 28 species in tropical terra firme forest in central Amazonia and concluded that the region's mild dry season is not long enough to deplete soil water, beyond the reach of the root system, which allows trees to grow at constant rates throughout the year. In the present study, the growth also remained constant, not being null during the evaluation period.

As for height, the species showed good elasticity in terms of low precipitation rates. According to (Sette et al. 2010), this result is explained by the availability of water from the rainy season, stored in the deeper layers of the soil.

Physiologically speaking, the assimilation of CO_2 from the atmosphere through foliar photosynthesis depends on temperature limits that allow the work of the enzymes that act in the process, the main one being Rubisco. Excessive temperature limits can not only inhibit Rubisco, but also cause damage to the plant's hydraulic system. This is because temperature is strongly related to vapor pressure deficit (VPD) which, in turn, has been identified as one of the main causes of tree mortality (McDowell and Allen, 2015, McDowell et al., 2018).

In a study to evaluate the growth in trunk diameter of *Eucalyptus grandis* trees and its relationship with climatic variables and mineral fertilization, (Sette et al. 2010) concluded that climatic variables influenced growth rates, where greater rainfall led to reductions in increments. Narducci et al. (2016) evaluated the growth of *Sclerolobium paniculatum* and the relationship between precipitation and diameter increment, in different planting spacings in dystrophic yellow latosol with annual precipitation of 2500 mm, and concluded that the correlation between precipitation and increment in diameter was moderate to strong, which, according to the authors, shows the sensitivity of the growth of this species to the availability of water. However, in the present study this correlation did not occur.

According to Mattos et al. (2015), rainfall from the previous year had a major contribution to the subsequent increase in diameter of Mimosa tenuiflora in seasonally dry tropical forest in Brazil. According to Santos et al. (2017), in places where there is an inventory to support the development and intervene in forest plantations, such as the choice of clones with higher productivity per site, information on rainfall, together with the analysis of growth curves in different types of soils, can help to define the most suitable clone for a given region.

According to Morais et al. (2017), *Tachigali vulgaris* presents strategies to water stress, which is correlated with increased leaf temperature. This promotes the elevation of leaf transpiration rates, serving as a strategy used to reduce leaf temperature, avoiding damages due to the exaggerated heating of the photosynthetic apparatus, since the process of evaporation of the water molecule by the plants causes a substantial loss of heat and constitutes one of the most important means they have to regulate the temperature. This is in agreement with the results found in the present study, where precipitation and maximum and average temperatures strongly influenced the dendrometric increments of *Tachigali vulgaris*. Narducci et al. (2016) also observed a correlation close to 0.6 between precipitation and diameter increment.

Soares and Cruz (2016) evaluated the influence of meteorological variables on the growth in diameter and height of paricá (*Schizolobium parahyba* var. *amazonicum*), using Pearson's correlation analysis, and found positive correlations, showing a directly proportional relationship between the meteorological variables and the increments in diameter and height of the trees of the species. In a study of the relationship of meteorological variables with the growth of planted trees of *Araucaria angustifolia* (Bertol.) Kuntze, it was found that the increase in precipitation positively influences the increase in diameter (Zanon & Finger 2010), which corroborates the results of the present study.

CONCLUSION

Precipitation was the climate variable that most positively influenced the increase in height and diameter of *Tachigali vulgaris* L. G. Silva & H. C. Lima plants,

The plants showed excellent elasticity, especially in periods of low rainfall,

The precipitation and maximum and average temperatures strongly influenced the dendrometric increments of *Tachigali vulgaris*,

In view of the results presented, there is a great possibility of indicating the planting of *Tachigali vulgaris* for regions with climate variations similar to this study.

REFERENCES

Bertolini, Í. C., Watzlawick, L. F., Sens, T. M. Z. G., Vantroba, A. P., Schran, J. A., Pott, C. A. 2020. Influence of climate variables on the diametric increment of Bauhinia forficata Link, Mimosa scabrella Benth. and Schinus terebinthifolius Raddi. *Research, Society and Development [S. l.]*, 9(4), e185942859.

Biagiotti, G., Valeri, S. V., Cruz, M. C. P. da, Vasconcelos, R. T. de. 2017. Fertilização potássica na implantação de *Corymbia citriodora* (Hook.) K.D. Hill & L.A.S. Jonhson. *Scientia Forestalis*, 45(113), 129-137.

Brienen, R. J., Gloor, M., Ziv, G. 2017. Tree demography dominates long-term growth trends inferred from tree rings. Global change biology, 23(2), 474-484.

Camargo, M. L. P., Moraes, C. B., Mori, E. S., Guerrini, I. A., Mello, E. J., Oda, S. 2004. Considerações sobre eficiência nutricional em *Eucalyptus*. *Cientifica*, 32(2), 191-196.

Costa, C. F. G., Figueiredo, R. de O., Oliveira, F. de A., Santos, I. P. de O. 2013. Escoamento superficial em Latossolo Amarelo distrófico típico sob diferentes agroecossistemas no nordeste paraense. *Revista Brasileira de Engenharia Agrícola e Ambiental*, 17, 162-169.

De Jesus, G. L., Longhi, S. J., Farias, K. J., Kanieski, M. R., Turmina, E., & Zangalli, C. 9019. Avaliação do Avaliação do crescimento de espécies nativas plantadas em área de compensação florestal. *Advances in Forestry Science*, 6(4), 819-826.

Dias, D. P. & Marenco R. A. 2016. Tree growth, wood and bark water content of 28 Amazonian tree species in response to variations in rainfall and wood density. *iForest*, 9, 445-451.

Forrester, D. I., Cowie, A. L., Bauhus, J., Wood, J. T., Forrester, R. I. 2006. Eûects of changing the supply of nitrogen and phosphorus on growth and interactions between *Eucalyptus globulus* and *Acacia mearnsii* in a pot trial. *Plant and Soil*, 280(1/2), 267-277.

Graciano, C., Goya, J. F., Frangi, J. L., Guiamet, J. J. 2006. Fertilization with phosphorus increases soil nitrogen absorption in young plants of *Eucalyptus grandis*. *Forest Ecology Management*, 236(2-3), 202-210.

Kanieski, M. R., Galvão, F., Santos, T.l., Milani, J. E. F., Botosso, P. C. 2017. Parâmetros Climáticos e Incremento Diamétrico de Espécies Florestais em Floresta Aluvial no Sul do Brasil. *Floresta e Ambiente*, 24(1), 1-11.

Kanieski, M. R., Santos, T. L., Graf Neto, J., Souza, T., Galvão, F., Roderjan, C. V. 2012. Influência da Precipitação e da Temperatura no Incremento Diamétrico de Espécies Floreastais Aluviais em Araucária-PR. *Floresta e Ambiente*, 19, 17-25.

Lyra, A., Imbach, P., Rodriguez, D., Chou, S. C., Georgiou, S., & Garofolo, L. 2017. Projections of climate change impacts on central America tropical rainforest. *Climatic Change*, 141(1), 93-105.

Mattos, P. P., Braz, E. M., Domene, V. D., Sampaio E. V. de S. B., Gasson, P., Pareyn, F. G. C., Alvarez, I. A., Baracat, A., Araújo, E. de L. 2015. Climate-tree growth relationships of *Mimosa tenuiflora* in seasonally dry tropical forest, brazil. *Cerne*, 21, 141-149.

McDowell, N., Allen, C.D., Anderson-Teixeira, K., Brando, P., Brienen, R., Chambers, J., Christoffersen, B., Davies, S., Doughty, C., Duque, A., Espirito-Santo, F., Fisher, R., Fontes, C.G., Galbraith, D., Goodsman, D., Grossiord, C., Hartmann, H., Holm, J., Johnson, D.J., Kassim, A.R., Keller, M., Koven, C., Kueppers, L., Kumagai, T., Malhi, Y., McMahon, S.M., Mencuccini, M., Meir, P., Moorcroft, P., Muller-Landau, H.C., Phillips, O.L., Powell, T., Sierra, C.A., Sperry, J., Warren, J., Xu, C. and Xu, X. 2018. Drivers and mechanisms of tree mortality in moist tropical forests. *New Phytologist*, 219, 851-869.

Mcdowell, N. G., & Allen, C. D. (2015). Darcy's law predicts widespread forest mortality under climate warming. *Nature Climate Change*, 5(7), 669.

Morais, R. R., Rossi L. M. B., Higa, R. C. V. 2017. Trocas gasosas de plantas jovens de tachi-branco submetidas à variação de temperatura foliar e suspensão da irrigação. *Ciência Florestal*, 27, 97-104.

Narducci, T. S., Yared, J. A. G., Brienza Junior, S. 2016. Growth and survival of *Sclerolobium paniculatum* Vogel AND the relationship between rainfall and the increment in diameter at different planting spacings. *Revista Árvore*, 40, 447-454.

Pinkard, E. A. 2003. Growth and physiological responses of Blackwood (*Acacia melanoxylon*) growing with a *Pinus radiate* nurse crop following applications of nitrogen and phosphorus. *Trees*, Berlin, 17(4), 325-335.

Rosim, C. C., Hsing, T. Y., Paula, R. C. de. 2016. Nutrient use efficiency in interspecific hybrids of eucalypt. *Revista Ciência Agronômica*, 47(3), 540-547.

Rousseau, G. X., Silva, P. R. dos S., Celentano, D., Carvalho, C. J. R. de. 2014. Macrofauna do solo em uma cronosequência de capoeiras, florestas e pastos no Centro de Endemismo Belém, Amazônia Oriental. *Acta Amazonica*, 44, 499-512.

Santos Neto, A. P. 2014. Crescimento inicial de mogno africano (*Khaya spp*.) sob diferentes condições microclimáticas associadas à deficiência hídrica. 2014. 66 p. Dissertação (Mestrado em Ciências Florestais) - Universidade Federal do Espírito Santo.

Santos, A. C. A., Silva, S., Leite, H. G., Cruz, J. P. da. 2017. Influência da variabilidade edafoclimática

no crescimento de clones de eucalipto no Nordeste baiano. *Pesquisa florestal brasileira*, 37, 259-268.

Sette Jr, C. R., Tomazello Filho, M., Dias, C. T. dos S., Laclau, J. P. 2010. Crescimento em diâmetro do tronco das árvores de *Eucalyptus grandis* W. HILL. EX. Maiden e relação com as variáveis climáticas e fertilização mineral. *Revista Árvore*, 34, 979-990.

Silva, M. de O., Santos, M. P. dos, Sousa, A. C. da P., Silva, R. L. V. da, Moura, I. A. A. de, SILVA, R. S. da, COSTA, K. D. da S. 2021. Qualidade do solo: indicadores biológicos para um manejo sustentável. *Brazilian Journal of Development*, v. 7, n. 1, p. 6853-6875.

Silva, S. B., Sousa, V. C., Santos, C. M., Mariano, D. C., Okumura, R. S. 2017. Levantamento florístico do componente arbustivo-arbóreo da vegetação ciliar de fragmento no rio Parauapebas. *Revista Agroecossistemas*, 9, 99-115.

Smethurst, P. J. 2010. Forest fertilization: trends in knowledge and practice compared to agriculture. *Plant and Soil*, 335(1/2), 83-100.

Soares, T. S. & Cruz, E. S. 2016. Influência de variáveis metereológicas no crescimento em diâmetro e altura de *Schizolobium parahyba* var. amazonicum. *Revista Univap*., 22(40), Edição Especial.

Sousa, V.g., Brienza Jr., S., Barbosa, M.g., Martorano, L.g., Silva, V.C. 2016. 37 p. Taxi-branco (*Tachigali vulgaris* L.F. Gomes da Silva & H.C. Lima): botânica, ecologia e silvicultura. Documentos Embrapa, 426.

Zanon, M. L. B, Finger C. A. G. 2010. Relação de variáveis meteorológicas com o crescimento das árvores de *Araucaria angustifolia* (Bertol.) Kuntze em povoamentos implantados. *Ciência Florestal*, 20, 467-476.

Zhang, F., Niu, J., Zhang, W., Chen, X., Li, C., Yuan, L., Xie, J. 2010. Potassium nutrition of crops under varied regimes of nitrogen supply. *Plant and Soil*, 335(1-2), 21-34.

Finito di stampare da
Logo s.r.l. – Borgoricco (PD) – Italia

RIGOROUS PEER REVIEW
Each submission to IJAm is subject to a rigorous quality control and peer-review evaluation process before receiving a decision. The initial in-house quality control check deals with issues such as competing interests; ethical requirements for studies involving human participants or animals; financial disclosures; full compliance with IJAm's data availability policy, etc.
Submissions may be returned to authors for queries, and will not be seen by our Editorial Board or peer reviewers until they pass this quality control check.
Each paper is subjected to critical evaluation and review by Field Editors with specific expertise in the different areas of interest and by the members of the international Editorial Board.

OPEN ACCESS POLICY
The Italian Journal of Agrometeorology provides immediate open access to its content. Our publisher, Firenze University Press at the University of Florence, complies with the Budapest Open Access Initiative definition of Open Access: By "open access", we mean the free availability on the public internet, the permission for all users to read, download, copy, distribute, print, search, or link to the full text of the articles, crawl them for indexing, pass them as data to software, or use them for any other lawful purpose, without financial, legal, or technical barriers other than those inseparable from gaining access to the internet itself. The only constraint on reproduction and distribution, and the only role for copyright in this domain is to guarantee the original authors with control over the integrity of their work and the right to be properly acknowledged and cited. We support a greater global exchange of knowledge by making the research published in our journal open to the public and reusable under the terms of a Creative Commons Attribution 4.0 International Public License (CC-BY-4.0). Furthermore, we encourage authors to post their pre-publication manuscript in institutional repositories or on their websites prior to and during the submission process and to post the Publisher's final formatted PDF version after publication without embargo. These practices benefit authors with productive exchanges as well as earlier and greater citation of published work.

COPYRIGHT NOTICE
Authors who publish with IJAm agree to the following terms:
Authors retain the copyright and grant the journal right of first publication with the work simultaneously licensed under a Creative Commons Attribution 4.0 International Public License (CC-BY-4.0) that allows others to share the work with an acknowledgment of the work's authorship and initial publication in IJAm.
Authors are able to enter into separate, additional contractual arrangements for the non-exclusive distribution of the journal's published version of the work (e.g., post it to an institutional repository or publish it in a book), with an acknowledgment of its initial publication in this journal.
Authors are allowed and encouraged to post their work online (e.g., in institutional repositories or on their website) prior to and during the submission process, as it can lead to productive exchanges, as well as earlier and greater citation of published work (See The Effect of Open Access).

PUBLICATION FEES
Unlike many open-access journals, the Italian Journal of Agrometeorology does not charge any publication fee.

WAIVER INFORMATION
Fee waivers do not apply at Firenze University Press because our funding does not rely on author charges.

PUBLICATION ETHICS
Responsibilities of IJAm's editors, reviewers, and authors concerning publication ethics and publication malpractice are described in IJAm's Guidelines on Publication Ethics.

CORRECTIONS AND RETRACTIONS
In accordance with the generally accepted standards of scholarly publishing, IJAm does not alter articles after publication: "Articles that have been published should remain extant, exact and unaltered to the maximum extent possible". In cases of serious errors or (suspected) misconduct IJAm publishes corrections and retractions (expressions of concern).

Corrections
In cases of serious errors that affect or significantly impair the reader's understanding or evaluation of the article, IJAm publishes a correction note that is linked to the published article. The published article will be left unchanged.

Retractions
In accordance with the "Retraction Guidelines" by the Committee on Publication Ethics (COPE) IJAm will retract a published article if:
- there is clear evidence that the findings are unreliable, either as a result of misconduct (e.g. data fabrication) or honest error (e.g. miscalculation)
- the findings have previously been published elsewhere without proper crossreferencing, permission or justification (i.e. cases of redundant publication)
- it turns out to be an act of plagiarism
- it reports unethical research.
- An article is retracted by publishing a retraction notice that is linked to or replaces the retracted article. IJAm will make any effort to clearly identify a retracted article as such.

If an investigation is underway that might result in the retraction of an article IJAm may choose to alert readers by publishing an expression of concern.

ARCHIVING
IJAm and Firenze University Press are experimenting a National legal deposition and long-term digital preservation service.

SUBMITTING TO IJAm
Submissions to IJAm are made using FUP website. Registration and access are available at: https://riviste.fupress.net/index.php/IJAm/submission
For more information about the journal and guidance on how to submit, please see https://riviste.fupress.net/index.php/IJAm/index

Principal Contact
Simone Orlandini, University of Florence
simone.orlandini@unifi.it

Support Contact
Alessandro Pierno, Firenze University Press
alessandro.pierno@unifi.it

GUIDE FOR AUTHORS
1. Manuscript should refer to original researches, not yet published except in strictly preliminary form.
2. Articles of original researches findings are published in Italian Journal of Agrometeorology (IJAm), subsequent to critical review and approval by the Editorial Board. External referees could be engaged for particular topics.
3. Three types of paper can be submitted: original paper, review, technical note. Manuscript must be written in English. All pages and lines of the manuscript should be numbered.
4. First Name, Last Name, position, affiliation, mail address, telephone and fax number of all the Co-Authors are required. Corresponding Authors should be clearly identified.
5. The abstract should be no longer than 12 typed lines.
6. Full stop, not comma, must be used as decimal mark (e.g. 4.33 and not 4,33).
7. Figures, tables, graphs, photos and relative captions should be attached in separate files. All images must be vector or at least 300 effective ppi/dpi to ensure quality reproduction.
8. Captions should be written as: Fig. x – Caption title, Tab. x – Caption title. Images should be referred to in the text as (Fig. x), (Tab. x).
9. Proof of the paper (formatted according to the Journal style) will be sent to the Corresponding Author for proof reading just one time. Corrections can be made only to typographical errors.
10. All the references in the text must be reported in the "References" section and vice-versa. In the text, only the Author(s) last name must be present, without the name or the first letter of the name (e.g. "Rossi, 2003" and not "Federico Rossi, 2003" or "F. Rossi, 2003"). If two authors are present, refer to them as: "Bianchi and Rossi, 2003" in the text (do not use "&" between the surnames). If more than two Authors are present, refer to them as: "Bianchi et al., 2003" in the text.
For journals, references must be in the following form:
Bianchi R., Colombo B., Ferretti N., 2003. Title. Journal name, number: pages.
For books:
Bianchi R., Colombo B., Ferretti N., 2003. Book title. Publisher, publishing location, total number of pages pp.
Manuscripts "in press" can be cited.

BECOME A REVIEWER
Peer review is an integral part of the scholarly publishing process. By registering as a reviewer, you are supporting the academic community by providing constructive feedback on new research, helping to ensure both the quality and integrity of published work in your field. Once registered, you may be asked to undertake reviews of scholarly articles that match your research interests. Reviewers always have the option to decline an invitation to review and we take care not to overburden our reviewers with excessive requests.
You must login before you can become a reviewer.
If you don't want to be a reviewer anymore, you can change your roles by editing your profile.

COMPETING INTERESTS
You should not accept a review assignment if you have a potential competing interest, including the following:
- Prior or current collaborations with the author(s)
- You are a direct competitor
- You may have a known history of antipathy with the author(s)
- You might profit financially from the work

Please inform the editors or journal staff and recuse yourself if you feel that you are unable to offer an impartial review.
When submitting your review, you must indicate whether or not you have any competing interests.

Italian Journal of Agrometeorology

Rivista Italiana di Agrometeorologia

n. 1 – 2024

Table of contents